AN ABSTRACT OF THE DISSERTATION OF

Radhika Naik for the degree of Doctor of Philosophy in Chemistry presented on October 11, 2007.

Title: Studying Fusion Reactions for Effect of P_{CN} on Heavy Nucleus Formation and for Nuclear Structure Effects.

Abstract approved: _____

Walter D. Loveland

The fusion reaction ^{208}Pb (^{50}Ti, xn) $^{258-x}Rf$ (x = 1-3) was studied to determine P_{CN} (probability that the mononucleus system evolves to form a compound nucleus inside the fission saddle point) and to establish the value of W_{sur} (survival probability) for the given reaction experimentally. The fission excitation function was measured at five beam energies. Angular distributions were fit using the Back et al. prescription to determine J_{CN} and σ_{CN}. The total fission cross section (σ_{fis}) and compound nucleus cross section (σ_{CN}) at each of the energies were used for calculating P_{CN}. These experimentally determined values of P_{CN} and σ_{fis} and the values of σ_{EVR} determined in previous studies of this system were used in the equation $\sigma_{EVR} = \sigma_c \times P_{CN} \times W_{sur}$ to arrive at W_{sur} for each of the energies. The experimental value of W_{sur} for 1n channel agrees very well with the one based on theoretical predictions of Möller et al. The subsequent lowering in W_{sur} with beam energy is attributed to onset of 2n and 3n evaporation channels.

The fusion reaction ^{9}Li+^{70}Zn was studied to determine the effects of nuclear structure of the projectile (neutron skin) on fusion. The fusion excitation function was measured at seven near- and sub-barrier beam energies. Radioactivity in the irradiated target was measured by γ-spectroscopy and in radiochemically separated EVRs by β-spectroscopy. The ^{9}Li fusion radius determined by fitting the excitation function with Wong formula was 12.1 ± 1.0fm, much larger than 2.5fm given by $R_0 \times A^{1/3}$. This extension of the radius is attributed to the presence of spatially extended neutron skin. The excitation function also showed a large sub-barrier fusion enhancement not explained by standard coupled channel model. An attempt was made at measuring the fusion excitation function with ^{11}Li projectile (neutron halo nucleus) which would enable us to do a comparative study as ^{9}Li is the core of ^{11}Li halo nucleus but it failed due to low beam intensity.

Studying Fusion Reactions for Effect of P_{CN} on Heavy Nucleus Formation and for Nuclear Structure Effects

by
Radhika Naik

A DISSERTATION

Submitted to

Oregon State University

in partial fulfillment of
the requirements for the
degree of

Doctor of Philosophy

Presented October 11, 2007
Commencement June 2008

Doctor of Philosophy dissertation of Radhika Naik presented on October 11, 2007

APPROVED:

Major Professor representing Chemistry

Chair of the Department of Chemistry

Dean of the Graduate School

I understand that any dissertation will become a part of the permanent collection of Oregon State University libraries. My signature below authorizes release of my dissertation to any reader upon request.

Radhika Naik, Author

ACKNOWLEDGEMENTS

There have been many people during the course of this work who have provided me with their time, money, expertise, patience, intellectual and moral support. It would be impossible to list you all here but you know who you are, I couldn't have done it without you.

This work was funded in part by The OSU Chemistry Department, the David P. Shoemaker Memorial Fellowship, the Benedict Award, the Director of Office of Energy Research, Division of Nuclear Physics of the Office of High Energy and Nuclear Physics of the U.S. Department of Energy, TRIUMF and the Natural Sciences and Engineering Research Council of Canada.

First and foremost, thanks go to my advisor Dr. Walter Loveland, who has been unfailingly patient and supportive throughout. Working under his guidance I have earned a great deal of scientific knowledge, experimental, technical and computational expertise which has made me able to work independently in the field of scientific research. A big thank you also goes to the following people,

My collaborators at Argonne National Lab (ANL), Don Peterson, Partha Choudhary, Frank Moore, C. Jiang, Shrabani Sinha, Xodong Tang and S. Zhu, John Greene of the target fabrication group for providing the Pb targets, Richard Pardo and the cyclotron operations staff.

My collaborators at Tri-University Meson Facility (TRIUMF), Mike Trinczeck, Marik Dombsky, Peter Machule, Dave Ottewell, David Cross, Kate Gagnon, and William. J. Mills, the cyclotron operations and health physics staff, in particular, Bob Laxdal, Marco Marchetto, Anne Trudel and Dave Hutcheon.

Peter Sprunger and A.M. Vinodkumar for helping me understand various aspects of scientific computing, electronics functioning and also nuclear physics on numerous occasions. Mike Conrady and Lucas Hart for computer support. Ted Hinke for machining various equipments and parts required for the experiments. The health physicists Scott Menn and Jim Darrough for making sure and making it easy to observe the safety requirements for radiochemical experiments. Leah Minc for making the γ detectors available when needed. The faculty and staff of the Radiation Center and Chemistry Department at Oregon State University.

My numerous friends in US and back home in India, especially Jasmine, Aaditi, Pranav, Amit, Aditi, Vibha, who have always known how to keep me smiling. The Phatak family and many others of the Indian community in Oregon for making me feel at home away from home.

And last but not the least, my parents and my fiancé, Ashish, for encouraging me and providing me strong and unfailing support to embark on and reach the destination of this journey for knowledge that has taken me thousands of miles away from home. You have been the most indispensable source of strength for me! Thank you for everything.

TABLE OF CONTENTS

Page

TABLE OF CONTENTS (Continued)

Page

TABLE OF CONTENTS (Continued)

Page

TABLE OF CONTENTS (Continued)

Page

LIST OF FIGURES

LIST OF FIGURES (Continued)

Figure Page

LIST OF FIGURES (Continued)

Figure Page

LIST OF FIGURES (Continued)

Figure Page

LIST OF FIGURES (Continued)

Figure Page

LIST OF TABLES

LIST OF TABLES (Continued)

Table Page

For
my mother, Vasundhara Pendse-Naik,
who has been my strongest support and closest friend
and
my father, Sudhir Naik,
who has always been there for me.

STUDYING FUSION REACTIONS FOR EFFECT OF P_{CN} ON HEAVY NUCLEUS FORMATION AND FOR NUCLEAR STRUCTURE EFFECTS

The study of fusion reactions that originally included only the lighter elements (A ≤ 56) has expanded over last few decades to involve heavier targets and projectiles (e.g.: actinides used as targets in hot fusion[1] or ^{208}Pb used as a projectile in an inverse kinematics[2] fusion reaction). The fusion reaction is now used for studying nuclear structure effects in various nuclei and for exploring different possibilities of synthesizing superheavy elements. Since the Coulomb repulsion between the nuclei needs to be overcome before they fuse, the projectile beam needs to be accelerated to substantial kinetic energy. Also since only a small fraction of the projectile nucleus undergoes nuclear reactions with the target nucleus the beam needs to have high intensity.

The different amounts of energy needed for the nuclei to interact with each other to various extents are illustrated in fig1. At low energies of the beam only scattering takes place which is not a nuclear reaction. The energy needed to bring the ions in contact, and thus to undergo nuclear reactions is the *interaction barrier*. Additional energy is required for the nuclei to surmount the fission saddle and to truly fuse and form a compound nucleus. A *compound nucleus* (CN) is a relatively long-lived reaction intermediate that is a result of complicated set of two-body interaction in which energy of projectile is distributed among all the nucleons of the composite system (Loveland 2005). The mode of decay of CN is independent of the mode of

[1] This particular type of fusion reaction is explained in section 1.1 of ^{50}Ti+^{208}Pb experiment.
[2] Usually fusion reactions are carried out with heavier element as target and lighter as the projectile. When this situation is reversed, the reaction carried out is termed as inverse kinematics fusion.

formation. While the statement is not true in general, it remains a useful tool in understanding some aspects of CN reactions.

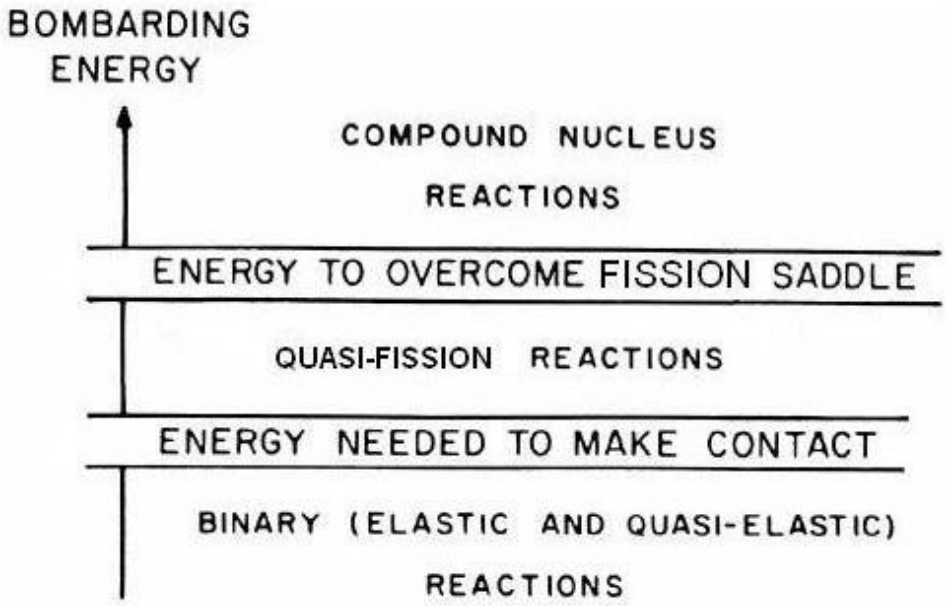

Figure 1 The different amounts of energy needed for the nuclei to interact with each other to various extents are illustrated in the figure. At low energies of the beam only scattering takes place which is not a nuclear reaction. The energy needed to bring the ions in contact, and thus to undergo nuclear reactions is the *interaction barrier*. Additional energy is required for the nuclei to surmount the fission saddle and to truly fuse and form a compound nucleus.

The probability of fusion is sensitive to the Coulomb force between the interacting nuclei and to the angular momentum. Fig2 shows the variation of nuclear potential (which is the sum of the Coulomb, the nuclear and the centrifugal potentials) as a function of angular momentum (l) and radial separation (R). At lower l, there are "pockets" in the potential curve which signify the combination of potential and radial separation at a given l when the interacting nuclei undergo fusion. For higher l, there are no such combinations and the fusion does not take place. Thus for a given projectile energy and Coulomb potential there is a critical value of angular momentum

(l_{crit}) above which no fusion occurs. The fusion probability is enhanced due to lowering of fusion barrier in case of deformed nuclei because the ions can contact at a greater value of R.

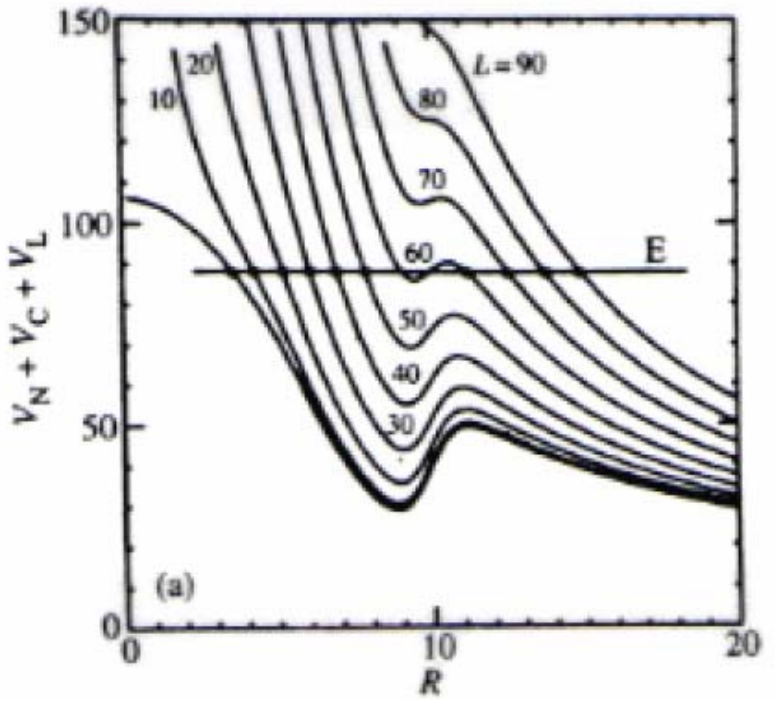

Figure 2 The figure shows the variation of nuclear potential (MeV, which is the sum of the Coulomb, the nuclear and the centrifugal potentials) as a function of angular momentum (l) and radial separation (R, fm). At lower l, there are "pockets" in the potential curve which signify the combination of potential and radial separation at a given l when the interacting nuclei undergo fusion. For higher l, there are no such combinations and the fusion does not take place. E is the bombarding energy of the projectile. [Source: (Loveland 2005)]

For superheavy element production, the system must evolve to a CN after passing over the fusion-barrier and the CN formed should survive by decaying through evaporation of few light particles without undergoing fission. The probability that the mononuclear complex evolves to form a CN (which is synonymous to the concept of

complete fusion (Bass 1980)) inside the fission saddle point (i.e. before it undergoes fission) is an important factor in heavy nucleus synthesis. Our study of the fusion reaction ^{208}Pb (^{50}Ti, xn) $^{258-x}$Rf (x = 1-3), involving a stable target and projectile combination, was aimed at determining this probability (P_{CN}) experimentally for the given system. It would possibly settle the contradiction over the theoretically determined values of survival probability (W_{sur}) for elements $Z \geq 102$ by employing the theoretical predictions of Möller et al. and Smolańczuk. The former part of this dissertation gives a detailed account of this experiment, the data analysis, and the results. Chapter 1 introduces the reader to heavy element synthesis, the previous experimental and theoretical studies performed involving this system and the theoretical contradiction in predicting the W_{sur} for elements Z = 102-120, resolution of which is the motivation behind this experiment. Chapter 2 deals with the details of experimental setup and data acquisition. The analysis of the data is described in detail in Chapter 3 and Chapter 4 contains the summary of results, their comparison with previous work, the consequences for heavy element synthesis and the possible future work to improve upon the same.

For last couple of decades, a large number of fusion reactions have been carried out using the radioactive projectiles, in addition to stable beams. The radioactive beams are produced using the ISOL (Isotope separator on-line) or PF (projectile fragmentation) techniques (Loveland 2005). The principal attraction of these studies is the ability to form and study reaction products or intermediates with unusual N/Z ratios by starting with very neutron- or proton-rich reactants. Also the radioactive projectiles which have an interesting nuclear structure, like the neutron-rich nuclei

with *skin* and *halo* structures[3], can be studied. There is considerable theoretical as well as experimental disagreement over the effect of these nuclear structures on fusion. Our second fusion study, which was a pilot study for the given system, involved a projectile with neutron-skin (^{9}Li) that fused with an intermediate mass neutron-rich target (^{70}Zn). By measuring the fusion excitation function for this reaction (for which P_{CN} is assumed to be unity) presence of any suppression or enhancement of sub-barrier fusion as compared with the theoretical predictions would be determined. (An attempt to measure the fusion excitation function for ^{11}Li (a neutron-halo nucleus) + ^{70}Zn was also made which did not yield statistically significant results due to low intensity of the beams). The latter part of this dissertation gives a detailed account of the ^{9}Li+^{70}Zn fusion experiment, the data analysis, and the results. Chapter 5 introduces the reader to nuclei with neutron skin and halo structure, the experimental and theoretical contradictions regarding the effect of these nuclear structures on fusion, which are the motivation behind this experiment, and the reasons behind studying this particular system. Chapter 6 describes the preparations done for this experiment. Chapter 7 deals with the details of experimental setup and data acquisition. The analysis of the data is described in detail in Chapter 8 and Chapter 9 contains the summary of results, their comparison with theoretical models as well as with experimental results of similar systems, the determination of fusion radius of ^{9}Li by Wong formula fit and the possible future work to improve upon the same.

The codes of the computer program routines used at various stages in the data analysis are enlisted in the appendices A (^{50}Ti+^{208}Pb) and B (^{9}Li+^{70}Zn). The paper

[3] Both types of nuclear structures are explained in section 1.1 of ^{9}Li+^{70}Zn experiment

based on the results of the $^{9}Li+^{70}Zn$ fusion experiment published in PRC is attached in appendix C.

DETERMINATION OF THE P_{CN} IN the $^{50}Ti + ^{208}Pb$ REACTION

1 INTRODUCTION

1.1 Heavy element synthesis

Besides the processes like neutron-capture, alpha particle-induced reaction etc. there are two well-established methods of synthesizing heavy nuclei which involve the fusion of the projectile and the target nuclei,

1. Fusion of a light projectile (Z = 6 to 20) with an actinide (Z = 90 to 103) target nucleus produces compound nuclei that have high excitation energy (E^*~30-60MeV). This reaction type is called *hot fusion* and has a lower fusion hindrance.
2. When a relatively heavier projectile (Z = 18 to 36) undergoes fusion with a *lead* (Pb) or *bismuth* (Bi) target the compound nuclei produced can have low excitation energy (E^*~10-15MeV). These reactions are termed as *cold fusion* and have a higher fusion hindrance.

The excitation energy (E^*) of a nucleus is related to its thermodynamic temperature (T) by the equation $E^* \approx aT^2$ (a – level density parameter proportional to mass of the nuclear system (A) with its value ranging A/12-A/8 MeV^{-1}). As the temperature increases with the increase in excitation energy the nuclei with higher E^* are "hot" and hence the name for the hot fusion. Similarly cold fusion is the reaction that produces compound nuclei that are "cold" due to low E^*. The survival probability of a given nucleus is inversely proportional to its E^*. The higher the E^* of a nucleus the greater is its tendency to decay via fission and have a lower survival probability as compared with the nuclei with low E^*.

It is a general observation that the half-lives ($t_{1/2}$) of the known transuranium nuclei decrease with increasing Z (with exception of nuclei with Z > 106) and that they decay by a combination of electron capture, alpha decay and spontaneous fission (SF). In late 60's and early 70's theoreticians predicted, based on techniques developed by Strutinski and Swiatecki, that the nuclear ground state of nuclei with proton number (Z) ≈ 114 and neutron number (N) ≈ 184 would be stabilized against decay by SF due to shell effects and hence it will be possible to synthesize long-lived ($t_{1/2} \approx 10^{10}$-10^{15} years) isotopes of *superheavy* elements on this 'island of stability'. However, it is now known on basis of various experiments that the elements with Z ≈ 114 are formed with extremely low cross sections (picobarns) and half-lives (<milliseconds). As N increases the half-life of the nucleus also increases. The underlying science of this observation is that as N/Z increases, both the SF and α–decay probability decrease with decrease in α–decay probability being lesser than that in SF probability. Hence, efforts are being directed towards synthesizing neutron (n)-rich isotopes of the heavier nuclei.

However, the synthesis of new element involves more than just colliding two nuclei whose atomic numbers are such that their sum is a Z value for which no element is known to the date. A nuclear reaction caused by head-on collision of two nuclei can proceed by two possible mechanisms in which full momentum transfer takes place. In the first one the compound nucleus is formed by complete fusion of the target and projectile nuclei. This CN then decays either by neutron (or rarely proton) evaporation to give the evaporation residues (EVRs) or by fission to emit fission fragments. The former is termed as 'fusion-evaporation' and the latter as 'fusion-

fission' mechanism. The other mechanism is a capture process in which the target and the projectile form a combined nuclear system but the system does not evolve inside the fission saddle point to form a CN. The system decays by subsequent fission and no EVRs are formed. This mechanism is called 'quasi-fission'. For the projectile trajectories that are in between the grazing and head-on collisions the reaction could proceed through 'deep inelastic scattering'. In this mechanism, the target and projectile interpenetrate partially, exchange some mass and energy, rotate as a partially fused complex and then reseparate under the influence of mutual Coulomb repulsion before a CN is formed. There is a large dissipation of projectile kinetic energy which results in its damping into the excitation energies of the target and projectile-like fragments (with some dispersion in mass possible) which are the products of this process. The full momentum transfer does not take place in this mechanism. The three processes are schematically shown in fig1.1.

The cross section for producing a heavy nucleus in a heavy ion reaction can be expressed as a product of three factors,

$$\sigma_{EVR}(E_{CM}) = \sigma_c(E_{CM}) \times P_{CN}(E_{CM}, J=0) \times W_{sur}(E_{CM}, J=0) \qquad \textbf{1-1}$$

where σ_c is the capture cross section (transition of the colliding nuclei over the Coulomb barrier and making contact with each other), P_{CN} is the probability that a mononuclear system is formed that evolves inside the fission saddle point to form the CN (which depends on the competition between complete fusion and quasi-fission) and W_{sur} is the survival probability of the CN thus formed. The 'production factors' (σ_c and P_{CN}) influence the yields of primary reaction products and the 'survival factor'

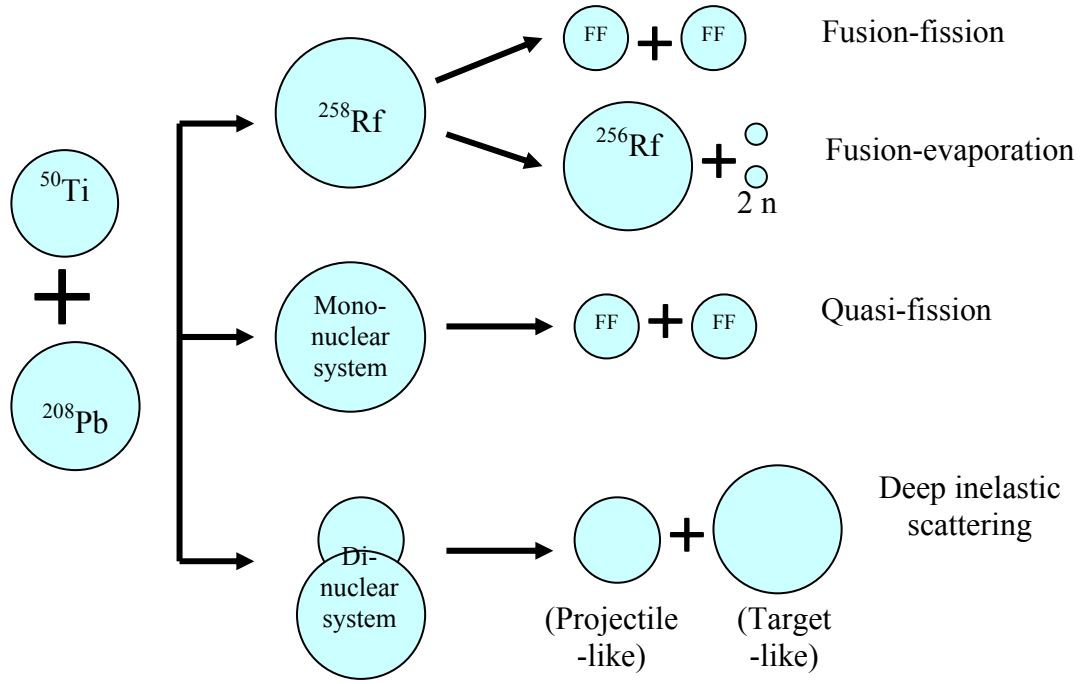

Figure 1.1 The figure schematically shows three possible mechanisms by which a nuclear reaction caused by collision of two nuclei can proceed. A] Compound nucleus (CN) is formed by complete fusion of the target and projectile which then decays either by neutron (or rarely proton) evaporation to give the evaporation residues (EVRs) or by spontaneous fission to give fission fragments (FFs). The former is termed as 'fusion-evaporation' and the latter as 'fusion-fission'. B] 'Quasi-fission' in which the target and the projectile form a combined nuclear system but the system does not evolve inside the fission saddle point to form a CN. The system decays by subsequent fission. C] For the projectile trajectories that are in between the grazing and head-on collisions the reaction could proceed through 'deep inelastic scattering' in which the target and projectile interpenetrate partially, exchange some mass and energy, rotate as a partially fused complex and then reseparate under the influence of mutual Coulomb repulsion before a CN is formed. This results in target and projectile-like fragments which have energies similar to that of FFs.

(W_{sur}) dictates whether the product nucleus decays by particle evaporation and hence survives or it decays by fission and hence gets destroyed.

For the fusion reaction $^{50}Ti + ^{208}Pb$ the quantity P_{CN} is an important one. Since Coulomb repulsion between the target and the projectile is significant the probability

of their overcoming the Coulomb barrier and forming a CN is a crucial factor. Since the CN formed in this reaction has low excitation energy it has higher W_{sur}.

1.2 Previous studies of ^{50}Ti + ^{208}Pb system

The lighter isotopes of element 104 (*rutherfordium* Rf) produced by the ^{50}Ti + ^{208}Pb fusion process have low excitation energy (E* ≈ 10-28MeV) and decay by neutron evaporation producing EVRs. This fusion reaction has therefore been studied numerous times and has been a subject of many publications. Below is the brief overview of these works and their significance to our experiment and data analysis.

Since CN decays either by formation of EVR or through fission the relationship between cross sections for fusion (σ_{fus}), fission ($\sigma_{fus\text{-}fis}$) and EVR formation (σ_{EVR}) is,

$$\sigma_{fus} = \sigma_{fus-fis} + \sigma_{EVR} \qquad \textbf{1-2}$$

Clerc et al. (Blank 1993) observed that the fusion cross section for this reaction was almost equal to the fission cross section ($\sigma_{fus} \approx \sigma_{fus\text{-}fis}$) as the evaporation residue cross section (σ_{EVR}) was about six orders of magnitude lower as compared to the $\sigma_{fus\text{-}fis}$ (fig1.2) and hence could be considered negligible. For the ^{40}Ar-induced reactions studied along with the aforementioned reaction, σ_{fus} values were in fair agreement with the ones predicted by the simple classical formula (Bass 1980),

$$\sigma = \pi R^2_{fus}\left(1 - \frac{V_B}{E}\right) \qquad \textbf{1-3}$$

where R_{fus} - Fusion radius given by $C_p + C_t + 1.14\text{fm}$

V_B - Fusion barrier as calculated from the Bass potential

C_p, C_t - 'Central radius' of projectile and target, respectively, given by $\mathrm{R} - (1\mathrm{fm}^2)/\mathrm{R}$ where $R = 1.28A^{1/3} - 0.76 + 0.8A^{-1/3}\,fm$

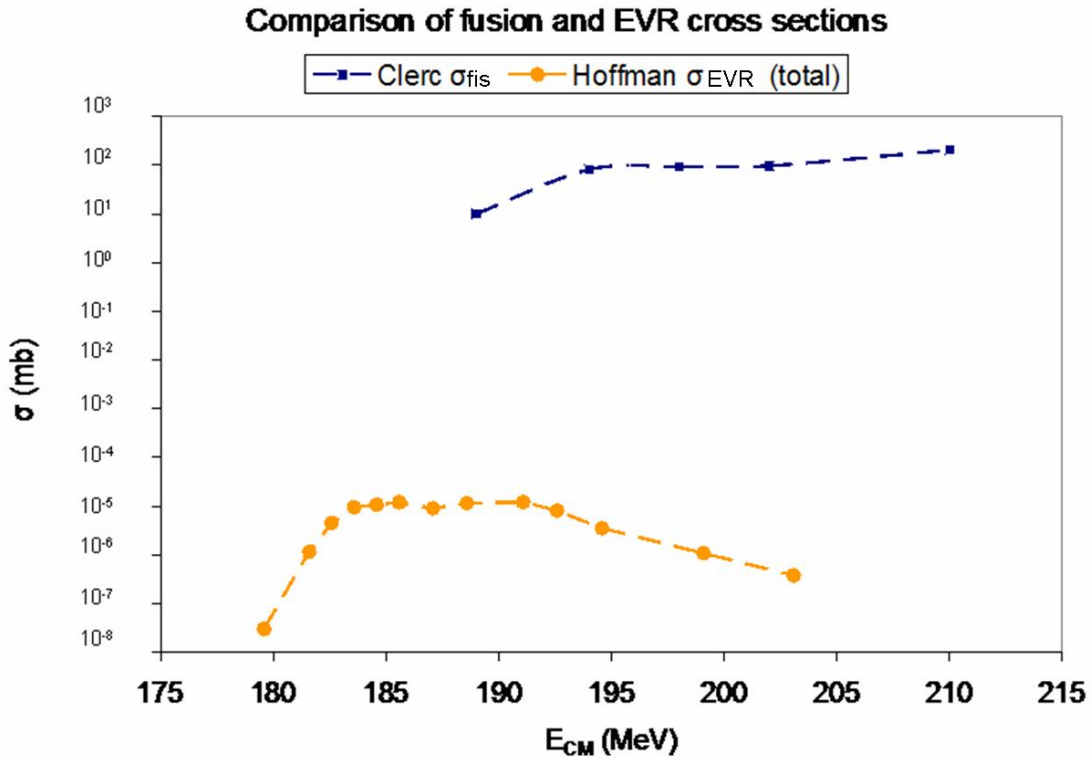

Figure 1.2 Fission cross sections (σ_{fis}) (squares) and evaporation residue cross sections (σ_{EVR}) (triangles) versus kinetic energy in the CM frame for the compound nucleus ^{258}Rf. The total neutron-evaporation-residue cross sections (Hofmann 2004) are shown in figure (1n-3n). The dashed lines are interpolations through the data points. As is clear from the figure, the σ_{EVR} are very low in magnitude (few nb) as compared with the measured fission cross sections (few hundred mb) (Blank 1993) and can be considered negligible.

However, the σ_{fus} for ^{50}Ti-induced reactions fell distinctly below the ones predicted by the formula in 1-3 but were well-described by the predictions based on Swiatecki's theory (Swiatecki 1982) which includes the "extra push" energy necessary for the heavy systems in achieving fusion.

In a study measuring the fission-like fragment angular distribution the observed $d^2\sigma/d\theta dZ$ distributions (Lützenkirchen 1986) showed large anisotropy at forward and backward angles as compared to the predictions based on the saddle-point transition-state theory (TST) and the rotating liquid-drop model (RLDM) saddle-point shapes. The projectile and target nuclei pass the 'conditional saddle point' for capture in entrance channel but they do not pass the 'true saddle point' to undergo fusion. This reaction channel, termed as quasi-fission, explains the anisotropy. This study, therefore, substantiated the coexistence of three distinct reaction channels, the complete fusion-fission, the quasi-fission and the deep inelastic scattering. We have tried to determine the contribution of QF to the capture cross section for the reaction $^{50}Ti + ^{208}Pb$ in our data analysis.

Heßberger et al. (Heßberger 1985) studied this reaction in order to reproduce the results of a previous study (Oganessian 1975). The study also included an asymmetric system ^{249}Cf (^{12}C, xn) $^{261-x}104$ which forms the same product nucleus. The σ_{EVR} for the 4n deexcitation for this carbon-induced reaction is 10 ± 2 nb. Therefore, expected σ_{EVR} for the more symmetric (and hence lower fissility) $^{50}Ti + ^{208}Pb$ was a few hundred nb but only 5 nb was observed. Also calculations with HIVAP simulation code (a statistical evaporation code which uses the standard evaporation theory (Reisdorf 1981)) were carried out for both these systems in which the fusion hindrance was taken into consideration in terms of the "extra push" energy. They reproduced the observed σ_{EVR} within 1% for the $^{12}C + ^{249}Cf$ reaction but it was a factor of 25 higher for the $^{50}Ti + ^{208}Pb$ reaction. These observations indicated a serious hindrance to CN formation for this system.

Further work by the same author (Heßberger 1997) produced the isotopes of element 104 with A=253-257 by bombarding ^{204,206,208}Pb targets with ^{50}Ti beams and the production cross sections for 1n, 2n and 3n decay channels which were measured to be $\sigma_{max,1n} = (10 \pm 1)$nb, $\sigma_{max,2n} = (12 \pm 1)$nb, $\sigma_{max,3n} = (0.7 \pm 0.5)$nb, were reached at excitation energies $E^*_{1n} = 15.6 \pm 0.1$MeV, $E^*_{2n} = 21.5 \pm 0.1$MeV, $E^*_{3n} = 29 \pm 1$MeV, respectively. (fig1.3). These measurements have however been updated in later studies (Hofmann 2004).

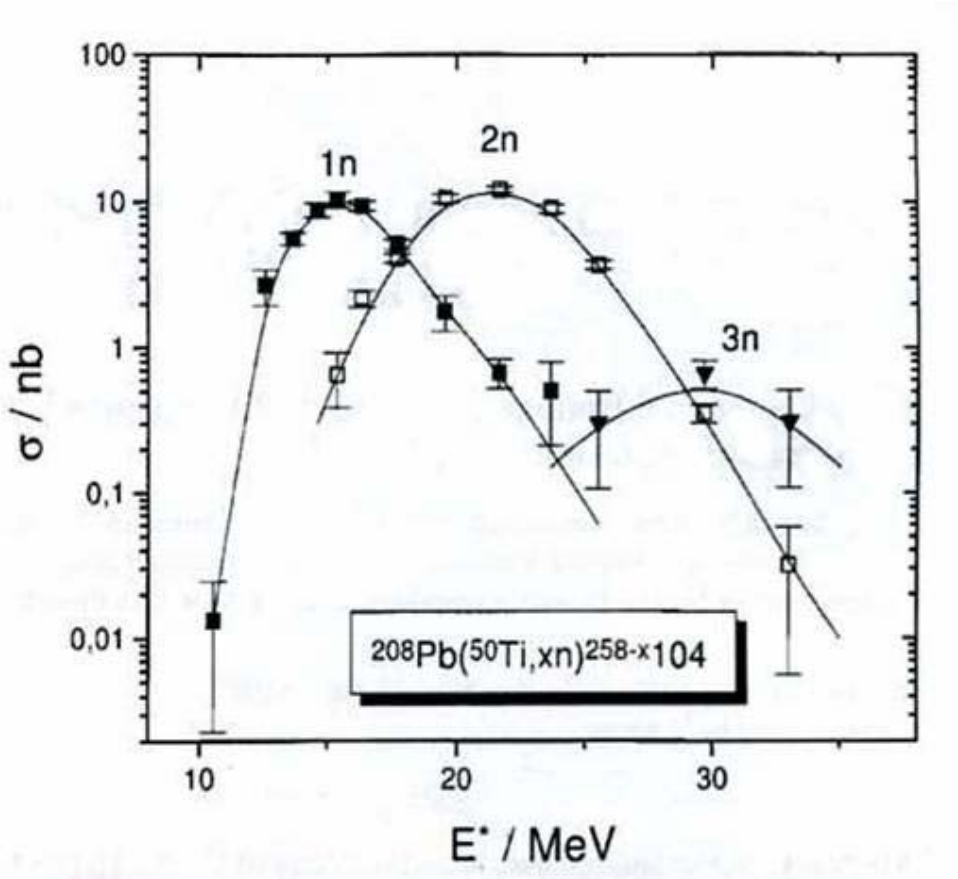

Figure 1.3 EVR excitation functions in irradiations of ^{208}Pb with ^{50}Ti for the 1n, 2n and 3n evaporation channels [Source: (Heßberger 1997)]. The lines are interpolations between the data points. The values of excitation energy (E^*) of the CN were calculated by using published mass excess data (Audi 1993). The uncertainties include only the statistical uncertainties.

1.3 Theoretical predictions of the survival probability (W_{sur})

The cross section for producing a heavy nucleus (σ_{EVR}) in a fusion reaction can be expressed as a product of three factors, the capture cross section (σ_c), the probability of CN formation inside the fission saddle point (P_{CN}) and the survival probability of the CN formed (W_{sur}). As mentioned in the previous section the reaction $^{50}Ti + {}^{208}Pb$ has been studied a number of times and σ_{EVR} (Heßberger 1997) and σ_C (Blank 1993) have been measured in previous works undertaken. The only unknown quantities for this reaction in the equation $\sigma_{ER} = \sigma_c \times P_{CN} \times W_{sur}$ are, therefore, P_{CN} and W_{sur}.

The W_{sur} can be calculated from the ratio of the partial widths of neutron evaporation and fission decay channels (Γ_n and Γ_f) as follows (Cherepanov 1980; Cherepanov 1983; Cherepanov 1984; Cherepanov 1999),

$$W_{sur}\left(E^*_{CN}, J\right) \approx P_{xn}\left(E^*_{CN}, J\right) \prod_{i=1}^{x} \frac{\Gamma_n\left((E^*_{CN})_i, (J)_i\right)}{\Gamma_n\left((E^*_{CN})_i, (J)_i\right) + \Gamma_f\left((E^*_{CN})_i, (J)_i\right)} \qquad \textbf{1-4}$$

These two partial widths can be calculated from the value of fission barrier (B_f) and neutron binding energies (B_n) for the reaction employing the following formula (Schröder 1984).

$$\frac{\Gamma_n\left(E^*_{CN}\right)}{\Gamma_f\left(E^*_{CN}\right)} = \frac{4A^{2/3}\left(E^*_{CN} - B_n\right)}{k\left(2\left[a\left(E^*_{CN} - B_f\right)\right]^{1/2} - 1\right)} \exp\left[2a^{1/2}\left(\left(E^*_{CN} - B_n\right)^{1/2} - \left(E^*_{CN} - B_f\right)^{1/2}\right)\right] \qquad \textbf{1-5}$$

where, P_{xn} – Probability of CN decaying through evaporation of x neutrons

E^*_{CN} – Excitation energy of the compound nucleus

J – Angular momentum quantum number of the compound nucleus

i – Index of evaporation step

Γ_n and Γ_f – Partial widths of neutron evaporation and fission

B_n – Binding energy of neutron

B_f – Fission barrier

k = 9.8MeV

a – Level density parameter

Since the B_f in the heaviest nuclei is defined by the shell corrections, its value depends on the excitation energy of the CN as $B_f = B_f (E^*_{CN} = 0) \exp [-E^*_{CN}/E_d]$ where $E_d = 5.48A^{1/3} / 1+1.3A^{-1/3}$ is the shell-damping energy.

Attempt has been made by Zubov et al. to calculate Γ_n/Γ_f and W_{sur} (Zubov 1999) for 1n evaporation reactions using the theoretical predictions of Smolańczuk (Smolańczuk 1995; Smolańczuk 1999) and Möller et al. (Möller 1988; Möller 1995). The values differ by more than an order of magnitude for most of the heavy elements, Z = 102-120 (fig1.4). This difference has been attributed to the difference in B_f given by each of these approaches as the B_n values in both approaches agree well with each other. For Z=104, which is the CN being produced in the reaction under investigation in our work, the values of Γ_n/Γ_f and W_{sur} for 1n evaporation are $2x10^{-2}$ and $1x10^{-3}$, respectively, using the former theoretical scheme and $2.5x10^{-3}$ and $1.2x10^{-4}$, respectively, using the latter. The details of these two theoretical approaches are summarized below.

Smolańczuk et al. analyze the spontaneous fission properties of the deformed superheavy nuclei which have relatively simple and thin fission barriers and for which the shell effects are very important. The potential energy of the nucleus is calculated in a macroscopic-microscopic approach. The Yukawa-plus-exponential model (Krappe 1979) with the standard values of its parameters (Möller 1981) is used for the

macroscopic part and the microscopic part is obtained from the Strutinski shell correction, based on Wood-Saxon single-particle potential (Ćwiok 1987). The residual pairing interaction is treated in the BCS approximation. The ratio of neutron-to-total width for the CN formed for 1n channel (which is the measure of the competition between the fission and n-evaporation) is given by the expression

$$G\left(E^{*},l\right)=\frac{\left(\Gamma n/\Gamma f\right)}{1+\left(\Gamma n/\Gamma f\right)} \qquad \textbf{1-6}$$

The partial widths of n-evaporation and fission processes are Γ_n and Γ_f, respectively. The ratio G(E*,l) depends on the neutron separation energy (S_n, which is 7.90MeV for the reaction of interest) and the height of static fission barrier (B_f^{stat}, which is 6.87MeV for the reaction of interest).

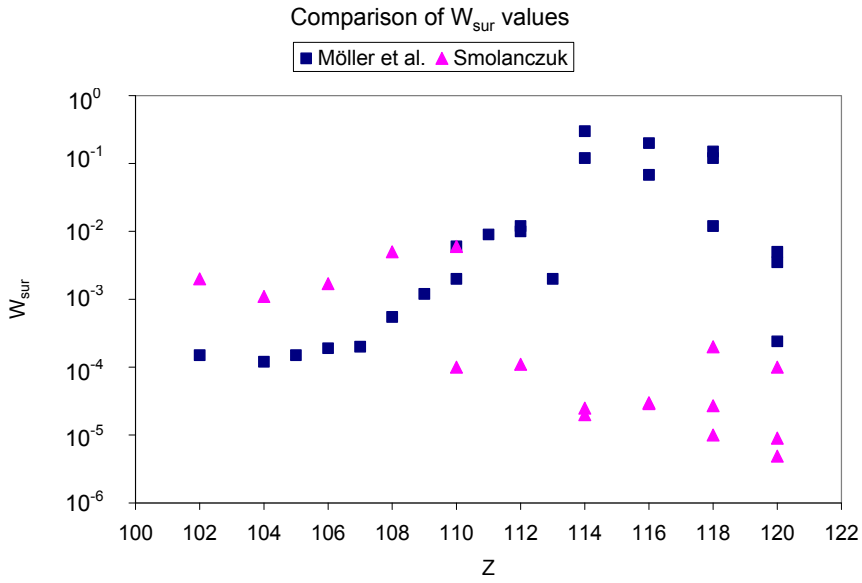

Figure 1.4 Plot of W_{sur} (for 1n channel) versus Z for nuclei with Z = 102-120. The plot highlights the difference in the values calculated by Zubov et al. using Γ_n/Γ_f based on Möller et al. theoretical predictions (Möller 1988; Möller 1995) (squares) and those based on Smolańczuk et al. theoretical predictions (Smolańczuk 1995; Smolańczuk 1999) (triangles).

Möller et al. use macroscopic-microscopic approach for their theoretical predictions of the ground-state mass excesses and deformations of 8979 nuclei ranging A = 16 to 339. The macroscopic models investigated in their work were the Finite-range liquid drop model (FRLDM) and the Finite-range droplet model (FRDM), the latter being an extension of the former which describes features such as nuclear compressibility and variation in the proton and neutron radii. The microscopic term represented the shell-plus-pairing correction which was determined based on the Strutinski shell correction and the Lipkin-Nogami version of BCS pairing model. The deficiency of the BCS model is that for large spacing between the single-particle levels at the Fermi surface no non-trivial solutions exist. The Lipkin-Nogami version does not have this flaw. The value of B_f (which is taken to be equal to the Shell correction) calculated with this theoretical prediction is 4.45MeV.

In order to decide which of the two abovementioned methods gives the accurate (or close to accurate) values of W_{sur} we proposed to carry out a fusion experiment with a well-studied reaction, $^{50}Ti + ^{208}Pb$. The aim of this experiment was to determine the P_{CN} for this reaction experimentally and hence deduce the W_{sur}.

2 EXPERIMENTAL AND SETUP DETAILS

2.1 Beam production and characteristics

The experiment was done at the Argonne Tandem Linear Accelerator System (ATLAS) (ANL 1993) facility at the Argonne National Lab (ANL). It is based on superconducting radio frequency (RF) resonator technology. Ion beams of nearly any atomic species with mass range of 6 to 238 are available from it. ATLAS consists of three major components (layout shown in fig2.1),

1. Positive Ion Injector (PII) which provides the capability of accelerating ions in the upper half of the table of isotopes.
2. FN tandem electrostatic injector, can provide beams with A<82.
3. Two-section superconducting LINAC.

Our experiment used the ^{50}Ti beam coming from the FN tandem electrostatic injector and further accelerated by the LINAC (area marked A in fig2.1). The FN tandem electrostatic injector consists of a negative ion source, a 12 MHz bunching system and a FN tandem electrostatic accelerator. The ion source is inverted cesium-sputter source type. In order for the LINAC to provide acceleration without introducing significant energy spread to the beam the injected beam is bunched into narrow time packets as it enters the first resonator of the LINAC. The bunching system has three stages. The first stage produces a pulse-train with a period of 82.5ns. In the second stage a room-temperature chopper removes the non-bunched beam to avoid producing components of beam significantly different in energy and time. The last stage refocuses the beam to produce a beam bunch of FWHM < 1000ps. The accelerator operates at terminal voltage of 8.5MV with thin carbon foil stripper in the

terminal of the machine in order to achieve good transmission and emittance characteristics. After acceleration through the injector, beam is passed through a stripper foil located upstream so as to raise its charge (to +12 in case of ^{50}Ti beam for our experiment) and then injected into main LINAC.

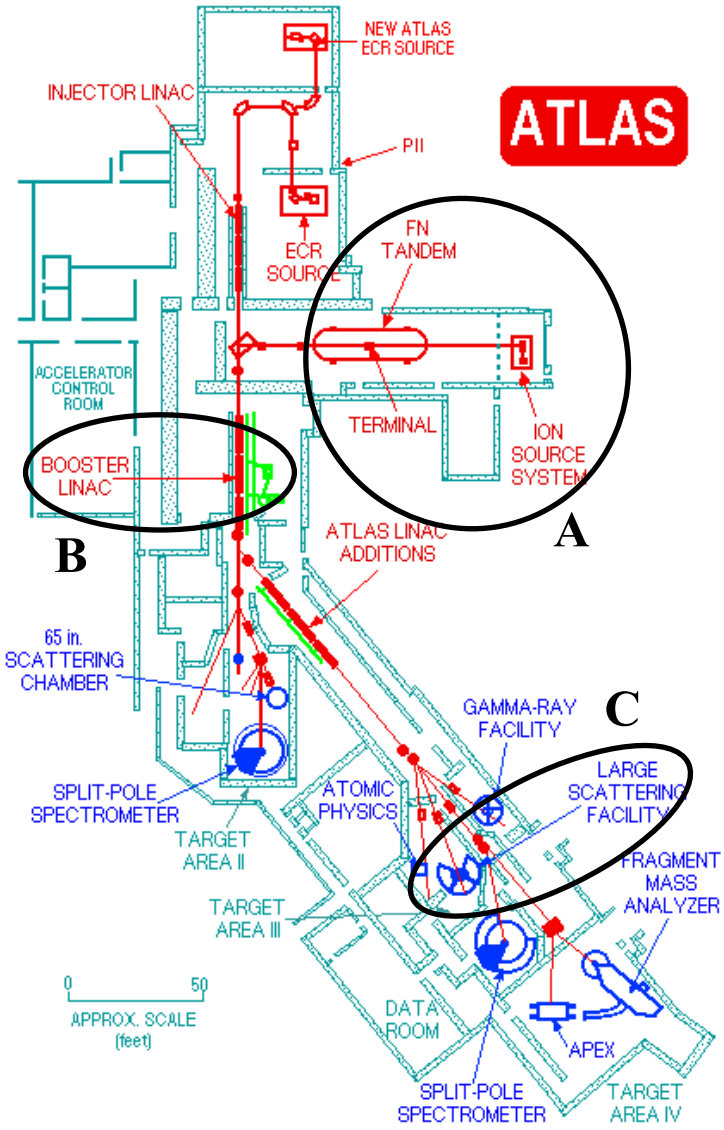

Figure 2.1 The layout of the Argonne Tandem-Linear Accelerator System (ATLAS) facility where the experiment was carried out. The figure shows the layout of the Ion Source, the LINAC and the Scattering Chamber. The 'large scattering facility' was used as the experimental chamber.

Final stage of acceleration occurs in a split-resonator superconducting LINAC cooled to 4.5K by liquid helium flow. Superconducting solenoids capable of peak fields of 7-8 Tesla are used as focusing elements. A single manually operated resonator located just upstream of the switching magnet rebunched the beam emerging from the LINAC to produce a time waist of < 1.0ns on the target (fig2.2). The time interval between consecutive beam bursts was 82ns.

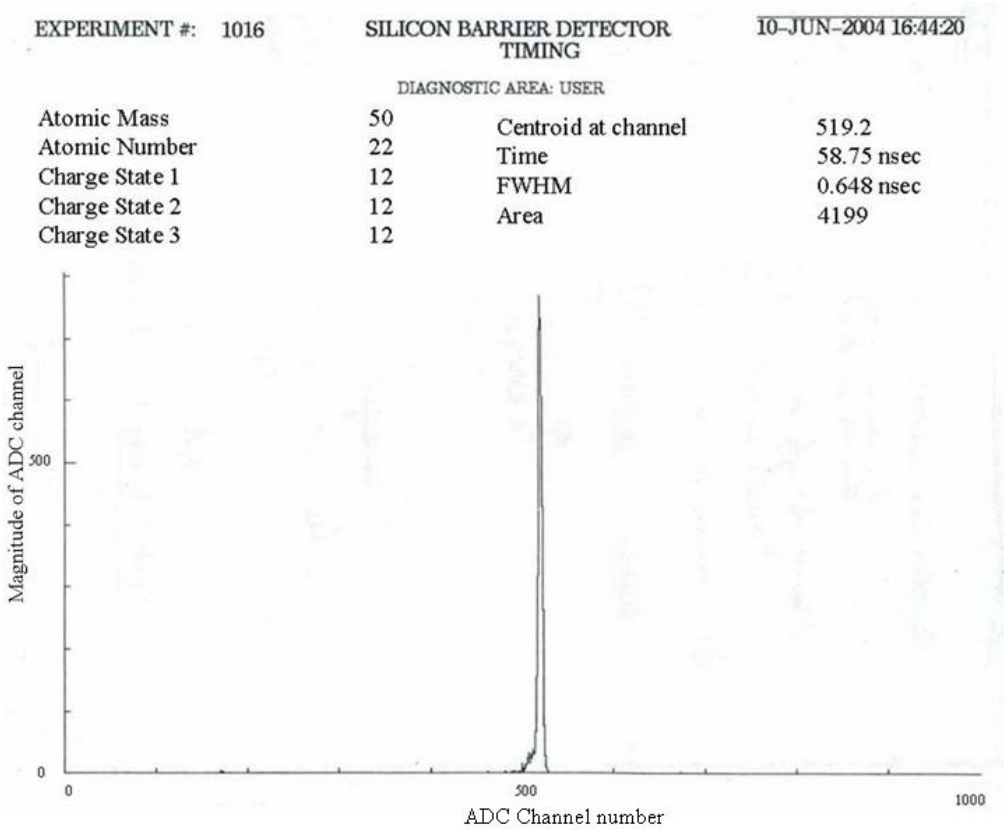

Figure 2.2 The timing spectrum of the ^{50}Ti beam coming from the FN tandem electrostatic injector and further accelerated by the LINAC. A single manually operated resonator located just upstream of the switching magnet rebunched the beam to produce a time waist of <1.0ns on the target (0.648ns in this case).

To characterize the excitation function the data were acquired at five beam energies bracketing the maximum of the 2n EVR excitation function at 238MeV (E* = 20.6MeV) (Heßberger 1985). At 230 and 233MeV (E* = 14.2MeV, 16.6MeV, respectively) the 1n evaporation channel is predominant with 230MeV being the maximum and the onset of 3n channel was expected at 243MeV (E* = 24.7MeV) with its maximum near 253MeV (E* = 33.7MeV) according to the previous work of Heßberger et al. Thus the data acquired spanned the 1n, 2n and 3n evaporation channels. The beam intensity was ~40enA (electrical nanoampere) based on the electrical current readout. The spot size on the target was about 2-3 mm diameter. Energy of the beam was continuously measured using the time-of-flight method.

2.2 Setup inside the experimental chamber

The ATLAS large scattering chamber (LSC), which was used as the experimental chamber, (area marked C in fig2.1) has 36in diameter and is divided into the lower fixed part and upper movable part. The lower fixed part of the chamber houses three independently movable gear rings on which the detectors were mounted. The chamber is equipped with Teflon seals and feedthroughs for various cables, controls, gas detector systems and coolant circulators. The various motions of the chamber are manually controlled.

The target ladder at the center of the chamber was designed to hold three target frames. Three targets mounted on the ladder (fig2.3) were a ^{208}Pb target to be used for the actual experiment, a 'hole' target (with a hole of 7.5mm diameter) to aid in tuning of the beam and a ^{197}Au target to be used for energy calibration. The ^{208}Pb target with an area density of 0.5mg/cm^2 was supported by a 40μg/cm^2 carbon backing and coated

with 10μg/cm^2 carbon film. The ^{197}Au target had an area density of 235μg/cm^2. This ladder could be rotated as well as raised or lowered to adjust the target position. The ^{208}Pb targets were prepared by the ANL target fabrication group using evaporation technique (boiling point of Pb = 962°C) and were ~100% pure. The ^{197}Au targets were Au foils provided by the OSU group. The beam intensity was monitored in terms of the integrated beam current reading (~40enA, electrical nanoampere) given by a Faraday cup mounted about 18in. downstream from the target.

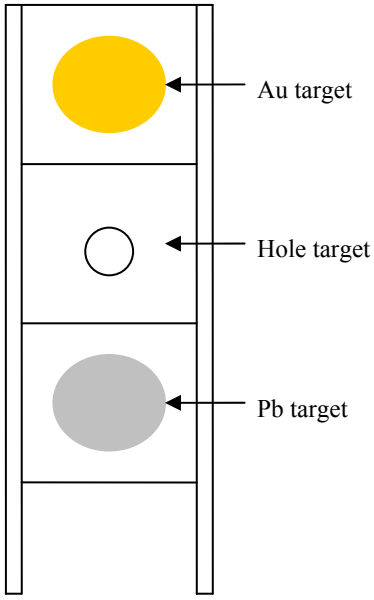

Figure 2.3 Schematic diagram of the target ladder which held three targets, ^{208}Pb target (area density of 0.5mg/cm^2) to be used for the actual experiment, a 'hole' target (with a hole of 7.5mm diameter) to aid in tuning of the beam and a ^{197}Au target (area density of 235μg/cm^2) to be used for energy calibration. The ^{208}Pb targets were produced by the ANL target fabrication group by evaporation and the Au foils were provided by the OSU group.

The schematic of the experimental setup is shown in fig2.4. Four double-sided silicon strip detectors (DSSDs) (A, B, C, D) of area 25cm^2 were placed at 22cm from

the target, two on each side of the beam. The pairs A-B and C-D were separated by folding angle for this reaction (~130°), centers of the detectors being at A = 65°, B = 65°, C = 35°, D = 95°. The 'folding angle' for a given reaction is the angle at which the two fission fragments coming out of the fused system are expected to be ejected with respect to each other in the laboratory reference frame. It can calculated based on the following equations,

$$P_{beam} = \sqrt{2 \times E_{beam} \times A_{beam}} \qquad \textbf{2-1}$$

$$P_{FF} = \sqrt{2 \times E_{FF} \times A_{FF}} \qquad \textbf{2-2}$$

$$\theta_{fld} = \left(\tan^{-1} \left[2 \times P_{FF} \Big/ P_{beam} \right] \right) \times 2 \qquad \textbf{2-3}$$

where, P_{beam} – Momentum of beam

E_{beam} – Kinetic energy of the projectile beam

P_{FF} – Momentum of fission fragments

E_{FF} – Fission fragment energy given by $0.5\left(Z_p Z_t e^2\right) \Big/ 1.8\left(A_p^{1/3} + A_t^{1/3}\right)$

Z_p, Z_t, A_p, A_t – Atomic numbers and masses of beam and target nuclei

A sample calculation for ^{50}Ti beam at 253MeV (E_{cot}[4] = 251MeV) and assuming symmetric fission is shown below,

$$P_{beam} = \sqrt{2 \times 251 \times 50} = 158$$

$$P_{FF} = \sqrt{2 \times 133 \times 129} = 185$$

$$\theta_{fld} = \left(\tan^{-1} \left[2 \times 185 \Big/ 158 \right] \right) \times 2 = \left(\tan^{-1} [2.34] \right) \times 2 = 133.72°$$

[4] Center-of-target, calculation explained in section 3.2.

Each DSSD had 16 vertical strips which were divided into eight groups by pairing two adjacent strips together. Seven individual silicon surface barrier (SB) detectors were setup at backward angles (on the left of the beam) at 30cm from the target covering the angles 133°-167°. Each circular detector had a surface area of 3cm^2.

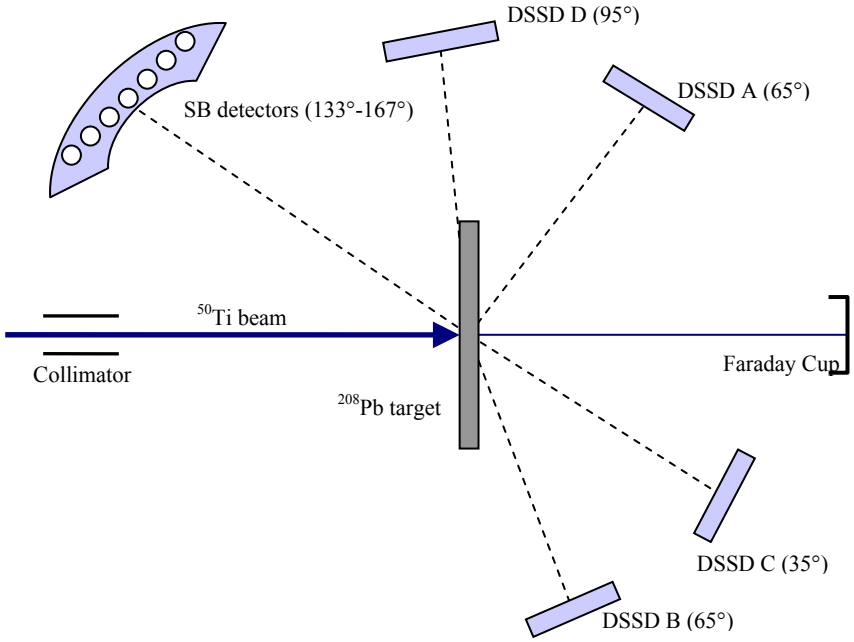

Figure 2.4 The experimental setup inside the chamber. The two pairs of double-sided strip detectors (DSSD), A-B and D-C, were separated by the 'folding angle' for the reaction (130°). An array of seven individual Si surface barrier (SB) detectors was placed at the backward angles. The beam current was measured by dumping the beam into a Faraday cup about 18in upstream of the target.

In addition to heavy ions, energetic electrons called 'delta (δ) electrons' are also produced in nuclear reactions. In an earlier attempt at this experiment the δ electrons produced with a flux of ~10^{14}/cm^2 extensively damaged the detectors at forward angles and data acquisition was impossible after about 8 hours. In the current experiment the target ladder was biased with +10,000V to avoid such damage. The

damage to the detectors was, however, only slowed down but not completely stopped. This resulted in DSSDs C and D becoming increasingly unreliable for DAQ after a first few runs and for bulk of the experiment data were acquired only from the DSSDs A and B and the Si SB detector array.

2.3 Electronics and Data Acquisition (DAQ) setup

The schematic of the electronic setup for the DSSDs and the SBs is shown in fig2.5. Each detector was biased through a pre-amplifier.

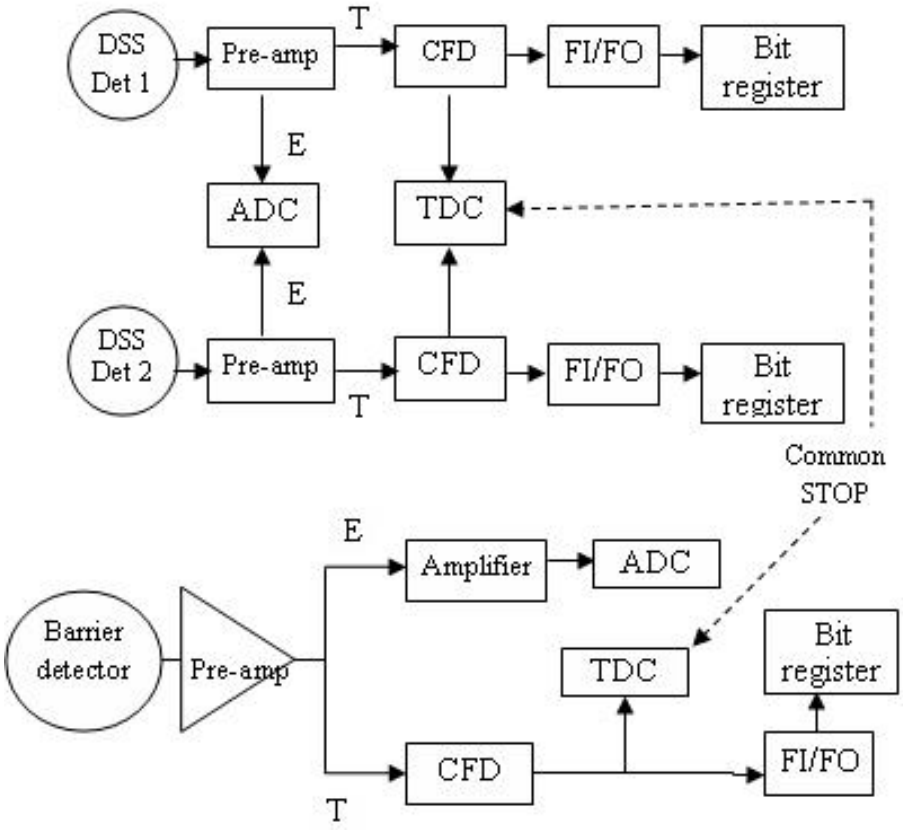

Figure 2.5 Schematic of the electronics layout for DSSD and SB detectors. Various modules and their role in the signal processing are discussed in detail in the text.

The slow signals from all the detectors were sent to an ‘analog-to-digital converter’ (ADC) to measure the energy of the incident particle. The fast timing signals were sent to a ‘constant fraction discriminator’ (CFD) to cut off low-level noise and the resulting pulse was sent to a ‘time-to-digital converter’ (TDC). The pulses from CFD were also input into a ‘fan- in/fan-out’ device (FI/FO) and then into a ‘bit register’. A FI/FO is a module that can take in one signal and ‘fan it out’ to many other modules without changing its amplitude or take in many signals and ‘fan them in’ to one output signal which has an amplitude equal to the sum of amplitudes of all signals taken in. A ‘bit register’ assigns one bit to each input and so it registers which detector(s) were triggered for a valid event and also the coincident triggering of multiple detectors.

Fig2.6 shows further layout of the electronic circuit. The output of each FI/FO was connected to a scaler that read continuously independent of event logic. This provided four scaler readouts, scaler A and B, one for each DSSD. The FI/FO outputs of A and B were combined in a logic box whose logic condition was set to OR for the singles mode and to AND for the coincidence mode data acquisition. The FI/FO signal from the SB detectors (‘array’ scaler) was combined with this signal through another OR. This signal, which also produced the ‘Master Gate raw’ (MGraw) scaler which indicated that at least one of all the 9 detectors had recorded an event, was passed through a logic veto which disallowed the recording of events when the DAQ system was busy thus giving the measure of system dead time in terms of scaler ‘MGacc’. The signal coming out of the logic veto was then passed through Gate Delay Generators (GDG), digitized and recorded in the computer DAQ.

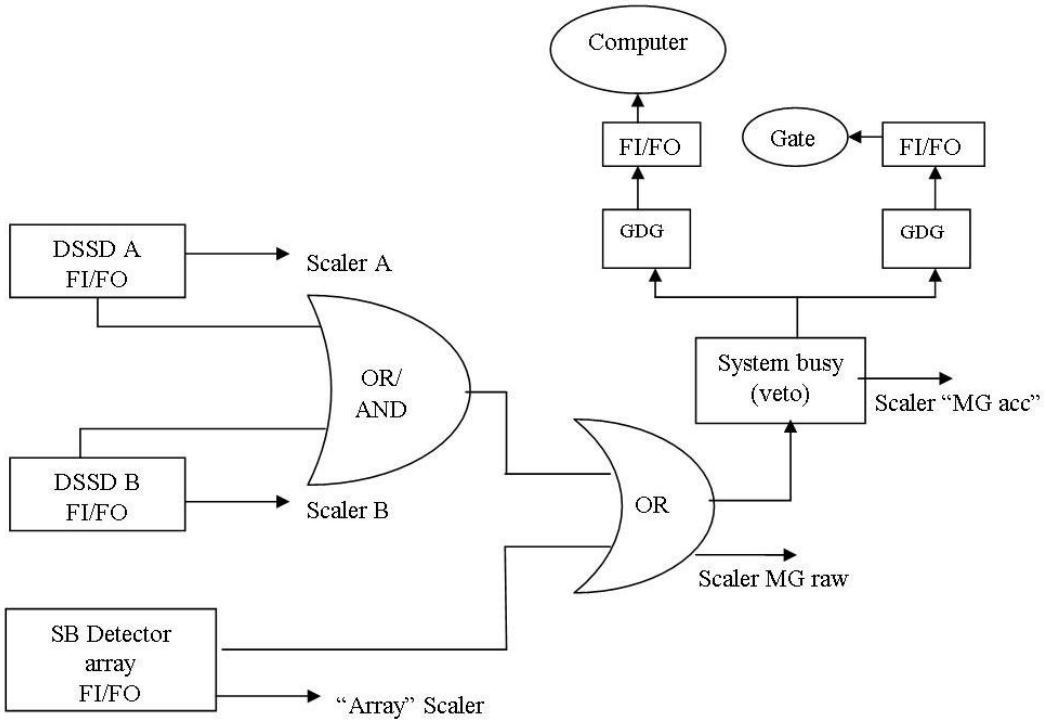

Figure 2.6 Further layout of electronics and logic modules processing the signals from the detectors and production of various scalers.

The DAQ required a 'start' and 'stop' signal between which the system recorded the data. The 'start' was occurrence of an event in any detector and a common 'stop' was then produced by delaying the accelerator RF signal. The logic behind the 'Time raw' and 'Time live' scalers resulting from this process is similar to that of the 'MGraw' and 'MGacc' scalers.

2.4 Experiment run details

2.4.1 Calibration runs

Before the experiment was started energy spectra were recorded with the ^{252}Cf spontaneous fission source in the position of the target ladder. These spectra were used for energy calibration of the detectors as the fission fragment energy for the ^{252}Cf fission is known (~185MeV). The calibration of the detectors is necessary in order to

nullify the Pulse Height Defect (PHD) affecting the data acquired from semiconductor detectors. This defect and the Schmitt-Kiker-Williams (SKW) method used for calibration are elaborated in section 3.4.1.

The first target to be put in was ^{197}Au and data were collected in singles mode[5] with a 243MeV ^{50}Ti beam incident on it. The target was then changed to ^{208}Pb and similar data collection was performed. The elastically scattered ^{50}Ti ions off the ^{197}Au and ^{208}Pb targets had energies in the range 230-85MeV. The peaks in energy spectra at these energies along with the 6MeV peak due to α-particles emitted from ^{252}Cf defined the energy scale.

2.4.2 ^{50}Ti + ^{208}Pb runs

After the data collection in singles mode all the further data collection with DSSDs was performed in 'coincidence mode'[6].The coincidence condition was put on each pair of strips of detectors A and B (strip A1 and strip B1 etc.) which were separated by the 'folding angle' for this reaction (130°). An event would only be recorded if the pair simultaneously detected a reaction product which signified the occurrence of fission. There was no coincidence condition put on the array of SB detectors at the backward angles and the data were acquired from these detectors in singles mode throughout the experiment. The data acquired from all the further runs were used for studying the fission fragment mass and angular distribution of the reaction.

The SB detector array was moved through an angle of 5° in forward or backward direction from its original position, in steps of 2.5° (Table 2.1). This would ensure that data acquired would better reflect the angular distribution of fission fragments at the

[5] In 'singles mode' the events from each detector are recorded independent of events in other detectors.
[6] In 'coincidence mode' the events are recorded only when there are simultaneous events in two or more detectors.

backward angles which was important in order to determine the contribution of quasi-fission to the capture cross section as will be detailed in the data analysis section.

Table 2.1 The angular distribution of the detectors over different runs. The SB detectors angle in the table signifies the angle of the center of the middle detector with three detectors on each side of it at ±5.67°, ±11.35° and ±17.05° from the center.

E_{cot} (MeV)	Run #	SB detectors (left of beam)	DSSD A (left of beam)	DSSD B (right of beam)
241	13	145°	65°	65°
251	20	150°	65°	65°
	25	152.5°	65°	65°
	26	155°	65°	65°
	28	157.5°	65°	65°
236	29	150°	65°	65°
	31	152.5°	65°	65°
	34	155°	65°	65°
	35	157.5°	65°	65°
	37	150°	65°	65°
231	39	152.5°	65°	65°
	40	155°	65°	65°
228	46	155°	65°	65°

3 DATA ANALYSIS

The experiment was carried out at five beam energies bracketing the maximum of the 2n EVR excitation function and ranging over 1n-3n evaporation channels of the reaction of interest. The DSSDs A and B and the array of SB Si detectors were the data sources as data acquisition with DSSDs C and D became increasingly unreliable after the first few runs.

The data for the experiment were recorded using the data acquisition (DAQ) system (NSCL 2004) developed at NSCL, MSU. All systems in the DAQ run on Linux operating system. The model of DAQ is that the data can be received from more than one computer for on-line analysis by more than one program running in a computer. Data is initially read in via the event readout program which describes how and when each input is read and is also capable of some data processing. It responds to a computer trigger by reading events from the hardware which is highly experiment dependent. Therefore, the DAQ system provides skeleton program routines that must be modified to produce the actual readout software. SpecTcl is a powerful nuclear event data analysis tool developed at the National Superconducting Cyclotron Laboratory of Michigan State University (NSCL 1999). It provides an object oriented C++ framework for histogramming and other data analysis operations. The Tcl/TK scripting language is embedded as the program's command language, providing the user with a powerful, extensible, command set as well as the ability to build custom graphical user interfaces or extend existing ones. The Xamine display program provides SpecTcl with a powerful visualization component. The program Stager, which works within this directory structure, runs from a graphical user interface and is

responsible for managing experimental data storage. Event buffers (events collected into convenient-sized blocks) are then transferred to another computer or a storage device for later detailed processing.

Energy and time spectra were recorded for each detector in terms of channel numbers which would later be converted to energy in MeV and time in nanoseconds (ns) prior to data analysis. The beam scaler and the beam current from the Faraday cup were also recorded in order to get the estimate of beam intensity for each energy. The data analysis was carried out using Physics Analysis Workstation (PAW). The raw data files were converted to hbook format suitable for processing in PAW with help of the FORTRAN program 'Ti+Pb.f' (modified for this experiment, from Don Peterson).

3.1 Detector angles and solid angle calculation

The centers of the DSSD and SB detectors in lab frame on both sides of the beam were at angles,

Detector A = 65° (left of beam) Detector B = 65° (right of beam)

Detector C = 35° (right of beam) Detector D = 95° (left of beam)

SB detector array = 150° (backward left of beam)

There were four strip-couplets on both sides of the center at ±1.63°, ±3.26°, ±4.89° and ±6.52° in case of the DSSDs and 3 detectors on both sides of the center detector at ±5.67°, ±11.35° and ±17.05° in the SB detector array. During the experiment the SB detector array was moved through an angle of 5° in forward or backward direction from its original configuration in order to obtain a better angular distribution of the fission fragments emitted at the backward angles (Table 2.1). Using distance of the

detectors from the target, and their dimensions, solid angle subtended (fig3.1) by each SB detector and each strip of the DSSD was calculated in units of steradian (sr).

$$Solid\ angle\ (\Omega) = \frac{A}{r^2} \qquad \textbf{3-1}$$

where, A – Area of the detector

r – Distance between the detector and the target ladder

These solid angle values were later used in the calculation of the differential cross sections (dσ/dΩ) details of which are given in section 3.6.1.

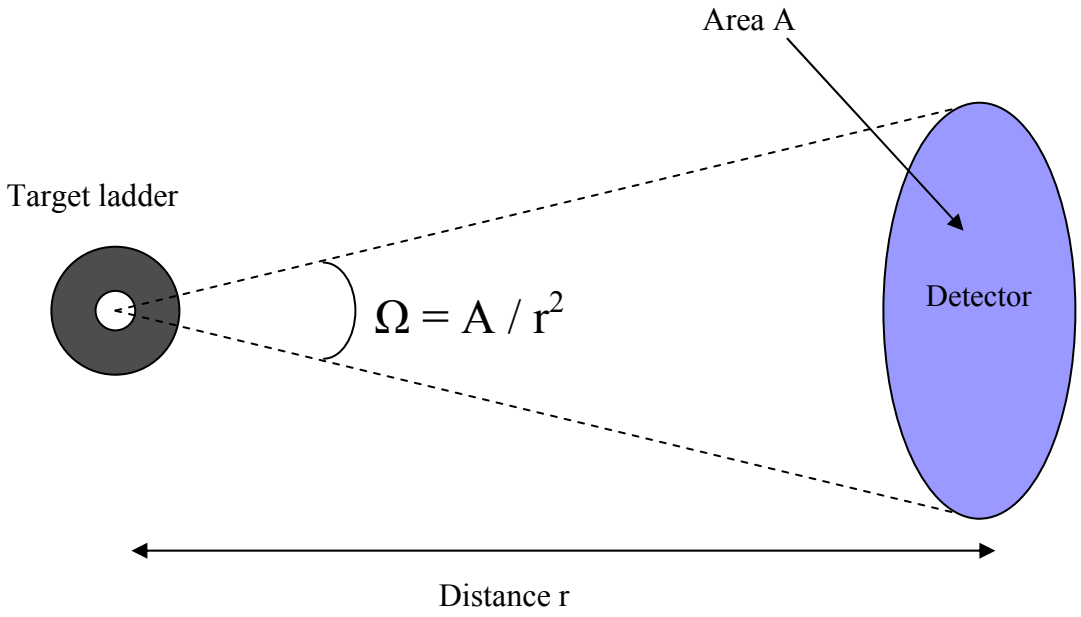

Figure 3.1 The figure illustrates the mathematical procedure for calculation of the solid angle (Ω) subtended by a particular detector at the target (in units of steradian (sr)). The area of the detector (A) and its distance from the target ladder (r) were used to arrive at the solid angle.

3.2 Energy loss calculations

When the beam strikes the target it loses some energy due to collisions with the target atoms in its path and this energy loss needs to be taken into consideration for

kinematical calculations and data analysis. The energy loss for ^{50}Ti beams in this experiment was calculated using the program package Stopping Power and Range of Ions in Matter (SRIM) (Ziegler 1985). The amount of energy lost (dE) is inversely proportional to the beam energy (E) as given by the expression,

$$\frac{dE}{dx} \approx \frac{MZ^2}{E} \qquad \textbf{3-2}$$

The energy loss for the ^{50}Ti beam passing half way through the ^{208}Pb target was ~2.0MeV for all beam energies and (Table 3.1) ~1.0MeV energy was lost from the 243MeV ^{50}Ti beam while passing half way through the ^{197}Au target.

Table 3.1 Beam energy in lab frame, energy loss for different beam energies and targets and beam energy at center-of-target (cot)

Target	E_{lab} (MeV)	Energy loss in beam (MeV)	E_{cot} (MeV)
^{208}Pb	253	1.9	251.1
^{208}Pb	243	2.0	241.0
^{208}Pb	238	2.0	236.0
^{208}Pb	233	2.0	231.0
^{208}Pb	230	2.0	228.0
^{197}Au	243	1.0	242.0

3.3 Fission fragment energy

The expected energy of the symmetric fission fragments (assuming the complete fusion-fission) for the ^{50}Ti + ^{208}Pb system was calculated to be 107.03MeV in CM frame employing the formula (Loveland 2005),

$$E_{FF} = \frac{e^2 \times Z_1 \times Z_2}{1.8 \times \left(A_1^{1/3} + A_2^{1/3}\right)} \times 0.5 \qquad \textbf{3-3}$$

where, Z_1, Z_2 – Atomic numbers of the projectile and target, respectively

A_1, A_2 – Atomic masses of the projectile and target, respectively

This FF energy (133MeV in lab frame) was used for determining the region of energy spectra to which the SKW calibration was to be applied and for checking the reliability of the energy and timing calibrations applied to the spectra (as described in next section). It also acted as an estimate for the cuts being performed on the E_1 vs E_2 (MeV vs MeV) spectra of the DSSD strips to arrive at the number of FFs emitted in order to calculate the cross section as detailed in section 3.6.1.

3.4 Detector calibration

3.4.1 Energy calibration

A typical raw energy spectrum from this experiment is shown in fig3.2 (left). Since the channel numbers are directly proportional to the energy of the ions detected the peak at lower channel numbers is ascribed to fission fragments and the elastically scattered ^{50}Ti produce the peak at higher channel numbers.

For very heavily ionizing particles (like those produced in most nuclear reactions), the high density of electron-hole pairs created in a semiconductor detector leads to space-charge phenomena which affect the ‘rise time’ and ‘pulse height’ of the resulting signal. The electron-hole pairs nullify the local charge created and therefore the rise time of pulse is longer than usual. During this delay, electrons and holes get a chance to recombine and therefore the collected charge is less than the created charge and the pulse height detected is smaller than actual. This is the Pulse Height Defect (PHD) which results in detector calibration being different for different particle types. In order to get rid of this defect affecting the data from semiconductor detectors they are calibrated using the Schmitt-Kiker-Williams (SKW) method (Schmitt 1965).

In SKW calibration coefficients a, a', b, b' are calculated for each detector/strip using the pulse heights of the ^{252}Cf SF source peaks as follows,

$$a = \frac{24.0203}{P_L - P_H} \quad \textbf{3-4}$$

$$a' = \frac{0.03574}{P_L - P_H} \quad \textbf{3-5}$$

$$b = 89.6083 - a \times P_L \quad \textbf{3-6}$$

$$b' = 0.1370 - a' \times P_L \quad \textbf{3-7}$$

where, P_L – Pulse height for light fragment peak

P_H - Pulse height for heavy fragment peak

Using these four coefficients into the following equation one can find the energy of a fission fragment of known mass,

$$E_{(MeV)} = \left[a + \left(a' \times M_{(amu)}\right)\right] \times P + \left[b + \left(b' \times M_{(amu)}\right)\right] \quad \textbf{3-8}$$

For our data analysis we assumed symmetric fission (M = 129amu) and program routine 'Ti+Pb.f' was modified to apply this energy calibration. The energy spectra from the singles runs and the expected energies of the FFs (calculated to be 107.03MeV in CM frame for symmetric fission of this system) and elastically scattered ^{50}Ti (using the Catkin kinematics spreadsheet (Catford 2002)) were used to check the reliability of the calibration. A typical energy spectrum after the calibration (in terms of MeV) is shown in fig3.2 (right).

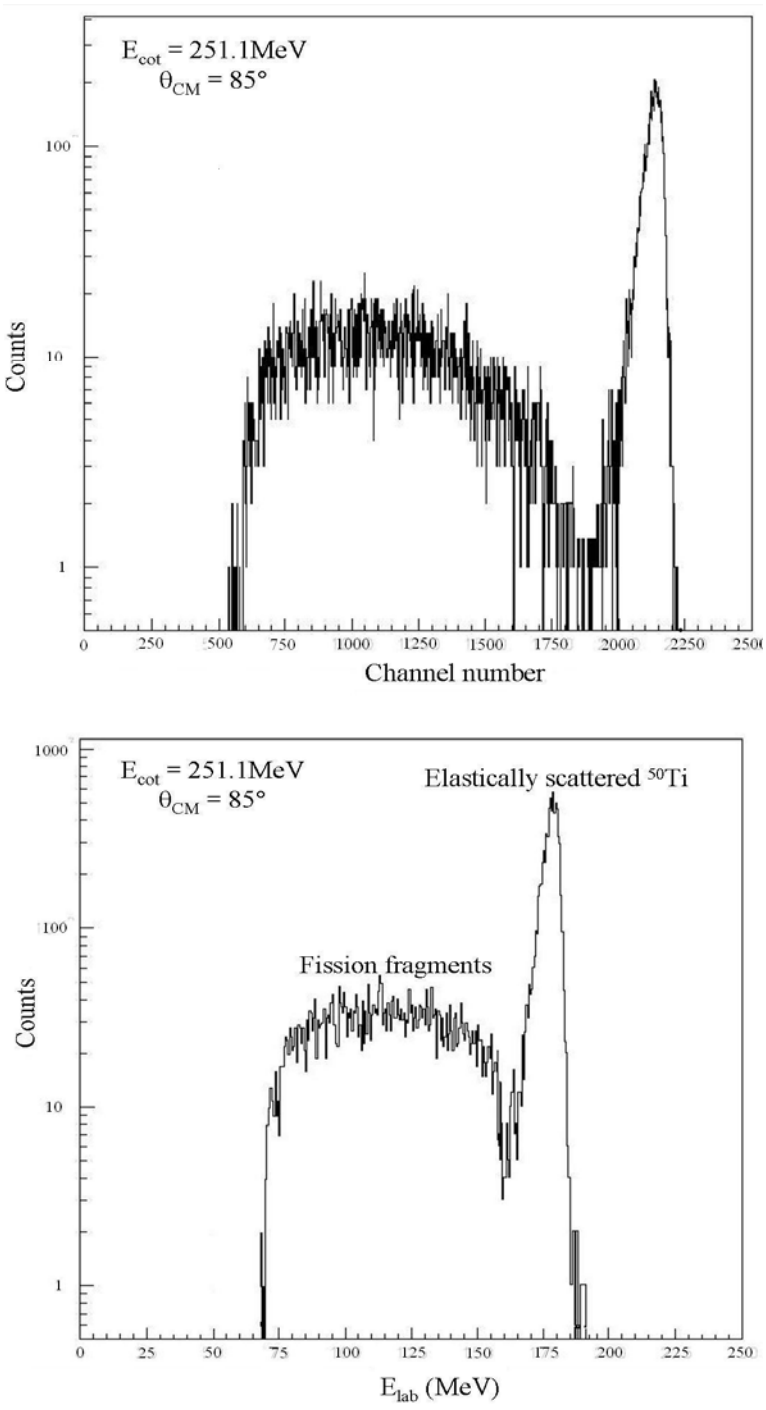

Figure 3.2 The figure shows a raw energy spectrum in terms of channel # (left) and the same spectrum, after energy loss and calibration has been applied, in terms of MeV (right) for a 253MeV ^{50}Ti beam on ^{208}Pb target. Since the channel numbers are directly proportional to the energy of the ions detected the peak at lower channel numbers is ascribed to fission fragments and the elastically scattered ^{50}Ti produce the peak at higher channel numbers.

3.4.2 Time calibration

A typical raw timing spectrum from this experiment is shown in fig3.3 (left). Since the channel numbers are inversely proportional to the timing of the ions detected (and since the timing spectra are recorded in reverse direction) the peak at lower channel numbers is ascribed to fission fragments and the elastically scattered ^{50}Ti produce the peak at higher channel numbers.

The energy of elastically scattered ^{50}Ti ions at various angles could be calculated from the Catkin kinematics spreadsheet (Catford 2002). Following formula was then utilized to arrive at the expected time (nanoseconds, ns) at which the particles would reach a particular detector at a given beam energy,

$$t = (0.72) \times l \times \sqrt{\frac{A}{E}} \qquad \textbf{3-9}$$

where, l – Distance of detector from target ladder (cm)

A – Mass of the beam particle (50 amu)

E – Energy of elastically scattered particle (MeV)

These expected times were then plotted versus the channel numbers of the centroids of the elastic peaks in the timing spectra for each detector or strip. The straight line equations obtained from these plots (fig3.4 for 8 strips of DSSD A) were then used in the 'Ti+Pb.f' to calibrate the timing spectra. The timing spectra from the single runs performed with the ^{197}Au target and the expected time calculated from the FF energy were once again useful as a cross-check for the correctness of the calibration. A typical timing spectrum after the calibration (in terms of ns) is shown in fig3.3 (right). As can be seen the time axis goes backward in the DAQ.

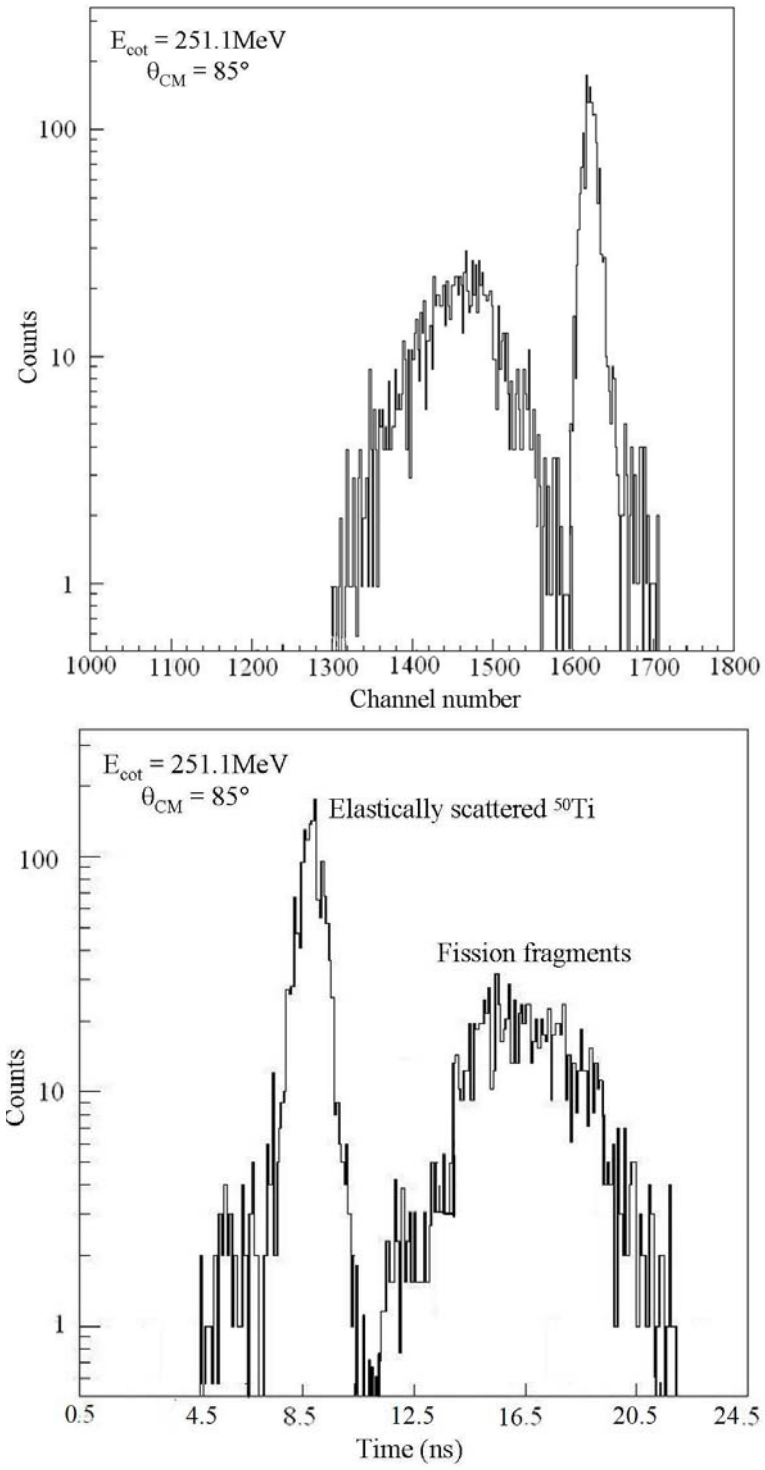

Figure 3.3 A figure analogous to fig3.2 for the timing spectra produced in this experiment. A typical raw timing spectrum in terms of channel # (left) and the same spectrum after calibration in terms of nanoseconds (right) for a 253MeV ^{50}Ti beam on ^{208}Pb target is shown. The timing spectrum is recorded in reverse direction with the DAQ and then converted to the right direction during calibration.

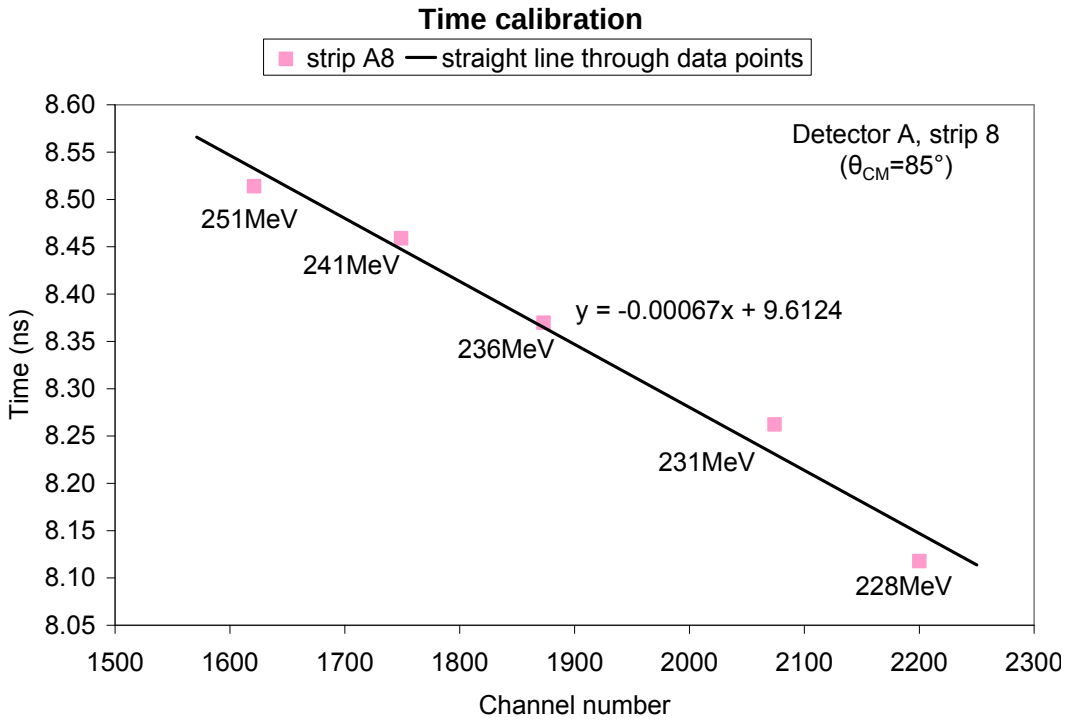

Figure 3.4 The times at which the elastically scattered ^{50}Ti were expected to reach a given detector at a given energy (indicated at each point) were plotted versus the channel numbers of the centroids of the elastic peaks. The straight line equations obtained from these plots were then used in the 'Ti+Pb.f' to calibrate the timing spectra. The negative slope of the lines indicates the fact that timing spectra are recorded in reverse direction.

3.5 Beam intensity calculations

The beam intensity was monitored in terms of the integrated beam current reading (~40enA, electrical nanoampere) given by a Faraday cup mounted about 18in. downstream from the target. This number was later converted to pnA (particle nanoampere), a unit independent of the charge on the particle (which was assumed to be 19.59 after charge equilibration takes place between ^{50}Ti and ^{208}Pb in a 0.5 mg/cm^2 target for beam of ~5MeV/A used in our experiment (Shima 1982)).

$$\text{Integrated beam current}\,(\text{pnA}) = \frac{\text{Integrated beam current}\,(\text{enA})}{\text{Charge on the particle}} \qquad \textbf{3-10}$$

The conversion of pnA to beam intensity in particles/s is based on the equation,

$$\text{Integrated beam intensity (particles/s)} = \text{pnA} \times \left(6.25 \times 10^{9} \text{ particles/s}\right) \qquad \textbf{3-11}$$

as 1pnA is equivalent to 6.25×10^{9} particles with charge one per second. The beam intensities at various beam energies are tabulated in Table 3.2. The number of particles incident on the target in a given run can therefore be determined by multiplying this beam intensity by the duration of run (sec).

Table 3.2 Duration of data acquisition and beam intensities for different beam energies.

E_{cot} (MeV)	Total duration on ^{208}Pb (hrs)	Time averaged beam intensity (particles/s)
251.1	17.90	3.82×10^{10}
241.0	17.48	1.10×10^{10}
236.0	16.77	3.71×10^{10}
231.0	18.27	3.55×10^{10}
228.0	21.93	4.84×10^{10}

3.6 Cross section calculations and deduction of P_{CN} and W_{sur}

3.6.1 Deep inelastic scattering and $\sigma_{fus\text{-}fis}$ calculations

A common mechanism by which a significant portion of the reaction proceeds when the trajectory of the projectile is in between head-on and grazing collisions is the 'deep inelastic scattering' (DIS). This mechanism is explained in section 1.1 and schematically depicted in fig1.1. It gives rise to reaction products with the mass comparable with the target and the projectile (with some dispersion to higher and lower masses) but energy near the fission fragments region. Previous work (Bock 1982) shows that considerable portion of the reaction proceeds through this mechanism at given energies of projectile. The data obtained in coincidence mode

with the DSSDs A-B placed at the angle 130° (the folding angle of this reaction), however, excludes the reaction products of DIS.

Knowing the number of fission events one can calculate the differential fission cross section ($d\sigma_{fis}/d\Omega$) utilizing the equation,

$$\frac{d\sigma_{fis}}{d\Omega} = \frac{\#\text{ fission events}}{(\#\text{ target atoms})(\#\text{ particles incident on target})(\text{Detector solid angle})} \qquad \textbf{3-12}$$

where the number of atoms in the target are given by,

$$\text{Number of target atoms} = \frac{\text{Weight of Target material} \times N_A}{A_t} \qquad \textbf{3-13}$$

where N_A– Avogadro's number (6.023×10^{23})

The number of fission events detected by each pair of strips of the DSSDs in coincidence was determined from the gate set on the E_1 vs E_2 (MeV vs MeV) plots (fig3.5).

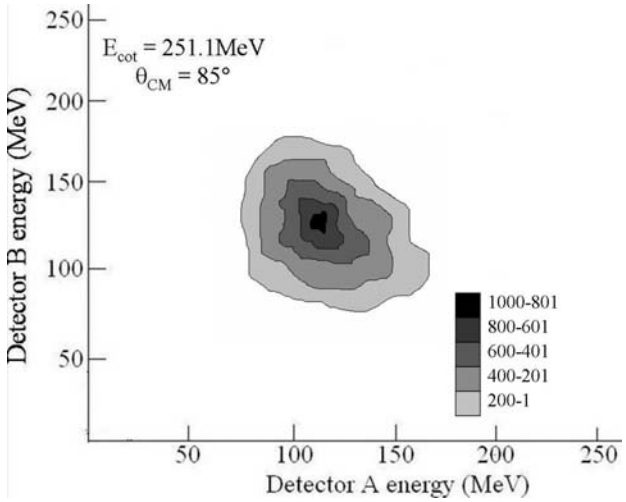

Figure 3.5 A typical E_1 vs E_2 (MeV vs MeV) plot from which the number of fission events in the DSSDs was determined. The expected E_{lab} for fission fragments is ~133MeV.

These data were used to calculate the $d\sigma_{fus\text{-}fis}/d\Omega$ according to the formula in 3-11. This was then integrated over the entire solid angle 4π to get the total $\sigma_{fus\text{-}fis}$ for each energy. The fusion-fission excitation function based on these cross sections is shown in fig3.6 and the values are tabulated in Table 3.3.

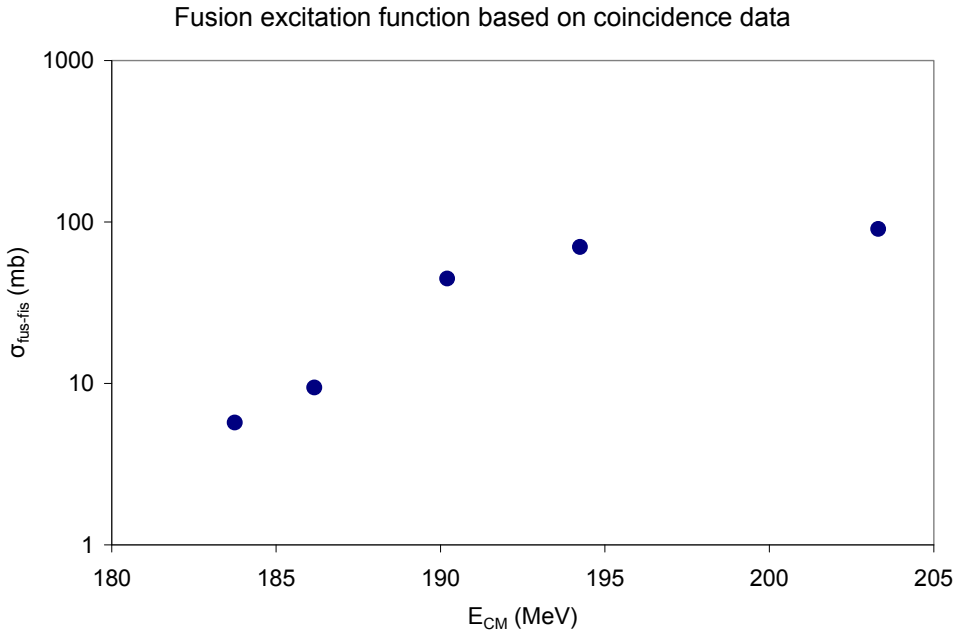

Figure 3.6 The fusion excitation function based on the cross sections calculated from the coincidence data from the DSSDs A and B. Coincidence condition was put on each pair of strips (strips A1 and B1). This ensured that they detected only the reaction products resulting from a mechanism that involves full momentum transfer, the fusion-fission. Error bars are smaller than the data points.

Table 3.3 The fusion cross sections calculated from the coincidence data and the errors (statistical) in the same (depicted graphically in fig3.6).

E_{cot} (MeV)	$\sigma_{fus\text{-}fis}$ (mb)	Error in $\sigma_{fus\text{-}fis}$
228.0	5.72	0.03
231.0	9.43	0.01
236.0	44.60	0.13
241.0	70.03	0.31
251.1	90.61	0.15

3.6.2 Differential fission cross section and angular distribution

The data were acquired in singles mode from the individual SB detectors and the number of fission fragments was determined from the gate set on the E vs A (MeV vs amu) spectra (fig3.7) which separated the reaction products caused by DIS from those of fusion-fission and quasi-fission mechanisms based on their masses.

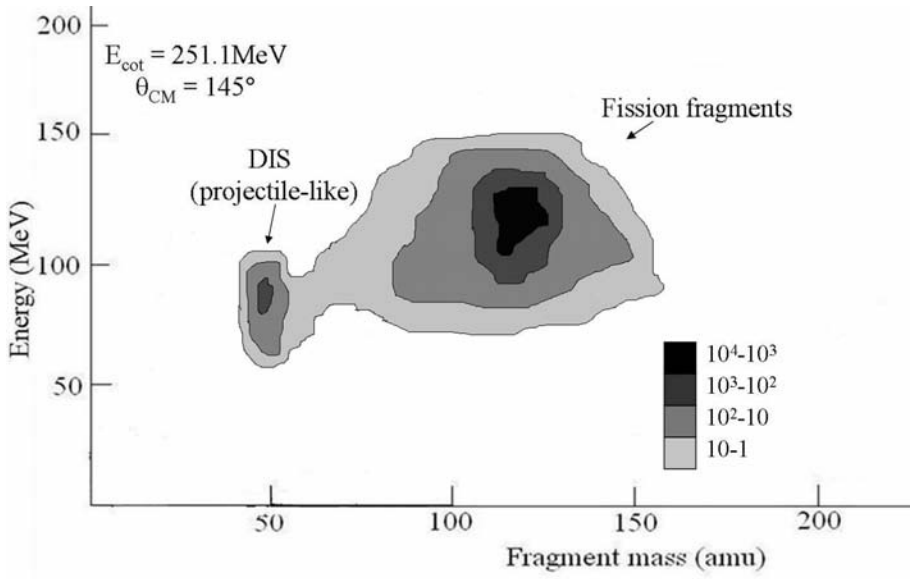

Figure 3.7 A typical E vs A (MeV vs amu) plot from which the number of fission events in the SB detectors was determined. The expected E_{lab} for fission fragments is ~133MeV.

Since the fission fragment emission is isotropic ($d\sigma_{fis}$ is constant as function of θ) the $d\sigma_{fis}/d\Omega$ should follow the shape of $1/\sin\theta$ (as $d\Omega$ is proportional to $\sin\theta\, d\theta$). The angular distribution (Table 3.4) for the SB detector array (in CM frame) shows significant rise in $d\sigma_{fis}/d\Omega$ as expected for the detectors at backward angles when compared with the $1/\sin\theta$ function (which was truncated at 10° and 170° for numerical integration) (fig3.8).

A five-point Savitsky-Golay filter (Savitzky 1964) was applied to these data which would preserve the structure of the data while removing any "noise" in it. The error bars represent statistical errors in the measurement of cross sections and the reproducibility of the measurements which are tabulated in Table 3.4.

Table 3.4 Differential fission cross sections and detector angles in CM frame for all the beam energies (at center-of-target) along with the errors.

E_{cot} (MeV)	θ_{CM} (degrees)	$d\sigma_{fis}/d\Omega$ (mb/sr)	Error in $d\sigma_{fis}/d\Omega$
228.0	145	0.90	0.17
	147	1.13	0.18
	150	1.02	0.18
	152	1.19	0.19
	159	1.11	0.18
	161	1.26	0.19
	163	1.44	0.21
	165	1.68	0.22
	168	1.79	0.24
	170	1.71	0.22
	172	1.95	0.24
	174	1.74	0.22
231.0	143	1.55	0.33
	145	1.51	0.32
	147	1.49	0.30
	148	1.68	0.34
	150	1.70	0.34
	152	1.78	0.35
	157	1.79	0.39
	159	1.82	0.40
	161	1.91	0.41
	161	2.53	0.41
	163	2.41	0.41
	165	3.10	0.59
	166	2.74	0.43
	168	2.65	0.43
	170	3.38	0.61
	170	2.81	0.44
	172	2.82	0.46
	174	3.39	0.61

Table 3.4 (Continued)

E_{cot} (MeV)	θ_{CM} (degrees)	$d\sigma_{fis}/d\Omega$ (mb/sr)	Error in $d\sigma_{fis}/d\Omega$
236.0	143	9.09	1.59
	145	7.08	1.37
	147	8.71	1.86
	148	10.00	1.65
	149	7.02	1.93
	150	8.12	1.49
	152	9.14	1.93
	154	9.57	2.28
	157	11.47	1.78
	159	9.09	1.56
	161	10.14	2.05
	161	13.28	1.92
	163	10.04	2.36
	163	11.82	1.81
	165	15.32	2.52
	166	13.82	1.94
	167	15.04	2.88
	168	12.74	1.86
	170	15.98	2.55
	170	15.60	2.04
	172	16.00	2.95
	172	13.54	1.90
	174	15.16	2.46
	176	16.40	2.95
241.0	139	10.14	0.75
	144	11.91	0.82
	153	13.30	0.87
	157	15.28	0.94
	162	17.84	1.00
	166	19.25	1.03

Table 3.4 (Continued)

E_{cot} (MeV)	θ_{CM} (degrees)	$d\sigma_{fis}/d\Omega$ (mb/sr)	Error in $d\sigma_{fis}/d\Omega$
251.1	143	15.15	1.68
	145	15.55	1.82
	147	15.13	1.77
	148	18.33	1.87
	149	15.67	2.21
	150	18.22	1.99
	152	16.69	1.88
	154	20.22	2.54
	157	21.57	2.05
	159	21.89	2.20
	161	20.30	2.10
	161	26.58	2.27
	163	23.47	2.76
	163	26.24	2.40
	165	23.49	2.25
	166	27.95	2.31
	167	25.50	2.87
	168	27.62	2.44
	170	25.77	2.34
	170	28.48	2.30
	172	29.04	2.48
	172	28.13	2.99
	174	28.22	2.42
	176	30.09	3.06

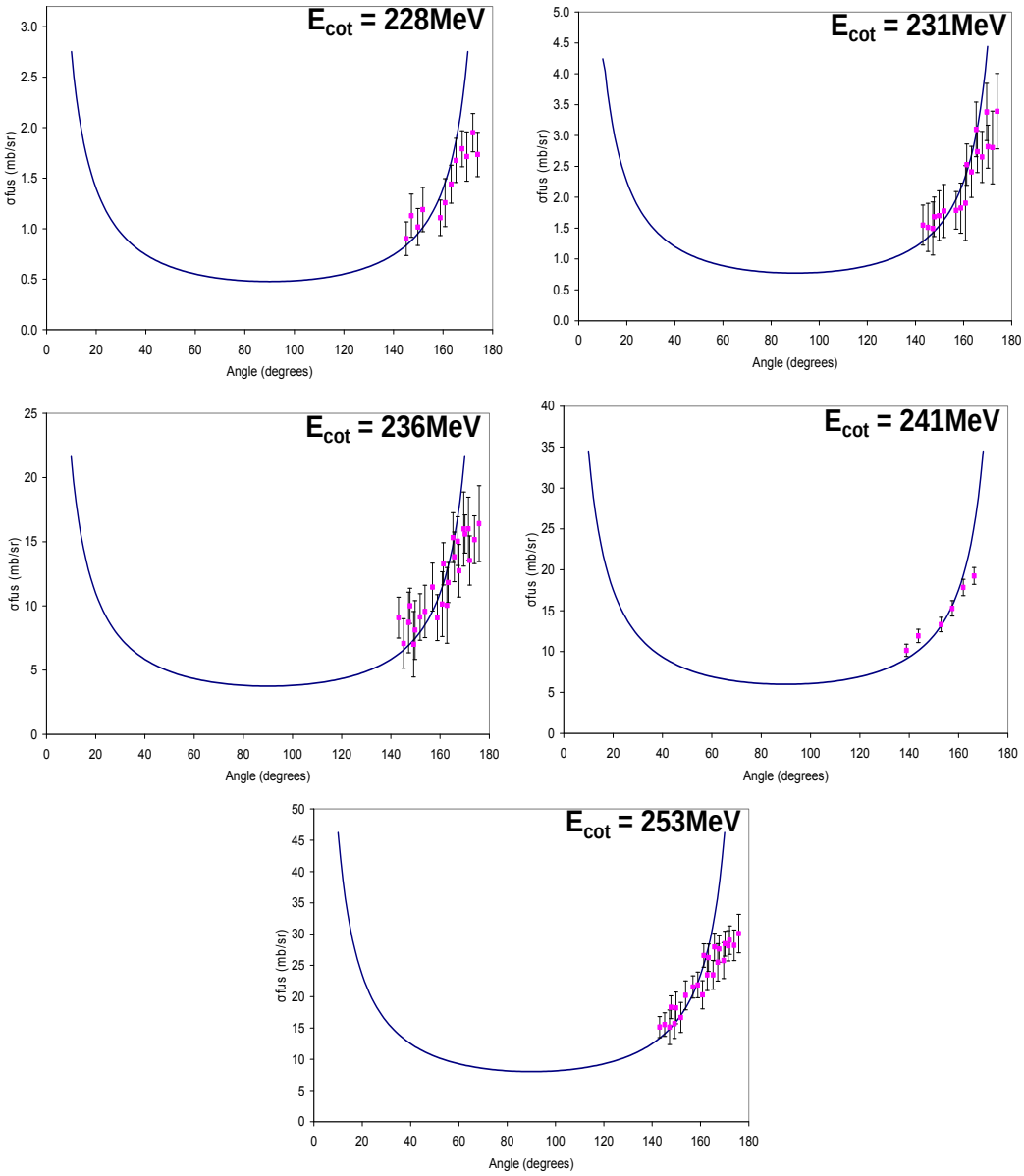

Figure 3.8 The fission angular distributions (in CM frame) for the SB detector array show significant rise in $d\sigma_{fis}/d\Omega$ as expected for the detectors at backward angles ($1/\sin\theta$ function is shown as solid line for comparison). The error bars represent statistical errors.

3.6.3 Vandenbosch-Huizenga fit and determination of J_{CN}, σ_{CN}

A method to describe the fission fragment distributions was taken from Vandenbosch and Huizenga (Vandenbosch 1973) which was used to fit the data and determine the relative contributions of compound nucleus formation and quasi-fission

to the total fission cross section according to the prescription given by Back (Back 1985b; Back 1985a). The FFs arise from the fusion-fission as well as quasi-fission. The fusion-fission angular distribution is isotropic whereas the quasi-fission angular distribution is forward and backward peaking. Therefore, the angular distribution of SB detectors at backward angles was fit in order to determine the quasi-fission contribution. In this method the fissioning nucleus is described as an axially symmetric top. The system can be defined by the angular momentum J, its projection on nuclear symmetry axis K and its projection along a space-fixed axis (defined as the beam axis) M (fig3.9).

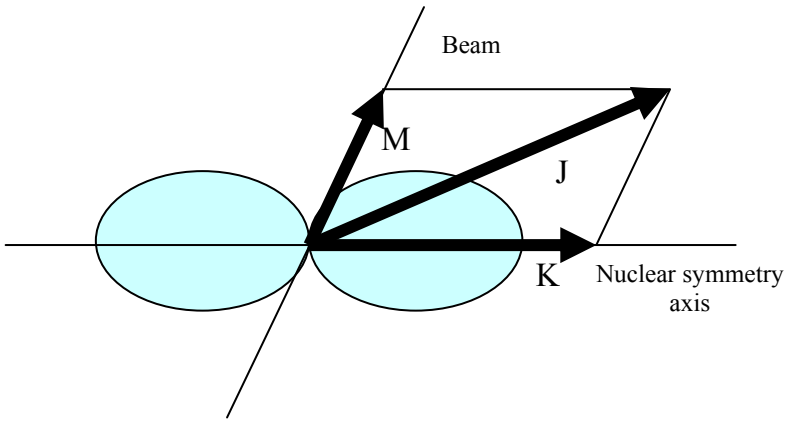

Figure 3.9 A depiction of a fissioning nuclear system as considered by Vandenbosch and Huizenga for their treatment of angular distribution fitting. The system is defined by the angular momentum J, its projection on nuclear symmetry axis K and its projection along a space-fixed axis (defined as the beam axis) M (Vandenbosch 1973).

The probability of emitting fragments in a given state (J,K,M) at a given angle θ can be written as (Bohr 1939)

$$W^{J}_{M,K}(\theta) = \frac{2J+1}{2}\left|d^{J}_{M,K}(\theta)\right|^{2} \qquad \textbf{3-14}$$

where the functions $d^{J}_{M,K}(\theta)$ are the symmetric top wavefunctions. If it is assumed that the projection M of the total angular momentum of the beam axis is small compared to J then for a given J the angular distribution of fission fragments is determined by K. The distribution of K values can be treated as a Gaussian function and the variance of this distribution (K_0^2) is taken to be

$$K_0^2 = \frac{TI_{eff}}{\hbar^2} \qquad \textbf{3-15}$$

where T – Thermodynamic temperature of the nucleus

I_{eff} – Effective moment of inertia of the nucleus

Using an approximate expression for the $d^{J}_{M,K}(\theta)$ functions an analytical expression is developed (Huizenga 1969) for the angular distribution of fission fragments.

$$W(\theta) \propto \sum_{J=0}^{\infty} \frac{(2J+1)^2 T_J \exp\left[\dfrac{-\left(J+\frac{1}{2}\right)^2 \sin^2\theta}{4K_0^2}\right] J_0\left[\dfrac{i\left(J+\frac{1}{2}\right)^2 \sin^2\theta}{4K_0^2}\right]}{erf\left[\dfrac{\left(J+\frac{1}{2}\right)}{\left(2K_0^2\right)^{1/2}}\right]} \qquad \textbf{3-16}$$

where J_0 – Zero-order Bessel function with an imaginary argument

erf(x) – The error function defined as $\frac{2}{\sqrt{\pi}}\int_0^x e^{-t^2}\,dt$

T_J – Transmission coefficient (determined using sharp cutoff approximation)

The angular distribution was fit with above function (fig3.10) according to the Back et al. prescription (Back 1985a) employing the FORTRAN routine ‘ang_dist.for’

(modified for this experiment, from Walter Loveland), a two-component fit in K_0^2. The inputs to this routine were J_{fis}, $\pi\lambda\!\!\!^{-2}$ (determined from the fission cross section data) and K_0^2 which gave the value J_{crit}, angular momentum at and below which complete fusion occurred.

It was assumed that the cross section consisted of two components; for angular momenta $J \leq J_{crit}$ compound nucleus formation occurred and $J \geq J_{crit}$ lead to quasi-fission. The moments of inertia for these partial waves were assigned as (Back 1985a),

$$\frac{I_0}{I_{eff}} = \left(\frac{I_0}{I_{eff}}\right)_{RLDM} \qquad \text{for } J \leq J_{crit} \qquad \textbf{3-17}$$

$$\frac{I_0}{I_{eff}} = 1.5 \qquad \text{for } J \geq J_{crit} \qquad \textbf{3-18}$$

where I_0 – Moment of inertia of a solid sphere given by $\frac{2}{5}mr^2$ (amu-fm^2)

r –Radius of the sphere given by $1.16A^{1/3}$ in case spherical nucleus of mass A

The values of I_0, I_{eff} and K_0^2, J_{fis} and $\pi\lambda\!\!\!^{-2}$ were determined for both complete fusion and quasi-fission and a best fit to the experimental data was obtained by varying J_{crit} for each of the five beam energies. A sample calculation is shown below for E_{lab} = 253MeV (E_{cot} = 251.1MeV, E_{CM} = 203.97MeV).

$$I_0 = \frac{2}{5}mr^2 = \frac{2}{5}(258)\left(1.16\times 258^{1/3}\right)^2 = 5628\ amu - fm^2$$

The values of $(I_0/I_{eff})_{RLDM}$ for each energy were determined using the equation max(a+bI^2,0.3) (Back 1985a) and values of parameters a and b obtained by fitting the

$^{16}O+^{238}U$ data from related literature (Back 1983). The values are tabulated in Table 3.5.

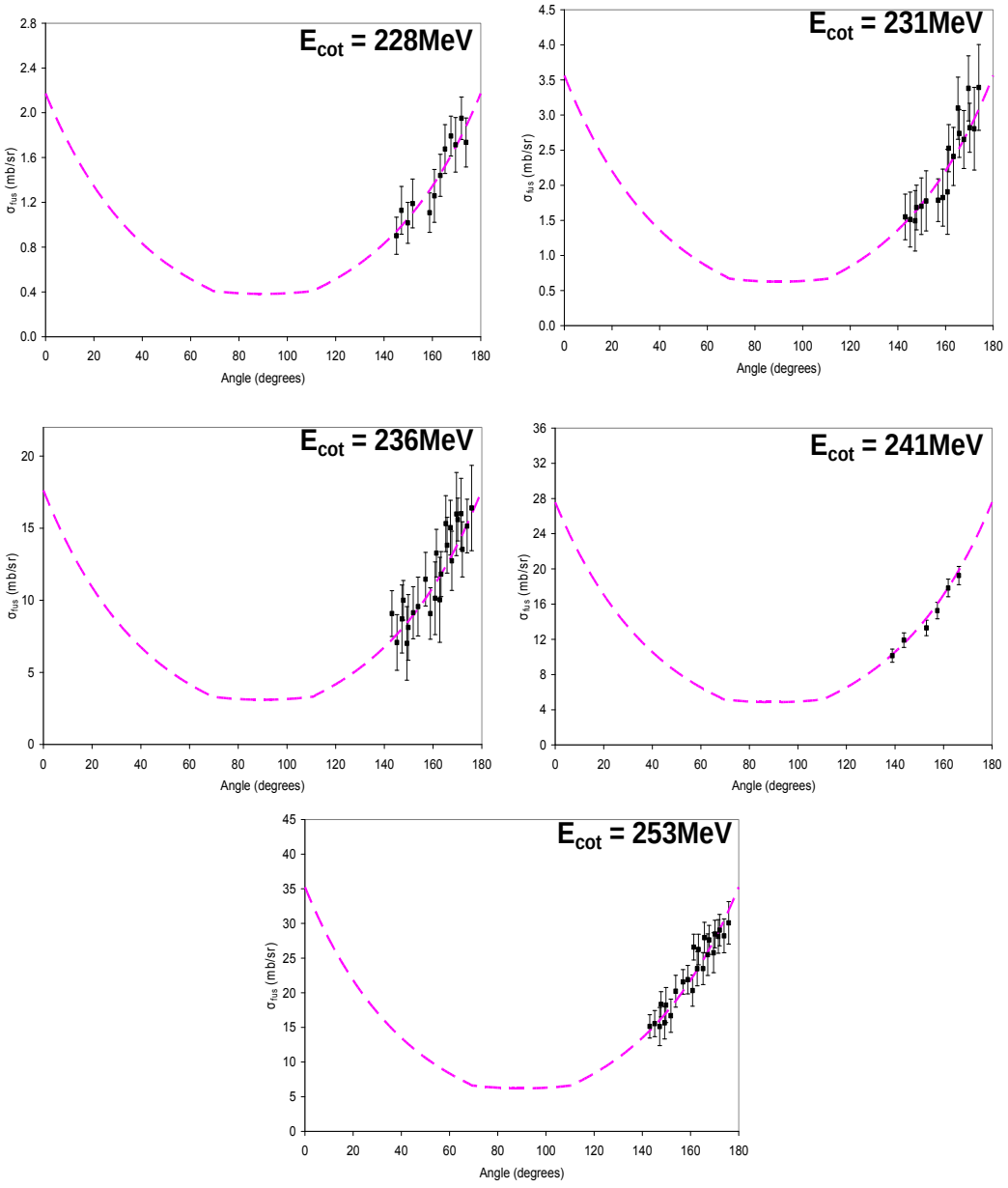

Figure 3.10 The fitting of angular distribution of SB detector array at backward angles using the Vandenbosch and Huizenga prescription (dashed line). The beam energies are in the center-of-target frame. The details of fitting procedure are discussed in the text.

$$I_{eff}\left(J \le J_{crit}\right) = \frac{I_0}{0.7} = \frac{6023}{0.7} = 8604\ amu - fm^2$$

$$I_{eff}\left(J \ge J_{crit}\right) = \frac{I_0}{1.5} = \frac{6023}{1.5} = 4015\ amu - fm^2$$

$$T = \left(\frac{8.5 \times \left(E^* - B_f - E_{rot}\right)}{A}\right)^{1/2} = \left(\frac{8.5 \times (34.39 - 4.65 - 2.35)}{258}\right)^{1/2} = 0.95MeV$$

For $J \geq J_{crit}$,

$$K_0^{\,2} = \frac{T\ Ieff}{\hbar^2} = \frac{(0.95MeV)(3751amu - fm^2)\left(931.5\,MeV/c^2 amu\right)}{\hbar^2}$$

$$= \frac{(0.95MeV)(3751amu - fm^2)\left(931.5\,MeV/amu\right)}{(\hbar c)^2}$$

$$= \frac{(0.95MeV)(3751amu - fm^2)\left(931.5\,MeV/amu\right)}{(197.33MeV - fm)^2}$$

$$= 85.27$$

$$\pi\lambda\!\!\!^{-2} = \pi\left(\frac{\hbar}{\sqrt{2mE_{CM}}}\right)^2 = \pi\frac{(197.33MeV - fm)^2}{(2)(40.31amu)\left(931.5\,MeV/amu\right)(203MeV)}$$

$$= 8.05 \times 10^{-3}\ fm^2$$

$$J_{fis} = \left(\frac{\sigma_{fus-fis}}{\pi\lambda\!\!\!^{-2}}\right)^{1/2} - 1 = \left(\frac{85.5 \times 10^{-27}\ cm^2}{8.05 \times 10^{-29}\ cm^2}\right)^{1/2} - 1 \quad = 32\hbar$$

Using the above values of parameters K_0^2, $\pi\lambda\!\!\!^{-2}$ and J_{fis} in the program routine gave an output of differential fission cross section for θ_{CM} = 0°-180° with steps of 1° and the value of J_{crit}. The total fission cross section (σ_{fis}) was calculated by integrating this fit over solid angle 4π. The cross sections calculated based on singles data from the SB detectors and those based on coincidence data from the DSSDs agree well with each other (fig3.11).

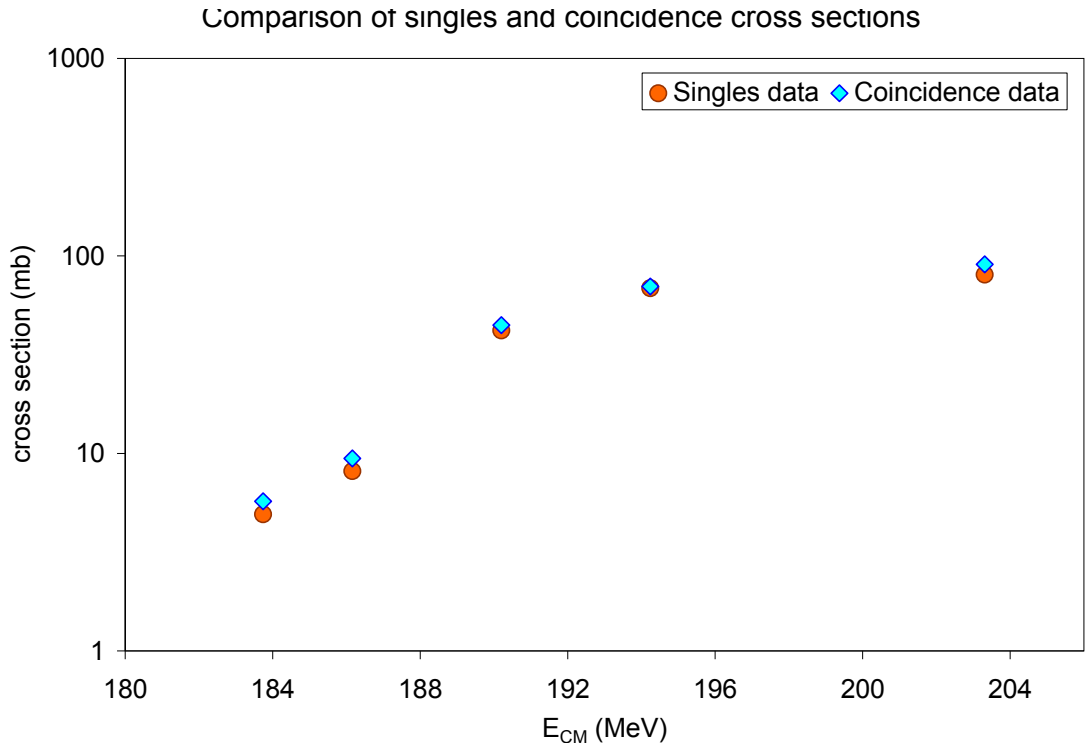

Figure 3.11 The figure showing the good agreement between the cross sections calculated based on singles data from the SB detectors and those based on coincidence data from the DSSDs. Error bars are smaller than data points.

From the J_{crit} (=J_{CN}) and σ_{fis} (which was taken as the average of the σ_{fis} values calculated from singles and coincidence data), the relative contribution of complete fusion was determined as (Back 1985a),

$$\frac{\sigma_{CN}}{\sigma_{fis}} = \frac{J_{CN}^2}{J_{fis}^2} \qquad \textbf{3-19}$$

Table 3.5 summarizes the values of K_0^2, $\pi\lambda^2$ and J_{fis} used for fitting the angular distributions according to the Back et al. prescription and Table 3.6 tabulates the values of J_{fis}, J_{CN}, σ_{fis} and σ_{CN} with errors, the reduced χ^2 and the degrees of freedom. The degrees of freedom = number of data points -1, J_{CN} being the variable parameter.

Table 3.5 Values of various parameters used for fitting the angular distributions by Back et al. prescription.

E_{cot} (MeV)	E^* (MeV)	$J>J_{CN}$ = Quasi-fission			$J<J_{CN}$ = Complete fusion			$\pi\lambda^2$ (fm^2)
		T (MeV)	I_0/I_{eff}	K_0^2	T(MeV)	I_0/I_{eff}	K_0^2	
228.0	14.16	0.62	3752	55.65	0.62	6327	93.84	$8.87x10^{-3}$
231.0	16.58	0.68	3752	61.03	0.68	6373	103.87	$8.75\ x10^{-3}$
236.0	20.62	0.74	3752	66.66	0.76	7013	127.94	$8.56\ x10^{-3}$
241.0	24.66	0.84	3752	75.39	0.86	7580	155.93	$8.32\ x10^{-3}$
251.1	33.73	0.95	3752	85.27	0.97	8638	200.45	$8.05\ x10^{-3}$

Table 3.6 J_{fis}, J_{CN}, σ_{fis} (average of singles and coincidence calculations) and σ_{CN} with errors, the reduced χ^2 and the degrees of freedom.

E_{cot} (MeV)	J_{fis} (ħ)	σ_{fis} (mb)	Degrees of freedom	Reduced χ^2	J_{CN} (ħ)	σ_{CN} (mb)
228.0	7	5.72±0.57	11	1.82	1	0.11±0.02
231.0	9	8.39±0.91	17	2.37	2	0.40±0.06
236.0	22	43.30±1.90	23	2.60	10	9.82±1.07
241.0	28	69.40±0.90	5	0.14	12	12.75±1.28
251.1	32	85.50±7.30	23	0.35	15	18.78±2.50

3.6.4 Determination of P_{CN} and W_{sur}

The σ_{fis} (which is also the σ_c) is calculated based on the fission events detected during the experiment. These fission fragments can originate from fission of compound nucleus formed by the fusion of target and projectile or from quasi-fission. Therefore the ratio σ_{CN}/σ_{fis} (determined by 3-16) gives the probability of the mononuclear complex formed after capture evolving to form a compound nucleus inside the fission saddle point (P_{CN}). The values of total σ_{EVR} for the beam energies used in our experiment were deduced from the interpolations between measured data points of the EVR excitation function in a previous work (Hofmann 2004). The errors were also deduced from errors in measured data points. Knowing these quantities in the equation $\sigma_{EVR} = \sigma_c \times P_{CN} \times W_{sur}$ the survival probability (W_{sur}) for the reaction ^{208}Pb (^{50}Ti, xn) $^{258-x}$Rf was determined for each beam energy. It is difficult to make meaningful

estimates of the uncertainties in the deduced values of P_{CN} given the fundamental systematic uncertainties in I_0/I_{eff} and thus in K_0^2. One estimate of the uncertainty in the deduced values of P_{CN} is from the comparison between the deduced values of P_{CN} based upon the fragment angular distributions (this work) and the fragment mass distributions (Itkis 2007) which correspond to an uncertainty of a factor of 1.8. This error is, however, not symmetric and could be lower on the negative side. There is a systematic uncertainty in the deduced Wsur values due to uncertainties in the measured values of σ_{EVR} which could make the estimates of Wsur a factor of 2.7 uncertain. The values of these four quantities are listed in Table 3.7.

Table 3.7 Values of σ_{EVR} from previous work (Hofmann 2004) and σ_c and P_{CN} values determined experimentally in this work were used to arrive at W_{sur} values.

E_{CM} (MeV)	σ_{EVR} (mbarns)	σ_c (mbarns)	P_{CN}	W_{sur}
183.74	$1.3 \times 10^{-5} \pm 2.0 \times 10^{-6}$	5.72±0.57	0.0201	1.22×10^{-4}
186.16	$1.6 \times 10^{-5} \pm 2.0 \times 10^{-6}$	8.39±0.91	0.0454	4.01×10^{-5}
190.20	$1.7 \times 10^{-5} \pm 2.0 \times 10^{-6}$	43.30±1.90	0.2268	1.78×10^{-6}
194.24	$6.0 \times 10^{-6} \pm 1.0 \times 10^{-6}$	69.40±0.90	0.1837	4.71×10^{-7}
203.31	$1.0 \times 10^{-6} \pm 1.0 \times 10^{-7}$	85.50±7.30	0.2197	5.32×10^{-8}

4 RESULTS AND CONCLUSION

4.1 Summary of the results

The quantities σ_{fis}, σ_{CN}, P_{CN} and W_{sur} were determined experimentally by analyzing the fission angular distribution of the reaction ^{208}Pb (^{50}Ti, xn) $^{258-x}$Rf (x = 1-3) at five different beam energies that bracketed the maximum of 2n EVR excitation function of this reaction. The details of the analysis procedure are outlined in the previous chapter and Table 4.1 summarizes the results. The determination of P_{CN} and in turn of W_{sur} is of importance to the heavy element production. The P_{CN} is the probability that complete fusion of the target and projectile will occur inside the fission saddle point and the W_{sur} is the survival probability of the compound nucleus formed.

The heavy element production with cross sections high enough to allow any study of the element formed can be possible only if these two quantities are favorable (i.e., high). Fig4.1 graphically depicts the trend of the two quantities. The P_{CN} increases with energy whereas the W_{sur} decreases. This decrease can be attributed to the combination of multiple decay channels at higher energies (Heßberger 1985). Theoretical estimates have been made about the numerical values of these two quantities. The W_{sur} estimates are especially very different from each other with different methods of calculation (Möller 1988; Möller 1995; Smolańczuk 1995; Smolańczuk 1999) and our attempt was at finding an experimental confirmation of either.

Table 4.1 Summary of the results obtained by the data analysis, i.e., experimentally determined values of σ_{fis}, σ_{CN}, P_{CN} and W_{sur}.

E_{CM} (MeV)	σ_c (mbarns)	σ_{CN} (mb)	P_{CN}	W_{sur}
183.74	5.72±0.57	0.11±0.02	0.0201	1.22×10^{-4}
186.16	8.39±0.91	0.40±0.06	0.0454	4.01×10^{-5}
190.20	43.30±1.90	9.82±1.07	0.2268	1.78×10^{-6}
194.24	69.40±0.90	12.75±1.28	0.1837	4.71×10^{-7}
203.31	85.50±7.30	18.78±2.50	0.2197	5.32×10^{-8}

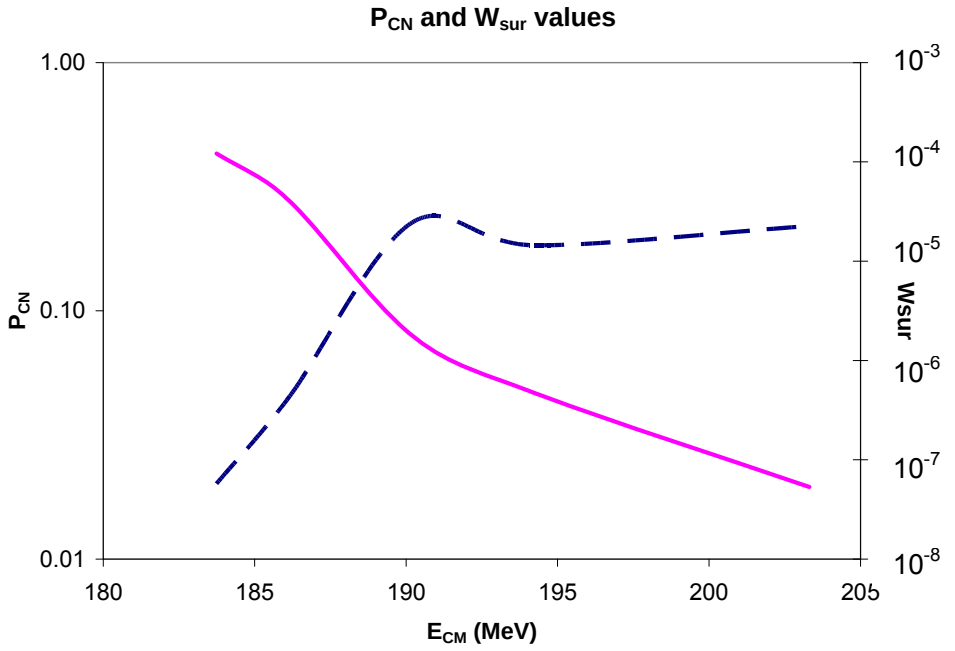

Figure 4.1 The figure graphically depicts the trend of the two quantities, P_{CN} (dashed) and W_{sur} (solid).

4.2 Comparison with previous work

4.2.1 Comparison of σ_{fis} with earlier measurements

An experiment was carried out at energies near and higher than the interaction barrier to study the binary reaction products from the interaction of ^{50}Ti, among other projectiles, with ^{208}Pb with aid of a position-sensitive ring counter operated in coincidence mode (Bock 1982). Cross section for mass equilibration reaction was

analyzed based on fusion models. Another experiment was carried out to determine the fusion-fission cross sections of numerous reactions with ^{40}Ar and ^{50}Ti projectiles and various actinide targets (Blank 1993). The cross sections were determined at energies bracketing the interaction barrier by measuring the energy and time-of-flight of the reaction products. The fission cross sections determined in our data analysis are a factor of ~4 higher than the ones measured by Clerc et al. except for the highest two energies where they are a factor of ~1.2 lower (fig4.2). The authors mention that the lower slope of excitation function as compared to model predictions could not be ascertained beyond doubt, which could explain higher values by our analysis.

The cross sections obtained by Bock et al. are lesser in magnitude than those measured in this work as well as by Clerc et al.

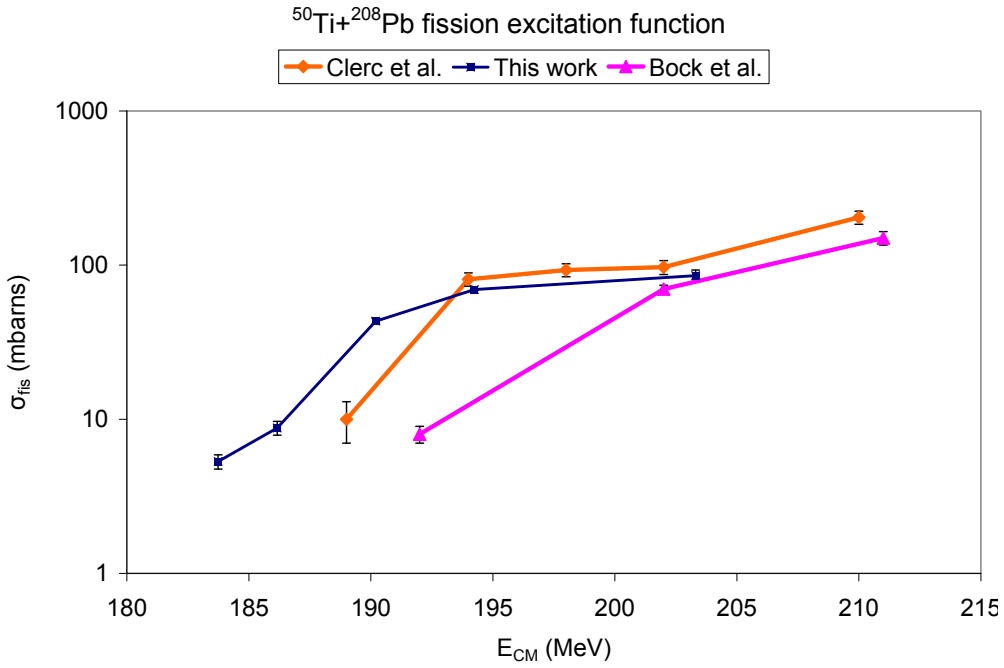

Figure 4.2 The comparison between fission cross sections determined in our data analysis (squares), the ones measured by Clerc et al. (Blank 1993) (diamonds) and those obtained by Bock et al. (Bock 1982) (triangles). The lines are interpolations through the data points.

4.2.2 Theoretical predictions of P_{CN}

The values of P_{CN} have been determined theoretically in a work (Adamian 2000) analyzing the dependence of fusion cross section on the isotopic composition of the colliding nuclei within a dinuclear system concept of the CN formation. It was found to depend decisively on the neutron numbers of the dinuclear system. The predicted value of P_{CN} = 0.07 for the ^{208}Pb (^{50}Ti, 2n) ^{256}Rf reaction with E^*_{CN} = 21.5MeV is a factor of 3.24 lower than the experimentally determined value of P_{CN} = 0.23 with E^*_{CN} = 20.6MeV, which is the maximum of 2n evaporation excitation function. Fig4.3 shows the comparison between the P_{CN} values determined for various cold fusion reactions and the experimentally determined average value of P_{CN} for the ^{208}Pb (^{50}Ti, 2n) ^{256}Rf reaction.

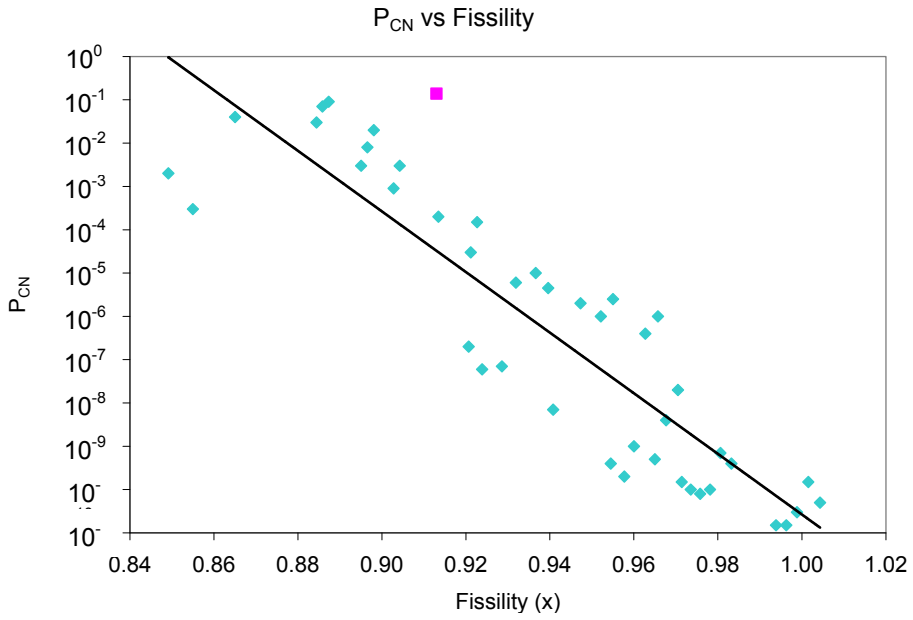

Figure 4.3 The values of P_{CN} have been determined theoretically in a work (Adamian 2000) within a dinuclear system concept of the CN formation. The figure shows the comparison between the P_{CN} values determined for various cold fusion reactions leading to formation of elements with Z = 100-118 (diamonds) and the experimentally determined average value of P_{CN} (square) for the ^{208}Pb (^{50}Ti, 2n) ^{256}Rf reaction. The solid line is a trendline between the data points.

In a recent publication "empirical" values of P_{CN} have been determined for $102 \leq Z \leq 113$ using standard statistical model Monte Carlo program SEQ (Siwek-Wilczynska 2005) for calculating the W_{sur}, reliably predicted σ_c based on diffused barrier formula (Siwek-Wilczynska 2004; Swiatecki 2005) and σ_{EVR} measured at GSI Darmstadt and RIKEN. This work reports an "empirical" value 0.01 for P_{CN} for the ^{208}Pb (^{50}Ti, 2n) ^{256}Rf reaction which is a factor of 23 lower than the experimentally determined value in our work, $P_{CN} = 0.23$.

4.2.3 Theoretical predictions of W_{sur}

The W_{sur} values have been calculated for 1n channel by Zubov et al. (Zubov 1999) by using the theoretical predictions for fission barrier heights from two different calculation schemes (Möller 1988; Möller 1995; Smolańczuk 1995; Smolańczuk 1999). The details of each of the theoretical approaches and the W_{sur} calculations have been outlined in section 1.3. The authors mention the possibility of higher differences in the W_{sur} values obtained with different approaches in the higher xn evaporation channels ($x \geq 2$). The authors therefore comment that only those calculations of W_{sur} should be of interest where a large enough number of reactions are considered within the same set of parameters and assumptions.

For our set of W_{sur} values, $W_{sur} = 1.22 \times 10^{-4}$ for $E^* = 14.16$MeV which is the maximum of 1n evaporation excitation function. This value is almost equal to that obtained by Möller et al. prescription for 1n channel, 1.2×10^{-4}. For next two energies the contribution of 1n channel to the decay of CN decreases and is substituted by 2n channel. The combination of two decay modes causes the W_{sur} to decrease over this energy range by just over an order of magnitude. Further decrease in W_{sur} is caused by

onset of 3n decay channel for the last two energies. Theoretical values for comparison with the W_{sur} for 2n and 3n channels are, however, not available at this point.

4.3 Conclusion and future work

The fusion reaction $^{50}Ti + ^{208}Pb$ has been carried out and studied for its various aspects numerous times in the past. Our goal of performing this experiment was to determine the P_{CN} (probability of the mononuclear complex formed after capture evolving into a compound nucleus inside the fission saddle point) for this much-studied reaction. The reaction was carried out at five beam energies (E_{cot} = 228.0-251.1MeV) bracketing the maximum of the 2n EVR excitation function, spanning 1n-3n evaporation channels. Data was acquired with two pairs of DSSDs, separated by the folding angle, in coincidence mode and with seven SB detectors at backward angles in singles mode. The singles data was analyzed to establish a fission angular distribution and fit with Back et al. procedure to arrive at the complete fusion contribution to the total fission cross section. The total fission cross sections were obtained by integrating these fits for each of the energies. Knowing the σ_{fis} and σ_{CN} the P_{CN} was determined. W_{sur} was calculated for each of the energies utilizing the σ_{EVR} from previous works and σ_c and P_{CN} determined experimentally.

The experimentally determined P_{CN} is a factor of 3.24 higher than the theoretical prediction for the P_{CN} of a system with the same fissility. The value of W_{sur} is, however, in good agreement with the deduced W_{sur} value based on the theoretical predictions of Möller et al. (Möller 1988; Möller 1995) for 1n channel. Experiments need to be carried out in future for the systems that would produce CN with $Z > 104$ to confirm the whether the trend of agreement with predictions of Möller et al. continues

for heavier nuclei. Experimentally determined W_{sur} values for a large number of nuclear systems will also help conclude whether any of the theories currently available are good theoretical models for explaining the heavy element production and decay mechanisms and whether the path leading to heavier element production should be that of cold fusion or hot fusion or an entirely new method needs to be thought of.

A publication based on these results is in the making and is expected to be published soon.

STUDY OF NEAR- AND SUB-BARRIER FUSION OF ^{9}Li + ^{70}Zn SYSTEM (AND AN ATTEMPT TO STUDY THE NEAR- AND SUB-BARRIER FUSION OF 'HALO' NUCLEUS ^{11}Li WITH ^{70}Zn)

5 INTRODUCTION

5.1 'Halo's and 'skin's in the nuclei near the neutron drip-line

In a nucleus made of protons (with positive charge) and neutrons (with no charge) the *nuclear strong force* plays a very important role in keeping it together. This is a short-range attractive force and works through the exchange of particles called *mesons*. Since the protons have positive charge they feel the repulsive Coulomb force acting between them. However at the very tiny distance (~10^{-15}m) at which the nucleons (as the protons and neutrons are collectively called) are placed from each other in the nucleus, the strong force prevails over the Coulomb force. This works particularly well for the lighter nuclei. As one goes towards higher Z and A, the Coulomb force becomes stronger with increasing number of protons. Hence only those nuclei survive which have more neutrons than protons thus making the strong force strong enough to overcome the repulsive Coulomb force and to keep the nucleus together. Hence the N/Z ratio goes on increasing with the Z and A of the nuclei. But at the same time the bulk of the nuclei also increases and a point is reached where the short-range (10^{-15}m) nuclear force can no longer keep the nucleus together. On the N vs. Z chart the *neutron drip line* identifies such an N/Z ratio beyond which the nuclei are unable to bind any additional neutrons.

When the attractive nuclear force is effective in keeping the nucleus together the density of nucleons over the entire nucleus is uniform. Also the ratio neutron-

density/proton-density is about the same as the N/Z ratio in the interior of the nucleus (Fukunishi 1993). The nucleons in the nuclei that are just inside the neutron drip line are, however, not uniformly distributed throughout. Some nucleons (usually 1 to 4) are placed well outside the bulk of the nuclear matter, at a radius much larger than the standard radius of $R_0 \times A^{1/3}$. These nucleons feel the attractive nuclear force less strongly as compared to others which are present in the 'core' (within the predicted nuclear radius) and hence form a sort of 'halo' around the core. The nuclei with this particular structure are called 'halo nuclei'. This uniqueness of nuclei was first discovered in 1985 (Tanihata 1985) when it was realized that ^{11}Li nucleus was abnormally spatially extended. ^{11}Li showed a rms matter radius of 3.27 ± 0.24 fm (fig5.1) as compared to that of ~2.5 fm on an average for the other Li isotopes ($^{6\text{-}9}$Li) and to 2.7fm predicted by $R_0 \times A^{1/3}$. This unusually large radius suggested a large deformation and/or long tail in matter distribution due to weakly bound nucleons. Later it was determined experimentally that there were two weakly bound neutrons that orbited the core ^{9}Li at a rms radius of 5.1±0.7fm (Gibbs 1991) which makes the strong interaction radius of ^{11}Li almost equal to that of much heavier ^{208}Pb. The nuclear charge radius (r_c) of ^{11}Li has been determined to be 2.217fm by high-precision laser spectroscopy (Sa´nchez 2006). The matter radius (r_m) and the neutron radius (r_n) are fixed at 2.44±0.08fm and 2.59fm, respectively, by a newly proposed and recently applied experimental method based on measurements of the differential cross sections dσ/dt for intermediate-energy proton-nucleus elastic scattering in inverse kinematics (Dobrovolsky 2004).

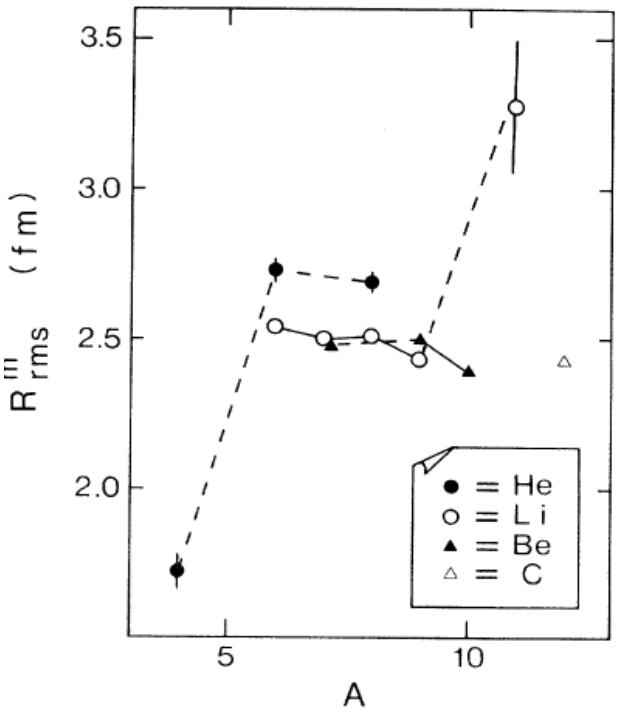

Figure 5.1 The figure [Source: (Tanihata 1985)] shows matter rms radius (R^{m}_{rms}) of different Li isotopes. Lines connecting the isotopes are only to guide the eye. Open circles represent the Li isotopes. The ^{11}Li shows matter rms radius much larger as compared to other Li isotopes.

It has been suggested (Migdal 1972/3) that even though the force between two neutrons is too weak to form a 'dineutron' cluster and even if the nucleus itself is unable to bind a single "extra" neutron to it the two entities, in presence of each other, can come together to form a three-body system consisting of the core nucleus and two relatively detached neutrons. This idea was applied to the nuclear structure of ^{11}Li (Hansen 1987) to explain its spatial extension. It was considered to be a nucleus with a ^{9}Li core and two neutrons orbiting it at a distance such that the interaction radius of this nucleus was almost equal to that of a much heavier ^{208}Pb nucleus (fig5.2). It is a "Borromean" nucleus, which means that when one of the three bodies involved (core and the two neutrons) is taken away from the system, the whole system breaks down.

This name is derived from the ancient symbol of the Borromean rings which is a set of three rings intertwined in such a way that if one of them is cut off, the remaining two also come apart.

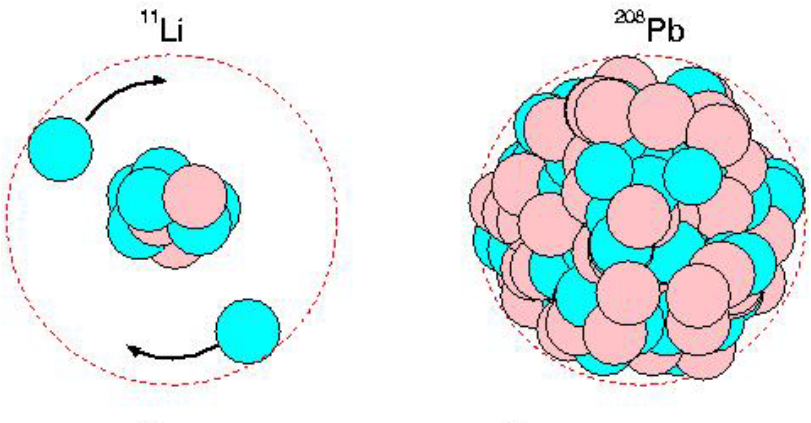

Figure 5.2 A schematic representation of the relative sizes of the halo nucleus ^{11}Li and the stable ^{208}Pb nucleus shows that the two have almost the same interaction radius although Li is a much lighter element. [Source: http://adam.phys.sci.osaka-u.ac.jp/study/intro/intro3.html]

Further speculations were made that this weak binding of the halo neutrons might lead to a nucleus having a soft dipole mode. The 'soft dipole mode' is a low energy branch (with excitation energy < 1MeV) of the 'giant dipole resonance'. The latter represents the oscillation of all the protons in a nucleus against the neutrons in it and the former symbolizes the halo neutrons oscillating against the core (fig5.3). Therefore the reaction $\text{halo nucleus} \rightarrow \text{core} + \text{halo neutrons}$ is possible through Coulomb collisions at a relatively low energy and that these nuclei might have only one bound state.

According to J. S. Al-Khalili (Al-Khalili 2003),

Halo nuclei are very weakly-bound exotic states of nuclear matter in which the outer one or two valence nucleons (usually neutrons) are spatially decoupled from a relatively tightly bound core such that they spend more than half their time beyond the range of the binding nuclear potential. In this sense, the halo is a threshold phenomenon in which the halo nucleons quantum tunnel out to large distances, giving rise to extended wavefunction tails and hence large overall matter radii. The halo nucleons tend to be in low relative orbital angular momentum states (s or p) so as not to be confined by the centrifugal barrier.

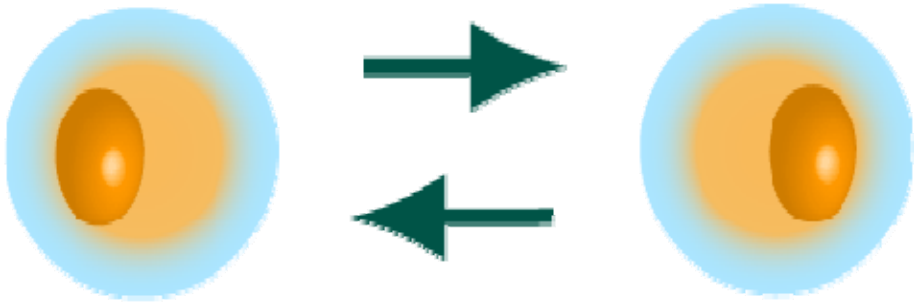

Figure 5.3 The figure gives a schematic representation of the 'Soft dipole mode', a low energy (E* < 1MeV) branch of the Giant Dipole Resonance (GDR), in which the halo nucleons oscillate against the core nucleons. [Source: http://ruby2.scphys.kyoto-u.ac.jp/person/kyoshida/physics.html]

Examples (fig5.4) of such nuclei are ^{11}Be and ^{19}C (1n halo), ^{11}Li, ^{14}Be, ^{17}B, ^{22}C (Borromean nuclei, 2n halo), ^{8}He and ^{19}B (4n halo) etc. There are a few other nuclei with very similar characteristics as the halo nuclei but the detached nucleons around them are called 'skin' as they are not as spatially extended as the halo nucleons. Examples of skin nuclei are ^{6}He, ^{6,7,9}Li (n skin), ^{7}Be, ^{8}B (p skin). The halos and skins have a very subtle difference between them. The number of nucleons and therefore their density in a 'skin' is relatively higher as compared to a halo in which the nucleon density is about 1/100th of the central nucleon density (Fukunishi 1993). Both are made from loosely bound nucleons which have very low binding energy. This makes

them very "detached" from the nucleus as whole and easily available for any nuclear reactions as compared to other nucleons in the nucleus.

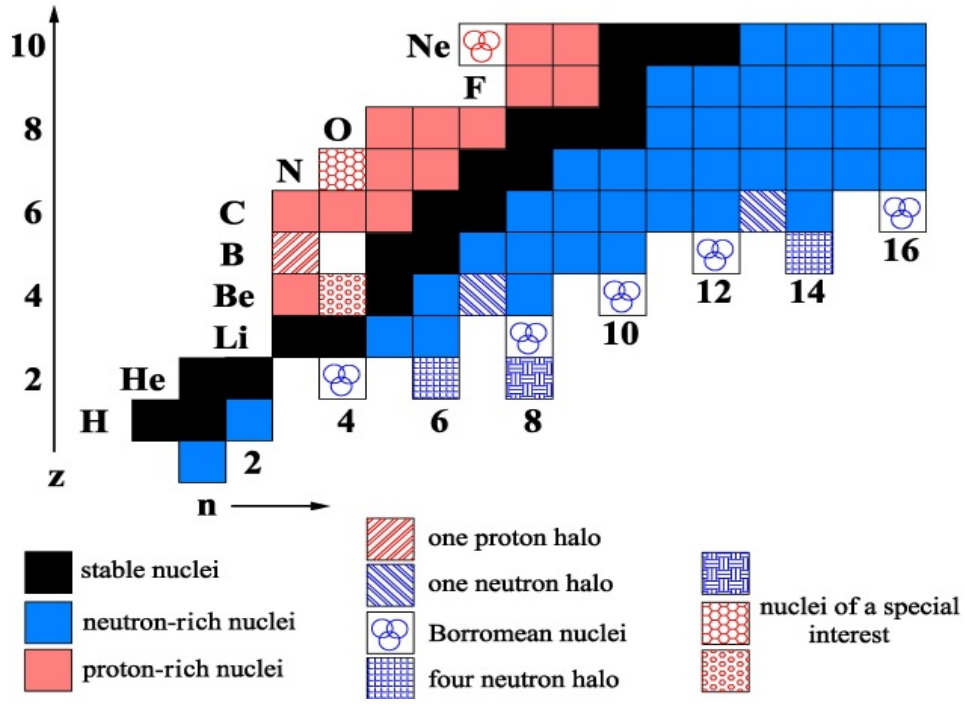

Figure 5.4 A depiction of chart of nuclides showing various types of proton and neutron-rich nuclei. [Source: http://www.ph.surrey.ac.uk/npg/confs/ecthalo.html]

However the halo nucleons behave completely independent of the core with regard to the reactions with impinging nuclei or particles. A proof of this "disconnectedness" of the halo nucleons would be to show that there are two components in a physical quantity such as transverse or longitudinal momentum observed in a high energy peripheral interaction of target and beam (Uchiyama 2003). Also the wave functions of halo nuclei should be able to be factorized in two components and that would become a signature of a halo nucleus. However, this total incoherence of loosely bound nucleons with the core nucleons is absent in case of the skin nuclei. The halo

can be considered to be a tunneling effect occurring in an *s* or *p* orbit whereas the skin can occur due to nucleons in any orbit. Also the spatial distribution of skin is not as extended as the one of the halo. The skin signifies the excess of a particular type of nucleon (neutrons or protons) near the nuclear surface whereas the halo symbolizes such an excess extending to a relatively larger distance from the nucleus (Bochkarev 1998).

The proton-halos are not common as Coulomb potential among protons, in spite of the attractive nuclear force, prevents the growth of the halo without unbinding of the nucleus. Hence the proton halos are less pronounced than the neutron halos. ^{8}B, ^{13}N and ^{17}Ne are examples of this rare phenomenon.

5.2 Contradictions concerning the fusion reactions with halo nuclei

The large halos of loosely bound neutrons tend to reduce the interaction barrier for the reactions involving these nuclei (Dasso 1994) due to the lower strength of the attractive nuclear force acting on them. The halo neutrons are also suspected to show the soft dipole mode of excitation (with excitation energy < 1MeV) which makes them easily available to take part in a nuclear reaction. Therefore when used as a projectile in a fusion reaction, these factors are expected to make the fusion of halo nuclei more probable as compared to the non-halo nuclei thus enhancing the fusion cross section.

Due to these reasons immense theoretical and experimental interest has been shown towards the halo nuclei. However, the breakup of the halo nuclei into core and separated halo nucleons might restrict the enhancement. There is a considerable division amongst nuclear theorists about how these competing factors will affect the fusion cross section and the experimental data obtained to the date are equivocal.

5.2.1 Theoretical contradictions

The contradicting theoretical predictions as well as the experiments done at energies above the Coulomb barrier have been summarized aptly by Signorini in a review article (Signorini 1997). The ^{11}Li + ^{208}Pb reaction has been a subject of many theoretical as well as experimental investigations. The system represents a reaction of a halo nucleus with a stable nucleus, both having almost the same radius. The system is, therefore, expected to show a large reaction cross section. This system has been theoretically studied for elastic scattering as well as fusion at energies below, near and above the fusion barrier. The current theoretical predictions for the fusion cross section (σ_{fus}) for this reaction are not very consistent with each other (fig5.5).

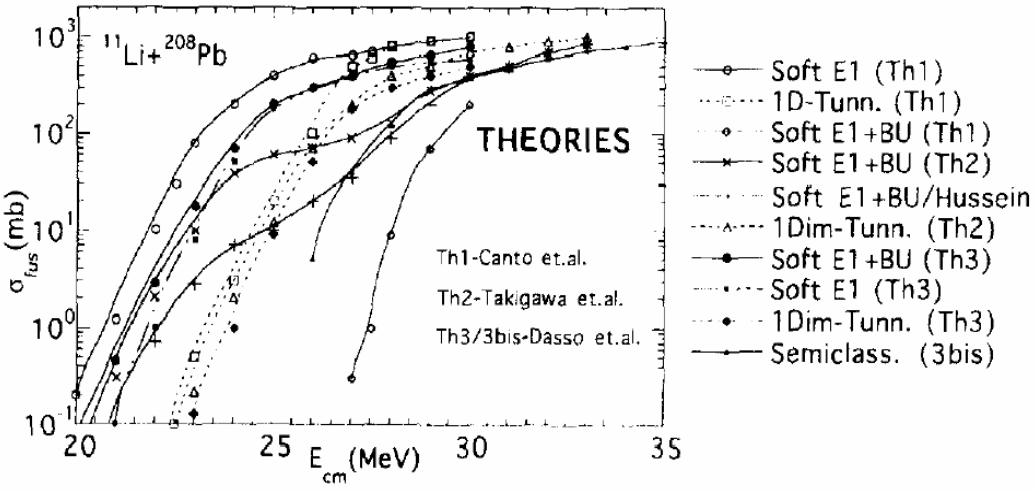

Figure 5.5 In this figure Signorini (Signorini 1997) aptly summarizes various theoretical predictions of the fusion excitation function for the ^{11}Li + ^{208}Pb reaction, considering all the different influencing factors, like the breakup of the halo nucleus, the availability of halo nucleons for fusion etc.

A Japanese group of scientists studying the ^{11}Li + ^{208}Pb system separated the σ_{fus} into two components (fig5.6), one for the 'entrance channel' (fusion of ^{11}Li with ^{208}Pb) and the other for 'breakup channel' (fusion of ^{9}Li core with ^{208}Pb) (Takigawa 1993).

The '^{9}Li + two-neutron cluster model' (Hansen 1987) was used when considering the intrinsic motion which is the motion of the two-neutron cluster and the ^{9}Li core with respect to each other. Their work showed that the σ_{fus} is dominated by the entrance channel at the lower energies and by breakup channel at higher energies. They also suggested that the effect of breakup on entrance channel alone should be considered when determining the factor by which the σ_{fus} is lowered due to breakup. However, they expected the fusion with halo nuclei to show significant enhancement over other isotopes (fig5.7) and did seek a confirmation of their results from the experimentalists.

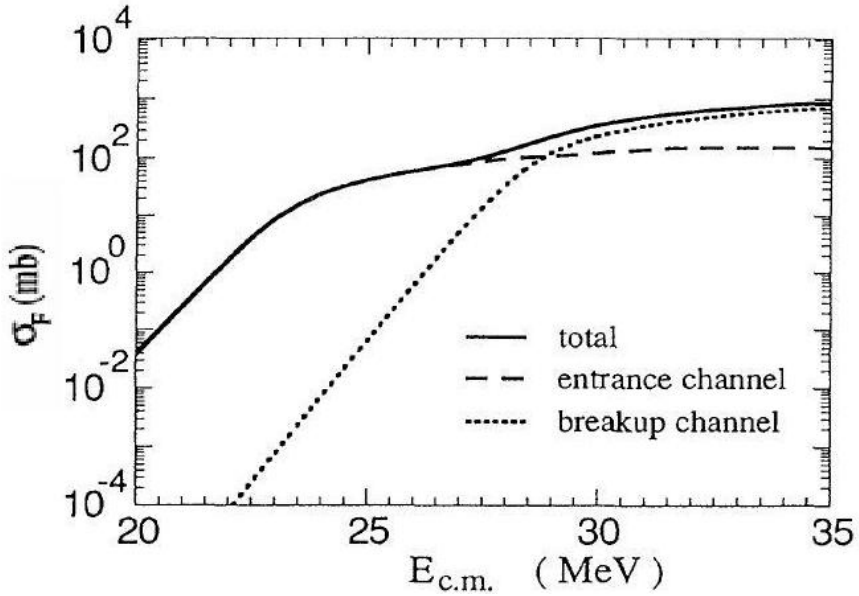

Figure 5.6 Decomposition of fusion cross section of ^{11}Li with ^{208}Pb into that in the entrance channel (dashed line) and in the breakup channel (dotted line). [Source: (Takigawa 1993)]

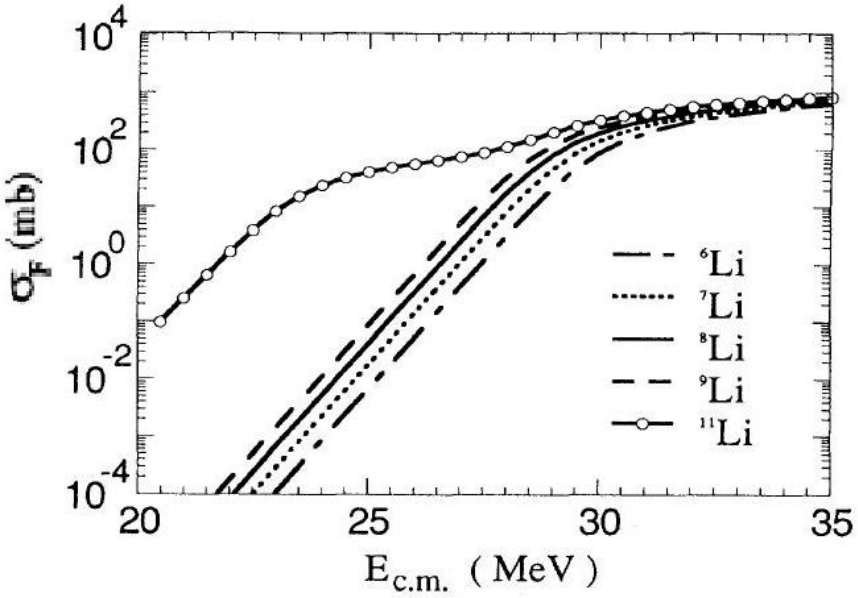

Figure 5.7 Comparison of the fusion cross section (σ_F) for the fusion of Li isotopes with ^{208}Pb from a work of Takigawa et al. (Takigawa 1993). The ^{11}Li-induced reaction shows significant sub-barrier enhancement (open circles) as compared with other isotopes (solid, dashed, dotted and dashed dotted lines).

Another study put forth the idea that the combined effects of the soft dipole mode and the break-up would lead to an abnormal fusion excitation function (fig5.8), with a small dip in the barrier region (Hussein 1995). The authors explained this in terms of the decay widths of the spreading channel (coupling of the soft dipole mode with the fine structure states in the host nucleus) and escape channel (coupling of the soft dipole mode with the various open decay modes) of a doorway state (Feshbach 1992). The 'doorway state' is an intermediate state of a reaction system lying between single-particle states and more complex states leading to formation of compound nuclei. The decay widths of these two channels are given by $\Gamma_d^{\downarrow}$ and $\Gamma_d^{\uparrow}$, respectively and Γ_d is the total decay width which is the sum of the former two quantities. Hence if $\Gamma^{\downarrow}_d \sim \Gamma$ then the fusion cross section would be slightly enhanced and if $\Gamma_d^{\uparrow} \sim \Gamma$ the fusion cross

section is lowered due to the breakup. Thus taking into account the effect of breakup on both the entrance and exit channels this group showed that fusion is considerably hindered if the reaction is taking place below the barrier and only slightly enhanced above it.

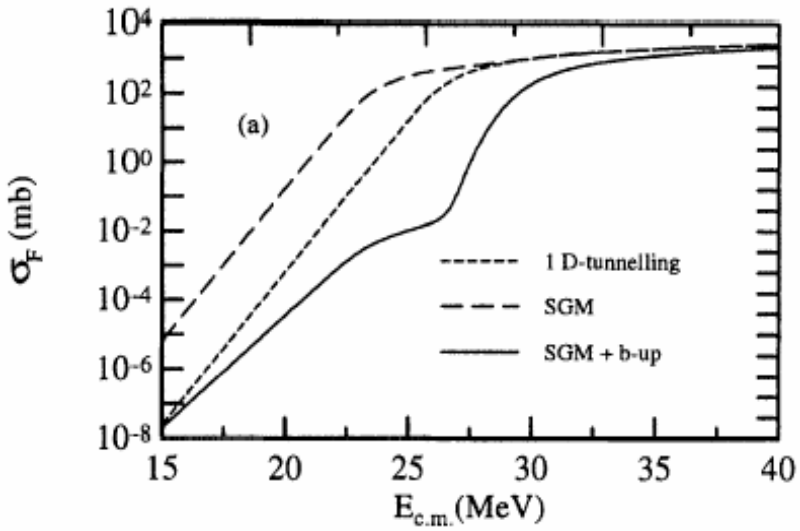

Figure 5.8 According to Hussein et al. (Hussein 1995), combined effect of the 'Soft Giant Dipole Mode' (SGM) and 'break-up' (b-up) will lead to an abnormal fusion excitation function with a small dip in the barrier region (solid line).

A theory very different than the above two theories is that the breakup will not necessarily lead to lowering of σ_{fus} (Dasso 1994). According to the authors of this article some basic characteristics of multidimensional quantal tunneling might have been ignored by the two previously mentioned groups of theoreticians. The transmitted flux which represents the fraction of particles undergoing the fusion reaction is sensitive to the magnitude of the transmission coefficients inside the potential barrier. The reflected flux which is the fraction not undergoing a nuclear reaction, however, depends wholly on the form factors outside the barrier. To check

the effect of the various quantal tunneling details mentioned above in case of the ^{11}Li + ^{208}Pb reaction, coupled channel tunneling calculations were performed with the barrier parameters and coupling form factors being the same as those used by Hussein et al. (Hussein 1992). The ^{11}Li channels considered were the ground state, the low-energy excited state (soft dipole mode) and the breakup into two neutrons and ^{9}Li. The results (fig5.9) showed a new trend in the excitation function in that when the breakup channel was coupled with the rest, the cross section showed enhancement as compared to the coupling of the entrance channel with the 'soft dipole mode' channel, especially at the energies below the barrier.

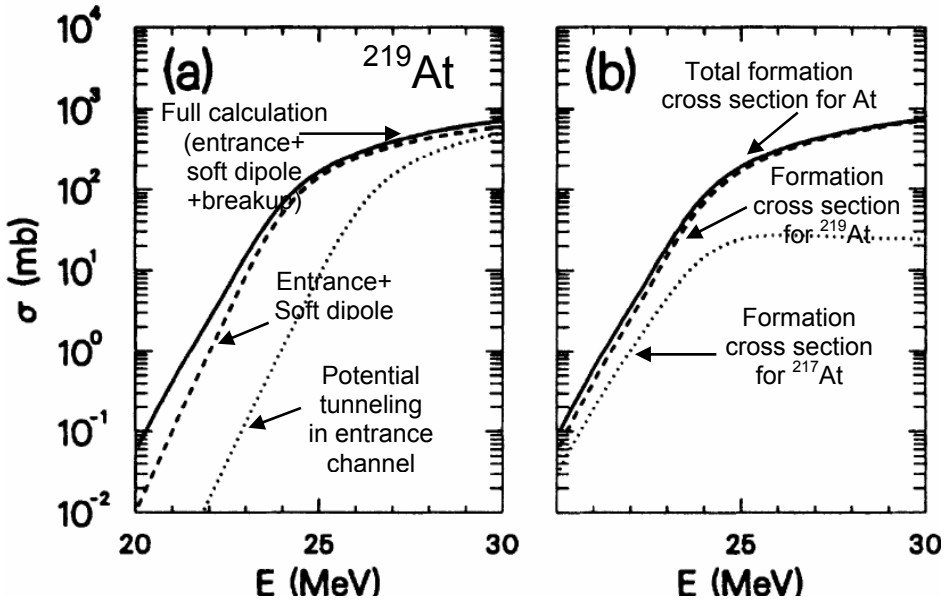

Figure 5.9 The calculated fusion excitation functions for the ^{11}Li + ^{208}Pb reaction [Source: (Dasso 1994)]. (a) Fusion cross sections leading up to the formation of ^{219}At. The full calculation includes three reaction channels, entrance, 'soft dipole mode' and breakup channel. For the first two channels, the parameters are V_B=25.9Mev, r_B=11.1fm, $\hbar\omega$=3MeV (Takigawa 1991) and for the third they are V_B=29Mev, r_B=11.1fm, $\hbar\omega$=4MeV (Broglia 1990). For the coupling between the three channels same parameters as Hussein et al. (Hussein 1992) have been used. (b) Total cross section for formation of As depicting contribution from two isotopes produced. Results incorporate all partial waves up to l=20.

5.2.2 Contradictory experimental results

Experiments with radioactive ion beams (RIBs) of halo or skin nuclei have not been very easy to perform due to either the non-availability of the beam or the extremely low intensity of the available beams. In the few experiments that have been done recently the data gathered have been scanty and the results in most cases are not conclusive and differ drastically from one another. Signorini has summarized the early experimental efforts made in the direction of better understanding the skin nuclei (Signorini 1997). However he has mentioned the need for more experiments to be carried out in order to confirm the results of the ones already performed. Some of the more recent studies have indicated the importance of the transfer reaction channels in the enhancement of sub-barrier fusion of weakly bound nuclei. Below is a short review of the experimental efforts made towards understanding the fusion of n-rich halo and skin nuclei and stable weakly bound nuclei in the past couple decades. ^{4,6}He, ^{6,7}Li and ^{9,11}Be have been studied the most.

The ^{6}He + ^{209}Bi fusion was studied at Dubna (Penionzhkevich 1995) and the fusion and EVR excitation functions were compared with the previously obtained results for ^{4}He + ^{209}Bi system (Khodai-Joopari 1966; Rattan 1992). As can be seen in fig5.10 the ^{6}He + ^{209}Bi fusion-fission cross sections showed an enhancement over the ones for the ^{4}He + ^{209}Bi system but no enhancement in the EVR excitation function is apparent. This was suggested to be due to the neutron halo structure of the ^{6}He nucleus. Similar studies carried out at University of Notre Dame (Kolata 1998c; Kolata 1998b; Kolata 1998a) showed no enhancement due to halo neutrons or suppression due to breakup of the nucleus in the fusion excitation function above the

barrier with ^{6}He but did observe a large sub-barrier enhancement in the fusion. They suggested this enhancement was due to a neutron-flow between target and projectile caused by the positive Q-value of the n-transfer reaction for the ^{6}He + ^{209}Bi system. A later study of the same system at the same venue (Aguilera 2000) lead to the observation of a large yield of ^{4}He fragments that contributed to the total reaction cross section. Based on the energy of these fragments it was suggested that the reactions ^{6}He→^{5}He+1n, ^{5}He→^{4}He+1n and ^{6}He→^{4}He+2n could be responsible for this yield along with the possibility of n-transfer to unbound states in ^{211}Bi. These authors propose that these transfer reaction channels and/or the breakup channel could be the doorway state that accounts for the sub-barrier enhancement in fusion cross section observed by the earlier group.

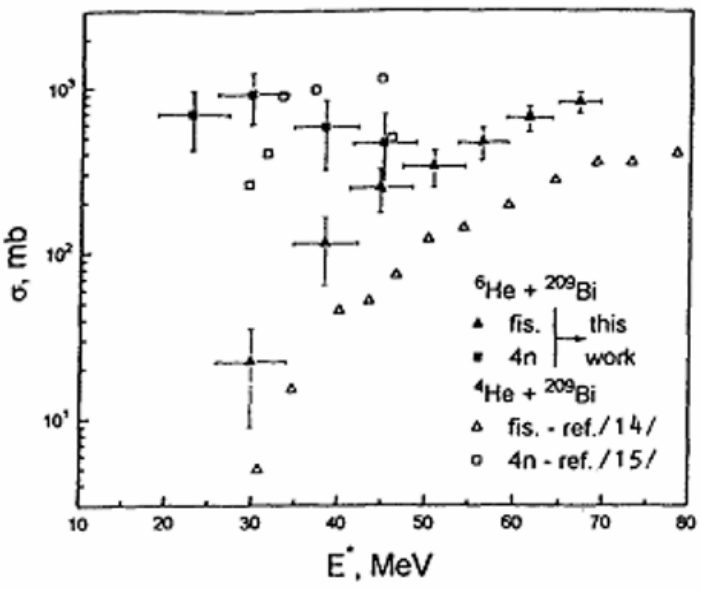

Figure 5.10 The figure [Source: (Penionzhkevich 1995)] shows the comparison between the fusion and EVR excitation functions for ^{6}He + ^{209}Bi and ^{4}He + ^{209}Bi systems. The ^{6}He + ^{209}Bi fusion-fission cross sections showed an enhancement over the ones for the ^{4}He + ^{209}Bi system but no enhancement in the evaporation residue excitation function is apparent. The ref./14/ and /15/ in the figure are (Khodai-Joopari 1966) and (Rattan 1992), respectively.

In order to confirm the contribution of the 1n- and 2n-transfer reactions to the large ^{4}He yield observed n-α correlation experiments were performed on the ^{6}He + ^{209}Bi system at the near-barrier energies (Bychowski 2004; DeYoung 2005). These experiments were based on the fact that there is a distinctive angular correlation between the neutrons and alpha particles emitted in transfer reactions. A conclusion was reached that the 1n-transfer reaction channel (Bychowski 2004) contributed 20% of the ^{4}He yield and the authors presumed that the remaining 80% was due to 2n-transfer and direct reactions. Later it was shown that beyond the grazing angle of this reaction 55% of the ^{4}He fraction resulted from the 2n-transfer reactions to unbound states of ^{211}Bi (DeYoung 2005). Both these pointed at the importance of transfer reaction channels in the fusion mechanism of the weakly bound nuclei.

In an experimental study of the ^{4,6}He+^{238}U it was deduced from the fusion experiment data (Trotta 2000) at near- and sub-barrier energies that the ^{6}He fusion showed what the authors called the “regular trend” of enhancement in fusion cross section below the barrier which could be attributed to its halo nuclear structure. The results of another fusion experiment carried out with the same system (Raabe 2004) showed, however, no substantial enhancement in fusion below the barrier. Most of the reactions lead to fission which was taken as the indication of the contribution of fusion and transfer channels to the cross section. Careful analysis of the data, which included measurements of fission fragments in coincidence with the α-particles produced by the breakup of ^{6}He, lead to the conclusion that enhancement in total sub-barrier cross section was due to 2n-transfer to excited states of ^{240}U with its subsequent fission with no enhancement in fusion probability.

In a study of the ^{6}He+^{64}Zn near-barrier fusion (Di Pietro 2004) the fusion cross section was measured by detecting the off-line atomic x-ray emission which follows the electron capture decay of the EVRs. These cross sections did not show any enhancement as compared to the similarly studied ^{4}He + ^{64}Zn system and almost 80% of the total cross section was proposed to be due to the breakup and transfer channels.

Fusion of ^{6,8}He with medium mass ^{63,65}Cu targets and heavier ^{188,190,192}Os targets was carried out at the SPIRAL facility (Navin 2004). A new technique of identifying the heavy reaction products by their characteristic γ rays was used in these experiments. The heavy reaction products measured in coincidence with the projectile-like charged particles provided the evidence for large transfer cross section for ^{6,8}He reactions as compared with the ^{4}He reaction with the same targets carried out at the Mumbai Pelletron® accelerator.

A very recent comparative study of the near- and sub-barrier fusions of the systems ^{4}He + ^{208}Pb and ^{6}He + ^{206}Pb (Penionzhkevich 2006), both of which produce ^{210}Po in 2n-evaporation channel, showed a very large sub-barrier enhancement in ^{6}He + ^{208}Pb fusion cross sections as compared to ^{4}He + ^{206}Pb. The possible mechanism for this sub-barrier fusion is proposed by authors to be the 'sequential fusion' (Zagrebaev 2003). The mechanism purports that there is an intermediate rearrangement of the valence neutrons with positive Q-value which leads to gain in the kinetic energy of the colliding nuclei. This increases the barrier penetrability and therefore increases the probability of the sub-barrier fusion. This mechanism has successfully explained the fusion enhancement in ^{40}Ca + ^{48}Ca vs. ^{48}Ca + ^{48}Ca, ^{40}Ca+^{96}Zr vs. ^{40}Ca + ^{90}Zr and ^{18}O + ^{58}Ni vs. ^{16}O + ^{60}Ni. This mechanism predicted that the fusion cross section for ^{6}He +

^{206}Pb would be three orders of magnitude higher than that for ^{4}He + ^{208}Pb for sub barrier energies as can be seen in fig5.11. The figure also indicates that the cross sections are comparable for both systems above the barrier.

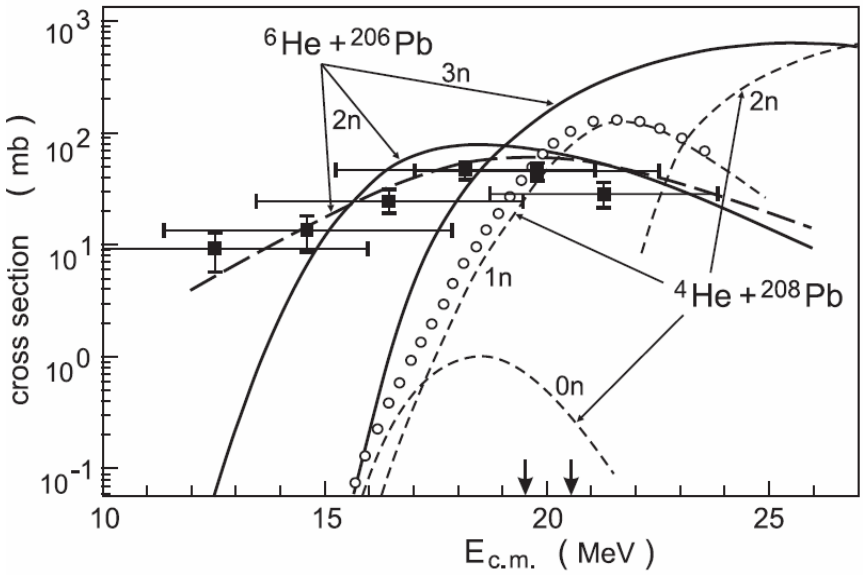

Figure 5.11 The 'sequential fusion' mechanism (Zagrebaev 2003) predicted that the fusion cross section for ^{6}He + ^{206}Pb (solid squares) would be three orders of magnitude higher than that for ^{4}He + ^{208}Pb (open circles) for sub barrier energies as can be seen in this figure [Source: (Penionzhkevich 2006)]. The figure also indicates that the cross sections are comparable for both systems above the barrier. The various dashed, dotted and solid lines represent EVR excitation functions for different evaporation channels as labeled in the figure.

In experiments at RIKEN (Yoshida 1995) the fusion excitation functions for the reaction of ^{9}Be and ^{11}Be with ^{209}Bi showed no enhancement of the cross section leading to evaporation residues for the halo nucleus ^{11}Be compared to the stable nucleus. Later experiments at Munich (Signorini 1998a) showed enhanced cross sections above the barrier for the ^{11}Be projectile but not below it. The authors however suggest a repetition of the experiment with a more intense ^{11}Be beam. Complications involving the breakup of the ^{9}Be projectile have been observed in a later work for the

^{9}Be + ^{209}Bi system (Signorini 1998b; Signorini 1999). Some of the recent fusion cross section measurements of ^{9}Be (which is a stable but weakly bound nucleus) with various targets performed with the new method of detection of reaction products using their characteristic γ rays (mentioned above) have put forth some unusual results. Non-inhibition of cross section has been observed for systems such as ^{9}Be + ^{64}Zn (Moraes 2000) at energies near and above the barrier and ^{9}Be + ^{9}Be (Mukherjee 1997) and ^{9}Be + ^{16}O (Cujec 1979) systems at sub-barrier energies despite the fact that ^{9}Be is a loosely bound (S_n = 51.67MeV) nucleus. On the other hand, the evaporation residue measurements for systems such as ^{9}Be + ^{28}Si (Eck 1980) and ^{9}Be + ^{29}Si (Figueira 1993) at energies well above the barrier and the α activity measurement for the ^{9}Be + ^{208}Pb system (Dasgupta 1999) at energies near and above the barrier show strong inhibition (only 68% of those predicted) of fusion cross sections.

Amongst the isotopes of Li, fusion of the stable but weakly bound ^{6}Li and ^{7}Li has been studied the most compared to the less studied radioactive ^{9}Li fusion. The reaction products in a fusion experiment of ^{6,7}Li with ^{16}O and ^{12,13}C (Mukherjee 2001) were detected by the new γ ray technique. The fusion cross sections thus measured have been shown to be larger than the ones measured earlier by the EVR techniques (Dennis 1982; Mateja 1984; Mateja 1986; Takahashi 1997), especially at the sub-barrier energies. The near-barrier fusion cross sections measured for the ^{7}Li+^{165}Ho (Tripathi 2002) were shown to be suppressed above-barrier and enhanced sub-barrier as compared to the one-dimensional barrier penetration model. The sub-barrier enhancement was attributed to the breakup of the ^{7}Li nucleus. The comparative study of ^{6,7}Li+^{59}Co fusion (Beck 2003) performed by identifying the products by their

characteristic γ rays showed a small enhancement for ^{6}Li below the barrier while the cross sections for both nuclides above the barrier were similar.

Thus as is apparent from the above discussion of various fusion studies carried out with different halo, skin and stable weakly bound nuclei the results obtained are not in agreement with each other for any of the systems pointing towards the need of many more fusion experiments to be performed with these nuclei. The important point to be noted is that the intensity of the projectile beams should be high in order to produce statistically reliable results.

5.3 Why study the ^{9,11}Li + ^{70}Zn system?

As mentioned in sections 5.2.1 and 5.2.2 there are theoretical as well as experimental contradictions regarding the outcome of fusion of halo nuclei. Therefore we proposed an experiment studying the fusion of ^{9}Li and ^{11}Li with ^{70}Zn. The ^{11}Li + ^{70}Zn fusion would be the pilot study for this particular system. The choice of ^{9}Li and ^{11}Li as projectiles would allow us to do a comparative study between a skin nucleus and a halo nucleus. Also the ^{9}Li is the core of ^{11}Li halo nucleus. The reasons for the interest in ^{11}Li have already been discussed at length in previous section. The reasons for choosing ^{9}Li as the other projectile and ^{70}Zn as target are summarized below.

^{9}Li is a very n-rich (N/Z = 2) nucleus having a significant neutron skin (Bertsch 1989) and ^{70}Zn is a n-rich (N/Z = 1.33) nucleus. The experimental runs performed with ^{9}Li projectile on ^{70}Zn target would give some insight into the nuclear structure of a very n-rich skin nucleus and reaction mechanism for its interaction with a n-rich target. Since ^{11}Li nucleus is made up of ^{9}Li core with a halo of two neutrons surrounding it, understanding of the nuclear structure and reactions of ^{9}Li would also

facilitate the understanding of the nuclear structure of ^{11}Li nucleus. Modeling of the reactions of ^{9}Li with other nuclei is made easy due to the nuclear structure of ^{9}Li being well-understood using the simple shell model. Non-fusion experiments such as the study of elastic scattering of ^{9,11}Li with ^{12}C target (Peterson 2003) and measurement of the total interaction cross section for the reactions of ^{9}Li with *carbon*, *aluminum*, *copper*, *tin* and *lead* targets (Blank 1993) have been carried out. Fusion studies have been performed at RIKEN on the ^{9,11}Li + Si system (Petrascu 1997) to determine whether the breakup process influenced the fusion cross section. The neutron spectra of the reactions ^{9}Li + Si and ^{11}Li + Si were taken and compared with the Monte-Carlo calculated fusion-evaporation spectra. The ^{9}Li + Si system showed good agreement with the calculated spectrum and in case of the ^{11}Li + Si system, $30 \pm 10\%$ of fusions were shown to be preceded by pre-emission of one or two neutrons. However, there is no information available on σ_{fus} in this article. Yoshida et al. (Yoshida 1994) studied the ^{9}Li + ^{209}Bi fusion also at RIKEN at ~36MeV energy. The integrated cross sections for 3n and 4n evaporation channels were calculated for the EVRs ^{215}Rn and ^{214}Rn, respectively but the quantity σ_{fus} was not measured in this experiment either. The EVR excitation function however did not match the predictions of the code CASCADE. Therefore an experiment was needed which measured the fusion cross section for a reaction of ^{9}Li.

The choice of ^{70}Zn for target was made for the following reasons. Since Li has Z = 3, the possible product nuclei by addition of nucleons to ^{70}Zn could be *gallium* (Ga), *germanium* (Ge) or *arsenic* (As) isotopes. As and Ge can be separated from each other by a radiochemical procedure with ease and can be detected with straightforward γ

spectroscopy. According to the PACE v.4.13 (Gavron 1980) and HIVAP (Reisdorf 1981) simulations ^{75}As, ^{76}As and ^{77}As EVRs are statistically the most probable ones (fig5.12) while Ge isotopes (^{75,77}Ge) are produced in much smaller quantities for the ^{9}Li+^{70}Zn fusion reaction. The percent yields predicted by these two simulation codes for the ^{11}Li+^{70}Zn fusion reaction are also very similar with PACE v.4.13 predicting ^{76,77}As as the major products with small amounts of ^{77}Ge and HIVAP predicts formation of only the As isotopes (fig5.13). The reason for such yields is that for sub- and near-barrier energies, particle evaporation is the dominant exit channel than the compound nucleus fission which would give a mixture of products with a wide range of Z values.

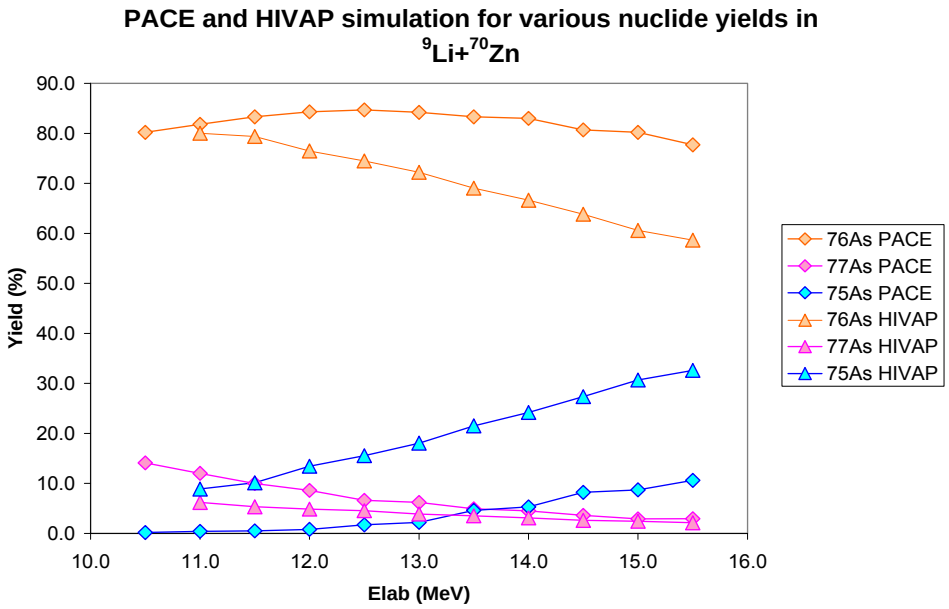

Figure 5.12 Figure shows the percent yields of ^{75}As, ^{76}As and ^{77}As, the major evaporation residues predicted for the ^{9}Li + ^{70}Zn fusion, according to PACE v.4.13 (diamonds) and HIVAP (triangles) simulations for sub- and near-barrier energies.

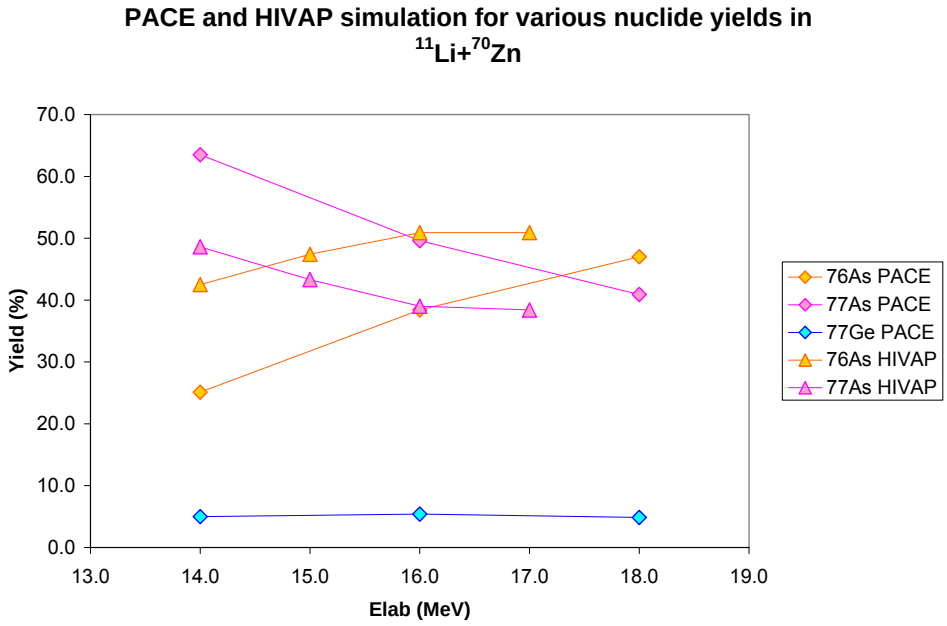

Figure 5.13 Figure shows the percent yields of ^{76}As, ^{77}As and ^{77}Ge, the major evaporation residues predicted for the ^{11}Li + ^{70}Zn fusion, according to PACE v.4.13 (diamonds) and HIVAP (triangles) simulations for sub- and near-barrier energies.

$^{9}\mathrm{Li} + {}^{70}\mathrm{Zn} \rightarrow {}^{79}\mathrm{As} \rightarrow {}^{75}\mathrm{As} + 4\mathrm{n}$, stable

$^{9}\mathrm{Li} + {}^{70}\mathrm{Zn} \rightarrow {}^{79}\mathrm{As} \rightarrow {}^{76}\mathrm{As} + 3\mathrm{n}$, $t_{1/2} = 1.09\mathrm{d}$

$^{9}\mathrm{Li} + {}^{70}\mathrm{Zn} \rightarrow {}^{79}\mathrm{As} \rightarrow {}^{77}\mathrm{As} + 2\mathrm{n}$, $t_{1/2} = 38.83\mathrm{h}$

$^{9}\mathrm{Li} + {}^{70}\mathrm{Zn} \rightarrow {}^{78}\mathrm{Ge} + \mathrm{p} \rightarrow {}^{77}\mathrm{Ge} + \mathrm{n}$, $t_{1/2} = 11.30\mathrm{h}$

$^{9}\mathrm{Li} + {}^{70}\mathrm{Zn} \rightarrow {}^{78}\mathrm{Ge} + \mathrm{p} \rightarrow {}^{75}\mathrm{Ge} + 3\mathrm{n}$, $t_{1/2} = 82.78\mathrm{m}$

$^{11}\mathrm{Li} + {}^{70}\mathrm{Zn} \rightarrow {}^{81}\mathrm{As} \rightarrow {}^{76}\mathrm{As} + 5\mathrm{n}$

$^{11}\mathrm{Li} + {}^{70}\mathrm{Zn} \rightarrow {}^{81}\mathrm{As} \rightarrow {}^{77}\mathrm{As} + 4\mathrm{n}$

$^{11}\mathrm{Li} + {}^{70}\mathrm{Zn} \rightarrow {}^{80}\mathrm{Ge} + \mathrm{p} \rightarrow {}^{77}\mathrm{Ge} + 3\mathrm{n}$

PACE (Projection Angular-momentum Coupled Evaporation) is a modified version of JULIAN, the Hillman-Eyal evaporation code. This code uses a Monte-Carlo calculation which follows the correct procedure for angular momentum coupling at each stage of deexcitation. PACE was first developed by A. Gavron (Gavron 1980). It is based on the statistical model that takes full account of angular momentum effects,

including the yrast levels and gamma emission at all stages of the evaporation. It has been successfully used for prediction of the fusion-evaporation products for various nuclear reactions. The PACE version 4.13 that has been used for all the simulations in our experiment is available as a part of the LISE software package (NSCL 2002). HIVAP is a statistical evaporation code (Reisdorf 1981) which uses the standard evaporation theory. It takes into account the competition between the various decay channels like the neutron and proton evaporation, alpha particle emission, gamma ray decay and fission. It uses the two-Fermi-gas-model angular momentum dependent level density formula with a few modifications (Reisdorf 1992). The coupling between orbital angular momentum of the emitted particles and the residual nuclear spin is accommodated in the code.

Another and more important reason for choosing ^{70}Zn target is availability of the maximum beam energy of 15.4 for ^{9}Li and 17.5MeV for ^{11}Li available at the ISAC1 facility at the TRIUMF lab, where the experiment was to be done. The interaction barrier (Bass 1980), which is the threshold bombarding energy in the center-of-mass system which is needed classically for two fragments to undergo a nuclear reaction, is 12.37MeV for the ^{9}Li + ^{70}Zn reaction and 12.08MeV for the ^{11}Li + ^{70}Zn. The interaction barrier (V_{int}) is calculated as follows (Loveland 2005),

$$R_i = 1.12A_i^{1/3} - 0.94A_i^{-1/3}\,fm \qquad \textbf{5-1}$$

$$R_{\text{int}} = R_1 + R_2 + 3.2\,fm \qquad \textbf{5-2}$$

$$V(R_{\text{int}}) = 1.44\frac{Z_1 Z_2}{R_{\text{int}}} - \frac{R_1 R_2}{R_1 + R_2} \qquad \textbf{5-3}$$

where R_i - Radius of a given nucleus (fm)

A_i - Atomic number of given nucleus

R_{int} - Interaction radius of the reaction involving nuclei 1 and 2 (fm)

$V(R_{\text{int}})$ - Interaction barrier of the reaction involving nuclei 1 and 2 (MeV)

Using 5-1, the radii for ^{9}Li and ^{70}Zn are

$$R_{^{9}Li} = 1.12(9)^{1/3} - 0.94(9)^{-1/3} = 1.88\,fm$$

$$R_{^{70}Zn} = 1.12(70)^{1/3} - 0.94(70)^{-1/3} = 4.39\,fm$$

Using 5-2 for the reaction ^{9}Li+^{70}Zn

$$R_{\text{int}} = 1.88 + 4.39 + 3.2 = 9.47\,fm$$

Using 5-3 the interaction barrier can be calculated as

$$V(R_{\text{int}}) = 1.44\frac{(3)(30)}{9.47} - (1)\frac{(1.88)(4.39)}{(1.88+4.39)} = 12.37MeV$$

It was possible to overcome this barrier with the available maximum beam energy of 15.4MeV for ^{9}Li and 17.5MeV for ^{11}Li at the experimental facility. The choice of target also rooted in the fact that it is a medium mass target where there are no special nuclear structure effects (shell closures etc).

6 PREPARATIONS FOR THE EXPERIMENT

The pre-experiment preparation involved,

1. Making ^{nat}Zn and ^{70}Zn targets by electroplating, the details of which are given in section 6.1.
2. Finding or developing an appropriate radiochemical separation procedure for the separation of the expected EVRs, As and Ge, and testing it. Section 6.2 discusses the details of the same.
3. Building a boron-loaded paraffin shield as a protection against the β delayed neutron emission from ^{9}Li, as described in section 6.3.

6.1 Making *zinc* targets by electroplating

The Zn targets prepared for use in the experiment were 1mg/cm^2 with area 2.83cm^2 (diameter = 1.9 cm). A 1mg/cm^2 thick target would provide a sufficient target density while the beam energy loss would be in the range 0.4-0.5MeV as calculated using the program SRIM (Ziegler 1985). The diameter of the collimator at the experimental facility was estimated to be 1 cm and hence the target over an area with diameter = 1.9 cm would ensure that the beam was well-focused on the target. The targets to be prepared were that of natural zinc (^{nat}Zn) and ^{70}Zn, an isotope of Zn with natural abundance of only 0.62%. Electroplating was the preferred method for making the targets due to its ~100% efficiency.

The choice of backing material for the Zn targets was limited by the experimental as well as electrochemical requirements. The backing had to be a light element in order to minimize back scattering of beam particles off the backing. This would ensure that the Faraday cup at the end of the beamline gave an accurate reading of the beam

current. The calculations detailed in section 8.1 indicate that the amount of ^{9}Li scattered due to backing were about 42% of the ones scattered by the ^{70}Zn. The backing material also had to be lower in electrochemical series than Zn (-0.7618 V). Therefore, the choice of *aluminum* (Al) as the backing material was ideal (Z=13, N=14, reduction potential = -1.662 V). Al foils of thickness 0.54-0.71mg/cm^2 were used.

Out of the numerous methods available in literature, a method (Parthasarathy 1989) using an acidic sulfate bath was employed for electroplating of Zn. The electrolyte is composed of 240g/l $ZnSO_4.7H_2O$, 30 g/l $Al_2(SO_4)_3.18H_2O$ and 15 g/l NH_4Cl. pH of the electrolyte is maintained at pH4 by $Al_2(SO_4)_3.18H_2O$ whereas NH_4Cl increases the conductivity of the solution (Laĭner 1970). Natural Zn is available as $ZnSO_4.7H_2O$ but for the ^{70}Zn, enriched ^{70}ZnO is the cheapest form available. The procedures therefore differed slightly for ^{nat}Zn and ^{70}Zn plating.

The electrolyte for electroplating of ^{nat}Zn targets was prepared by dissolving 1760mg $ZnSO_4.7H_2O$, 220mg $Al_2(SO_4)_3.18H_2O$ and 110mg NH_4Cl in 100ml deionized (DI) water. This gave a solution 4mg/ml in Zn. The electroplating cell was assembled as shown in fig6.1 and 1ml of electrolyte was added to it along with a small amount of DI water to increase the volume. The Zn wire was connected to the positive terminal of the voltage source and the negative terminal was attached to the *copper* (Cu) base of the plating cell. The Al-foil rested on the Cu base and was held in place by a polyvinyl ring which exposed only 1.9cm diameter area at the center of the foil. The Zn^{2+} ions were released in the solution and were attracted to

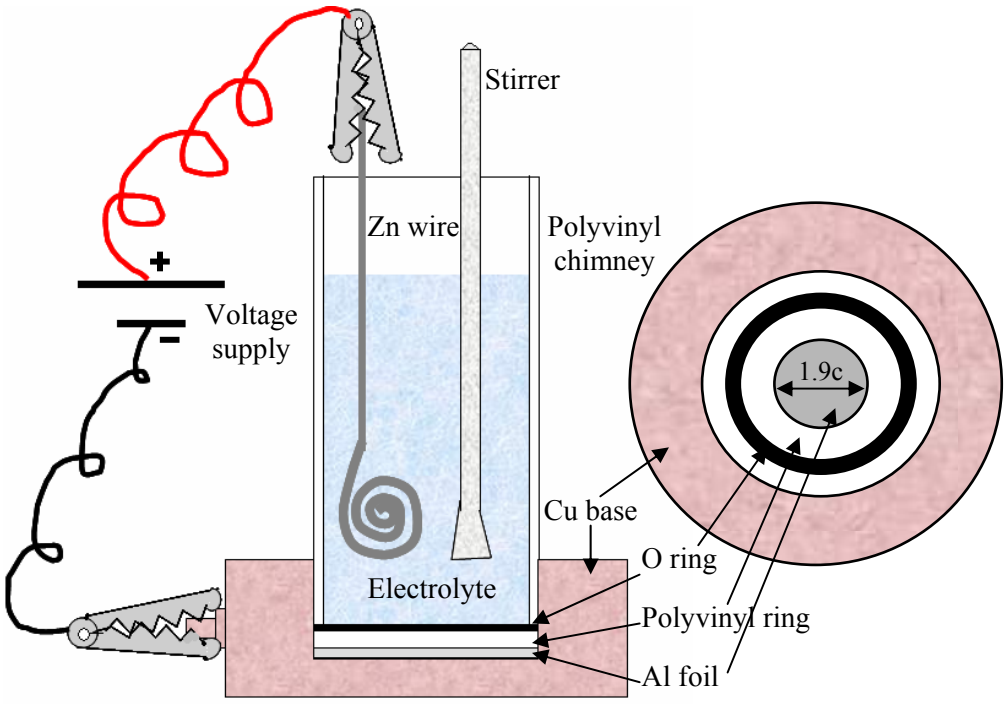

Figure 6.1 A schematic of the electroplating cell used for making Zn-targets. The Zn wire acted as the anode and Cu base of the cell was the cathode. The Al-foil on which Zn metal got deposited by reduction from the electrolyte was placed between the two electrodes. The electrolyte was composed of 1760mg $ZnSO_4.7H_2O$, 220mg $Al_2(SO_4)_3.18H_2O$ and 110mg NH_4Cl in 100ml deionized (DI) water for ^{nat}Zn targets. For ^{70}Zn targets 498mg ^{70}ZnO was dissolved in minimum amount of dil.H_2SO_4 and this solution along with 220mg $Al_2(SO_4)_3.18H_2O$ and 110mg NH_4Cl was dissolved in 100ml DI water.

the negative cathode. The Al-foil, however, being placed between the solution and the Cu-base, Zn^{2+} metal got deposited on it by reduction from the electrolyte. The electrochemical reactions involved were as follows,

$$Zn_{(\text{zinc wire})} \rightarrow Zn^{2+}{}_{(\text{goes in eletrolyte})} + 2e^-$$

$$Zn^{2+}{}_{(\text{from electrolyte})} + 2e^- \rightarrow Zn_{(\text{plated on Al-foil})}$$

A current of 1mA was passed through the electrolyte for about 20 minutes while it was also being stirred. This gave the deposit of ~1mg/cm^2 thickness. The solution had to

be maintained at pH 3-4. If it dropped below pH3 hydrogen evolution would make the deposit non-uniform and flaky. At pH higher than 4 precipitation of $Al(OH)_3$ took place dissolving the backing foil. The deposition carried out under such conditions was stopped after approximately 20 minutes and the cell was dismantled. The Al-foil with the Zn deposit was then allowed to dry and then weighed to determine the accurate area density of that particular deposit. Al-foil with the Zn deposit was clamped (fig6.2) between an octagonal steel flap and a steel square with help of four screws.

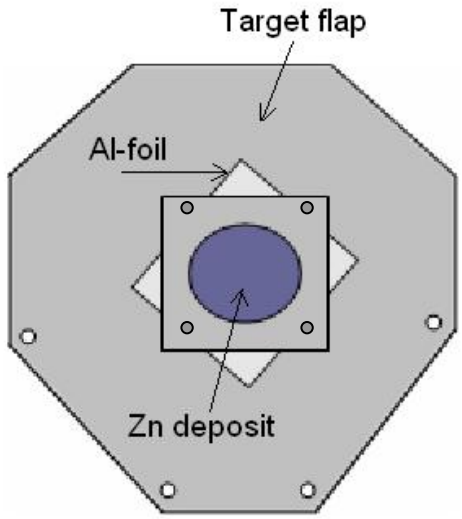

Figure 6.2 The figure shows the target flap assembly. Al-foil with the Zn deposit was clamped between an octagonal steel flap and a steel square with help of four screws. The square had a hole of diameter 1.9cm in the center which exposed the Zn layer on the Al-foil to the beam. The octagonal flap was used for mounting the targets on the target wheel in the experimental chamber as shown in fig7.3.

The square had a hole of diameter 1.9cm in the center which exposed the Zn layer on the Al-foil to the beam. The octagonal flap was used for mounting the targets on the target wheel in the experimental chamber.

For making the ^{70}Zn targets ^{70}ZnO (>95% enriched, obtained from Trace Sciences International) was used. The procedure for deposition differed a little in that the water-insoluble ^{70}ZnO had to be dissolved in H_2SO_4 to convert it to soluble $ZnSO_4$. Hence to make the electrolyte, 498mg ^{70}ZnO was dissolved in minimum amount of dil.H_2SO_4 and this solution along with 220mg $Al_2(SO_4)_3.18H_2O$ and 110mg NH_4Cl was dissolved in 100ml DI water. This gave a solution 4mg/ml in ^{70}Zn. The electrodeposition procedure remained the same as did the specifications of the targets. Table 6.1 gives the thicknesses of the targets prepared. Isotopic purity of the ^{70}Zn targets was determined to be 80.58% ^{70}Zn with minor contributions from other Zn isotopes (especially ^{64}Zn) by carrying out a neutron activation analysis (NAA). The details of the activation, counting and calculations are given in section 8.3.

Table 6.1 Details of ^{70}Zn targets prepared by electrodeposition

Year 2005		
Target #	Weight of deposit (mg)	Area density (mg/cm^2)
1	2.5	0.89
2	3.6	1.28
3	3.0	1.07
4	2.5	0.89
5	2.8	1.00
6	3.4	1.21
7	3.4	1.21
8	2.9	1.04
9	3.5	1.25
10	2.6	0.93

Year 2006		
Target #	Weight of deposit (mg)	Area density (mg/cm^2)
1	2.9	1.02
2	3.0	1.06
3	3.0	1.06
4	2.4	0.85
5	2.7	0.95
6	2.4	0.85

6.2 Separation of the As and Ge EVRs by Solvent Extraction

The expected EVRs from this fusion reaction were the isotopes of As and Ge. A solvent extraction procedure was developed for separation of the As isotopes from the Ge isotopes by modifying a procedure in literature (Marinsky 1961). This procedure utilizes the difference in ease of extraction of Ge (VI) and As (III) iodides into *chloroform* ($CHCl_3$) in presence of *hydriodic acid* (HI). The flowchart of the process is shown in fig6.3 and the procedure is summarized below.

A mixture of 1 ml each of 10mg/ml As and Ge standard carriers (purchased from Alfa Aesar, Specpure©) was heated to near dryness to get rid of the NO^{3-} ions as they tend to oxidize some of the HI (added later in the procedure) to I_2. The irradiated target was dissolved in 3.7ml of 6M *hydrochloric acid* (HCl). The near-dried liquid mixture of the two standards was added to it with aid of 11.2ml of deionized (DI) water making the resulting 15ml solution 3M in HCl. This solution was then transferred to a separation funnel and 4 ml of 47% HI was added. The As combined with the I^- to form AsI_3,

$$As^{3+} + 3I^- \rightarrow AsI_3$$

20 ml of $CHCl_3$ was then added to the separation funnel and the funnel was shaken to equilibrate the aqueous and the organic layers. 15-20 minutes were allowed for the two layers to equilibrate and separate again. During the equilibration process, the AsI_3 was preferably extracted into the organic layer ($CHCl_3$) and Ge remained in the aqueous phase. The organic layer was drained in an Ehrlenmeyer flask and 10 ml of $CHCl_3$ was added to the separation funnel in order to repeat the equilibration and separation process. This ensured that any AsI_3 remaining in the aqueous layer was

extracted into the organic layer completely. The new 10ml organic fraction was drained into the Ehrlenmeyer flask with the earlier 20ml organic layer.

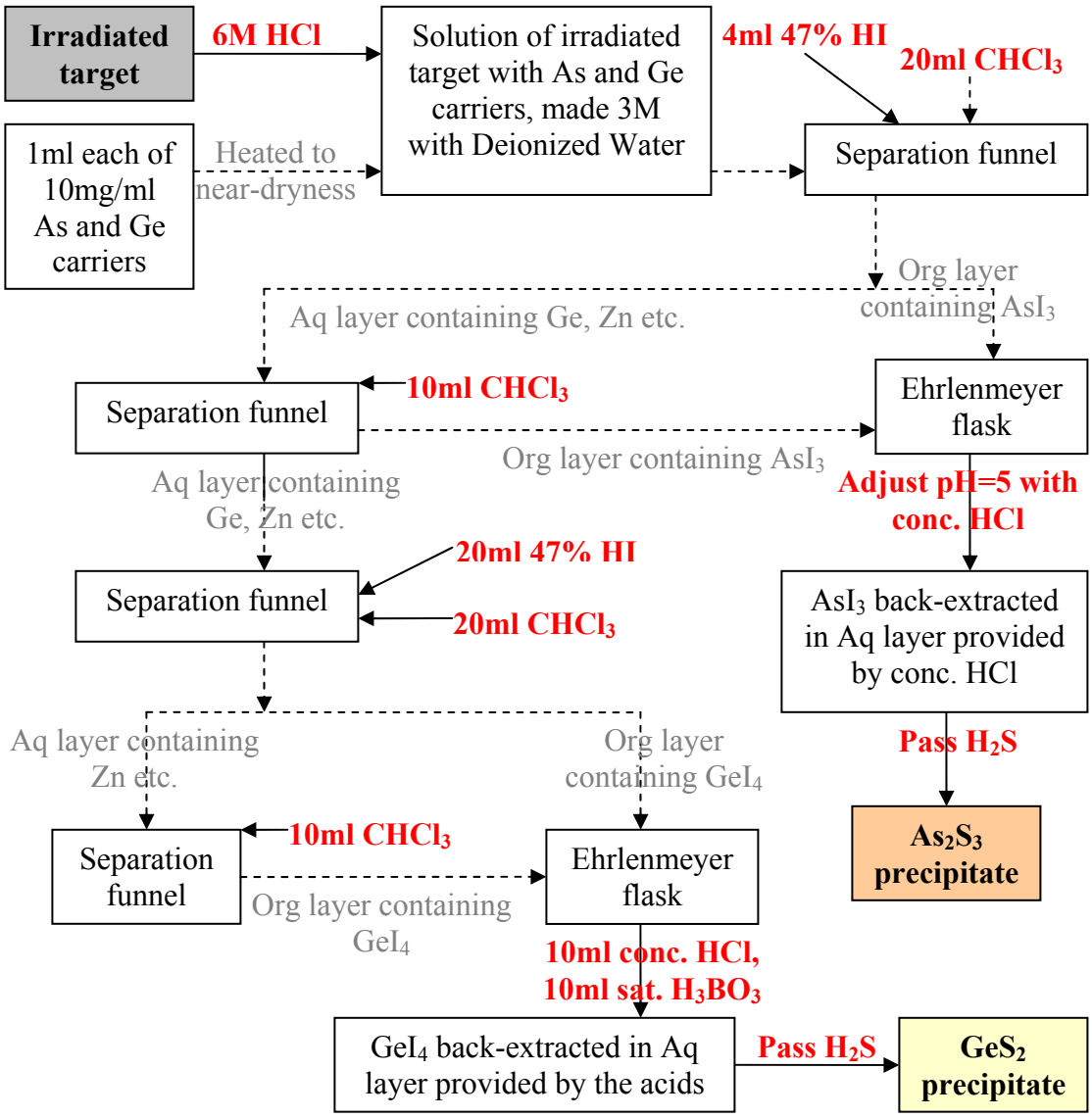

Figure 6.3 Flowchart of the solvent extraction procedure for separation of As isotopes and Ge isotopes from each other. This procedure utilizes the difference in ease of extraction of Ge (VI) and As (III) iodides into chloroform ($CHCl_3$) in presence of hydriodic acid (HI).

The pH of this fraction was adjusted to pH5 by addition of appropriate amount of conc. HCl which also provided the aqueous phase in which the As got back extracted. H_2S was passed through the mixture for about 10 minutes to precipitate As as a bright yellow As_2S_3 in the aqueous phase.

$$2AsI_3 + 3H_2S \rightarrow As_2S_3 + 6HI$$

It was then filtered through a glass-fiber filter paper, air-dried and weighed to determine the percent yield.

The fraction in the separation funnel was treated with 20 ml HI. This provided an excess of I^- to make sure that the Ge remaining in the aqueous layer reacted completely to form GeI_4.

$$Ge^{4+} 4I^- \rightarrow GeI_4$$

The equilibration and separation process was performed on this fraction in exact same way as on the As fraction to ensure the complete extraction of GeI_4 into the organic layer. The organic layer was drained in an Ehrlenmeyer flask and 10 ml of conc. HCl and 10 ml saturated Boric Acid (sat. H_3BO_3) was added to it. The addition of the two acids provided the aqueous phase for the back extraction of Ge and the acidic medium for precipitation of Ge with H_2S. A white precipitate of GeS_2 was obtained in the aqueous phase by passing H_2S for about 10 minutes.

$$GeI_4 + 2H_2S \rightarrow GeS_2 + 4HI$$

The solution was left undisturbed for about 6 hours to let the GeS_2 precipitate out completely as it is known to undergo incomplete precipitation and to form an almost colloidal solution in the acidic medium. It was then filtered, air-dried and weighed to determine the percent yield.

A more accurate determination of percent yields was done by post-irradiation neutron activation which ranged from 27 to 100% (average = 63%) for As and from 3 to 32% (average = 22%) for Ge. Details of the activation and calculations are given in section 8.4. The reasons for especially low yields for GeS_2 seem to be the tendency to undergo incomplete precipitation in acidic medium and formation of colloidal precipitate which is difficult to filter. These precipitates were counted in a Tennelec LB1000 low-background beta detector. Each one was counted for several days in order to establish a decay curve to identify the isotope(s) in the precipitate. The details of counting process and data analysis are given in section 8.2.

6.3 Preparation of a *boron*-loaded paraffin shield

^{9}Li is a 178ms (Alburger 1976) β emitter with a Q_β ~13.6MeV (Ajzenberg-Selove 1979) with ~50% decays resulting in n-emission. We therefore designed and prepared a shield of 5% *boron*-loaded paraffin (fig6.4) as protection against these delayed n-emissions. It was a cube of volume ~0.063m^3 with dimensions 15.75in x 15.75in x 16.25in made of 1/32in thick Cu sheets. Alternate layers of paraffin blocks and Borax powder were put in the cube. Molten paraffin was poured into it after each layer to hold the paraffin blocks together. The shield had a hollow cylindrical space 8in deep with diameter of 4in in the center in order for it to fit around the Faraday cup. This configuration put the end of the beamline approximately at the center of the shield.

Paraffin is a common name for a group of alkane hydrocarbons with general formula C_nH_{2n+2}. The solid paraffin is called paraffin wax (which was used for making the shield) for which $n \geq 20$. Thus the amount of *hydrogen* (H) atoms is ~67% and the amount Borax added was such that the *boron* (B) was ~5% in the shield. The

hydrogen acts as a very effective 'moderator' for the neutrons emitted from the ^{9}Li beam because the mass of *hydrogen* is almost the same as the neutron mass. Therefore the energetic neutrons that enter this paraffin block are scattered from several hydrogen atoms until their energy has become very low (thermal neutrons). The *boron* in the block then absorbs these thermalized neutrons effectively ($\sigma_{\text{thermal neutron}}$ = 5mb for ^{11}B [~80% abundance]). For a delayed n-emission intensity of $>10^{7}$ particles/s the measured neutron dose at 3m was 0.1 μSv/hr.

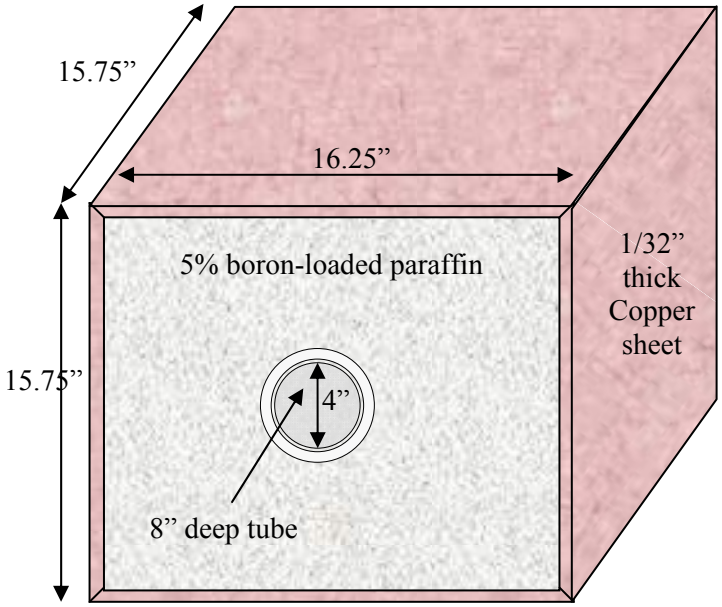

Figure 6.4 A shield of 5% boron-loaded paraffin as protection against the delayed n-emissions from ^{9}Li. Alternate layers of paraffin blocks and Borax powder were put in the cube and molten paraffin poured in to hold the paraffin blocks together. The shield had a hollow cylindrical space 8in deep with diameter of 4in in the center.

7 EXPERIMENTAL AND SETUP DETAILS

The experiment was performed at the Isotope Separator and Accelerator (ISAC) facility at TRIUMF which is designed to produce radioactive ion beams (RIB) using the protons from the 500MeV H^- cyclotron. Short-lived nuclei are produced in thick targets using the proton beam (with the maximum operational intensity being 100μA) and converted to a radioactive ion beam using the ISOL (Isotope Separation On-Line) method (Dombsky M. 2004). Fig7.1 shows the side and front view of the target and surface ion source assembly (Bricault P. 2003). The working of the target-ion source assembly and details of beam production are given in section 7.1. This facility was able to provide the ^{9}Li and ^{11}Li beams at required energies for measuring the fusion excitation functions for both isotopes with ^{70}Zn target (the intensities of both the beams were much less than the ones that were thought to be producible). The energy ranges were chosen such that they were below or near the fusion barrier for these reactions as given by the Bass model (calculations in section 5.2.3) and had intensities high enough to produce statistically significant fusion data.

The experiment was carried out at seven different energies of ^{9}Li beam. For each of the beam energy a new ^{70}Zn target was mounted in the chamber and it was irradiated for 1-3 days depending on the beam intensity so that all the targets received approximately the same beam dose. After the irradiation the target was counted in the γ counter for about a day (in the 2006 attempt) and subjected to radiochemical solvent extraction separation procedure subsequently. In the 2005 attempt low beam doses produced low activity in the target difficult to discern in the γ spectroscopy. The γ

counter also suffered from electronics malfunction and the *lead* bricks used for shielding were contaminated with *uranium* which produced a huge background.

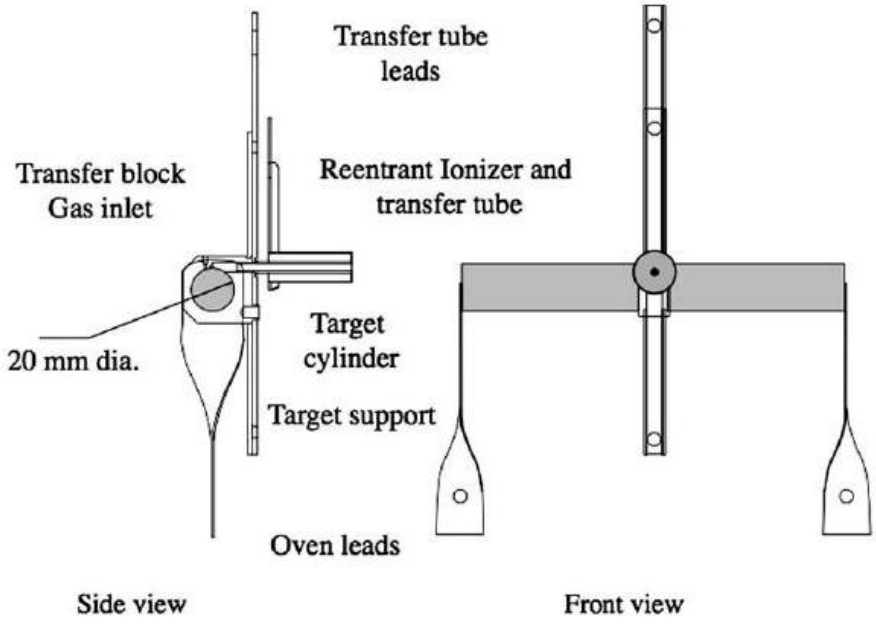

Figure 7.1 The side and front view of the target and surface ion source assembly at the ISAC facility at TRIUMF. It produces radioactive ion beams using the protons from the 500MeV H^- cyclotron. Short-lived nuclei are produced in thick targets using the proton beam (with the maximum operational intensity being 100μA) and converted to a radioactive ion beam using the ISOL method (Dombsky M. 2004).

The target was, therefore, directly subjected to radiochemical separation. The separated and dried precipitates of As_2S_3 and GeS_2 were then counted on the β counter for several days to establish the decay curve of the isotopes present.

7.1 Beam production and characteristics

500MeV proton beams with intensities ranging from 50-85μA (particle dose ~10^{20}) (100μA beam in case of the ^{11}Li beam production) struck the *tantalum* (Ta) metal production targets. The target design consists of a 19mm diameter tube made of

tantalum-tungsten (1:0.025) alloy in which the 18mm diameter discs of Ta metal (thickness ~25g/cm^2) are stacked perpendicular to the proton beam axis. The target is heated to ≈2200°C by passing DC current (Joule heating) through the target container. The high temperature aids the diffusion and effusion of the product nuclei. However as the proton beam intensity increases it results in heating up of the target and therefore the beam dumps are necessary for moderating the amount of energy transferred to the target. This decreases the need for the heating with DC current and the beam heating and Joule heating need to be balanced carefully in order to maintain the target temperature. Cooling is done by enclosing the targets within a water-cooled Cu heat shield (Dombsky 2004). Radioactive beams of ^{9}Li and ^{11}Li were extracted with energies up to 60eV, mass-separated by passage through two dipole magnets and accelerated to their final energy by radiofrequency (RF) quadrupole and drift tube linear accelerators. The beam struck the ^{70}Zn target mounted in the chamber and the intensities were monitored by measuring the elastic scattering in the two monitor detectors at ±16.2° and also by a suppressed Faraday Cup. The primary proton beam currents and the beam intensities in the two attempts made in 2005 and 2006 are given in Table 7.1.

The fusion excitation function for the reaction of ^{9}Li with ^{70}Zn was measured at seven different energies ranging between 11.5-15.4MeV and an attempt was made to measure the same with ^{11}Li beam at energies 16.5 and 17.5MeV. (The measurements with ^{11}Li were originally planned at beam energies in the range 12-18MeV. However, due to the low intensity (~700 particles/s) of the beams at 17.5MeV and 16.5MeV irradiations were not performed at lower energies.)

Table 7.1 The beam energy in lab frame, target thicknesses, energy loss in the beam when passing through the target, beam energy at center-of-target, radioactive beam dose and intensities for each beam energy of ^{9,11}Li.

Nuclide	E_{lab} (MeV)	Target thickness (mg/cm^2)	Energy loss (MeV)	E_{cot} (MeV)	Beam dose (particles)	Average beam intensity (particles/s)
^{9}Li	15.4	0.89	0.4	15.0	$3.08\text{x}10^{11}$	$8.45\text{x}10^{6}$
	15.4	1.21	0.5	14.9	$5.35\text{x}10^{11}$	$5.35\text{x}10^{6}$
	15.1	1.02	0.4	14.7	$4.16\text{x}10^{11}$	$3.38\text{x}10^{6}$
	14.5	1.06	0.4	14.1	$5.87\ \text{x}10^{11}$	$3.80\text{x}10^{6}$
	14.0	0.85	0.4	13.6	$5.76\text{x}10^{11}$	$4.00\text{x}10^{6}$
	13.5	1.28	0.5	13.0	$2.29\text{x}10^{11}$	$3.80\text{x}10^{6}$
	12.5	1.06	0.5	12.0	$1.07\text{x}10^{12}$	$3.51\text{x}10^{6}$
	11.5	1.07	0.5	11.0	$3.41\text{x}10^{11}$	$6.71\text{x}10^{6}$
^{11}Li	17.5	1.25	0.5	17.0	$1.19\text{x}10^{8}$	$7.79\text{x}10^{2}$
	17.5	0.95	0.4	17.1	$2.06\text{x}10^{8}$	$1.07\text{x}10^{3}$
	16.5	0.99	0.4	16.1	$7.77\ \text{x}10^{7}$	$4.56\ \text{x}10^{2}$

7.2 Setup in the beamline and detector lab

7.2.1 Experimental chamber setup

The experimental setup in the beamline is shown in fig7.2. The experiment was carried out in a large volume scattering chamber at the end of the straight-through HEBT (High Energy Beam Transport) beamline. The chamber had an inner diameter of 20in and two ports at angles ±16.2° with respect to the incident beam at beam height. A collimator was placed just inside the chamber wall in front of the opening which connected the beamline to the chamber. The target wheel was 6in upstream from the center of the chamber on which the target flaps could be mounted such that the targets would be perpendicular to the beam axis. The target wheel rotation mechanism was computer controlled. It had four positions for attaching flaps on it, in a vertical plane (fig7.3). The beam exit port extended about 30in and the Faraday cup was placed at a distance of 25in. A port in the bottom of the chamber was used for evacuating it to ~$5\text{x}10^{-6}$ torr. The chamber lid had a circular opening in which the

target wheel fit so that it could be manipulated without removing the entire chamber lid.

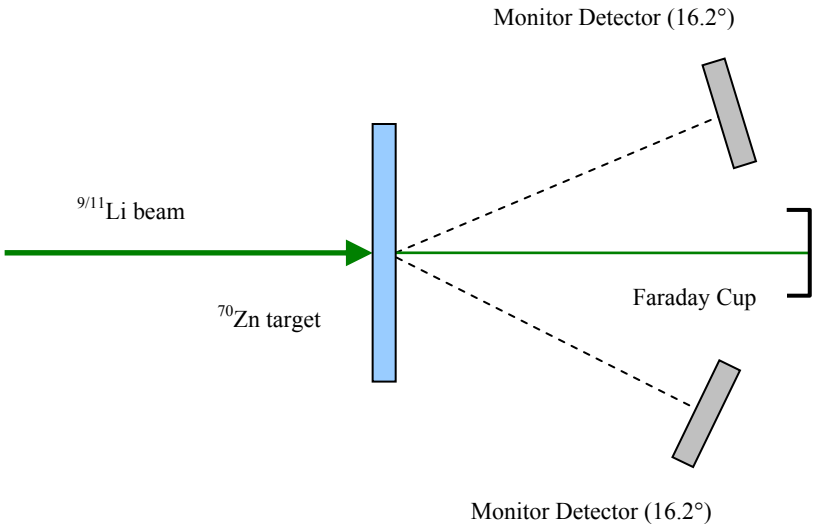

Figure 7.2 The figure shows the experimental setup in the chamber. Two silicon surface barrier (SB) detectors were mounted at about 40cm from the target at an angle of 16.2° on both sides of the beam to detect the elastically scattered fragments. A Faraday cup was situated at the end of the beamline, 35in downstream from the target. The target was perpendicular to the beam axis throughout the experiment.

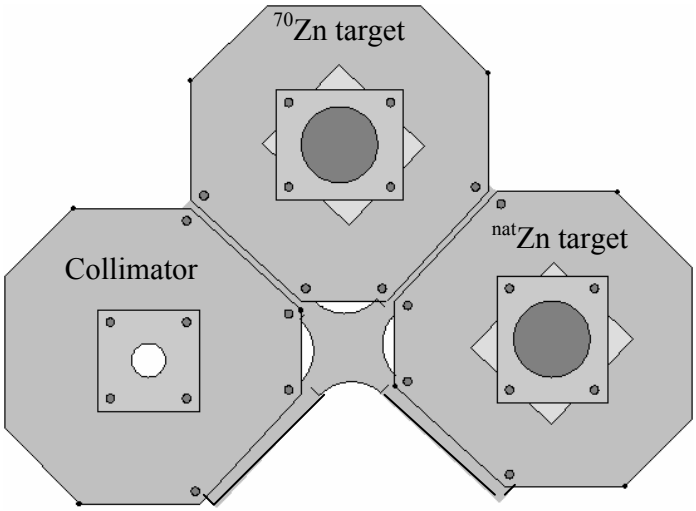

Figure 7.3 The target wheel had four positions for attaching the flaps, in a vertical plane. The collimator, a ^{nat}Zn target and a ^{70}Zn target could all be mounted at once in three different positions on the wheel as shown in the figure and rotated into position as needed with a computer controlled mechanism.

The ^{nat}Zn targets were used for checking the functioning of the electronics and the data acquisition (DAQ) and the isotopically enriched (~95%) ^{70}Zn targets were used for the actual experimental runs. The collimator for beam tuning, ^{nat}Zn target for a short check-run and ^{70}Zn target for actual run were all mounted at once in three different positions on the wheel and rotated into position as needed.

A 300mm^2 *silicon* surface barrier (SB) detector was mounted in each port at about 40cm from the target at an angle of ±16.2° to detect the elastically scattered fragments. These counts were used to calculate the beam intensities (particles/sec) as a backup to the Faraday cup readout. The emission of 13.6MeV β particles from ^{9}Li might have made the Faraday cup respond unexpectedly and hence this additional way of monitoring the beam intensity was used. The β emission has a branch of 50.80% resulting in delayed n-emission which, given the intensities of the ^{9}Li beams (~5x10^6 particles/s), was a considerable flux of neutrons (~2.5x10^6 particles/s).

7.2.2 Beta counter setup

A Tennelec LB1000 low background beta counter, with 6.6% detection efficiency, was used for counting the activity of the separated As and Ge EVRs. This system has been designed for ultra low-level detection of alpha and beta radiation. The system has two basic parts, the detector/shielding assembly with its associated gas transport unit and the electronics assembly. The detector/shielding are made up of sliding sample holder, a sample gas flow proportional counter and a guard gas flow proportional counter. The P-8 gas is supplied from a gas bottle to the proportional counters at the rate of 0.125scfh (cubic feet per hour at standard temperature and pressure). The shielding plays a dual role of reducing the background as well as acting as housing for

the detector tray. The electronic modules include the pre-amplifiers, the amplifier/analyzers, timers and scalers. The detector was calibrated using β sources with β endpoint energies ranging 0.156-0.709MeV and efficiency of the detector was also determined using these data. The details of these calculations are given in section 8.2.1.

7.2.3 Gamma counter setup

The detector used for γ counting of the irradiated target was an ORTEC High Purity Germanium (HPGe) coaxial γ detector with 2.0% detection efficiency. The detector assembly consists of two main parts, the detector system and the cryostat. The detector is cooled using liquid *nitrogen* (LN_2) and the cryostat functions as the connection and supply-route between the LN_2 Dewar flask and the detector system. The detector system consists of a high voltage supply, an HPGe detector and a pre-amplifier which are all enclosed in a casing. The detector bias supply, the precision pulse generator, the amplifier and the count rate meter are situated outside the detector casing. The data were acquired using the ORTEC DSpec module which was connected to a computer where the γ spectra were stored for later analysis. The detector was calibrated using the NIST (National Institute of Standards and Technology) calibrated ^{60}Co, ^{137}Cs, ^{152}Eu γ ray standards and efficiency of the detector was determined using these data. Details of these calculations are given in section 8.2.2.

7.3 Electronics and Data acquisition in the beamline and detector lab

7.3.1 Experimental chamber setup

The electronics setup in the experimental chamber (fig7.4) consisted of connecting the appropriate electronic and logic modules to the two SB monitor detectors. Each

detector was biased to +50V through a pre-amplifier. The outputs of pre-amplifier were split and connected to a timing filter amplifier (TFA) and to a slow amplifier.

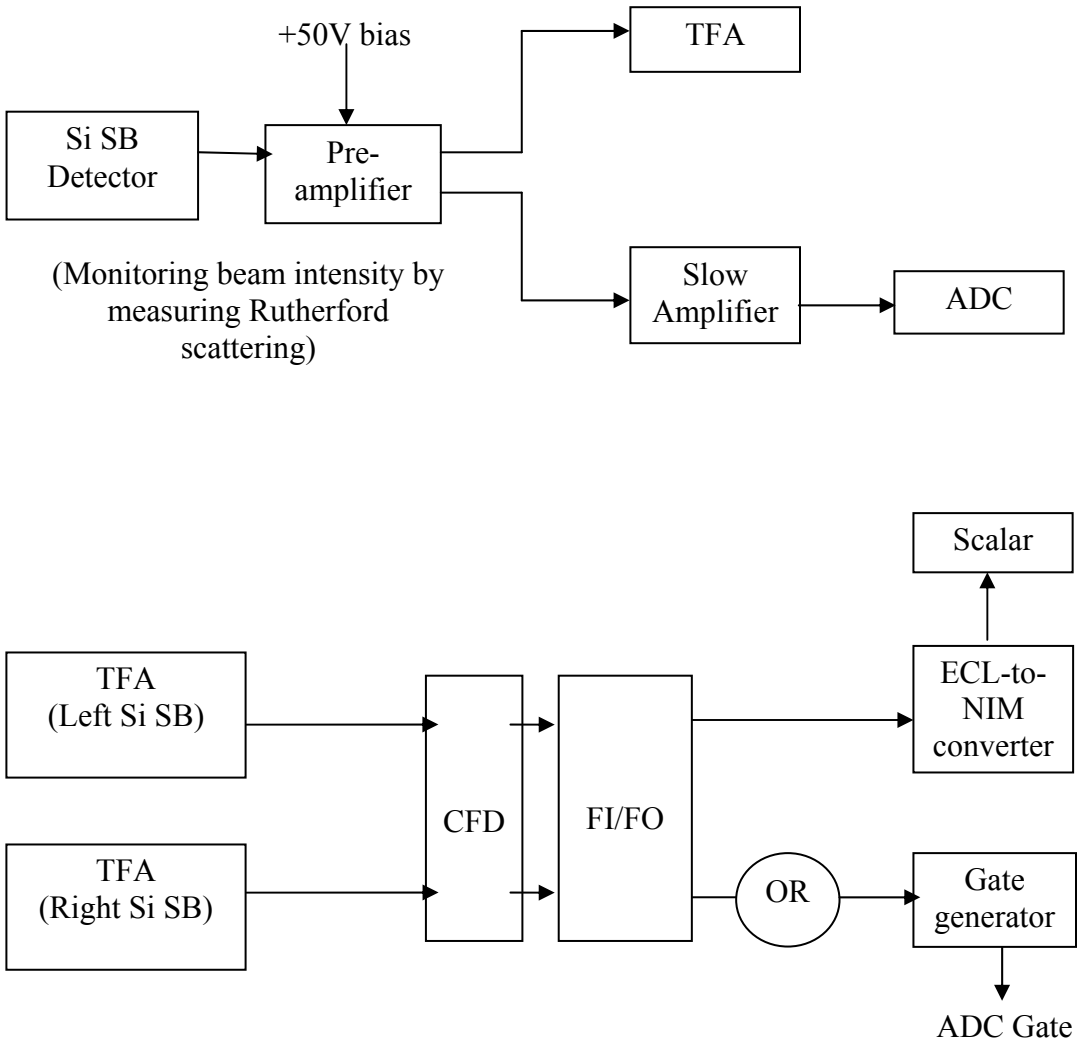

Figure 7.4 The electronics setup in the experimental chamber depicts the connection made from the SB monitor detectors to produce the signals and scalers for DAQ.

The output of the slow amplifier was then fed into an analog-to-digital converter (ADC). The outputs of the TFA's of all the three Si detectors were fed into a constant fraction discriminator (CFD) and then connected to a fan-in-fan-out (FI/FO) module. One output of the FI/FO was sent to an ECL-to-NIM converter, output of which gave a scaler for each detector. These scalers, which signified the number of particles undergone Rutherford scattering, were later used to calculate the beam dose for each run. The other output of the FI/FO was fed into logic OR which sent its output to a gate generator which produced the gate for data acquisition in the ADC's.

The data acquisition (DAQ) at the beamline, which recorded the data acquired from the Si monitor detectors and the Faraday cup, was done using the MIDAS software in 2005 attempt and using SpecTcl software in 2006. The communication between various controls like the vacuum system, the beam characteristics etc. and their display on computer monitors was made possible through the EPICS system in use at TRIUMF.

The Maximum Integrated Data Acquisition System (MIDAS) is a general-purpose system for event based data acquisition in small and medium scale physics experiments (TRIUMF 2000). It has been developed at the Paul Scherrer Institute (Switzerland) and TRIUMF (Canada) between 1993 and 2000. It is based on a modular networking capability and a central database system. MIDAS consists of a C library and several applications. They run on many different operating systems like UNIX-like, WindowsNT and MS-DOS and can be used with CAMAC, VME and FASTBUS systems. The MIDAS DAQ provides data collection from a local and/or remote hardware source and data recording to common storage media along with full

data-flow control. It is also capable of event-by-event analysis through PAW or Root-based applications.

SpecTcl is a powerful nuclear event data analysis tool developed at the National Superconducting Cyclotron Laboratory of Michigan State University (NSCL 1999). It provides an object oriented C++ framework for histogramming and other data analysis operations. The Tcl/TK scripting language is embedded as the program's command language, providing the user with a powerful, extensible, command set as well as the ability to build custom graphical user interfaces or extend existing ones. The Xamine display program provides SpecTcl with a powerful visualization component. It runs on the Linux operating system.

Experimental Physics and Industrial Control System (EPICS) is a set of software tools and applications which provide a software infrastructure for use in building distributed control systems to operate devices such as particle accelerators, large experiments and major telescopes (ANL 1993). Such distributed control systems typically comprise tens or even hundreds of computers, networked together to allow communication between them and to provide control and feedback of various parts of the device from a central control room, or even remotely over the internet. It was originally written jointly by Los Alamos National Laboratory and Argonne National Laboratory EPICS uses Client/Server and Publish/Subscribe techniques to communicate between the various computers. Most servers (called Input/Output Controllers or IOCs) perform real-world I/O and local control tasks, and publish this information to clients using the Channel Access (CA) network protocol.

7.3.2 Beta counter setup

The electronic setup for the β counter is shown in fig7.5. The β counter consisted of a sample gas flow proportional counter and a guard gas flow proportional counter which were filled with P-8 gas.

In proportional counters the conducting walls are the cathodes and a thin metal wire is the anode. A positive bias voltage is applied to the anode from a high voltage power supply. When a charged particle (in this case β) enters the proportional counter the filled gas is ionized. The electrons flow to the anode which gives rise to a pulse whose magnitude is proportional to the number of electrons produced.

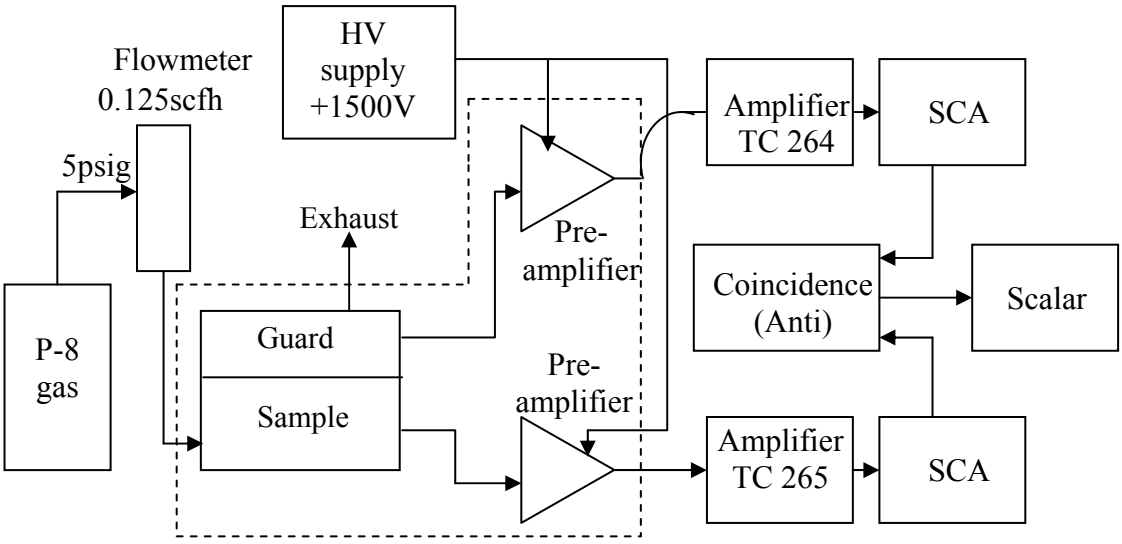

Figure 7.5 Figure shows the electronics setup within and outside the Tennelec LB 1000 low background β counter. The guard and sample gas flow proportional counters as well as the pre-amplifiers are enclosed inside the detector casing. The P-8 gas is supplied from a gas bottle at the rate of 0.125scfh. The data were acquired with 'anti-coincidence' condition put on the SCA outputs.

Both the counters were biased to +1500V through pre-amplifiers. The pre-amplifiers were connected to amplifiers (TC264 for guard counter and TC265 for

sample counter) whose outputs were fed into single channel analyzers (SCA). The pulses from both the SCAs were sent to a scaler which showed the number of ionizing particles detected in a digitized form.

The guard proportional counter is employed for canceling high energy cosmic rays and electronic noise from counting. The low energy (soft) cosmic rays are stopped by the lead shielding surrounding the counter unlike the high energy (hard) cosmic rays. Such cosmic rays penetrate both the sample and the guard counters and produce large pulses in both counters. The counts are, therefore, registered in the scaler only when the sample counter produces a pulse and there is no pulse from the guard. This 'anti-coincidence' condition put on the outputs of the SCAs ensures that cosmic rays are not counted. The counts resulting from this logic condition were output on a scaler readout which was then recorded manually at the end of each counting period.

7.3.3 Gamma counter setup

The electronics circuit for the γ counter is shown in fig7.6. The connections between pre-amplifier and the detector and between the high voltage filter and the detector are made through the cryostat vacuum feedthroughs beforehand as these parts are housed inside the electronics shield. The detector was cooled with LN_2 and then the remaining electronics connections were made as shown in the figure. Bias voltage was supplied to the detector by passing it through the high voltage filter. Attenuated output of a precision pulse generator was connected to test input of the pre-amplifier and its output was fed into an amplifier. The amplifier output was connected to the DSpec data acquisition module and the spectra were saved on a computer using the MAESTRO software.

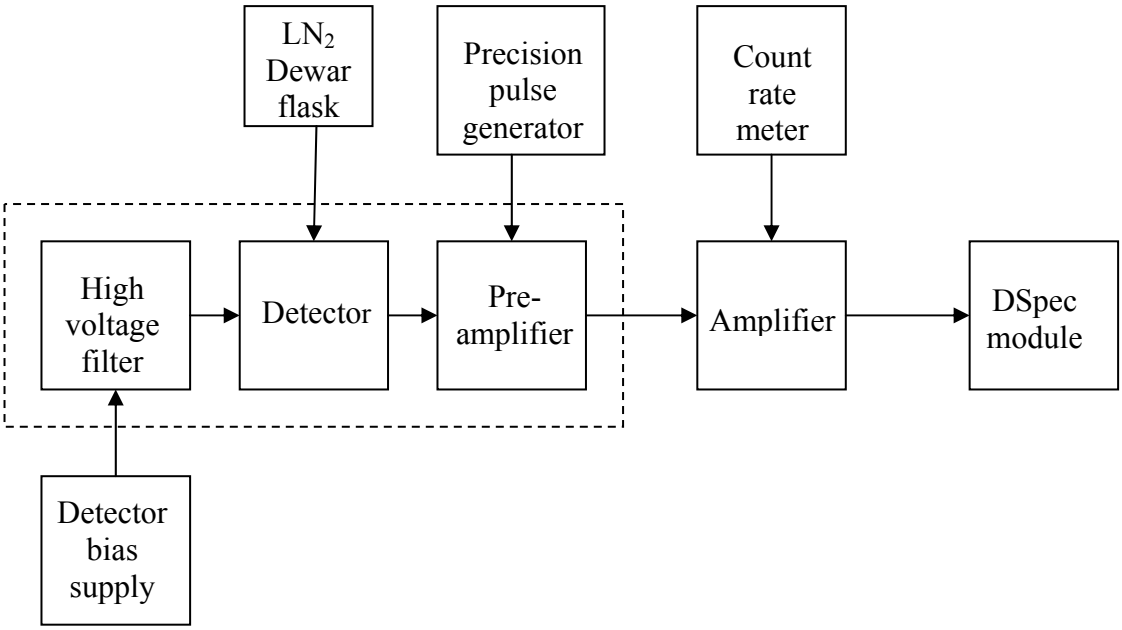

Figure 7.6 Figure shows the electronics setup within and outside the ORTEC HPGe coaxial γ detector. The high voltage filter, the detector and the pre-amplifier are enclosed inside the cryostat casing. The LN_2 gas is supplied from a Dewar flask. The data were acquired with DSpec module.

8 DATA ANALYSIS

8.1 Calculation of beam dose from elastically scattered particles

The beam dose was monitored by detecting the elastically scattered beam using two monitor detectors at ±16.2° with respect to the beam. The counts were recorded in the logbook intermittently along with the time of recording from which the duration of each of the runs was obtained. The 'ruthwaltcor3.for' program (from Walter Loveland) was used to obtain the integrated beam dose for each run. The program takes as an input the atomic and mass numbers of both target and projectile, the beam energy (MeV/A), number of particles undergone Rutherford scattering (scalers recorded from the two monitor detectors), the target thickness (mg/cm^2) and the total duration of the run (sec). From these parameters it calculates the differential Rutherford cross sections ($d\sigma_{Ruth}/d\Omega$) in center-of-mass and lab frames of reference as well as the total beam current (pnA) for that run. For the ^{9}Li+^{70}Zn system and beam energies used in our experiment, the grazing angle in lab frame ($\theta_{gr\ (lab)}$) = 45°-61° as calculated by formulas given below (GSI 2001).

$$\theta_{gr(lab)} = \frac{2.88 \times Z_1 Z_2 \times \left[931.5 + \left(E_{lab}/A_P\right)\right]}{A_P\left[\left(E_{lab}/A_P\right)^2 + \left\{1863 \times \left(E_{lab}/A_P\right)\right\}\right]} \times \frac{1}{R_{\text{int}}} \qquad \textbf{8-1}$$

$$R_{\text{int}} = 1.2 \times \left(A_P^{\,1/3} + A_T^{\,1/3}\right) + 3.2 \qquad \textbf{8-2}$$

The $\theta_{gr\ (lab)}$ is given in units of radians (rad) by 8-1 and the interaction radius used in the calculation is given by 8-2. The monitor detectors were at ±16.2° with respect to the beam, well inside $\theta_{gr\ (lab)}$ where $\sigma_{Ruth} = \sigma_{elas}$. Therefore, the $d\sigma_{Ruth}/d\Omega$ calculated by the program routine can be used to calculate the beam dose.

The formulae employed by the program to calculate various quantities are discussed in some detail below. The beam energy was converted from lab frame to center-of-mass (CM) frame using the formula

$$E_{CM} = E_{lab}\frac{A_t}{A_p + A_t} \qquad \textbf{8-3}$$

where, E_{lab} - Energy per nucleon of projectile beam in lab frame (MeV/A)

A_p, A_t - Mass numbers of projectile and target, respectively

The angles at which the monitor detectors were placed were converted from degrees to radians and then from lab frame to center-of-mass frame as follows

$$\theta_{CM} = \arcsin\left(A_p\frac{\sin\theta_{lab}}{A_t}\right) + \theta_{lab} \qquad \textbf{8-4}$$

The differential Rutherford cross section was calculated by means of formula

$$\left(\frac{d\sigma_{RUTH}}{d\Omega}\right)_{CM} = \left(\frac{3.6\times10^{-14}\times Z_p\times Z_t}{E_{CM}}\right)^2 \Bigg/ \left(\sin\left(\frac{\theta_{CM}}{2}\right)\right)^4 \qquad \textbf{8-5}$$

The most important step in the calculation was the conversion of the $(d\sigma_{RUTH}/d\Omega)_{CM}$ to $(d\sigma_{RUTH}/d\Omega)_{lab}$. This Jacobian transformation was performed via the formula below.

$$\left(\frac{d\sigma_{RUTH}}{d\Omega}\right)_{lab} = \frac{1.00}{\cos(\theta_{CM}-\theta_{lab})}\times\left(\frac{d\sigma_{RUTH}}{d\Omega}\right)_{CM}\times\left(\frac{\sin\theta_{CM}}{\sin\theta_{lab}}\right)^2 \qquad \textbf{8-6}$$

The number of target atoms was calculated utilizing the formula

$$\text{Number of target atoms} = \frac{\text{Weight of target material}\times N_A}{A_t} \qquad \textbf{8-7}$$

where N_A– Avogadro's number ($6.023\text{x}10^{23}$)

Using this number and the number of Rutherford scattered particles the rate of projectile bombardment was calculated. The beam current was then calculated in particle nanoamperes (pnA).

$$\text{pnA} = \frac{\text{Rate of projectile bombardment}}{6.25\times10^{9}\,\text{particles of charge one per second}} \qquad \textbf{8-8}$$

The energy loss of the elastically scattered ^{9}Li off ^{70}Zn as well as the ^{27}Al-foil backing of the target was calculated using the kinematics calculation spreadsheet 'Catkin' (Catford 2002). The energy loss of the 15.4MeV beam elastically scattered off of the ^{27}Al backing was 0.385MeV and of that scattered off of the ^{70}Zn target material was 0.149MeV at the angle of 16.2°. The differential cross section ($d\sigma_{RUTH}/d\Omega$) was calculated using 8-5 where the beam energy in center-of-mass frame is given by 8-3. Using 8-3 kinetic energy of ^{9}Li beam at 15.4MeV is calculated in center-of-mass frame as

$$T_p^{\,CM} = 15.0\left(\frac{27}{9+27}\right) = 11.25MeV$$

Using this value in 8-5 the differential Rutherford cross section for the ^{9}Li + ^{27}Al is

$$\frac{d\sigma_{RUTH}}{d\Omega} = \left(\frac{(3)(13)(1.44)}{(4)(11.25)}\right)^{2}\frac{1}{\sin^{4}(16.2/2)} = 395157\,fm^{2}/sr = 3.9\times10^{4}\,mb/sr$$

Carrying out similar calculation for ^{9}Li + ^{70}Zn gives ($d\sigma_{RUTH}/d\Omega$) of 1.51x10^{5}mb/sr.

The number of particles scattered off of both the target and the backing can be calculated as

$$N\sigma = \frac{\text{Weight of target material}}{A_t}\times N_A \times \left(\frac{d\sigma}{d\Omega}\right) \qquad \textbf{8-9}$$

Putting the appropriate values for ^{70}Zn target in 8-9

$$N\sigma = \frac{1\times10^{-3}}{70}\times\left(6.023\times10^{23}\right)\times\left(1.48\times10^{5}\right)=1.3\times10^{24}$$

Performing similar calculation for ^{27}Al backing foil one gets a value of 5.44x10^{23}. These numbers indicate that the amount of ^{9}Li scattered due to backing were about 42% of the ones scattered by the ^{70}Zn. This fact was taken into consideration in the calculation of the beam doses for all the runs and appropriate corrections were made.

8.2 Detector calibration and efficiency calculations

The efficiencies of both Tennelec LB1000 low background β counter and the high purity Germanium (HPGe) γ detector were determined using the β calibration standards with $E_{max}\beta$ = 0.156-0.709MeV and the NIST (National Institute of Standards and Technology) calibrated γ ray standards ^{60}Co, ^{137}Cs and ^{152}Eu, respectively.

8.2.1 Beta counter calibration and efficiency calculations

The efficiency of the β counter is inversely proportional to the energy of the particle being detected. Therefore various β emitters with their β end point energies ($E_{max}\beta$) spread over a range were used for calculating the efficiency of the β counter. 10min counts were taken using ^{14}C, ^{36}Cl, ^{90}Sr, ^{99}Tc and ^{147}Pm calibrated β sources and the efficiency of the detector was determined for each one. A sample calculation is shown below with a ^{90}Sr ($t_{1/2}$ = 28.78yrs) source calibrated at 1295Bq on October 1, 1992. The calculations for the expected activity on February 20, 2007 were done as follows,

$$A_t = A_0 e^{-\frac{0.693}{t_{1/2}}\times t} \qquad \textbf{8-10}$$

$$A_t = (1295)e^{-\left(\frac{0.693}{28.78}\right)\times 15.39} = 894\text{Bq}$$

The observed counts in 10min were 60720 giving the disintegration rate of 101.2Bq. Therefore the efficiency was calculated to be

$$\text{Efficiency} = \frac{\text{Observed disintegration rate}}{\text{Expected disintegration rate}} \times 100\% \qquad \textbf{8-11}$$

$$\text{Efficiency} = \frac{101.2}{894.0} \times 100 = 11.32\%$$

Similar calculations were done for all the calibrated β sources and the results are summarized in Table 8.1. The β end point energies of these nuclides ranged from 0.156MeV to 0.709MeV. Since the β end point energy of ^{76}As is 2.97MeV the efficiency of the β counter for this nuclide was determined by extrapolation (fig8.1) to be 6.6% and was incorporated in all cross section calculations based on beta counter data.

Table 8.1 Details of the counts and calculations to determine the efficiency of β counter

Nuclide	E_{max} β (MeV)	$t_{1/2}$ (y)	Calibration date	Expected activity (dps)	Observed activity (dps)	Efficiency (%)
^{14}C	0.156	5715	Aug 6, 1985	5831	703.2	12.06
^{147}Pm	0.225	2.6	Mar 28, 1985	11	1.3	11.97
^{99}Tc	0.292	$2.1\text{x}10^5$	Oct13, 1983	1406	168.2	11.96
^{90}Sr	0.546	28.78	Oct 1, 1992	894	101.2	11.32
^{36}Cl	0.709	$3\text{x}10^5$	Apr 4, 1985	677	74.7	11.04

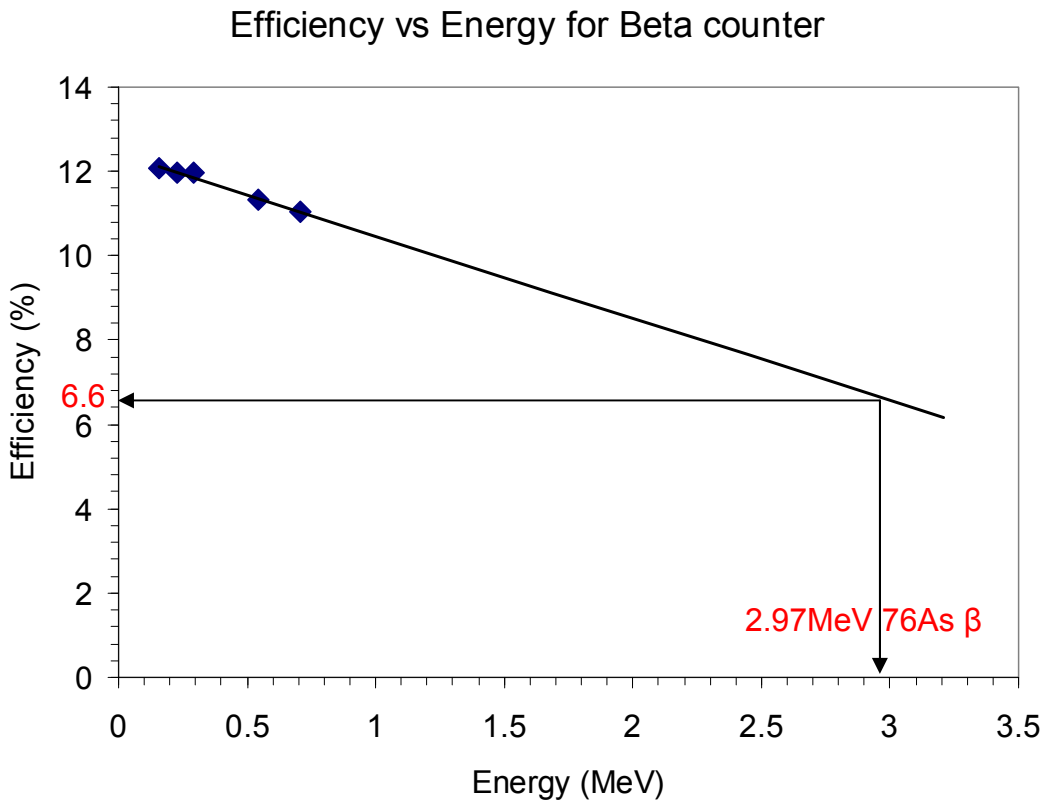

Figure 8.1 The plot shows the percent efficiencies of the beta counter for five different energies of beta particles emitted by the radionuclides ^{14}C, ^{36}Cl, ^{90}Sr, ^{99}Tc and ^{147}Pm. The efficiency for the 2.97MeV β emission is determined to be 6.6% by extrapolation.

8.2.2 Gamma counter calibration and efficiency calculations

The standards used for efficiency determination of the γ counter were ^{60}Co, ^{137}Cs and ^{152}Eu. The calculations were similar to those done for the β counter efficiency. Several 10min counts were taken with each source. Expected disintegration rate was calculated based on 8-10 and the efficiency was calculated for each one using 8-11. A sample calculation for the ^{60}Co source calibrated as having disintegration rate of 2.8×10^5Bq on August 23, 1966 is shown below.

$$A_t = \left(2.8\times10^5\right)e^{-\left(\frac{0.693}{5.27}\right)\times39.77} = 1499.41Bq$$

$$\text{Efficiency} = \frac{53.07}{1499.41}\times100 = 3.53\%$$

The efficiency of the counter was obtained by plotting the efficiencies for the γ lines of ^{60}Co (1.17 and 1.33MeV), ^{137}Cs (0.66MeV) and ^{152}Eu (0.12, 0.24, 0.34, 0.44, 0.78, 0.87, 0.11, 0.13 and 0.14MeV) against the energies and fitting the data. This plot is shown in fig8.2 which gave an efficiency of 2.0% for the 559keV γ line emitted by ^{76}As.

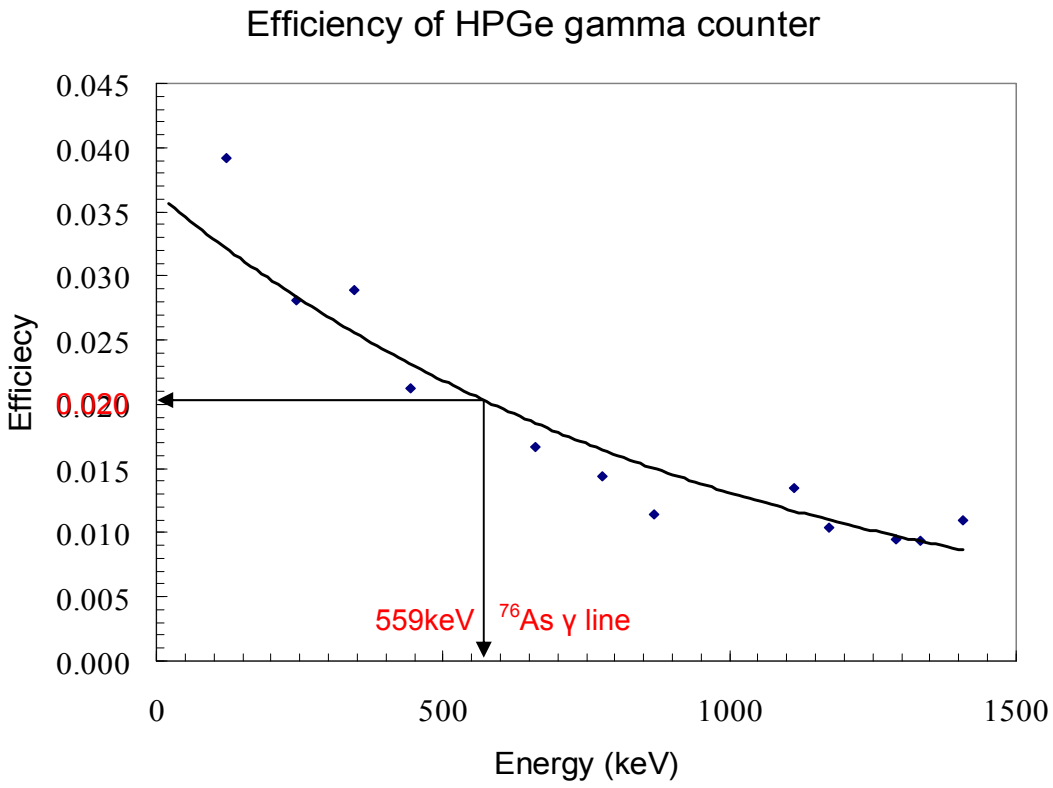

Figure 8.2 The efficiency was obtained by plotting the detector efficiencies for γ lines of ^{60}Co (1.17 and 1.33MeV), ^{137}Cs (0.66MeV) and ^{152}Eu (0.12, 0.24, 0.34, 0.44, 0.78, 0.87, 0.11, 0.13 and 0.14MeV) and fitting the data. The plot, shown in the figure, gave an efficiency of 2.0% for the 559keV γ line emitted by ^{76}As.

8.3 Isotopic purity of ^{70}Zn targets

The isotopic purity of the targets was determined by carrying out a neutron activation analysis (NAA) of one of the targets. The isotopic composition of the target was expected to be nearly 100% ^{70}Zn with some impurities of ^{nat}Zn. The prominent radioactive nuclide that would be produced by NAA of the target was ^{71}Zn ($t_{1/2}$ = 3.97h). The ^{70}Zn coated on the Al-backing foil was dissolved with dil. HNO_3 and the foil was rinsed with DI water which was added to the ^{70}Zn solution in HNO_3. This solution was then subjected to an hour long thermal neutron irradiation along with a standard solution of ^{70}Zn. Both the samples were counted for 5min each after an hour long irradiation. Knowing the activity present in the sample (A_t) at given time after activation (t) the end-of-bombardment (EOB) activity (A_0) was calculated using 8-10. Details of counting and activities are summarized in Table 8.2.

Comparative analysis was done based on the weight of ^{70}Zn in the standard (0.34mg) and the EOB activities calculated for both the standard and the target to arrive at the weight 2.77mg for ^{70}Zn in the target. Therefore, the isotopic composition of the target (3.46mg of electroplated material) was 80.58% ^{70}Zn. The remaining 19.42% was assumed to be other isotopes of Zn (predominantly ^{64}Zn indicated by the presence of 1115keV γ line) due to the absence of any other prominent γ lines. These results for the isotopic composition of the target were incorporated in the fusion cross section calculations by both β and γ analysis.

8.4 Chemical yields of As and Ge precipitates

Even though the percent chemical yields for As and Ge precipitates were calculated based on the weights recorded at the end of each separation, a more

accurate calculation was performed by neutron activation of the precipitates along with 1ml standard As and Ge carriers used. The samples were irradiated for an hour in the 1.1MW TRIGA reactor at OSU. The percent chemical yield for each As and Ge precipitate at each beam energy was calculated based on formula

$$\text{Percent chemical yield} = \frac{\text{Counts from precipitate}}{\text{Counts from standard}} \times 100\% \qquad \textbf{8-12}$$

Table 8.2 Details of activated sample counting to determine the isotopic composition of the targets used in the experiment

Nuclide (Sample)	Counts (per 5min)	A_t (cps)	Time since irradiation (h)	A_0 (cps)	Weight (mg)	Isotopic composition (%)
^{71}Zn (standard)	125	0.42	20.20	14.29	0.34	-
^{71}Zn (target)	1086	3.62	19.88	116.46	2.77	80.58

The counts at EOB (A_0) were calculated from the counts observed at the counting time (A_t), half-life of the nuclide ($t_{1/2}$) and the time interval (t) utilizing formula given in 8-10. A sample calculation for the As precipitate from the ^{9}Li run with beam energy 13.5MeV is shown below. Calculation of activity at EOB for the 1ml As (^{76}As $t_{1/2}$ = 1.07d) standard counted 2.04hrs after EOB,

$$A_0 = \frac{A_t}{e^{-\frac{0.693}{t_{1/2}} \times t}} = \frac{165348}{e^{-\frac{0.693}{25.68} \times 2.04}} = 174706$$

Calculation of activity at EOB for the As (^{76}As $t_{1/2}$ = 1.07d) precipitate counted 2.39hrs after EOB,

$$A_0 = \frac{A_t}{e^{-\frac{0.693}{t_{1/2}} \times t}} = \frac{158835}{e^{-\frac{0.693}{25.68} \times 2.39}} = 169417$$

Employing 8-12 for obtaining the percent chemical yield

$$Percent\ chemical\ yield = \frac{169417}{174706} \times 100\% = 96.97\%$$

Table 8.3 gives a summary of the percent chemical yields for all the precipitates produced with the ^{9}Li and the ^{11}Li beams.

Table 8.3 The percent chemical yields for the As and Ge precipitates obtained by radiochemical separation from the irradiated target (beam energies in laboratory frame)

Projectile	E_{lab} (MeV)	Precipitate	Chemical yield (%)
Year 2005			
^{9}Li	15.4	As	34.2
	13.5	As	96.9
	11.5	As	90.9
^{11}Li	15.5	As	99.7
Year 2006			
^{9}Li	15.1	As	27.1
		Ge	31.9
	14.5	As	43.5
		Ge	22.4
	12.5	As	52.2
		Ge	28.3
	14.0	As	43.5
		Ge	23.9
^{11}Li	17.5	As	63.7
		Ge	3.0
	16.5	As	59.3

8.5 Beta counting analysis

A Tennelec LB1000 low background beta counter, with efficiency of 6.6%, was used for counting the activity in separated As and Ge EVRs. The decay of these precipitates was followed for several days in order to obtain a decay curve for establishing the identity of the isotopes present in the precipitates. The activity was measured and recorded in 100min intervals. The counts were plotted versus time using

ORIGIN (fig8.3). The decay data were then resolved using DECHAOS software which consists of various FORTRAN program routines.

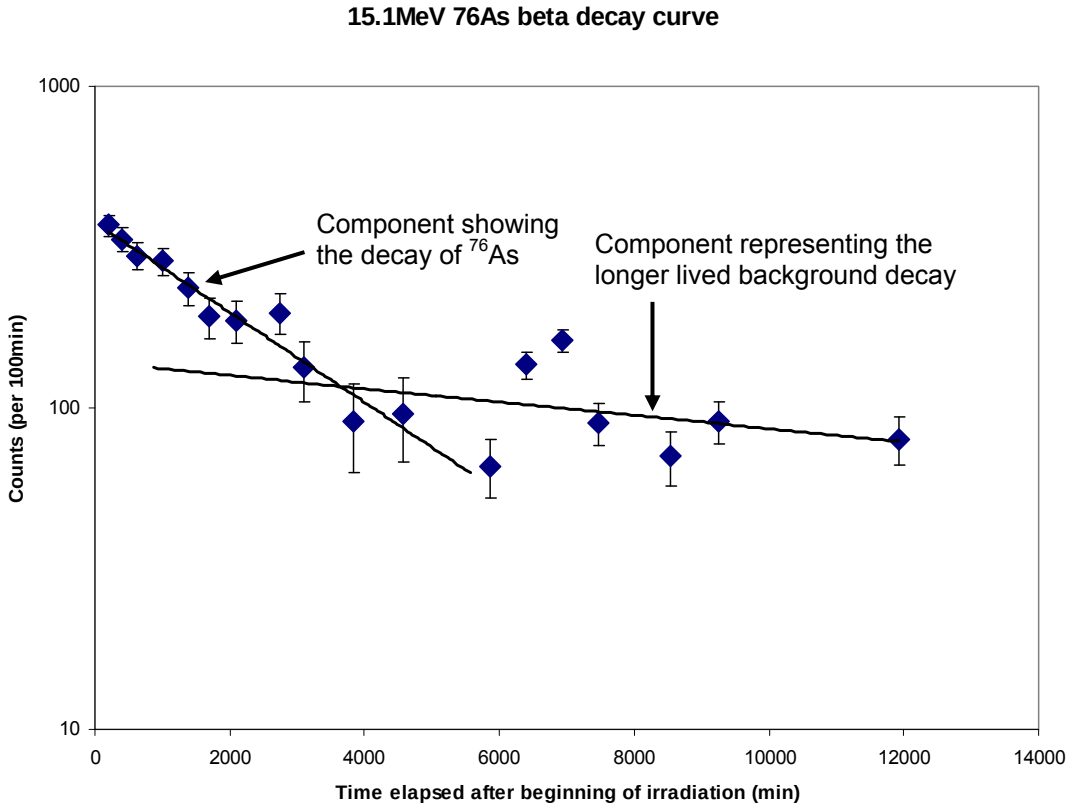

Figure 8.3 The decay of radiochemically separated As and Ge precipitates was followed for several days to establish their decay curves. These data were recorded manually during the experiment and were plotted using ORIGIN later. The figure shows one such decay curve for the As precipitate from the 14.7MeV ^{9}Li + ^{70}Zn. The resolution of the curve into two components is apparent, one representing ^{76}As decay and other depicting long-lived background.

'Dehl2.for' (from Walter Loveland) is an error weighed least squares decay curve fitting program which read in the counting data and gave the half-life ($t_{1/2}$) and initial activity (A_0) of the given nuclide, error in the initial activity (σ_{A0}) and data-fitting plots with χ^2 values. 'Desort.for' (from Walter Loveland) read in this output and

converted the error to percent error. The absolute activity at EOB and the half-life values, along with the beam doses calculated from monitor detector scalers, were then used in the program 'CROSS.for' (from Walter Loveland) to arrive at the production cross sections (σ_{prod}) with the corrections for the detector efficiency, the chemical yield and isotope correction applied to them. Details of the calculations are given in section 8.7.1. This analysis was performed only with the As precipitates data since from the half-life values given by the DECHAOS analysis ^{76}As was the predominant isotope and Ge precipitates did not show statistically significant activity. The upper limit cross sections (2σ) for the ^{75}Ge and ^{77}As were calculated as 0.1mb.

The counting was done by utilizing the As_2S_3 precipitates on filter papers produced in the radiochemical separation procedure. For such samples 'self-absorption correction' needs to be applied as some of the β emissions tend to get absorbed in the precipitate and are not detected. The thicknesses of these precipitates ranged from 5 to 18 mg/cm^2. ^{76}As tracer was produced by irradiating 1ml of 10mg/ml As standard and five As_2S_3 precipitates were made with 0.1ml tracer in each. The thicknesses ranged 3.71-25.98 mg/cm^2 (details in Table 8.4). The precipitation efficiency was determined to be ~90% for all the precipitates by weighing the completely dried precipitates. All precipitates were counted in the β counter along with a 0.1ml irradiated As standard. A plot was made of precipitate thickness against the correction factor (fig8.4) obtained by comparative analysis of the counts obtained from the standard and each of the precipitates. Based on the precipitation efficiency 90% of the observed counts for standard were used in calculations. The self-absorption correction factors for the precipitates used for β counting analysis were determined based on this curve and are

tabulated in Table 8.5. These were incorporated in the cross section calculations with β data.

Table 8.4 Details of self-absorption correction analysis and the correction factors obtained.

Tracer (ml)	Standard (ml)	^{76}As (mg)	Total As (mg)	Area density (mg/cm^2)	Counts (1min)	Correction factor
0.1	0.0	1	1	Liquid	2605	-
0.1	0.3	1	4	3.71	2579	0.99
0.1	1.1	1	12	11.14	2532	0.97
0.1	1.9	1	20	18.56	2364	0.91
0.1	2.7	1	28	25.98	2219	0.85

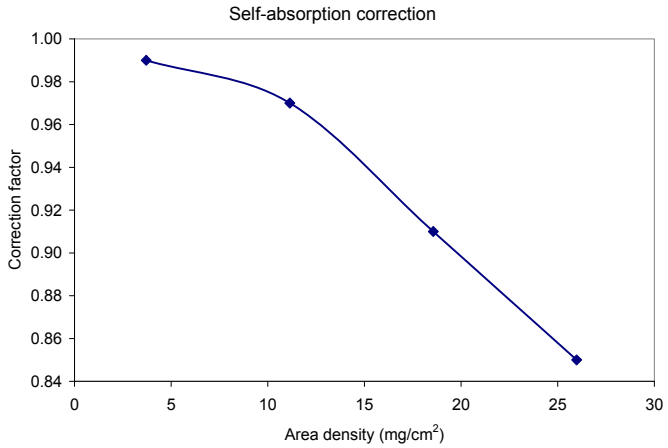

Figure 8.4 Plot of self-absorption correction factor vs. area density of As_2S_3 targets. This plot was used to deduce the correction factors for the precipitates produced in the experiment and incorporated into the β data analysis of the same.

Table 8.5 The self-absorption correction factors for the precipitates used for β counting analysis determined based on the curve shown in fig8.4 are tabulated.

E_{lab} (MeV)	Target thickness (mg/cm^2)	Self-absorption correction
15.4	6.35	0.987
15.1	5.03	0.990
14.5	8.07	0.980
14.0	8.07	0.980
13.5	17.98	0.909
12.5	9.69	0.978
11.5	16.87	0.920

8.6 Gamma counting analysis

The detector used for γ counting was a large volume high purity Germanium (HPGe) γ detector with efficiency ~2%. The efficiency was determined using the NIST (National Institute of Standards and Technology) calibrated γ ray standards. The analysis was performed only for the data taken at 14.0, 14.5 and 15.1MeV ^{9}Li beams. The reasons for not considering the 2005 data are listed in chapter 7. The beam intensity for the lowest energy of ^{9}Li in 2006 was too low to produce a statistically significant activity in the target and the data from this run was, therefore, not used for calculations either.

The program 'Handanal.for' (from Walter Loveland) read in the ASCII γ spectra and gave the peak areas and uncertainties. The formulae used for the calculations were,

$$\text{Absolute area of peak} = \text{Area of peak} - \text{Background} \qquad \textbf{8-13}$$

$$\text{Uncertainty} = \sqrt{\text{Absolute area of peak} + \text{Background}} \qquad \textbf{8-14}$$

These peak areas and uncertainties were input into DECHAOS software (programs 'Dehl2.for' and 'Desort.for') which fitted the data and gave the half-life and absolute activity at EOB with percent error. These values and the beam dose were then processed through 'CROSS.for' to output the σ_{prod} with the appropriate corrections applied.

8.7 Calculation of the cross sections

8.7.1 Production cross section (σ_{prod})

The calculation of production cross section (σ_{prod}) was carried out in the program 'CROSS.for'. The input of the program was the beam dose given to the target, the

half-life of the isotope for which the cross section was to be calculated and the EOB activity (along with the error) in the target for the same. The later two quantities were obtained by employing the DECHAOS software. The former was calculated using the 'ruthwaltcor3.for' program for intervals of four hours each. The beam flux for each interval was calculated using the formula,

$$\phi_i \times \left(1 - e^{-\frac{0.693 t_i}{t_{1/2}}}\right) \times \left(e^{-\frac{0.693 t_d}{t_{1/2}}}\right) \qquad \textbf{8-15}$$

where ϕ_i - Beam flux on the target in the given interval.

t_i - Duration of the irradiation

t_d - Time elapsed between EOB and counting

$t_{1/2}$ - Half-life of the isotope of interest

All these φ_i were then summed over the entire run to get the total flux (φ). The total activity (dps) in the target at EOB (A_0) was calculated as a weighed mean of all the EOB activities for each interval based on the branching ratio and the error.

$$W_i = Br_i \Big/ (err_i)^2 \qquad \textbf{8-16}$$

$$A_0 = \frac{\sum (A_{0i} \times W_i)}{\sum W_i} \qquad \textbf{8-17}$$

where W_i - Weight for activity recorded in each interval

Br_i - Branching ratio for the γ line of the nuclide

err_i - Error in the activity measurement

A_{0i} - Activity measured in the given interval

The number of target atoms (N_t) was calculated using 8-7 and the cross section could then be calculated in units of millibarns (mb = $10^{-27}cm^2$) with formula given below.

$$\sigma = \frac{A_0 \times 10^{27}}{\phi \times N_t} \qquad \textbf{8-18}$$

The error in the activity was calculated based on the standard deviation.

$$\text{err} = \sqrt{\sum W_i \times (A_0 - A_{0i})^2 \Big/ \sum W_i} \qquad \textbf{8-19}$$

Thus the error in the cross section was calculated employing the formula given below.

$$\text{err}_\sigma = \frac{\text{err} \times 10^{27}}{\phi \times T_n} \qquad \textbf{8-20}$$

The correction factors that needed to be taken into account (and incorporated in the program routine) were the chemical yields, the isotopic purity of the targets, the branching ratios, the self absorption correction (for β counter data), the detector efficiencies and the temporal variation of the beam intensity.

8.7.2 Fusion cross sections from β (σ_{fus}-β) and γ (σ_{fus}-γ) data

The fusion cross section (σ_{fus}) was obtained from the σ_{prod} by correcting it for the unobserved fusion products. The correction factor was taken as the average of the two ratios (σ_{fus}) as computed by PACE4.13$/(\sigma^{76}\text{As})$ as computed by PACE4.13 and (σ_{fus}) as computed by HIVAP$/(\sigma^{76}\text{As})$ as computed by HIVAP. The details about PACE v.4.13 and HIVAP simulation codes are given in section 5.2.3. The values of the averages ranged between 0.72-0.83 for different energies and are given in Table 8.6. The σ_{fus}-γ and σ_{fus}-β for each energy were obtained by dividing the σ_{prod} by these

correction factors and the uncertainties in cross sections included the uncertainties in activity measurement and systematic uncertainties along with the uncertainties in σ_{prod} calculations mentioned above (Table 8.7). For the ^{11}Li+^{70}Zn system only the upper limits of cross sections (2σ) are reported as the data obtained for this system were statistically insignificant thus making the cross sections unreliable.

Table 8.6 The ratios of the production cross section and the cross sections for ^{76}As as computed by PACE v.4.13 and HIVAP and their average (beam energies at the center of target)

Projectile	E_{cot} (MeV)	$\left(\sigma_{prod}/\sigma^{76}As\right)_{PACE4.13}$	$\left(\sigma_{prod}/\sigma^{76}As\right)_{HIVAP}$	Average
^{9}Li	11.0	0.821	0.840	0.831
	12.0	0.840	0.810	0.825
	13.0	0.841	0.765	0.803
	13.7	0.844	0.724	0.784
	14.1	0.835	0.703	0.769
	14.7	0.805	0.647	0.726
	15.0	0.795	0.647	0.721
^{11}Li	16.0	0.378	0.553	0.466
	17.0	0.433	0.555	0.494

Table 8.7 The fusion cross sections based on beta and gamma data with isotope corrections applied (beam energies in laboratory frame)

Projectile	E_{lab} (MeV)	Analysis method	σ_{fus}-γ (mb)	σ_{fus}-β (mb)
^{9}Li	11.5	β	-	30.0±5.8
	12.5	β	-	45.4±20.4
	13.5	β	-	69.6±10.7
	14.0	γ, β	205.5±19.5	167.3±28.0
	14.5	γ, β	285.8±20.1	202.2±26.2
	15.1	γ, β	421.8±26.3	302.7±20.4
	15.4	β	-	299.8±31.9
^{11}Li	16.5	β	-	<55000 (2σ upper limit)
	17.5	β	-	<27000 (2σ upper limit)

9 RESULTS AND CONCLUSIONS

9.1 Fusion cross section (σ_{fus}) and comparison with similar systems

The cross sections calculated using the γ data were on an average 1.34 times larger (Table 9.1) than the ones based on the β data with shapes of both the excitation functions being relatively the same (fig9.1). This discrepancy is attributed to the possibility of loss of some radioactivity during the transfer of the irradiated target from experimental chamber to radiochemistry lab and during the dissolution of target for radiochemical separation after which the β counting was done. For 13.7, 14.1 and 14.7MeV beam energies where cross sections were calculated by means of both β and γ data the average of σ_{fus}-γ and σ_{fus}-β was taken to be the σ_{fus} and for all other energies the σ_{fus}-β was the σ_{fus}. Table 9.2 lists the σ_{fus}-γ, σ_{fus}-β and σ_{fus} values for each beam energy and Table 9.3 provides relevant experimental details.

In order to make the ^{9}Li+^{70}Zn fusion relevant in context of other fusion reactions carried out with similar systems of targets and projectiles the reduced excitation functions of reactions ^{6,7}Li+^{64}Zn were plotted along with that of ^{9}Li+^{70}Zn system. To arrive at the reduced excitation function data points the fusion cross section (σ_{fus}) was divided by the square of the Bass model fusion radius (R_B) and the beam energy in CM frame (E_{CM}) was divided by the Bass model fusion barrier height (V_B) (Bass 1980).

Table 9.1 The fusion cross sections as given by calculations done with β and γ spectroscopy data and their ratio

E_{lab}(MeV)	σ_{fus}-γ (mb)	σ_{fus}-β (mb)	σ_{fus}-γ/σ_{fus}-β
14.0	205.5±19.5	167.3±28.0	1.2±0.7
14.5	285.8±20.1	202.2±26.2	1.4±0.8
15.1	421.8±26.3	302.7±20.4	1.4±0.3

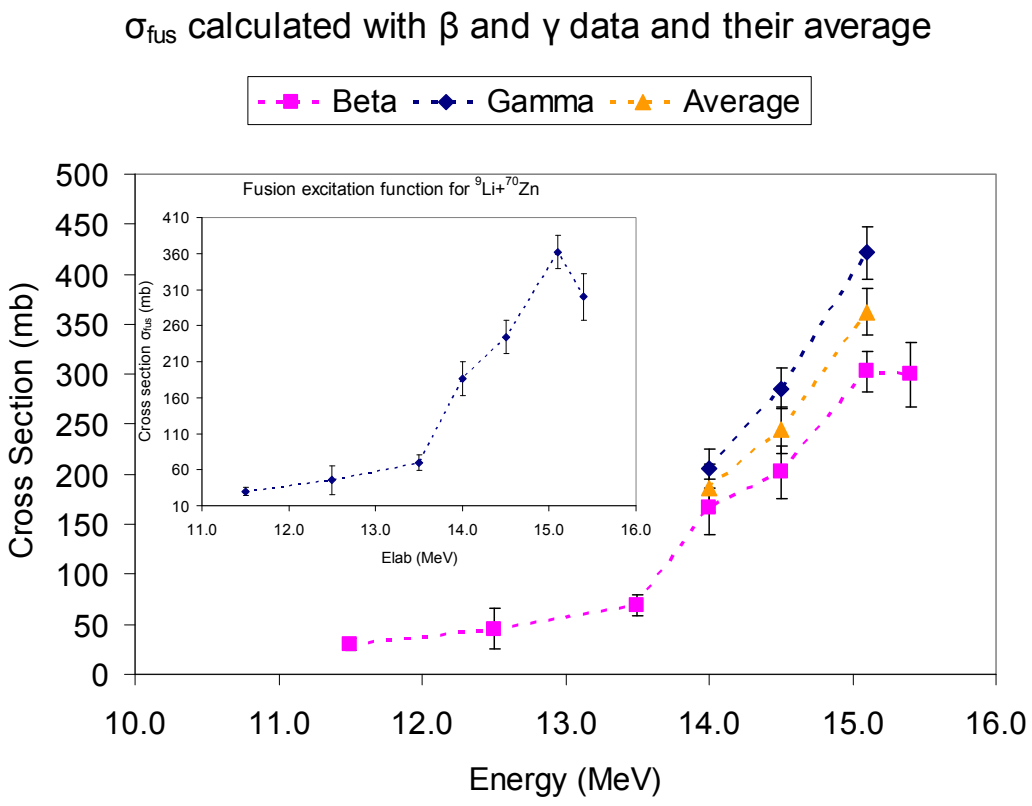

Figure 9.1 The excitation functions based on the β (squares) and the γ (diamonds) data. Shapes of both the excitation functions are relatively similar however the absolute values of the cross sections differ by a factor of 1.4. An average (triangles) of σ_{fus}-γ and σ_{fus}-β was taken as σ_{fus} for the energies 14.0, 14.5 and 15.1MeV. The fusion excitation function as plotted with the average of σ_{fus}-γ and σ_{fus}-β for concerned energies is also shown (inset).

Table 9.2 The values of σ_{fus}-γ, σ_{fus}-β and σ_{fus} at all beam energies of ^{9}Li

E_{lab}(MeV)	σ_{fus}-γ (mb)	σ_{fus}-β (mb)	σ_{fus}
11.5	-	30.0±5.8	30.0±5.8
12.5	-	45.4±20.4	45.4±20.4
13.5	-	69.6±10.7	69.6±10.7
14.0	205.5±19.5	167.3±28.0	186.4±23.7
14.5	285.8±20.1	202.2±26.2	244.0±23.2
15.1	421.8±26.3	302.7±20.4	362.2±23.4
15.4	-	299.8±31.9	299.8±31.9

Table 9.3 The beam energies (in laboratory and center-of-mass frames and at the center of target), irradiation time, beam dose and the method of analysis along with the cross sections for fusion with ^{9}Li projectile

E_{lab} (MeV)	E_{cot} (MeV)	E_{CM} (MeV)	T_{irr} (min)	Dose (particles/s)	Analysis method	Cross section (mb)
11.5	11.0	9.7	848	$3.4x10^{11}$	β	30.0±5.8
12.5	12.0	10.6	5099	$2.6 x10^{11}$	β	45.4±20.4
13.5	13.0	11.5	1006	$2.3 x10^{11}$	β	69.6±10.7
14.0	13.7	12.1	2395	$6.5 x10^{11}$	β, γ	186.4±23.7
14.5	14.1	12.5	2577	$5.9 x10^{11}$	β, γ	244.0±23.2
15.1	14.7	13.0	2062	$4.2 x10^{11}$	β, γ	362.2±23.4
15.4	15.0	13.4	1196	$3.9 x10^{11}$	β	299.8±31.9

The beam energies E_{lab} and E_{CM}, cross section σ_{fus}, scaling parameters R_B, V_B (Padron 2002) and the scaled quantities $\sigma_{fus}/(R_B)^2$ and E_{CM}/V_B are given in Table 9.4 for ^{6}Li+^{64}Zn, in Table 9.5 for ^{7}Li+^{64}Zn and in Table 9.6 for ^{9}Li+^{70}Zn. The reduced excitation functions thus obtained from the scaled parameters were plotted for the abovementioned systems (fig9.2). As seen in the figure the measurements taken by us for the ^{9}Li+^{70}Zn system are at much lower energies. The Bass barrier (Bass 1980) for the ^{9}Li+^{70}Zn system is 12.5MeV and most of our data are collected near- or sub-barrier. The plot indicates that the reduced excitation function of the ^{9}Li+^{70}Zn system follows a similar trend as the two other systems involving similar targets and projectiles.

Table 9.4 The beam energies E_{lab} and E_{CM}, cross section σ_{fus}, scaling parameters R_B, V_B and the scaled quantities $\sigma_{fus}/(R_B)^2$ and E_{CM}/V_B for the $^{6}Li+^{64}Zn$ system

E_{lab} (MeV)	E_{CM} (MeV)	σ_{fus} (mb)	$\sigma_{fus}/(R_B)^2$ [R_B=7.95fm]	E_{CM}/V_B [V_B=13.56MeV]
24	21.94	597±45	9.44±0.71	1.62
28	25.60	823±59	13.02±0.93	1.85
31	28.34	869±50	13.75±0.79	2.09
34	31.08	984±60	15.57±0.95	2.29
37	33.83	1053±71	16.66±1.12	2.49
40	36.57	1022±65	16.17±1.03	2.69
43	39.31	1166±71	18.45±1.12	2.90

Table 9.5 The beam energies E_{lab} and E_{CM}, cross section σ_{fus}, scaling parameters R_B, V_B and the scaled quantities $\sigma_{fus}/(R_B)^2$ and E_{CM}/V_B for the $^{7}Li+^{64}Zn$ system

E_{lab} (MeV)	E_{CM} (MeV)	σ_{fus} (mb)	$\sigma_{fus}/(R_B)^2$ [R_B=8.25fm]	E_{CM}/V_B [V_B=13.22MeV]
24	21.94	656±56	9.64±0.82	1.66
28	25.60	883±66	12.97±0.97	1.94
31	28.34	922±64	13.55±0.94	2.14
34	31.08	1002±69	14.72±1.01	2.35
37	33.83	1134±77	16.66±1.13	2.56
40	36.57	1105±75	16.23±1.10	2.77
43	39.31	1254±81	18.42±1.19	2.97

Table 9.6 The beam energies E_{lab} and E_{CM}, cross section σ_{fus}, scaling parameters R_B, V_B and the scaled quantities $\sigma_{fus}/(R_B)^2$ and E_{CM}/V_B for the $^{9}Li+^{70}Zn$ system

E_{lab} (MeV)	E_{CM} (MeV)	σ_{fus} (mb)	$\sigma_{fus}/(R_B)^2$ [R_B=8.80fm]	E_{CM}/V_B [V_B=12.50MeV]
11.5	9.7	30.0±5.8	0.39±0.08	0.78
12.5	10.6	45.4±20.4	0.59±0.26	0.85
13.5	11.5	69.6±10.7	0.90±0.14	0.92
14.0	12.1	186.4±23.7	2.41±0.31	0.97
14.5	12.5	244.0±23.2	3.15±0.30	1.00
15.1	13.0	362.2±23.4	4.68±0.30	1.04
15.4	13.4	299.8±31.9	3.87±0.41	1.07

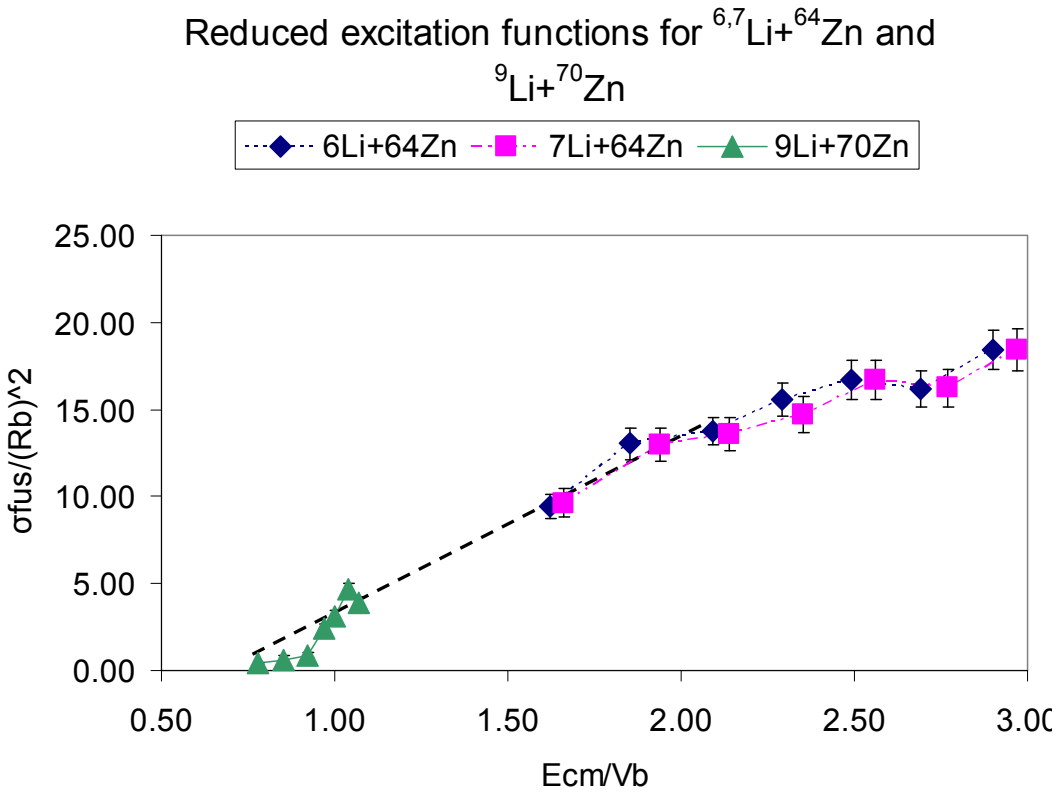

Figure 9.2 The reduced excitation functions $[\sigma_{fus}/(R_B)^2$ vs $E_{CM}/V_B]$ of reactions $^{6}Li+^{64}Zn$ (diamonds), $^{7}Li+^{64}Zn$ (squares) and $^{9}Li+^{70}Zn$ (triangles). The fusion radius (R_B) and the fusion barrier height (V_B) were as given by the semi empirical Bass model (Bass 1980) and the beam energies and cross sections for the $^{6,7}Li+^{64}Zn$ reaction have been published earlier (Padron 2002). The beam energies and cross sections for the $^{9}Li+^{70}Zn$ system are from this work. The dotted line is an extrapolation of data-trendline.

9.2 Comparison with theoretical model simulations

The values of σ_{fus} obtained for $^{9}Li+^{70}Zn$ fusion were compared with the predictions of theoretical model simulations PACE v.4.13 and HIVAP (fig9.3). The details about both PACE and HIVAP are given in section 5.2.3. The predictions of the two codes differ significantly from one another and the experimental cross sections conform to the general trend differing from either in absolute values.

Coupled-channel calculations were also performed for the system under consideration. CCFULL is a FORTRAN77 program for coupled-channel calculations with all order couplings for heavy-ion fusion reactions (Hagino 1999). The program calculates fusion cross section and mean angular momentum of the compound nucleus under the influence of couplings between the relative motion and several nuclear collective motions, like rotational and vibrational coupling. The linear coupling approximation used in most coupled-channel calculations is inadequate for analyses of such high precision data as those gathered in the fusion experiments. Therefore the program takes into account the effects of nonlinear couplings to all orders, which have been shown to play an important role in heavy-ion fusion reactions at sub-barrier energies. The 'no-Coriolis approximation' is employed to reduce the dimension of coupled-channel equations with full space which are too large for practical purposes. This approximation replaces the angular momentum of the relative motion in each channel by the total angular momentum and it has been shown to work well for heavy-ion fusion.

The input parameters are system parameters like the mass and charge of the projectile and target, the parameters used in coupling Hamiltonian like the radius parameters, property of the intrinsic motion of the projectile and target (which when set to 0 vibrational coupling is assumed and when set to 1 rotational coupling is assumed), target excitation parameters like the excitation energy of single phonon state, deformation parameter and multipolarity of vibrational excitation.

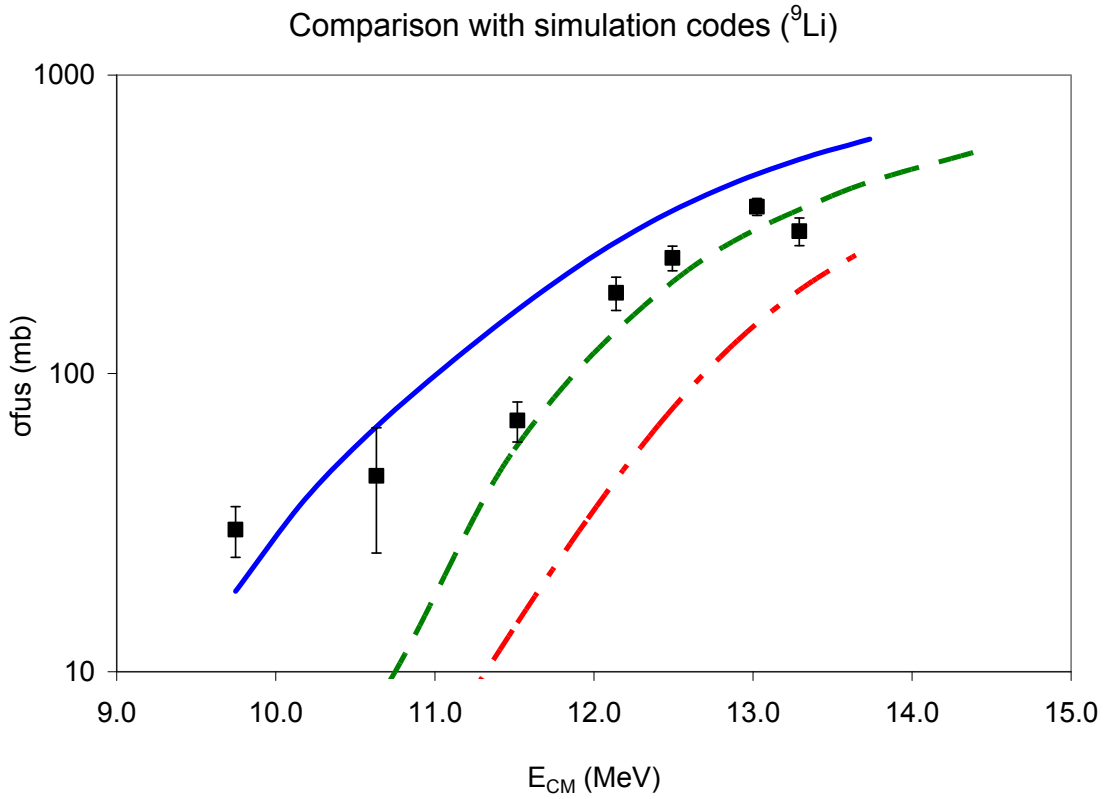

Figure 9.3 Comparison of the fusion cross sections obtained in this experiment (squares) with the predictions of the simulation codes PACE v.4.13 (dashed dotted line), HIVAP (solid line) and CCFULL (dashed line). More information about each code is given in the text. The experimental cross sections conform to the general trend but show a large sub-barrier enhancement which is not predicted and explained by the coupled-channel calculations.

The number of rotational states to be included also needs to be given. CCFULL can perform calculations for multiple excitation modes and parameters for projectile excitation can also be input if required. The nuclear potential in entrance channel, the radius parameter, surface diffuseness parameter, minimum and maximum colliding energy, interval in energy scale, matching radius and the mesh of integration complete the set of input parameters. The last two control the accuracy of calculations. For our calculations inelastic excitation of the first vibrational 2+ and 3- states in ^{70}Zn and the

rotational states of ^{9}Li were included along with the two neutron transfer channel. The Q-value for two neutron transfer $^{9}Li + ^{70}Zn \rightarrow ^{7}Li + ^{72}Zn$ is +8.612MeV which makes it necessary to include the coupling with this channel. A Woods-Saxon type nuclear potential with V_0 = 105MeV, R_0 = 1.12fm and a_0 = 0.65fm was used.

As can be seen from fig9.4 the experimental cross sections show a large sub-barrier enhancement which is not predicted and explained by the coupled-channel calculations. In a recent work in theoretical physics (Zagrebaev 2007) near-barrier fusion of neutron-rich nuclei was studied within the semi-empirical channel coupling model for intermediate neutron rearrangement.

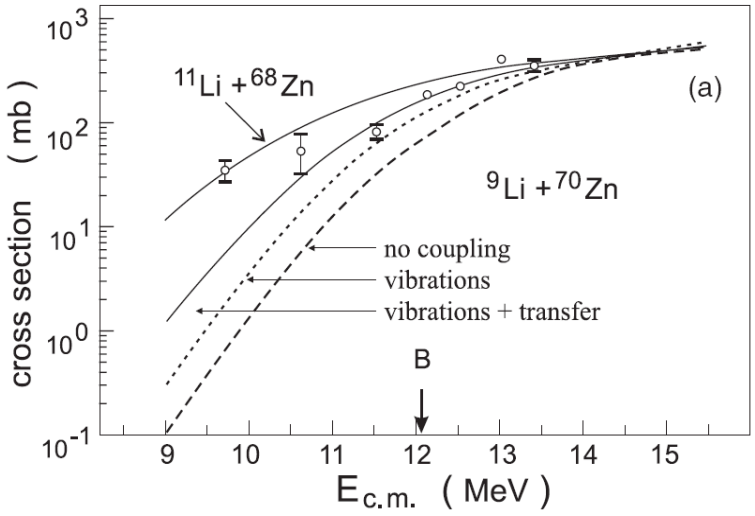

Figure 9.4 In a recent work in theoretical physics (Zagrebaev 2007) near-barrier fusion of neutron-rich nuclei was studied within the semi-empirical channel coupling model for intermediate neutron rearrangement. The deep sub-barrier enhancement was attributed to an increased barrier penetrability due to neutron transfer with positive Q-value.

A huge enhancement of deep sub-barrier fusion probability was found for light neutron-rich weakly bound nuclei which was attributed to an increased barrier penetrability due to neutron transfer with positive Q-value. For the reaction studied in

our work neutron rearrangement with positive Q-values is possible as mentioned earlier. The excitation function calculated for this fusion reaction showed a significant increase in sub-barrier fusion probability when the effect of neutron rearrangement was considered. However this sub-barrier enhancement was not sufficient to explain the experimental results. The authors state that this could be due to more probable "di-neutron" transfer as compared to the sequential neutron transfer used in their calculations.

The comparison of ^{11}Li+^{70}Zn fusion cross sections with simulation codes (fig9.5) shows a difference of almost two orders of magnitude between the two. The reported measured cross sections are, however, the upper limit cross sections and not reliable due to the meager statistics for this system. Therefore further attempts at studying this system with much higher beam intensity need to be done.

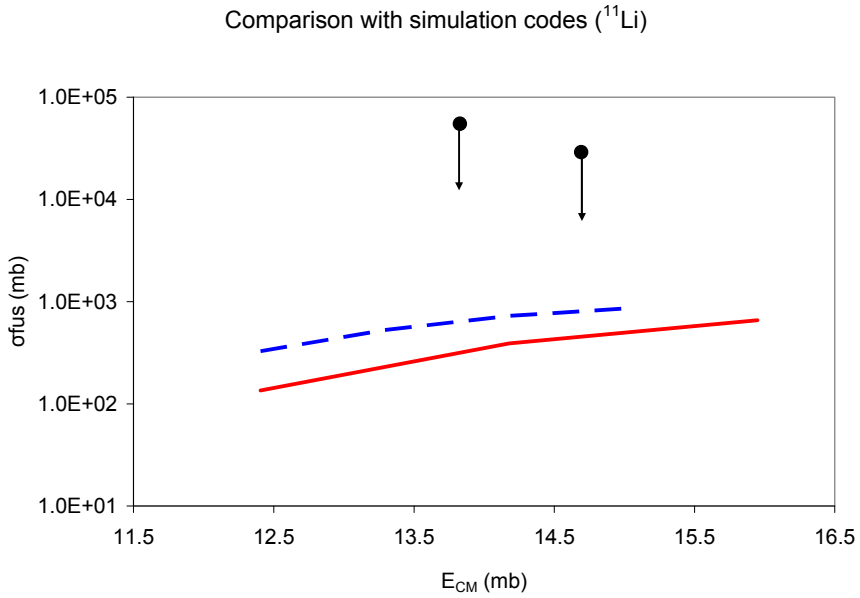

Figure 9.5 The figure reflects the large difference (almost two orders of magnitude) between the experimental upper limit fusion cross sections (circles) and those predicted by PACE v.4.13 (solid line) and HIVAP (dashed line) for the ^{11}Li+^{70}Zn system.

9.3 Wong formula and fusion radius (R_B) of ^{9}Li

Most of the data taken in the ^{9}Li+^{70}Zn fusion experiment were at near- or sub-barrier energies. The results of the calculations for fusion cross section show that the fusion took place below the barrier and in explaining such a sub-barrier fusion the importance of the nuclear structure of ^{9}Li is very high. The ^{9}Li nucleus has been described as having a neutron skin of thickness 0.48fm (Dobrovolsky 2004). A simple analytic expression for nucleon densities which correctly incorporates the two basic physical requirements, the asymptotic behavior ($r \rightarrow \infty$) and the behavior near the centre ($r \rightarrow 0$), has been proposed (Bhagwat 2001). The expression provides separately the neutron and proton densities and is suitable for the description of the loosely bound systems such as the nuclei in the neutron-halo region. The calculations carried out for $^{6\text{-}9,11}$Li using this expression were consistent with the experimental values. The density distribution of ^{9}Li was found to show a significant tail with $\rho=10^{-4}$ nucleon/fm^3 at 6.5fm. According to shell model (Borremans 2005) ^{9}Li is a combination of ^{4}He, ^{3}H and two neutrons. The Q-value for two neutron transfer $^{9}\mathrm{Li}+^{70}\mathrm{Zn}\rightarrow^{7}\mathrm{Li}+^{72}\mathrm{Zn}$ is +8.612MeV.

All the above mentioned factors make it very likely that ^{9}Li has a large fusion radius. To demonstrate numerically whether this is true one can fit the fusion excitation function with an appropriate theoretical formula and find the value of the radius parameter. Wong formula (Wong 1973) represents the fusion barrier (subscript 'B' in the equation representing 'barrier') as a parabola and describes the fusion cross section in a semi-empirical equation

$$\sigma_W = \frac{\hbar\omega_B R^2{}_B}{2E} \ln\left\{1 + \exp\left[\frac{2\pi}{\hbar\omega_B}\left(E - V_B\right)\right]\right\} \qquad \textbf{9-1}$$

where σ_w - Fusion cross section as described by Wong formula (mb)

$\hbar\omega_B$ - Barrier curvature of the fusion barrier (MeV)

R_B - Fusion radius (fm)

E - Beam energy in CM frame (MeV)

V_B - Fusion barrier height (MeV)

The above equation is arrived at by integrating over all the partial waves *l*, to which the quantities R_l and $\hbar\omega_l$ are insensitive. The fission excitation functions for reactions of ^{4}He, ^{11}B, ^{14}N, ^{16}O and ^{40}Ar with ^{238}U have been fitted extremely well with this expression. The fits to ^{9}Li+^{70}Zn seven-point fusion excitation function were performed by varying all the parameters and by fixing the value for V_B to 12.5MeV, the Bass barrier for the system. The values of the parameters and asymptotic standard errors[7] obtained for each fit given in Table 9.7 indicate that the fit performed by varying all parameters was statistically not significant.

Table 9.7 The seven-point fusion excitation function was fit using the Wong formula. The fit method, values of the parameters and asymptotic standard errors obtained for each fit are given in the table.

Parameter status	Parameter value	Asymptotic standard error
Fit 1		
R_B (variable)	18.1 fm	160.1%
V_B (variable)	13.8MeV	35.42%
$\hbar\omega$ (variable)	6.8MeV	37.09%
Fit 2		
R_B (variable)	12.1 fm	8.03%
V_B (fixed)	12.5MeV	-
$\hbar\omega$ (variable)	5.7MeV	13.97%

[7] An error applied to a non-linear equation but calculated assuming the equation is linear.

The data was best described by the fit where value for V_B was fixed (fig9.6). The values of the fusion radius (R_B) and barrier curvature ($\hbar\omega$) obtained by this fit are 12.1fm and 5.7MeV, respectively.

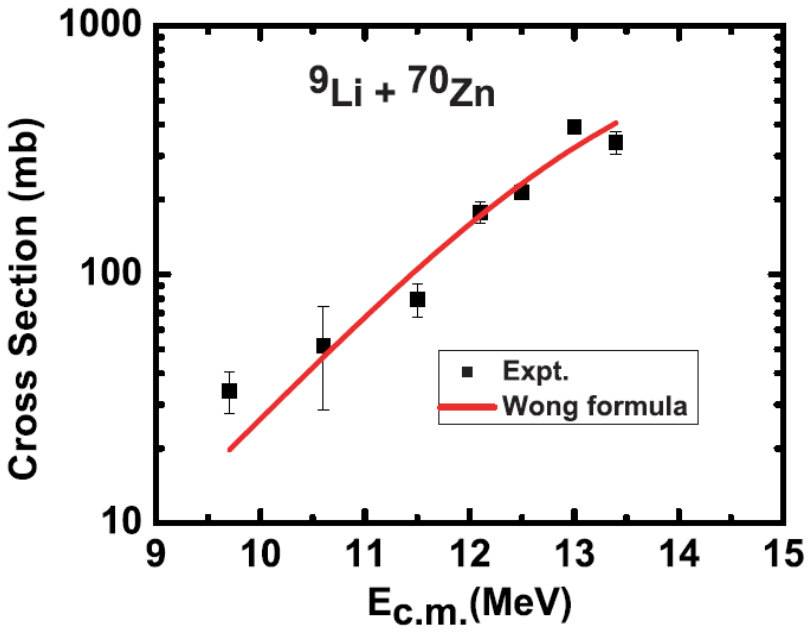

Figure 9.6 The fusion excitation function for ^{9}Li+^{70}Zn system is fit with Wong formula by fixing the value of barrier potential (V_B) = 12.5MeV, fusion radius (R_B) and barrier curvature ($\hbar\omega$) being the free parameters. This fit described the data well and the values of R_B and $\hbar\omega$ obtained were 12.1fm and 5.7MeV, respectively.

9.4 Conclusion and future work

An experiment was carried out at the ISAC accelerator facility at TRIUMF, Canada to measure the fusion excitation function of the ^{9}Li+^{70}Zn and ^{11}Li+^{70}Zn systems. ^{9}Li projectile reacting with the ^{70}Zn target at seven different beam energies gave rise to measurable amount of EVRs, viz., As and Ge isotopes. These EVRs were stopped in the ^{70}Zn target itself and γ spectra acquired of this irradiated target showed characteristic γ lines for the concerned nuclides. The target was then subjected to a

radiochemical solvent extraction which separated the As and Ge from eachother and these separated fractions were then monitored for decay in the radioactivity by β spectroscopy. The radioactivity produced in the targets due to ^{11}Li bombardment at two energies was not detectable above background in γ spectroscopy and too low to be statistically significant in the β counting of the separated As and Ge fractions.

The identity of the EVRs was established by the half-lives calculated from β counting data. Both β and γ spectra were resolved using DECHAOS software and CROSS.for processed the data to give the fusion cross sections along with uncertainties. The seven-point excitation function obtained for the ^{9}Li+^{70}Zn system showed a large sub-barrier enhancement not explained by the coupled channel calculations. Comparison of the reduced excitation function for this system with that of similar systems ^{6,7}Li+^{64}Zn shows that ^{9}Li+^{70}Zn follows the general trend although the measurements done in our work for this system are at much lower energies. Fitting the excitation function with the Wong formula gives a large fusion radius value for ^{9}Li, $R_B = 12.1 \pm 1.0$fm, which can be attributed to the existence of 'neutron skin' around it and its spatially extended neutron density. Thus this study indicates the necessity of taking into account the sub-barrier fusion enhancement shown by ^{9}Li while trying to explain the same for ^{11}Li halo nucleus for which ^{9}Li is the core. An extension of this work for future experiments could be the experiments carried out at beam energies lower than the ones used in present work in order to determine the limit of the sub-barrier fusion.

For the ^{11}Li+^{70}Zn fusion reaction only the upper limit cross sections for the two beam energies could be obtained due to the scanty statistics available. These numbers

however cannot be of any significance as shown by their large magnitude when compared with the theoretical predictions. Thus they point to the need of similar experiments being done in future with much larger beam intensities of ^{11}Li in order to obtain reliable statistics.

The results of this work have been published (Loveland 2006) however some modifications in the results have occurred based on the corrections applied to the data analysis after the publication.

BIBLIOGRAPHY

Adamian, G. G., N.V. Antonenko, W. Scheid (2000). "Isotopic dependence of fusion cross sections in reactions with heavy nuclei." Nucl. Phys. A **678**(1-2): 24.

Aguilera, E. F., J. J. Kolata, F. M. Nunes, F. D. Becchetti, P. A. DeYoung, M. Goupell, V. Guimarães, B. Hughey, M. Y. Lee, D. Lizcano, E. Martinez-Quiroz, A. Nowlin, T. W. O'Donnell, G. F. Peaslee, D. Peterson, P. Santi, and R. White-Stevens (2000). "Transfer and/or Breakup Modes in the ^{6}He+^{209}Bi Reaction near the Coulomb Barrier " Phys Rev Lett **84**(22): 5058 - 5061.

Ajzenberg-Selove, F. (1979). "Energy levels of light nuclei A = 5–10." Nuclear Physics A **320**(1): 1-224.

Al-Khalili, J. S. (2003). Structure of halo nuclei: overview of theoretical status. International Workshop XXXI on Gross Properties of Nuclei and Nuclear Excitations, Hirschegg, Austria, Gesellschaft für Schwerionenforschung (GSI) Darmstadt (web-book).

Alburger, D. E., Wilkinson, D. H. (1976). "Beta decay of ^{16}C and ^{17}N." Phys Rev C **13**(2): 835 - 846.

ANL. (1993, 20 Feb 2006). "Experimental Physics and Industrial Control System." Retrieved Feb 22, 2006, from http://www.aps.anl.gov/epics/index.php.

Audi, G., A.H. Wapstra (1993). "The 1993 atomic mass evaluation : (I) Atomic mass table." Nucl Phys A **565**: 1.

Back, B. B. (1985a). "Complete fusion and quasifission in reactions between heavy ions." Phys Rev C **31**(6): 2104

Back, B. B. (1985b). "Erratum: Complete fusion and quasifission in reactions between heavy ions." Phys Rev C **32**(5): 1786.

Back, B. B., R. R. Betts, K. Cassidy, B. G. Glagola*, J. E. Gindler, L. E. Glendenin, and B. D. Wilkins (1983). "Experimental Signatures of Quasifission Reactions." Phys Rev Lett **50**: 818.

Bass, R. (1980). Nuclear Reactions with Heavy Ions. New York, Springer.

Beck, C., F. A. Souza, N. Rowley, S. J. Sanders, N. Aissaoui, E. E. Alonso, P. Bednarczyk, N. Carlin, S. Courtin, A. Diaz-Torres, A. Dummer, F. Haas, A. Hachem, K. Hagino, F. Hoellinger, R. V. F. Janssens, N. Kintz, R. Liguori Neto, E. Martin, M. M. Moura, M. G. Munhoz, P. Papka, M. Rousseau, A. Sànchez i Zafra, O. Stézowski, A. A. Suaide, E. M. Szanto, A. Szanto de Toledo, S. Szilner, and J. Takahashi (2003). "Near-barrier fusion of weakly bound ^{6}Li and ^{7}Li nuclei with ^{59}Co." Phys Rev C **67**(5): 054602.

Bertsch, G. F., B. A. Brown, H. Sagawa (1989). "High-energy reaction cross sections of light nuclei." Phys. Rev. C **39**(3): 1154 - 1157.

Bhagwat, A., Y. K. Gambhir and S. H. Patil (2001). "Nuclear densities of Li isotopes." Journal of Physics G: Nuclear and Particle Physics **27**: B1–B7.

Blank, B., J. -J. Gaimard, H. Geissel, K. -H. Schmidt, H. Stelzer and K. SümmererD. Bazin, R. Del Moral, J. P. Dufour, A. Fleury and F. HubertH. -G. Clerc, M. Steiner (1993). "Total and 2n-removal cross sections of the neutron-rich isotopes ^{8,9,11}Li." Nuclear Physics A **555**(2): 408-434.

Bochkarev, O. V., L.V. Chulkov, P. Egelhof, H. Geissel, M.S. Golovkov, H. Irnich, Z. Janas, H. Keller, T. Kobayashi, G. Kraus, G. MÄunzenberg, F. Nickel, A.A.

Ogloblin, A. Ozawa, A. Piechaczek, E. Roeckl, W. Schwab, K. SÄummerer, T. Suzuki, I. Tanihata, K. Yoshida (1998). "Evidence for a neutron skin in ^{20}N." Eur Phys J A **1**: 15-17.

Bock, R., T. Chu, M. Dakowski, A. Gobbi, E. Grosse, A. Olmi, H. Sann, D. Schwam, U. Lynen, W. Müller, S. Bjørnholm, H. Esbensen, W. Wölfli, E. Morenzoni (1982). "Dynamics of the fusion process." Nucl Phys A **388**: 334.

Bohr, N., J.A. Wheeler (1939). "The Mechanism of Nuclear Fission." Phys Rev **56**(5): 426.

Borremans, D., D. L. Balabanski, K. Blaum, W. Geithner, S. Gheysen, P. Himpe, M. Kowalska, J. Lassen, P. Lievens, S. Mallion, R. Neugart, G. Neyens, N. Vermeulen and D. Yordanov (2005). "New measurement and reevaluation of the nuclear magnetic andquadrupole moments of ^{8}Li and ^{9}Li." Phys Rev C **72**: 044309.

Bricault P., M. D., A. Dowling, M. Lane (2003). "High power target developments at ISAC." Nuclear Instruments and Methods in Physics Research B **204**: 6.

Broglia, R. A., Winther, Aage (1990). Heavy Ion Reactions. New York, Addison-Wesley Publishing Company.

Bychowski, J. P., P.A. DeYoung, B.B. Hilldorea, J.D. Hinnefeld, A. Vida, F.D. Becchetti, J. Lupton, T.W. O'Donnell, J.J. Kolata, G. Rogachev, M. Hencheck (2004). "^{209}Bi(^{6}He, α) reaction mechanisms studied near the Coulomb barrier using n–α coincidence measurements." Phys Lett B **596**: 26–31.

Catford, W. N. (2002). Catkin**:** Relativistic kinematics program in Excel

Cherepanov, E. A. (1999). Dubna, JINR.

Cherepanov, E. A., A.S. Iljinov, and M.V. Mebel (1983). "Systematics of the effective ratio ($\Gamma_n/\ \Gamma_f$) of neutron emission and fission partial widths for transcurium nuclei." J. Phys. G **9**: 931.

Cherepanov, E. A. a. A. S. I. (1980). Lett Nuovo Cimento Soc Ital Fis **25**: 611.

Cherepanov, E. A. a. A. S. I. (1984). Proceedings of International Symposium on In-Beam Nuclear Spectropscopy, Debrecen.

Cujec, B., S.-C. Wu, and C.A. Barnes (1979). "Alpha transfer at sub-coulomb energies in the ^{9}Be + ^{16}O reaction." Phys Lett B **89**: 151.

Ćwiok, S., J. Dudek, W. Nazarewicz, J. Skalski and T. Werner (1987). Comput Phys Commun **46**: 379.

Dasgupta, M., et al. (1999). "Fusion versus Breakup: Observation of Large Fusion Suppression for ^{9}Be+^{208}Pb." Phys Rev Lett **82**: 1395.

Dasso, C. H., Vitturi, A. (1994). "Does the presence of ^{11}Li breakup channels reduce the cross section for fusion process?" Phys. Rev. C **50**(1): R12.

Dennis, L. C., K.M. Abdo, A.D. Frawley, and K.W. Kemper (1982). "Fusion of Li and C and a search for entrance channel limitations to fusion cross sections." Phys Rev C **26**: 981.

DeYoung, P. A., Patrick J. Mears, J. J. Kolata, E. F. Aguilera, F. D. Becchetti, Y. Chen, M. Cloughesy, H. Griffin, C. Guess, J. D. Hinnefeld, H. Jiang, Scott R. Jones, U. Khadka, D. Lizcano, E. Martinez-Quiroz, M. Ojaniega, G. F. Peaslee, A. Pena, J. Rieth, S. VanDenDriessche, and J. A. Zimmerman (2005). "Two-neutron transfer in the ^{6}He+^{209}Bi reaction near the Coulomb barrier." Phys Rev C **71**: 051601(R).

Di Pietro, A., P. Figuera, F. Amorini, C. Angulo, G. Cardella, S. Cherubini, T. Davinson, D. Leanza, J. Lu, H. Mahmud, M. Milin, A. Musumarra, A. Ninane, M. Papa, M. G. Pellegriti, R. Raabe, F. Rizzo, C. Ruiz, A. C. Shotter, N. Soić, S. Tudisco, and L. Weissman (2004). "Reactions induced by the halo nucleus ^{6}He at energies around the Coulomb barrier." Phys Rev C **69**: 044613.

Dobrovolsky, A. V., G.D. Alkhazova, M.N. Andronenko, A. Bauchet, P. Egelhof, S. Fritz, H. Geissel, C. Gross, A.V. Khanzadeev, G.A. Korolev, G. Kraus, A.A. Lobodenko, G. Münzenberg, M. Mutterer, S.R. Neumaier, T. Schäfer, C. Scheidenberger, D.M. Seliverstov, N.A. Timofeeva, A.A. Vorobyov, V.I. Yatsouraa (2004). "Study of the nuclear matter distribution in neutron-rich Li isotopes." Nuclear Physics A **766**: 1–24.

Dombsky, M., P. Bricault, V. Hanemaayer (2004). "Increasing beam currents at the TRIUMF-ISAC Facility; techniques and experiences." Nucl. Phy. A **746**: 8.

Dombsky M., P. B., V. Hanemaayer (2004). "Increasing beam currents at the TRIUMF-ISAC Facility; techniques and experiences." Nucl. Phy. A **746**: 8.

Eck, J. S., J.R. Leigh, T.R. Ophel, and P.D. Clark (1980). "Total fusion cross section for the ^{9}Be+^{28}Si system." Phys Rev C **21**: 2352.

Feshbach, H. (1992). Theoretical nuclear physics: Nuclear reactions. New York, John Wiley and Sons.

Figueira, M. C. S., E.M. Szanto, R.M. Anjos, N. Added, N. Carlin, L. Fante, Jr., R. Matheus, and A. Szanto de Toledo (1993). "Complete fusion of ^{9}Be + ^{29}Si." Nuclear Physics A **561**: 453.

Fukunishi, N., T. Otsuka, I. Tanihata (1993). "Neutron-skin and proton-skin formations in exotic nuclei far from stability." Phys Rev C **48**(4): 1648 - 1655.

Gavron, A. (1980). "Statistical model calculations in heavy ion reactions." Physical Review C **21**(1): 230.

Gibbs, W. R., Hayes, A. C. (1991). "Determination of the radius of the ^{11}Li neutron halo from pion double charge exchange." Phys Rev Lett **67**(11): 1395-1398.

GSI. (2001). "Calculation of the Grazing Angle." Retrieved May 17, 2007, from http://www-aix.gsi.de/~wolle/EB_at_GSI/FRS-WORKING/grazing.html.

Hagino, K., N. Rowley, and A.T. Kruppa (1999). "A program for coupled-channels calculations with all order couplings for heavy-ion fusion reactions." Comput. Phys. Comm **123**: 143.

Hansen, P. G., B. Jonson (1987). "The neutron halo of extremely neutron-rich nuclei." Europhys. Lett. **4**(4): 409.

Heßberger, F. P., Hoffman, S., Ninov, V., Armbruster, P., Folger, H., Münzenberg, G., Schött, H.J., Popeko, A.G., Yeremin, A.V., Andreyav, A.N., Saro, S. (1997). "Spontaneous fission and alpha-decay propoerties of neutron deficient isotopes $^{257-253}$104 and ^{258}106." Z Phys A **359**: 415.

Heßberger, F. P., Münzenberg, G., Hoffman, S., Reisdorf, W., Schmidt, K-H, Schött, H.J., Armbruster, P., Hingmann, R., Thuma, B., Vermeulen, D. (1985). "Study of evaporation residues produced in reactions of ^{207,208}Pb with ^{50}Ti." Z Phys A **321**: 317.

Hofmann, S., F.P. Heßberger, D. Ackermann, S. Antalic, P. Cagarda, B. Kindler, P. Kuusiniemi, M. Leino, B. Lommel, O.N. Malyshev, R. Mann, G.

Mu¨nzenberg, A.G. Popeko, S. S´aro, B. Streicher and A.V. Yeremin (2004). "Properties of heavy nuclei measured at the GSI SHIP." Nucl Phys A **734**: 93.

Huizenga, J. R., A.N. Bekhami, L.G. Moretto (1969). "Note on interpretation of fission-fragment angular distributions at moderate excitation energies." Phys Rev **177**(4): 1826.

Hussein, M. S., Bertulani, C.A., Canto, L.F., Donangelo, R., Pato, M.P., De Toledo-Piza, A.F.R. (1995). "Fusion of Halo nuclei." Nucl. Phys. A **588**(1): 85c.

Hussein, M. S., M.P. Pato, L.F. Canto, R. Donangelo (1992). "Near-barrier fusion of ^{11}Li with heavy spherical and deformed targets." Phys Rev C **C46**: 377.

Itkis, M. G., et al. (2007). "The processes of fusion-fission and quasi-fission of superheavy nuclei." Nucl Phys A **787**: 150.

Khodai-Joopari, A. (1966). UCRL-16489. Berkeley, University of California, Berkeley. **PhD**.

Kolata, J. J. (1998a). "Fusion of a neutron skin nucleus : ^{209}Bi(^{6}He,4n) reaction." Phys. Rev. C **58**: 3442.

Kolata, J. J., Guimarães, V., Peterson, D., Santi, P., White-Stevens, R., DeYoung, P.A., Peaslee, G.F., Hughey, B., Atalla, B., Kern, M., Jolivette, P.L., Zimmerman, J.A., Lee, M.Y., Becchetti, F.D., Aguilera, E.F., Martinez-Quiroz, E., Hinnenfeld, J.D. (1998b). "Sub-barrier fusion of ^{6}He with ^{209}Bi." Phys. Rev. Lett. **81**(21): 4580.

Kolata, J. J., Guimarães, V., Peterson, D., Santi, P., White-Stevens, R., von Schwarzenberg, J., Hinnenfeld, J.D., Aguilera, E.F., Martinez-Quiroz, E., Roberts, D.A., Becchetti, F.D., Lee, M.Y.. Kryger, R.A. (1998c). "^{6}He + ^{209}Bi fusion-fission reaction." Phys. Rev. C **57**(1): R6.

Krappe, H. J., J. R. Nix and A. J. Sierk (1979). "Unified nuclear potential for heavy-ion elastic scattering, fusion, fission, and ground-state masses and deformations." Phys Rev C **20**: 992.

Laĭner, V. I. (1970). Modern electroplating (Translated from Russian), Jerusalem, Israel Program for Scientific Translations.

Loveland, W., A. M. Vinodkumar, R. S. Naik, P. H. Sprunger, B. Matteson, J. Neeway, M. Trinczek, M. Dombsky, P. Machule, D. Ottewell, D. Cross, K. Gagnon, and W. J. Mills (2006). "Subbarrier fusion of ^{9}Li with ^{70}Zn." Phys Rev C **74**.

Loveland, W. D., D.J. Morrissey, G.T. Seaborg (2005). Modern Nuclear Chemistry. Hoboken, NJ, John Wiley and Sons, Inc.

Lützenkirchen, K., Kratz, I.V., Wirth, G., Brüchle, W., Sümmerer, K., Lucas, R., Poitou, J., Grégoire, C. (1986). "Angular distributions in quasi-fission reactions." Nucl Phys A **452**: 351.

Marinsky, J. A., Ed. (1961). Monographs on radiochemistry of Germanium. NAS-NRC Nucl. Sci. Series.

Mateja, J. F., A.D. Frawley, L.C. Dennis, and K. Sartor (1986). "Comparison of ^{6} and ^{7}Li induced fusion cross sections on ^{16}O." Phys Rev C **33**: 1649.

Mateja, J. F., J. Garman, D.E. Fields, R.L. Kozub, A.D. Frawley, and L.C. Dennis (1984). "Fusion cross sections for four heavy-ion entrance channels leading to the ^{23}Na compound nucleus " Phys Rev C **30**: 134.

Migdal, A. B. (1972/3). Yad. Fiz. (English translation: Sov. J. Nucl. Phys.) **16 (16)**: 427 (238).

Möller, P., J. R. Nix (1988). "Nuclear masses from a unified macroscopic-microscopic model." Atomic Data and Nuclear Data Tables **39**(2): 213.

Möller, P., J. R. Nix, W. D. Myers, W. J. Swiatecki (1995). "Nuclear Ground-State Masses and Deformations." Atomic Data and Nuclear Data Tables **59**(2): 185.

Möller, P. a. J. R. N. (1981). "Nuclear mass formula with a Yukawa-plus-exponential macroscopic model and a folded-Yukawa single-particle potential." Nucl Phys A **361**: 117.

Moraes, S. B., P.R.S. Gomes, J. Lubian, J.J.S. Alves, R.M. Anjos, M.M. Sant'Anna, J. Padron, and C. Muri (2000). "Fusion and elastic scattering of ^{9}Be+^{64}Zn: A search of the breakup influence on these processes." Phys Rev C **61**: 064608.

Mukherjee, A. a. B. D. (1997). "Fusion cross sections for ^{7}Li + ^{11}B and ^{9}Be + ^{9}Be reactions at low energies." Nuclear Physics A **614**: 238.

Mukherjee, A. a. B. D. (2001). "Breakup vs fusion inhibition of Li-induced reactions at low energies " Phys Rev C **63**(1): 017604.

Navin, A., V. Tripathi, Y. Blumenfeld, V. Nanal, C. Simenel, J. M. Casandjian, G. de France, R. Raabe, D. Bazin, A. Chatterjee, M. Dasgupta, S. Kailas, R. C. Lemmon, K. Mahata, R. G. Pillay, E. C. Pollacco, K. Ramachandran, M. Rejmund, A. Shrivastava, J. L. Sida, and E. Tryggestad (2004). "Direct and compound reactions induced by unstable helium beams near the Coulomb barrier." Phys Rev C **70**: 044601.

NSCL. (1999, October 28, 2003). "SpecTcl Home page." Retrieved Feb 22, 2006, from http://docs.nscl.msu.edu/daq/spectcl/index.htm.

NSCL. (2002). "Simulation of fragment separators." 2006, from http://groups.nscl.msu.edu/lise/lise.html.

NSCL. (2004). "NSCL Data Acquisition." Retrieved May 6, 2007, from http://groups.nscl.msu.edu/userinfo/daq/dataacquisition.html.

Oganessian, Y. T., Demin, A.G., Iljinov, A.S., et. al. (1975). "Experiments on the synthesis of neutron-deficient Kurchatovium isotopes in reactions induced by ^{50}Ti Ions." Nucl Phys A **239**: 157.

Padron, I., P. R. S. Gomes, R. M. Anjos, J. Lubian, C. Muri, J. J. S. Alves, G. V. Martı´, M. Ramı´rez, A. J. Pacheco, O. A. Capurro, J. O. Ferna´ndez Niello, J. E. Testoni, D. Abriola, M. R. Spinella (2002). "Fusion of stable weakly bound nuclei with ^{27}Al and ^{64}Zn." Phys Rev C **66**(4): 044608.

Parthasarathy, N. V. (1989). Practical electroplating handbook, Englewood Cliffs, N.J. : Prentice Hall.

Penionzhkevich, Y. E. (1995). "The experimental investigation of exotic nuclei properties in Dubna." Nuclear Physics A **588**(1): 259c--266c.

Penionzhkevich, Y. E., V. I. Zagrebaev, S. M. Lukyanov, and R. Kalpakchieva (2006). "Deep Sub-Barrier Fusion Enhancement in the ^{6}He+^{206}Pb Reaction." Phys Rev Lett **96**: 162701.

Peterson, D., J. J. Kolata, P. Santi, J. von Schwarzenberg, D. Bazin, B. M. Sherrill (2003). "Elastic scattering of ^{9}Li and ^{11}Li from ^{12}C at 50 MeV per nucleon." Phys. Rev. C **67**.

Petrascu, M., I. Tanihata, T. Kobayashi, A. Isbasescu, H. Petrascu, A. Korsheninnikov, E. Nikolski, S. Fukuda, H. Kumagai, S. Momota, A. Ozawa, K. Yoshida, C. Bordeanu, I. David, I. Lazar, I. Mihai, G. Vaman, M. Giurgiu (1997). "Neutron pre-emission at the fusion of ^{11}Li halo nuclei with Si targets." Physics Letters B **405**(3-4): 224-229.

Raabe, R., J. L. Sida, J. L. Charvet, N. Alamanos, C. Angulo, J. M. Casandjian, S. Courtin, A. Drouart, D. J. C. Durand, P. Figuera, A. Gillibert, S. Heinrich, C. Jouanne, V. Lapoux, A. Lepine-Szily, A. Musumarra, L. Nalpas, D. Pierroutsakou, M. Romoli, K. Rusek & M. Trotta (2004). "No enhancement of fusion probability by the neutron halo of ^{6}He." Nature **431**: 823.

Rattan, S. S. e. a. (1992). Radiochim Acta **57**: 7.

Reisdorf, W. (1981). "Analysis of fissionability data at high excitation energies." Zeitschrift für Physik A Hadrons and Nuclei **300**(2-3): 227.

Reisdorf, W., M. Schadel, (1992). "How well do we understand the synthesis of heavy elements by heavy-ion induced fusion?" Zeitschrift für Physik A Hadrons and Nuclei **343**(1): 47-57.

Sa´nchez, R., W. No¨rtersha¨user, G. Ewald, D. Albers, J. Behr, P. Bricault, B. A. Bushaw, A. Dax, J. Dilling, M. Dombsky, G.W. F. Drake, S. Go¨tte, R. Kirchner, H.-J. Kluge, Th. Ku¨hl, J. Lassen, C. D. P. Levy, M. R. Pearson, E. J. Prime, V. Ryjkov, A. Wojtaszek, Z.-C. Yan, and C. Zimmermann (2006). "Nuclear Charge Radii of ^{9,11}Li: The Influence of Halo Neutrons." Phys Rev Lett **96**: 033002.

Savitzky, A. a. M. J. E. G. (1964). "Smoothing and Differentiation of Data by Simplified Least Squares Procedures." Anal Chem **36**(8): 1627.

Schmitt, H. W., Kiker, W. E., Williams, C. W. (1965). "Precision Measurements of Correlated Energies and Velocities of ^{252}Cf Fission Fragments." Phys Rev **137**(4B): B837.

Schröder, W. U., J.R. Huizenga (1984). Treatise on heavy-ion science. NYC, Plenum Press.

Shima, K., Toyoyuki Ishihara and Takashi Mikumo (1982). "Empirical formula for the average equilibrium charge-state of heavy ions behind various foils." Nuclear Instruments and Methods in Physics Research **200**(2-3): 605-608.

Signorini, C. (1997). "Fusion and breakup at the barrier with unstable nuclei." Nucl. Phys. **A616**(1-2): 262c.

Signorini, C., Liu, Z.H., Li, Z.C., Löbner, K.E.G., Müeller, L., Ruan, M., Rudolph, K., Soramel, F., Zotti, C., Andrighetto, A., Stroe, L., Vitturi, A., Zhang, H.Q. (1999). "Does break-up affect ^{9}Be + ^{209}Bi fusion at the barrier?" Eur. Phys. J. **A5**: 7.

Signorini, C., Liu, Z.H., Yoshida, A., Fukuda, T., Li, Z.C., Löbner, K.E.G., Müeller, L., Pu, Y.H., Rudolph, K., Soramel, F., Zotti, C., Sida, J.L. (1998a). "Fusion around the barrier in ^{11,9}Be + ^{209}Bi." Eur. Phys. J. **A2**: 227.

Signorini, C., Liu, Z.H., Yoshida, A., Fukuda, T., Li, Z.C., Löbner, K.G.E., Müller, L., Pu, Y.H., Rudolph, K., Soramel, F., Zotti, C., Andrighetto, A., Sida, J.L. (1998b). "Fusion cross-sections around the barrier in ^{11,9}Be + ^{209}Bi." Nuovo Cimento A **111**(8-9): 917.

Siwek-Wilczynska, K., I. Skwira, J. Wilczynski (2005). "Tests of the fission-evaporation competition in the deexcitation of heavy nuclei." Phys Rev C **72**: 034605.

Siwek-Wilczynska, K., J. Wilczynski (2004). "Empirical nucleus-nucleus potential deduced from fusion excitation functions." Phys Rev C **69**: 024611.

Smolańczuk, R. (1999). "Production mechanism of superheavy nuclei in cold fusion reactions." Phys Rev C **59**(5): 2634.

Smolańczuk, R., Skalski, J., Sobiczewski, A. (1995). "Spontaneous-fission half-lives of deformed superheavy nuclei." Phys Rev C **52**(4): 1871.

Swiatecki, W. J. (1982). "The dynamics of the fusion of two nuclei." Nucl Phys A **376**: 275.

Swiatecki, W. J., K. Siwek-Wilczynska, J. Wilczynski (2005). "Fusion by diffusion. II. Synthesis of transfermium elements in cold fusion reactions." Phys Rev C **71**: 014602.

Takahashi, J., M. Munhoz, E.M. Szanto, N. Carlin, N. Added, A.A.P. Suaide, M.M. de Moura, R. Liguori Neto, A. Szanto de Toledo, and L.F. Canto (1997). "Is Fusion Inhibited for Weakly Bound Nuclei?" Phys Rev Lett **78**: 30.

Takigawa, N., Kuratani, M., Sagawa, H. (1993). "Effect of breakup reactions on the fusion of a halo nucleus." Phys. Rev. **C47**(6): R2470.

Takigawa, N., Sagawa, H. (1991). "Interaction potential and fusion of a halo nucleus." Phys Lett B **265**(1-2): 23-28.

Tanihata, I., H. Hamagaki, O. Hashimoto, Y. Shida, N. Yoshikawa (1985). "Measurements of interaction cross sections and nuclear radii in the light p-shell region." Phys. Rev. Lett. **55**(24): 2676.

Tripathi, V., A. Navin, K. Mahata, K. Ramachandran, A. Chatterjee, and S. Kailas (2002). "Angular Momentum and Cross Sections for Fusion with Weakly Bound Nuclei: Breakup, a Coherent Effect " Phys Rev Lett **88**(17): 172701.

TRIUMF. (2000). "Midas Data Acquisition." Retrieved Feb 22, 2006, from http://ladd00.triumf.ca/~daqweb/doc/midas/html/index.html.

Trotta, M., J. L. Sida, N. Alamanos, A. Andreyev, F. Auger, D. L. Balabanski, C. Borcea, N. Coulier, A. Drouart, D. J. C. Durand, G. Georgiev, A. Gillibert, J. D. Hinnefeld, M. Huyse, C. Jouanne, V. Lapoux, A. Lépine, A. Lumbroso, F. Marie, A. Musumarra, G. S. Ottini, R. Raabe, S. Ternier, P. Van Duppen, K. Vyvey, C. Volant, and R. Wolski (2000). "Large Enhancement of the Sub-barrier Fusion Probability for a Halo Nucleus " Phys Rev Lett **84**(11): 2342 - 2345.

Uchiyama, F. (2003). "Is a neutron halo nothing but a large neutron skin?" Nuclear Theory **nucl-th/0309080**: 12.

Vandenbosch, R., J.R. Huizenga (1973). Nuclear Fission. N.Y. and London, Academic Press.

Wong, C. Y. (1973). "Interaction barrier in charged-particle nuclear reactions." Physical Review Letters **31**(12): 766.

Yoshida, A., Aoi, N., Fukuda, T., Hirai, M., Ishihara, M., Kobinata, H., Mizoi, Y., Mueller, L., Nagashima, Y., Nakano, J., Nomura, T., Pu, Y.H., Scarlassala, F., Signorini, C., Watanabe, Y. (1995). "Measurement of fusion cross section with neutron halo nuclei." Nucl. Phys. A **588**: 109c.

Yoshida, A., Watanabe Y., Ishihara M., Liu G.H., Fukuda T, Nomurs T., Pu Y.H., Mizoi Y., Signorini C., Mueller L., Scarlassara F., Sekine T, Ueno H., Nagashima Y., Sakurai H., Tanikawa M., Kimura K. (1994). Measurement of the fusion cross section with unstable neutron rich nuclei. Heavy-ion fusion: exploring the variety of nuclear properties, Padova, Italy, World Scientific.

Zagrebaev, V. I. (2003). "Sub-barrier fusion enhancement due to neutron transfer " Phys Rev C **67**: 061601.

Zagrebaev, V. I. a. V. V. S., Walter Greiner (2007). "Sub-barrier fusion of neutron-rich nuclei and its astrophysical consequences." Phys Rev C **75**.

Ziegler, J. (1985, 2006). "PARTICLE INTERACTIONS WITH MATTER." Retrieved June 1, 2007, from http://www.srim.org/.

Zubov, A. S., Adamian, G.G., Antoneko, N.V., Ivanova, S.P., Scheid, W. (1999). "Survival probability of superheavy nuclei." Phys Rev C **65**: 024308.

APPENDICES

APPENDIX A

1. Ti+Pb.f

```
** -*- mode: FORTRAN; mode: fold -*-
      PROGRAM Ti+Pb

C{{{** Variables for processing the .EVT file
      Character*75 evtfile
      Character*45 runname
      Character*23 basedir
      Logical ixst,needswap,printit

      Integer MAXPAR,BUFSIZ
      PARAMETER (MAXPAR=170,BUFSIZ=8192)

      Integer*2 ibuf(BUFSIZ)
      Integer*2 swap2,GetDataWord
      Integer evtlen,buflen,buftyp
      Integer ipt,evtnum,epoint
      Integer bufproc,evtproc ! number of bufs/evts processed
      Integer i,j,iosb
C}}}
C{{{** Variables for packing the Ntuple
      Integer hitpatAB, hitpatCD, hitpatSiA
      Integer Aen, Ben, Cen, Den
      Real AenMeV, BenMeV, CenMeV, DenMeV
      Real EmaxA, EmaxB, EmaxC, EmaxD
      Integer unus1
      Integer Sien
      Real SienMeV
      Integer unus2
      Integer Atm, Btm, Ctm, Dtm
      Real Atmns, Btmns, Ctmns, Dtmns
      Real TmaxA, TmaxB, TmaxC, TmaxD
      Integer Sitm
      Real Sitmns
      Integer unus3
      Integer idata
      Integer StripnumA, StripnumB, StripnumC, StripnumD, StripnumSi
      Integer SmaxA, SmaxB, SmaxC, SmaxD
      Character*300 chform
      Real dA(8), dB(8), dC(8), dD(8), dSi(7)
        Data (dA(i), i = 1, 8) /21.8577, 21.9199, 21.9644, 21.9911, 21.9911, 21.9644,
21.9199, 21.8577/
```

```
      Data (dB(i), i = 1, 8) /21.8577, 21.9199, 21.9644, 21.9911, 21.9911, 21.9644,
21.9199, 21.8577/
      Data (dC(i), i = 1, 8) /21.8577, 21.9199, 21.9644, 21.9911, 21.9911, 21.9644,
21.9199, 21.8577/
      Data (dD(i), i = 1, 8) /21.8577, 21.9199, 21.9644, 21.9911, 21.9911, 21.9644,
21.9199, 21.8577/
      Data (dSi(i), i = 1, 7) /29.0000, 29.5600, 29.9000, 30.0000, 29.9000, 29.5600,
29.0000/
     Real vA, vB, vC, vD, vSi
     Integer massA, massB, massC, massD, massSi
     Real mA(8), mB(8), mC(8), mD(8), mSi(7)
      Data (mA(i), i = 1, 8) /0.0842, 0.1175, 0.0856, 0.0694, 0.0649, 0.0819, 0.0827,
0.0892/
      Data (mB(i), i = 1, 8) /0.1128, 0.1128, 0.0856, 0.0944, 0.0641, 0.0716, 0.0639,
0.0721/
      Data (mC(i), i = 1, 8) /0.0740, 0.0679, 0.0672, 0.0659, 0.0693, 0.0680, 0.0775,
0.0682/
      Data (mD(i), i = 1, 8) /0.0702, 0.0748, 0.0694, 0.0765, 0.0765, 0.0715, 0.0702,
0.0743/
      Data (mSi(i), i = 1, 7) /0.0779, 0.1042, 0.0277, 0.0812, 0.1258, 0.1082, 0.1101/
     Real a1A(8), a1B(8), a1C(8), a1D(8), a1Si(7), a2A(8), a2B(8), a2C(8), a2D(8),
a2Si(7)
     Real b1A(8), b1B(8), b1C(8), b1D(8), b1Si(7), b2A(8), b2B(8), b2C(8), b2D(8),
b2Si(7)
      Data (a1A(i), i = 1, 8) /0.0666, 0.0733, 0.0729, 0.0622, 0.0568, 0.0882, 0.0889,
0.0844/
      Data (a1B(i), i = 1, 8) /0.0640, 0.0640, 0.0899, 0.0640, 0.0647, 0.0744, 0.0667,
0.0719/
      Data (a1C(i), i = 1, 8) /0.1117, 0.1316, 0.0944, 0.0986, 0.0977, 0.1025, 0.0634,
0.0698/
      Data (a1D(i), i = 1, 8) /0.0693, 0.0734, 0.0705, 0.0782, 0.0763, 0.0774, 0.0664,
0.0667/
      Data (a1Si(i), i = 1, 7) /0.0700, 0.0985, 0.0665, 0.0693, 0.1059, 0.1018, 0.0897/
      Data (a2A(i), i = 1, 8) /0.000099, 0.000114, 0.000109, 0.000093, 0.000085,
0.000131, 0.000132, 0.000088/
      Data (a2B(i), i = 1, 8) /0.000090, 0.000090, 0.000134, 0.000090, 0.000096,
0.000111, 0.000099, 0.000107/
      Data (a2C(i), i = 1, 8) /0.000166, 0.000196, 0.000140, 0.000147, 0.000145,
0.000152, 0.000054, 0.000104/
      Data (a2D(i), i = 1, 8) /0.000103, 0.000109, 0.000105, 0.000116, 0.000114,
0.000115, 0.000099, 0.000099/
      Data (a2Si(i), i = 1, 7) /0.000104, 0.000147, 0.000099, 0.000103, 0.000158,
0.000151, 0.000133/
      Data (b1A(i), i = 1, 8) /10.434, 4.073, 3.894, 0.884, 9.594, -10.072, -3.205, -
2.844/
```

```
      Data (b1B(i), i = 1, 8) /-2.540, -2.540, -12.265, -2.540, -2.260, -1.820, 0.640,
4.369/
      Data (b1C(i), i = 1, 8) /-38.899, -71.058, -27.821, -34.942, -26.736, -31.318,
7.410, 7.410/
      Data (b1D(i), i = 1, 8) /4.173, 1.934, 2.701, -0.485, 3.452, 0.138, 8.626, 14.503/
      Data (b1Si(i), i = 1, 7) /-1.915, -6.715, -0.848, -1.586, 1.766, -8.050, 1.292/
      Data (b2A(i), i = 1, 8) /0.0192, 0.0103, 0.0094, 0.0050, 0.0179, -0.0113, -0.0011,
-0.0011/
      Data (b2B(i), i = 1, 8) /0.0640, 0.0640, -0.0145, 0.0640, 0.0003, 0.0009, 0.0046,
0.0102/
      Data (b2C(i), i = 1, 8) /-0.0542, -0.1020, -0.0377, -0.0483, -0.0361, -0.0429,
0.0147, 0.0147/
      Data (b2D(i), i = 1, 8) /0.0099, 0.0065, 0.0077, 0.0030, 0.0088, 0.0038, 0.0165,
0.0252/
      Data (b2Si(i), i = 1, 7) /0.00082, -0.00632, 0.00240, 0.00131, 0.00629, -0.00830,
0.00559/
    Real Aanglval(8), Banglval(8), Canglval(8), Danglval(8), Sianglval(7)
        Data (Aanglval(i), i = 1, 8) /66.63, 71.52, 68.26, 61.74, 63.37, 58.48, 60.11,
69.89/
        Data (Banglval(i), i = 1, 8) /99.89, 98.26, 91.74, 101.52, 96.63, 90.11, 88.48,
93.37/
        Data (Canglval(i), i = 1, 8) /31.74, 28.48, 36.63, 30.11, 38.26, 33.37, 41.52,
39.89/
        Data (Danglval(i), i = 1,8) /58.48, 61.74, 66.63, 63.37, 68.26, 60.11, 69.89,
71.52/
        Data (Sianglval(i), i = 1, 7) /132.95, 138.65, 167.05, 144.33, 150.00, 155.67,
161.35/
    Real cAtm(8), cBtm(8), cCtm(8), cDtm(8), cSitm(7)
        Data (cAtm(i), i = 1, 8) /8.9297, 9.0974, 9.1383, 9.2495, 9.5236, 9.5036,
9.5554, 9.6232/
        Data (cBtm(i), i = 1, 8) /9.9817, 0.0000, 10.157, 10.294, 10.602, 10.648,
10.863, 10.236/
        Data (cCtm(i), i = 1, 8) /0.0075, 0.0072, 0.0074, 0.0074, 0.0074, 0.0070,
0.0085, 0.0070/
        Data (cDtm(i), i = 1,8) /8.1617, 7.9533, 8.3622, 8.1828, 8.0346, 0.0095,
7.9527, 8.8211/
        Data (cSitm(i), i = 1, 7) /14.872, 15.461, 0.0400, 16.159, 16.592, 16.113,
15.832/
    Real mAtm(8), mBtm(8), mCtm(8), mDtm(8), mSitm(7)
        Data (mAtm(i), i = 1, 8) /-0.0004, -0.0005, -0.0005, -0.0005, -0.0006, -0.0005,
-0.0006, -0.0006/
        Data (mBtm(i), i = 1, 8) /0.0005, 0.0001, -0.0005, -0.0006, -0.0007, -0.0007, -
0.0007, -0.0003/
        Data (mCtm(i), i = 1, 8) /-0.0008, -0.0005, -0.0009, -0.0007, -0.0005, 0.0070, -
0.0004, -0.0011/
```

```
      Data (mDtm(i), i = 1,8) /0.0135, 0.0102, 0.0100, 0.0105, 0.0085, 0.0095,
0.0083, 0.0086/
      Data (mSitm(i), i = 1, 7) /-0.0011, -0.0012, 0.0009, -0.0009, -0.0012, -0.0010, -
0.0016/
    Integer Aangl, Bangl, Cangl, Dangl, Siangl
** NTUPLE COMMON BLOCKS
    COMMON /HitPat/hitpatAB, hitpatCD, hitpatSiA
    COMMON /Energy/ Aen(8), Ben(8), Cen(8), Den(8), Sien(7)
    COMMON /Unused1/ unus1(1)
    COMMON /Unused2/ unus2(4)
    COMMON /Time/ Atm(8), Btm(8), Ctm(8), Dtm(8),Sitm(7)
    COMMON /Timens/ Atmns(8), Btmns(8), Ctmns(8), Dtmns(8), Sitmns(7)
    COMMON /Tmax/TmaxA, TmaxB, TmaxC, TmaxD
    COMMON /Unused3/ unus3(5)
    COMMON /EnergyMeV/ AenMeV(8), BenMeV(8), CenMeV(8), DenMeV(8),
SienMeV(7)
    COMMON /Emax/EmaxA, EmaxB, EmaxC, EmaxD
    COMMON /Stripnum/ StripnumA(8), StripnumB(8), StripnumC(8),
StripnumD(8), StripnumSi(7)
    COMMON /Smax/SmaxA, SmaxB, SmaxC, SmaxD
    COMMON /Angle/ Aangl(8), Bangl(8), Cangl(8), Dangl(8), Siangl(7)
    COMMON /Velocity/ vA(8), vB(8), vC(8), vD(8), vSi(7)
    COMMON /Mass/ massA(8), massB(8), massC(8), massD(8), massSi(7)
C}}}

** Paw COMMON stuff
    INTEGER icycle
    PARAMETER (MXBK=1000000)
    COMMON /PAWC/ PAW(MXBK)
    COMMON /QUEST/IQUEST(100)
    COMMON /HBOOK/ LRECL
    CALL HLIMIT(MXBK)
    IQUEST(10)=64000

    needswap = .true.
    basedir = '/store/naikra/EVTfiles/'
** Establish output file
    call hbset('BSIZE',8192,ISTAT)
    call hropen(3,'Rf','Rfentm.hbook', 'NQP', 8192,ISTAT)
C{{{** Form CWN
    call hbnt(100,'Ti+Pb=Rf',' ')

C{{{ Hitpatterns
    chform = 'hitpatAB[0,4096]:i'
    call hbname(100, 'HitPatAB',hitpatAB, chform)
```

```
      chform = 'hitpatCD[0,4096]:i'
      call hbname(100, 'HitPatCD',hitpatCD, chform)

      chform = 'hitpatSiA[0,4096]:i'
      call hbname(100, 'HitPatSiA', hitpatSiA, chform)
C}}}
C{{{ Detector A Energies
      chform = 'Aen(8)[0,4096]:i'
      call hbname(100, 'Aenergy', Aen(1), chform)
C}}}
C{{{ Detector A Energies in MeV
      chform = 'AenMeV(8):r'
      call hbname(100, 'AenergyMeV', AenMeV(1), chform)
C}}}
C{{{ Detector A Max Energy
      chform = 'EmaxA:r'
      call hbname(100, 'EmaxA', EmaxA, chform)
C}}}
C{{{ Detector A strip numbers
      chform = 'StripnumA(8)[0,4096]:i'
      call hbname(100, 'StripnumA', StripnumA(1), chform)
C}}}
C{{{ Detector A max strip number
      chform = 'SmaxA[0,4096]:i'
      call hbname(100, 'SmaxA', SmaxA, chform)
C}}}
C{{{ Detector A Angles
      chform = 'Aangl(8)[0,4096]:i'
      call hbname(100, 'Aangle', Aangl(1), chform)
C}}}
C{{{ Detector A Velocity
      chform = 'vA(8):r'
      call hbname(100, 'velA', vA(1), chform)
C}}}
C{{{ Detector A Mass
      chform = 'massA(8):i'
      call hbname(100, 'massA', massA(1), chform)
C}}}
C{{{ Detector B Energies
      chform = 'Ben(8)[0,4096]:i'
      call hbname(100, 'Benergy', Ben(1), chform)
C}}}
C{{{ Detector B Energies in MeV
      chform = 'BenMeV(8)r'
      call hbname(100, 'BenergyMeV', BenMeV(1), chform)
C}}}
```

```
C{{{ Detector B Max Energy
      chform = 'EmaxB:r'
      call hbname(100, 'EmaxB', EmaxB, chform)
C}}}
C{{{ Detector B strip numbers
      chform = 'StripnumB(8)[0,4096]:i'
      call hbname(100, 'StripnumB', StripnumB(1), chform)
C}}}
C{{{ Detector B max strip number
      chform = 'SmaxB[0,4096]:i'
      call hbname(100, 'SmaxB', SmaxB, chform)
C}}}
C{{{ Detector B Angles
      chform = 'Bangl(8)[0,4096]:i'
      call hbname(100, 'Bangle', Bangl(1), chform)
C}}}
C{{{ Detector B Velocity
      chform = 'vB(8):r'
      call hbname(100, 'velB', vB(1), chform)
C}}}
C{{{ Detector B Mass
      chform = 'massB(8):i'
      call hbname(100, 'massB', massB(1), chform)
C}}}
C{{{ Detector C Energies
      chform = 'Cen(8)[0,4096]:i'
      call hbname(100, 'Cenergy', Cen(1), chform)
C}}}
C{{{ Detector C Energies in MeV
      chform = 'CenMeV(8):r'
      call hbname(100, 'CenergyMeV', CenMeV(1), chform)
C}}}
C{{{ Detector C Max Energy
      chform = 'EmaxC:r'
      call hbname(100, 'EmaxC', EmaxC, chform)
C}}}
C{{{ Detector C strip numbers
      chform = 'StripnumC(8)[0,4096]:i'
      call hbname(100, 'StripnumC', StripnumC(1), chform)
C}}}
C{{{ Detector C max strip number
      chform = 'SmaxC[0,4096]:i'
      call hbname(100, 'SmaxC', SmaxC, chform)
C}}}
C{{{ Detector C Angles
      chform = 'Cangl(8)[0,4096]:i'
```

```
      call hbname(100, 'Cangle', Cangl(1), chform)
C}}}
C{{{ Detector C Velocity
      chform = 'vC(8):r'
      call hbname(100, 'velC', vC(1), chform)
C}}}
C{{{ Detector C Mass
      chform = 'massC(8):i'
      call hbname(100, 'massC', massC(1), chform)
C}}}
C{{{ Detector D Energies
      chform = 'Den(8)[0,4096]:i'
      call hbname(100, 'Denergy', Den(1), chform)
C}}}
C{{{ Detector D Energies in MeV
      chform = 'DenMeV(8):r'
      call hbname(100, 'DenergyMeV', DenMeV(1), chform)
C}}}
C{{{ Detector D Max Energy
      chform = 'EmaxD:r'
      call hbname(100, 'EmaxD', EmaxD, chform)
C}}}
C{{{ Detector D strip numbers
      chform = 'StripnumD(8)[0,4096]:i'
      call hbname(100, 'StripnumD', StripnumD(1), chform)
C}}}
C{{{ Detector D max strip number
      chform = 'SmaxD[0,4096]:i'
      call hbname(100, 'SmaxD', SmaxD, chform)
C}}}
C{{{ Detector D Angles
      chform = 'Dangl(8)[0,4096]:i'
      call hbname(100, 'Dangle', Dangl(1), chform)
C}}}
C{{{ Detector D velocity
      chform = 'vD(8):r'
      call hbname(100, 'velD', vD(1), chform)
C}}}
C{{{ Detector D Mass
      chform = 'massD(8):i'
      call hbname(100, 'massD', massD(1), chform)
C}}}
C{{{ Si-Array Detector Energies
      chform = 'Sien(7)[0,4096]:i'
      call hbname(100, 'Sienergy', Sien(1), chform)
C}}}
```

```
C{{{ Si-Array Detector Energies in MeV
      chform = 'SienMeV(7):r'
      call hbname(100, 'SienergyMeV', SienMeV(1), chform)
C}}}
C{{{ Si-array strip numbers
      chform = 'StripnumSi(7)[0,4096]:i'
      call hbname(100, 'StripnumSi', StripnumSi(1), chform)
C}}}
C{{{ Si-Array Detector Angles
      chform = 'Siangl(7)[0,4096]:i'
      call hbname(100, 'SiAangle', Siangl(1), chform)
C}}}
C{{{ Detector Si velocity
      chform = 'vSi(8):r'
      call hbname(100, 'velSi', vSi(1), chform)
C}}}
C{{{ Detector Si Mass
      chform = 'massSi(7):i'
      call hbname(100, 'massSi', massSi(1), chform)
C}}}
C{{{ Detector A Times
      chform = 'Atm(8)[0,4096]:i'
      call hbname(100, 'Atime', Atm(1), chform)
C}}}
C{{{ Detector A Absolute Times
      chform = 'Atmns(8):r'
      call hbname(100, 'Atimens', Atmns(1), chform)
C}}}
C{{{ Detector A Max Time
      chform = 'TmaxA:r'
      call hbname(100, 'TmaxA', TmaxA, chform)
C}}}
C{{{ Detector B Times
      chform = 'Btm(8)[0,4096]:i'
      call hbname(100, 'Btime', Btm(1), chform)
C}}}
C{{{ Detector B Absolute Times
      chform = 'Btmns(8):r'
      call hbname(100, 'Btimens', Btmns(1), chform)
C}}}
C{{{ Detector B Max Time
      chform = 'TmaxB:r'
      call hbname(100, 'TmaxB', TmaxB, chform)
C}}}
C{{{ Detector C Times
      chform = 'Ctm(8)[0,4096]:i'
```

```
      call hbname(100, 'Ctime', Ctm(1), chform)
C}}}
C{{{ Detector C Absolute Times
      chform = 'Ctmns(8):r'
      call hbname(100, 'Ctimens', Ctmns(1), chform)
C}}}
C{{{ Detector C Max Time
      chform = 'TmaxC:r'
      call hbname(100, 'TmaxC', TmaxC, chform)
C}}}
C{{{ Detector D Times
      chform = 'Dtm(8)[0,4096]:i'
      call hbname(100, 'Dtime', Dtm(1), chform)
C}}}
C{{{ Detector D Absolute Times
      chform = 'Dtmns(8):r'
      call hbname(100, 'Dtimens', Dtmns(1), chform)
C}}}
C{{{ Detector D Max Time
      chform = 'TmaxD:r'
      call hbname(100, 'TmaxD', TmaxD, chform)
C}}}
C{{{ Si-Array Detector Times
      chform = 'Sitm(7)[0,4096]:i'
      call hbname(100, 'Sitime', Sitm(1), chform)
C}}}
C{{{ Si-array Detector Absolute Times
      chform = 'Sitmns(7):r'
      call hbname(100, 'Sitimens', Sitmns(1), chform)
C}}}
C{{{Unused parameters
      chform = 'unus1(1)[0,4096]:i'
      call hbname(100, 'Unused1', unus1(1), chform)
C}}}
C{{{Unused parameters
      chform = 'unus2(4)[0,4096]:i'
      call hbname(100, 'Unused2', unus2(1), chform)
C}}}
C{{{Unused parameters
      chform = 'unus3(5)[0,4096]:i'
      call hbname(100, 'Unused3', unus3(1), chform)
C}}}

**      chform = 'nmult[0,12]:i, fmult(2)[0,16]:i, '//
**     &  'bmult(2)[0,16]:i, tmult(2)[0,16]:i'
**      call hbname(100, 'MULT', nmult, chform)
```

```
**C}}}

      evtproc=0
C{{{ Locate data file(s)
      open(1,file='runlist.txt',status='old')
 1    READ(1,'(a)') runname
      If (runname(1:3).eq.'end' .OR. runname(1:3).eq.'END') Then
        CLOSE(1)
        Goto 999
      EndIf

      evtfile = basedir//runname
      inquire(file=evtfile,exist=ixst)
      If (.NOT. ixst) Then
        Print*, 'Error:  file not found; ',evtfile
        STOP
      EndIf
C}}}
** Open file(s)
      open(20,file=evtfile,access='direct',recl=bufsiz*2,status='old')
      bufproc=0

 2    CONTINUE
** Read next buffer
      bufproc = bufproc+1
      evtproc = evtproc + evtnum
      read(20,rec=bufproc,err=997,iostat=IOSB)ibuf
      If (iosb .ne. 0) Then
        If (iosb.ne.-1) Print*, 'IOSB=',iosb
        Goto 11
      EndIf

C{{{ Zero parameters for hitpatterns
        hitpatAB = 0
        hitpatCD = 0
        hitpatSiA  = 0
C}}}
      Do i=0,7
C{{{Zero parameters for DSSD energies
        Aen(i+1) = 0
        Ben(i+1) = 0
        Cen(i+1) = 0
        Den(i+1) = 0
C}}}
       EndDo
      Do i=0,7
```

```
C{{{Zero parameters for DSSD energies in MeV
       AenMeV(i+1) = -100
       BenMeV(i+1) = -100
       CenMeV(i+1) = -100
       DenMeV(i+1) = -100
C}}}
      EndDo
     Do i=0,7
C{{{Zero parameters for DSSD max energies in MeV
      EmaxA = 0
      EmaxB = 0
      EmaxC = 0
      EmaxD = 0
C}}}
      EndDo
     Do i=0,7
C{{{Zero parameters for DSSD max energies in MeV
      SmaxA = 0
      SmaxB = 0
      SmaxC = 0
      SmaxD = 0
C}}}
      EndDo
     Do i=0,7
C{{{Zero parameters for DSSD max energies in MeV
      TmaxA = 0
      TmaxB = 0
      TmaxC = 0
      TmaxD = 0
C}}}
      EndDo
     Do i=0,7
C{{{Zero parameters for DSSD strip numbers
       StripnumA(i+1) = 0
       StripnumB(i+1) = 0
       StripnumC(i+1) = 0
       StripnumD(i+1) = 0
C}}}
      EndDo
     Do i=0,7
C{{{Zero parameters for DSSD angles
       Aangl(i+1) = 0
       Bangl(i+1) = 0
       Cangl(i+1) = 0
       Dangl(i+1) = 0
C}}}
```

```
      EndDo
     Do i=0,7
C{{{Zero parameters for DSSD velocities
      vA(i+1) = 0
      vB(i+1) = 0
      vC(i+1) = 0
      vD(i+1) = 0
C}}}
      EndDo
     Do i=0,7
C{{{Zero parameters for DSSD masses
      massA(i+1) = 0
      massB(i+1) = 0
      massC(i+1) = 0
      massD(i+1) = 0
C}}}
      EndDo
C{{{Zero parameter for unused
         unus1(1) = 0
C}}}
      Do i=0,6
C{{{Zero parameters for Si-array energy
      Sien(i+1) = 0
C}}}
      EndDo
      Do i=0,6
C{{{Zero parameters for Si-array energy in MeV
      SienMeV(i+1) = 0
C}}}
      EndDo
      Do i=0,6
C{{{Zero parameters for Si-array strip numbers
      StripnumSi(i+1) = 0
C}}}
      EndDo
      Do i=0,6
C{{{Zero parameters for Si-array angles
      Siangl(i+1) = 0
C}}}
      EndDo
      Do i=0,6
C{{{Zero parameters for Si-array velocity
      vSi(i+1) = 0
C}}}
      EndDo
      Do i=0,6
```

```
C{{{Zero parameters for Si-array mass
       massSi(i+1) = 0
C}}}
      EndDo
      Do i=0,3
C{{{Zero parameter for unused
          unus2(i+1) = 0
C}}}
      EndDo
      Do i=0,7
C{{{Zero parameters for DSSD times
       Atm(i+1) = 0
       Btm(i+1) = 0
       Ctm(i+1) = 0
       Dtm(i+1) = 0
C}}}
     EndDo
      Do i=0,7
C{{{Zero parameters for DSSD absolute times
       Atmns(i+1) = 0
       Btmns(i+1) = 0
       Ctmns(i+1) = 0
       Dtmns(i+1) = 0
C}}}
     EndDo
     Do i=0,6
C{{{Zero parameters for Si-array time
       Sitm(i+1) = 0
C}}}
     EndDo
     Do i=0,6
C{{{Zero parameters for Si-array absolute time
       Sitmns(i+1) = 0
C}}}
     EndDo
     Do i=0,4
C{{{Zero parameters for unused
          unus3(i+1) = 0
C}}}
     EndDo

     evtnum = 0


C{{{** Find Buffer (useful) length and type
     If (needswap) Then
```

```
      buflen = swap2(ibuf(1))
      buftyp = swap2(ibuf(2))
    Else
      buflen = ibuf(1)
      buftyp = ibuf(2)
    EndIf
**        write(*,*)'buflen and buftyp =',buflen,buftyp
**        write(*,*)
    If (buftyp .ne. 1) Then
      WRITE(*,'(a,i5,a,i3)') 'Buffer ',bufproc,' was type ',buftyp
      If (buftyp .eq. 12) Goto 11 ! "END_RUN" BUFFER
      Goto 2 ! Skip to next buffer if this isn't data
    EndIf
C}}}

    ipt = 17  !get past Buffer Header to real data
** Loop over events in the buffer
    Do While (ipt .le. buflen)
C{{{
      evtnum = evtnum+1
      printit = .false.
      idata = GetDataWord(needswap,ibuf(ipt))
      If (printit) WRITE(*,9999) evtnum,ipt,idata
      evtlen = idata !Get Event Length
      epoint = ipt   ! Note beginning of event packet (pointer for event)
      endpt = epoint+evtlen
      If (printit) WRITE(*,*) 'STARTING EVENTS: ',evtlen,epoint,ipt
      Do While (ipt .lt. endpt) ! Loop through this event packet
      ipt = ipt+1

C{{{ Read all channels set in Hitpattern of A and B ADC
            idata = GetDataWord(needswap,ibuf(ipt))
            If (printit) WRITE(*,9999) evtnum,ipt,idata
            idata = IAND(idata,'0fff'x) ! data is in lower 12 bits
            hitpatAB = idata
C}}}
          ipt = ipt+1
C{{{ Read all channels set in Hitpattern of C and D ADC
            idata = GetDataWord(needswap,ibuf(ipt))
            If (printit) WRITE(*,9999) evtnum,ipt,idata
            idata = IAND(idata,'0fff'x) ! data is in lower 12 bits
            hitpatCD = idata
C}}}
          ipt = ipt+1
C{{{ Read all channels set in Hitpattern of Si-array ADC
            idata = GetDataWord(needswap,ibuf(ipt))
```

```
            If (printit) WRITE(*,9999) evtnum,ipt,idata
            idata = IAND(idata,'0fff'x) ! data is in lower 12 bits
            hitpatSiA = idata
C}}}
          ipt = ipt+1
C{{{ Read all A energies, convert to MeV, read angles
         Do j = 0,7
            idata = GetDataWord(needswap,ibuf(ipt+j))
            If (printit) WRITE(*,9999) evtnum,ipt+j,idata
            idata = IAND(idata,'0fff'x) ! data is in lower 12 bits
            Aen(j+1) = idata
            AenMeV(j+1) = mA(j+1)*idata
                  If (AenMeV(j+1) .lt. 150.00) then
                  AenMeV(j+1) = (a1A(j+1)+(a2A(j+1)*128.00))*idata +
(b1A(j+1)+(b2A(j+1)*128.00))
                  endif
                  If (AenMeV(j+1) .gt. EmaxA) then
                        EmaxA = AenMeV(j+1)
                     SmaxA = j+1
                  endif
                  StripnumA(j+1) = j+1
                  Aangl(j+1) = Aanglval(j+1)
         EndDo
           ipt = ipt+8
C}}}
C{{{ Read active channels in B energies ADC
         Do j = 0,7
            idata = GetDataWord(needswap,ibuf(ipt+j))
            If (printit) WRITE(*,9999) evtnum,ipt+j,idata
            idata = IAND(idata,'0fff'x) ! data is in lower 12 bits
            Ben(j+1) = idata
            BenMeV(j+1) = mB(j+1)*idata
                  If (BenMeV(j+1) .lt. 115.00) then
                  BenMeV(j+1) = (a1B(j+1)+(a2B(j+1)*128.00))*idata +
(b1B(j+1)+(b2B(j+1)*128.00))
                  endif
                  If (BenMeV(j+1) .gt. EmaxB) then
                        EmaxB = BenMeV(j+1)
                     SmaxB = j+1
                  endif
                  StripnumB(j+1) = j+1
                  Bangl(j+1) = Banglval(j+1)
         EndDo
           ipt = ipt+8
C}}}
C{{{ Read active channels in C energies ADC
```

```
          Do j = 0,7
             idata = GetDataWord(needswap,ibuf(ipt+j))
             If (printit) WRITE(*,9999) evtnum,ipt+j,idata
             idata = IAND(idata,'0fff'x) ! data is in lower 12 bits
             Cen(j+1) = idata
             CenMeV(j+1) = mC(j+1)*idata
                   If (CenMeV(j+1) .lt. 190.00) then
                   CenMeV(j+1) = (a1C(j+1)+(a2C(j+1)*128.00))*idata +
(b1C(j+1)+(b2C(j+1)*128.00))
                   endif
                   If (CenMeV(j+1) .gt. EmaxC) then
                         EmaxC = CenMeV(j+1)
                        SmaxC = j+1
                   endif
                   StripnumC(j+1) = j+1
                   Cangl(j+1) = Canglval(StripnumC(j+1))
          EndDo
            ipt = ipt+8
C}}}
C{{{ Read active channels in D energies ADC
          Do j = 0,7
             idata = GetDataWord(needswap,ibuf(ipt+j))
             If (printit) WRITE(*,9999) evtnum,ipt+j,idata
             idata = IAND(idata,'0fff'x) ! data is in lower 12 bits
             Den(j+1) = idata
             DenMeV(j+1) = mD(j+1)*idata
                   If (DenMeV(j+1) .lt. 150.00) then
                   DenMeV(j+1) = (a1D(j+1)+(a2D(j+1)*128.00))*idata +
(b1D(j+1)+(b2D(j+1)*128.00))
                   endif
                   If (DenMeV(j+1) .gt. EmaxD) then
                         EmaxD = DenMeV(j+1)
                        SmaxD = j+1
                   endif
                   StripnumD(j+1) = j+1
                   Dangl(j+1) = Danglval(StripnumD(j+1))
          EndDo
            ipt = ipt+8
C}}}
C{{{ Read active channels in unused ADC
             idata = GetDataWord(needswap,ibuf(ipt))
             If (printit) WRITE(*,9999) evtnum,ipt,idata
             idata = IAND(idata,'0fff'x) ! data is in lower 12 bits
             unus1(1) = idata
           ipt = ipt+1
C}}}
```

```
C{{{ Read active ADC channels in Si-array energies
        Do j = 0,6
           idata = GetDataWord(needswap,ibuf(ipt+j))
           If (printit) WRITE(*,9999) evtnum,ipt+j,idata
           idata = IAND(idata,'0fff'x) ! data is in lower 12 bits
           Sien(j+1) = idata
           SienMeV(j+1) = mSi(j+1)*idata
                 StripnumSi(j+1) = j+1
                 Siangl(j+1) = Sianglval(StripnumSi(j+1))
        EndDo
         ipt = ipt+7
C}}}
C{{{ Read all active ADC channel in unused
        Do j = 0,3
           idata = GetDataWord(needswap,ibuf(ipt+j))
           If (printit) WRITE(*,9999) evtnum,ipt+j,idata
           idata = IAND(idata,'0fff'x) ! data is in lower 12 bits
           unus2(j+1) = idata
        EndDo
         ipt = ipt+4
C}}}
C{{{ Read all active ADC channels in A times
      Do j = 0,7
           idata = GetDataWord(needswap,ibuf(ipt+j))
           If (printit) WRITE(*,9999) evtnum,ipt+j,idata
           idata = IAND(idata,'0fff'x) ! data is in lower 12 bits
           Atm(j+1) = idata
                 Atmns(j+1) = mAtm(j+1)*idata + cAtm(j+1)
                 If (Atmns(j+1) .gt. TmaxA) TmaxA = Atmns(j+1)
                 vA(j+1) = dA(j+1) / Atmns(j+1)
                 massA(j+1) = (2*AenMeV(j+1)) / (vA(j+1)**2)
**               If (AenMeV(j+1) .gt. 50) write(21,*) bufproc, (j+1), AenMev(j+1),
Atm(j+1), Atmns(j+1), massA(j+1), vA(j+1), (vA(j+1)**2)
        EndDo
         ipt = ipt+8
C}}}
C{{{ Read all active ADC channels in B times
      Do j = 0,7
           idata = GetDataWord(needswap,ibuf(ipt+j))
           If (printit) WRITE(*,9999) evtnum,ipt+j,idata
           idata = IAND(idata,'0fff'x) ! data is in lower 12 bits
           Btm(j+1) = idata
                 Btmns(j+1) = mBtm(j+1)*idata + cBtm(j+1)
                 If (Btmns(j+1) .gt. TmaxB) TmaxB = Btmns(j+1)
                 vB(j+1) = dB(j+1) / Btmns(j+1)
                 massB(j+1) = (2*BenMeV(j+1)) / (vB(j+1)**2)
```

```
          EndDo
            ipt = ipt+8
C}}}
C{{{ Read all active ADC channels in C times
       Do j = 0,7
             idata = GetDataWord(needswap,ibuf(ipt+j))
             If (printit) WRITE(*,9999) evtnum,ipt+j,idata
             idata = IAND(idata,'0fff'x) ! data is in lower 12 bits
             Ctm(j+1) = idata
                   Ctmns(j+1) = mCtm(j+1)*idata + cCtm(j+1)
                   If (Ctmns(j+1) .gt. TmaxC) TmaxC = Ctmns(j+1)
                   vC(j+1) = dC(j+1) / Ctmns(j+1)
                   massC(j+1) = (2*CenMeV(j+1)) / (vC(j+1)**2)
          EndDo
            ipt = ipt+8
C}}}
C{{{ Read all active ADC channels in D times
        Do j = 0,7
             idata = GetDataWord(needswap,ibuf(ipt+j))
             If (printit) WRITE(*,9999) evtnum,ipt+j,idata
             idata = IAND(idata,'0fff'x) ! data is in lower 12 bits
             Dtm(j+1) = idata
                   Dtmns(j+1) = mDtm(j+1)*idata + cDtm(j+1)
                   If (Dtmns(j+1) .gt. TmaxD) TmaxD = Dtmns(j+1)
                   vD(j+1) = dD(j+1) / Dtmns(j+1)
                   massD(j+1) = (2*DenMeV(j+1)) / (vD(j+1)**2)
          EndDo
            ipt = ipt+8
C}}}
C{{{ Read all active ADC channels in Si-array times
       Do j = 0,6
             idata = GetDataWord(needswap,ibuf(ipt+j))
             If (printit) WRITE(*,9999) evtnum,ipt+j,idata
             idata = IAND(idata,'0fff'x) ! data is in lower 12 bits
             Sitm(j+1) = idata
                   Sitmns(j+1) = mSitm(j+1)*idata + cSitm(j+1)
                   vSi(j+1) = dSi(j+1) / Sitmns(j+1)
                   massSi(j+1) = (2*SienMeV(j+1)) / (vSi(j+1)**2)
          EndDo
            ipt = ipt+7
C}}}
C{{{ Read all active ADC channels in unused
       Do j = 0,4
             idata = GetDataWord(needswap,ibuf(ipt+j))
             If (printit) WRITE(*,9999) evtnum,ipt+j,idata
             idata = IAND(idata,'0fff'x) ! data is in lower 12 bits
```

```
            unus3(j+1) = idata
          EndDo
           ipt = ipt+5
C}}}
            idata = GetDataWord(needswap,ibuf(ipt))  ! dead
            If (printit) WRITE(*,9999) evtnum,ipt,idata
            idata = IAND(idata,'0fff'x) ! data is in lower 12 bits
            idata = IAND(idata,'07ff'x) ! data is in lower 11 bits
            ipt = ipt+1

            idata = GetDataWord(needswap,ibuf(ipt))  !ffff
            ipt= ipt+1
          If (idata .ne. -1) Then
           WRITE(*,*) 'Error in (xffff) event ',evtnum,' at ipt', ipt
           ipt = endpt
           Goto 3
          EndIf
C}}}
3       EndDo !End Packet

       call hfnt(100)

C{{{ Zero parameters for next event
C{{{ Zero parameters for hitpatterns
       hitpatAB = 0
       hitpatCD = 0
       hitpatSiA = 0
C}}}
      Do i=0,7
C{{{Zero parameters for DSSD energies
       Aen(i+1) = 0
       Ben(i+1) = 0
       Cen(i+1) = 0
       Den(i+1) = 0
C}}}
      EndDo
     Do i=0,7
C{{{Zero parameters for DSSD energies in MeV
       AenMeV(i+1) = -100
       BenMeV(i+1) = -100
       CenMeV(i+1) = -100
       DenMeV(i+1) = -100
C}}}
      EndDo
     Do i=0,7
C{{{Zero parameters for DSSD max energies in MeV
```

```
      EmaxA = 0
      EmaxB = 0
      EmaxC = 0
      EmaxD = 0
C}}}
      EndDo
     Do i=0,7
C{{{Zero parameters for DSSD max energies in MeV
      SmaxA = 0
      SmaxB = 0
      SmaxC = 0
      SmaxD = 0
C}}}
      EndDo
     Do i=0,7
C{{{Zero parameters for DSSD max energies in MeV
      TmaxA = 0
      TmaxB = 0
      TmaxC = 0
      TmaxD = 0
C}}}
      EndDo
      Do i=0,7
C{{{Zero parameters for DSSD strip numbers
       StripnumA(i+1) = 0
       StripnumB(i+1) = 0
       StripnumC(i+1) = 0
       StripnumD(i+1) = 0
C}}}
      EndDo
      Do i=0,7
C{{{Zero parameters for DSSD angles
       Aangl(i+1) = 0
       Bangl(i+1) = 0
       Cangl(i+1) = 0
       Dangl(i+1) = 0
C}}}
      EndDo
     Do i=0,7
C{{{Zero parameters for DSSD velocities
       vA(i+1) = 0
       vB(i+1) = 0
       vC(i+1) = 0
       vD(i+1) = 0
C}}}
      EndDo
```

```
      Do i=0,7
C{{{Zero parameters for DSSD masses
       massA(i+1) = 0
       massB(i+1) = 0
       massC(i+1) = 0
       massD(i+1) = 0
C}}}
      EndDo
C{{{Zero parameter for unused
          unus1(1) = 0
C}}}
      Do i=0,6
C{{{Zero parameters for Si-array energy
       Sien(i+1) = 0
C}}}
      EndDo
      Do i=0,6
C{{{Zero parameters for Si-array energy in MeV
       SienMeV(i+1) = 0
C}}}
      EndDo
      Do i=0,6
C{{{Zero parameters for Si-array strip numbers
       StripnumSi(i+1) = 0
C}}}
      EndDo
      Do i=0,6
C{{{Zero parameters for Si-array angles
       Siangl(i+1) = 0
C}}}
      EndDo
      Do i=0,3
C{{{Zero parameter for unused
          unus2(i+1) = 0
C}}}
      EndDo
      Do i=0,7
C{{{Zero parameters for DSSD times
       Atm(i+1) = 0
       Btm(i+1) = 0
       Ctm(i+1) = 0
       Dtm(i+1) = 0
C}}}
     EndDo
      Do i=0,7
C{{{Zero parameters for DSSD absolute times
```

```
       Atmns(i+1) = 0
       Btmns(i+1) = 0
       Ctmns(i+1) = 0
       Dtmns(i+1) = 0
C}}}
     EndDo
     Do i=0,6
C{{{Zero parameters for Si-array time
       Sitm(i+1) = 0
C}}}
     EndDo
     Do i=0,6
C{{{Zero parameters for Si-array absolute time
       Sitmns(i+1) = 0
C}}}
     EndDo
     Do i=0,4
C{{{Zero parameters for unused
          unus3(i+1) = 0
C}}}
     EndDo
C}}}
C}}}
     EndDo !End Buffer

     Goto 2
 11   CLOSE(20)
 998  WRITE(*,111) evtfile,bufproc-1,evtproc
 111  FORMAT ('End of file: ',a,/,1i7,' buffers,',1i7,' events')
     close(2)
     Goto 1

 997  CONTINUE
     WRITE(*,*) 'ERROR IN FILE: ',IOSB

 999  CONTINUE
     call hprnt(100)
     call hrout(100,icycle,' ')
     call hrend('Rf')

 9999 FORMAT('Event ',i4,':  ipt =',i6,' idata =',z10.4)
 9998 FORMAT('Next header is ',z6.4)
 9997 FORMAT('Evt, ipt, Bitreg: ',i3,1x,i6,1x,z6.4)
     END
```

```
      INTEGER*2 FUNCTION GetDataWord(needswap,word)
C{{{
      LOGICAL needswap
      Integer*2 GetDataWord,word,swap2
      If (needswap) Then
        GetDataWord = swap2(word)
      Else
        GetDataWord =  word
      EndIf
      RETURN
C}}}
      END

      INTEGER*2 FUNCTION swap2(raw)
C{{{
      Integer*2 raw,swap2
      Integer*2 out/0/,copy,i
      Character*1 inbytes(4),oubytes(4)
      Equivalence (out,oubytes)
      Equivalence (inbytes,copy)

      copy=raw
      Do i=1,2
        oubytes(i)=inbytes(3-i)
**          WRITE(*,101), i,inbytes(i),oubytes(i)
      EndDo
 101  FORMAT(i4,1x,2z6.4)
      swap2 = out
      RETURN
C}}}
      END
```

2. ang_dist.for

```
      PROGRAM Ang_Dist

c   data from 243 MeV perpendicular target run;
c   MODIFIED to fit only backward angles.
c
c    Program to calculate fusion/quasifission ratios from the fission fragment angular
c distributions using the formula from Vandenbosch and Huizenga.  You need to
c calculate K-naught squared for both the RLDM case and for I(0)/I(eff)=1.5 (Back
c quasifission); also J(max) and pi*lambdabar^2 for each energy (from the fission
c cross section data).  J(crit) increases in the minimization routine, so start it low.
c
c   RN April 2007
```

```
c
      implicit none

      character*20 title,head1,head2, head3
      integer i,k,l,m,n,p,q,s,t,entries
      integer counter
      data head1,head2,head3/'Theta(rad)','W(theta)',’W(theta)/correct’/
      integer j,jmin,jmax,jmaxfus
      real exper(24),runval(24)
      integer angle1,angle2,angle3,angle4,angle5, angle6
      real*8 bessio,erf,erftot,bessel,correct
      real theta(180), Wtheta(180),factor(6),sigmaj
      real j1,kzero,kzeroqf,thetaold,trig,pi,pilambda
      real*8 zee,erfarg,Wtop,sigma,sigmaold,delold,delsigma
      data runval/10.14,11.91,13.30,15.28,17.84,19.25/
      data angle1,angle2,angle3,angle4,angle5,angle6/
     *128,134,145,151,156,162/
      parameter(pi=3.14159)

  100 open(40,file='ang_dist243.out',status='new')
      jmin=0
      write(*,120)
  120 format(5x,'Input the value of J max ')
      read(*,'(I6)')jmax
      write(*,130)
  130 format(5x,'Starting value for J crit?')
      read(*,'(I6)')jmaxfus
      write(*,140)
  140 format(5x,'K-naught-squared for quasifission?')
      read(*,'(f6.2)')kzeroqf
      write(*,150)
  150 format (5x,'K-naught-squared (RLDM)?')
      read(*,'(f6.2)')kzero
      write(*,160)
  160 format(5x,'Enter pi*lambdabar^2 ')
      read(*,'(f6.4)')pilambda

      sigma=7000000000000000.
      delsigma=999999999999.

c  *** start the loop through theta values ***
  205 n=1
      theta(n)=0
  210 thetaold=theta(n)
      n=n+1
      theta(n)=thetaold+0.017
```

```
      IF(theta(n).GT.pi)then
        go to 900
      Endif
      trig=(SIN(theta(n)))**2

c  ******** calculate W(theta) ********
      j1=REAL(j)
      Wtheta(n)=0
      do j=jmin,jmaxfus            ! sum over J-values

c  ******* zee is the argument of the bessel function *******
        zee=((j1+0.5)**2)*trig/(4*kzero)
        bessel=BESSIO(zee)
        erfarg=(j1+0.5)/(SQRT(2*kzero))
        erftot=ERF(erfarg)
        Wtop=((2*j1+1)**2)*pilambda*(EXP(-zee))*bessel
        Wtheta(n)=Wtheta(n)+Wtop/erftot
      enddo
      do j=jmaxfus+1,jmax
        zee=((j1+0.5)**2)*trig/(4*kzeroqf)
        bessel=BESSIO(zee)
        erfarg=(j1+0.5)/(SQRT(2*kzeroqf))
        erftot=ERF(erfarg)
        Wtop=((2*j1+1)**2)*pilambda*(EXP(-zee))*bessel
        Wtheta(n)=Wtheta(n)+Wtop/erftot
      enddo
c
c  ******** try to optimize the J-crit parameter with respect
c   to the experimental data.  Just trying to minimize
c   S-squared... not tremendously glamorous. **********

      IF(NINT(theta(n)*100).EQ.angle1)Then
        exper(1)=Wtheta(n)
      ELSEIF(NINT(theta(n)*100).EQ.angle2)Then
        exper(2)=Wtheta(n)
      ELSEIF(NINT(theta(n)*100).EQ.angle3)Then
        exper(3)=Wtheta(n)
      ELSEIF(NINT(theta(n)*100).EQ.angle4)Then
        exper(4)=Wtheta(n)
      ELSEIF(NINT(theta(n)*100).EQ.angle5)Then
        exper(5)=Wtheta(n)
      ELSEIF(NINT(theta(n)*100).EQ.angle6)Then
        exper(6)=Wtheta(n)
      ENDIF
 400  goto 210           !next theta
```

```
c  ********************************************************
 900  correct=0
      Do t=1,6
        factor(t)=exper(t)/runval(t)
        correct=correct+factor(t)
      enddo
      correct=correct/6
      sigma=0
      Do q=1,6
        exper(q)=exper(q)/correct
        sigma=sigma+(exper(q)-runval(q))**2
      Enddo
      do i=1,6
        write(*,'(a8,i2,a5,f10.2)')' exper(',i,') = ',exper(i)
      enddo
      delold=delsigma
      delsigma=ABS(sigma-sigmaold)
c     write(*,'(f10.2,1x,I8,2f20.10)')correct,jmaxfus,delsigma,
c     *  delold
c     write(*,'(f10.2,2x,f10.2)')sigmaold,sigma
c     pause

      sigmaold=sigma
      IF(delsigma.LT.delold)Then
        jmaxfus=jmaxfus+1
        goto 205
      EndIf

      counter=(n-1)
      print*,'  Title line for output file?'
      read(*,'(a40)')title
      write(40,'(5x,a40)')title
c     write(40,'(a20,f6.2)')' k-naught-squared = ',kzero
      write(40,'(a20,I8)')' J crit = ',jmaxfus
c     write(40,'(a20,f10.2)')' s-squared = ',sigma
      write(40,930)head1,head2, head3
 930  format(3x,a10,8x,a10, 8x, a20)

      do s=1,counter
        write(40,950)theta(s),Wtheta(s),Wtheta(s)/correct
 950    format(3x,f10.2,3x,f15.2,3x,f15.2)
      enddo

 999  close(40)
      end
c ********************************************************
```

```
      REAL FUNCTION ERF(X)          ! Error function, gamma function,
                                    ! and Bessel function routines
      If(X.LT.0.)Then               ! taken from _Numerical Recipes_
        ERF=-GAMMP(.5,X**2)
      Else
        ERF=GAMMP(.5,X**2)
      Endif
      return
      end

c *********************************************************
      REAL FUNCTION GAMMP(A,X)

      If(X.LT.0..OR.A.LE.0.)Pause
      If(X.LT.A+1.)Then
        Call GSER(GAMMP,A,X,GLN)
      Else
        Call GCF(GAMMCF,A,X,GLN)
        GAMMP=1.-GAMMCF
      Endif
      return
      end

c *********************************************************
      SUBROUTINE GSER(GAMSER,A,X,GLN)

      parameter(itmax=100,eps=3.E-7)
      GLN=GAMMLN(A)
      If(X.LE.0.)Then
        If(X.LT.0.)pause
        GAMSER=0.
        return
      Endif
      AP=A
      SUM=1./A
      DEL=SUM
      Do n=1,itmax
        AP=AP+1
        DEL=DEL*X/AP
        SUM=SUM+DEL
        If(ABS(DEL).LT.ABS(SUM)*eps)GO TO 1
      Enddo
      Continue
      PAUSE 'A too large; ITMAX too small'
    1 GAMSER=SUM*EXP(-X+A*LOG(X)-GLN)
      RETURN
```

```
      END

c ************************************************************
      SUBROUTINE GCF(gammcf,a,x,gln)

      parameter(itmax=100,eps=3.E-7)
      gln=GAMMLN(A)
      GOLD=0
      a0=1
      a1=x
      b0=0
      b1=1
      fac=1
      do n=1,itmax
        an=FLOAT(n)
        ana=an-a
        a0=(a1+a0*ana)*fac
        b0=(b1+b0*ana)*fac
        anf=an*fac
        a1=x*a0+anf*a1
        b1=x*b0+anf*b1
        If(a1.NE.0.)Then
          fac=1./a1
          g=b1*fac
          If(ABS((g-GOLD)/g).LT.eps)Go To 1
          GOLD=g
        Endif
        Enddo
        Continue
      PAUSE 'A too large; ITMAX too small'
    1  gammcf=EXP(-x+a*ALOG(x)-gln)*g
      return
      end

c ************************************************************
      REAL FUNCTION GAMMLN(XX)

      real*8 cof(6),stp,half,one,fpf,x,tmp,ser
      data cof,stp/76.18009173D0,-86.50532033d0,24.01409822d0,
     *  -1.231739516D0,0.120858003d-2,-0.536382d-5,
     *  2.50662827465d0/
      data half,one,fpf/0.5d0,1.0d0,5.5d0/
      x=xx-one
      tmp=x+fpf
      tmp=(x+half)*LOG(tmp)-tmp
      ser=one
```

```
      do j=1,6
        x=x+one
        ser=ser+cof(j)/x
      enddo
      continue
      gammln=tmp+LOG(stp*ser)
      return
      end

c *************************************************************
      REAL FUNCTION BESSIO(x)

      real*8 y,p1,p2,p3,p4,p5,p6,p7
      real*8 q1,q2,q3,q4,q5,q6,q7,q8,q9
      data p1,p2,p3,p4,p5,p6,p7/1.0d0,3.5156229d0,
     *  3.0899424d0,1.2067492d0,0.2659732d0,0.360768d-1,
     *  0.45813d-2/
      data q1,q2,q3,q4,q5,q6,q7,q8,q9/0.39894228d0,
     *  0.1328592d-1,0.225319d-2,-0.157565d-2,0.916281d-2,
     *  -0.2057706d-1,0.2635537d-1,-0.1647633d-1,
     *  0.392377d-2/

      If(ABS(x).LT.3.75)Then
        y=(x/3.75)**2
        BESSIO=p1+y*(p2+y*(p3+y*(p4+y*(p5+y*(p6+y*p7)))))
      Else
        ax=ABS(x)
        y=3.75/ax
        BESSIO=(EXP(ax)/SQRT(ax))*(q1+y*(q2+y*(q3+y*(q4
     *   +y*(q5+y*(q6+y*(q7+y*(q8+y*q9))))))))
      Endif
      return
      end
```

APPENDIX B

1. Ruthwaltcor3.for

```
C-------------------------------------------------------------------------------------------------
C Calculates currents, cross sections for eff.=1 etc. from the rutherford counting rate.
C rutherford detectors are placed at 16.2 degree upstream at a distance of 396.24 mm
C from target
      character*1 ckey
C-----definition of constants
      pi=3.141593
      epna=6.242e9
C-----radius of collimator in mm
      rdet=9.77
C-----lab. angle between detector and beam axis
      th=16.2
C-----distance target detector in mm
      rdt=397.51
C-------------------------------------------------------------------------------------------------

10    write(*,11)
11    format(1x,'Give  Zp,Ap,Zt,At : ',$)
      read(*,*) izp,iap,izt,iat
      write(*,12)
12  format(1x,'Give  E/A,n. Ruth.,Targ. thickn.: ',$)
      read(*,*) ep,nruth,tth
      write(*,13)
13  format(1x,'Give total measuring time in sec.: ',$)
      read(*,*) itm
      ecm=ep*iap*iat/(iap+iat)
      fac1=3.6e-14*izp*izt/ecm
      th1=pi*th/180.0
      thcm=asin(iap*sin(th1)/iat)+th1
      thcm1=180.0*thcm/pi
      dsdomcm=(fac1**2)/(sin(thcm/2))**4
      dsidomlab=(1./cos(thcm-th1))*dsdomcm*(sin(thcm)/sin(th1))**2
      dom=pi*(rdet/rdt)**2
      sidet=dom*dsidomlab
      apat=nruth/sidet
      tarat=0.001*tth*6.0225e23/iat
      prat=apat/tarat
      pna=prat/epna
      write(*,100)
100   format(1x,70('-')/,
     +8x,'evaluates counting rate of rutherford-detector'/,
     +1x,70('-'))
      write(*,102) izp,izt,iap,iat,ep*iap,ecm,tth,tarat,
     +rdt,2*rdet,th,thcm1,
```

```
     +dsdomcm,dsidomlab,dom,
     +prat,pna/itm,apat
102   format(8x,'Projectile (Z,A) = ',i2,2x,i3/,
     +8x,'Target     (Z,A) = ',i2,2x,i3/,
     +8x,'kin. Ener. (lab) =',F7.2,' MeV',
     +8x,'kin. Ener. (cm) = ',F7.2,' MeV'//,
     +8x,'Target Thickness  =',F6.3,' mg/cm^2'/,
     +8x,'Numb. of targ. atoms = ',E8.3,' cm^-2'//,
     +8x,'Distance Detector Target = ',F7.2,' mm'/,
     +8x,'Detector Diameter        = ',F7.2,' mm'//,
     +8x,'Th (lab) =   ',F7.2,' deg',
     +8x,'Th (cm)  =   ',F7.2,' deg'/,
     +8x,'dSi/dOm (lab) = ',e8.2,
     +8x,'dSi/dOm (cm) = ',e8.2/,
     +8x,'solid angle   = ',e8.2/,
     +8x,'Number of projectiles = ', e9.4/,
     +8x,'average current       = ',f6.1,' PnA '/,
     +8x,'proj. atoms x targ. atoms = ',e9.4,' cm^-2'/,
     +1x,70('-')/)
200   write(*,104)
104   format(1x,'continue (y/n) : ', $)
      read(*,105,err=200) ckey
105   format(A1)
      if(ckey.EQ.'Y'.OR.ckey.EQ.'y') goto 10
      stop
      end
```

2. Dehl2.for

```
C-------------------------------------------------------------------------------------------------
C version 87-feb-87
C revised 7/2006
C This is an error weighted least squares decay curve fitting program. The program
C was designed for analyzing gamma ray data and by altering the input files. I am
C using it to analyze our beta counter data from TRIUMF.
C-------------------------------------------------------------------------------------------------

PROGRAM DEHL2
      implicit integer*2(i-n)
      implicit character(g-h)
      implicit real*8(a-f,r-z)
      common vel,zel,ea,tact,adta,bdta,cdta,ddta,icom,icn,idata,iord
     x,fram,ipr
      dimension vel(10,10),wel(10,10),zel(10),hfix(10),fram(10),
     %rfram(10),xel(10,10),yel(10,10),abu(10),absa(10),efix(10),
     %sabsa(10),ipr(10)
```

```
      dimension adta(200),bdta(200),cdta(200),ddta(200),ea(200),
     %usum(200),tact(200),sbar(200),rcor(200),bsav(200),
     %sih(200),sil(200)
      dimension gline(80),gr(125),xths(50),xa0s(50),xe(50),xie(50),
     %xthf(50),xa0f(50),a00(5),kz(5)
      character*78 head
      character*8 gnuc,gid(10),gxid(50),gz2,gskip
      character*3 gunit,gdel
      character*2 gok
      character*1 gz1,gxie(50),gabu(10),check,gmd(50)
C Room for 10 variable parameters and 200 data points
      open(1,file='dehl2.dat',status='old')
      open(10,file='dehl2.res',status='new')
      open(11,file='defit.res',status='new')
      open(12,file='desort.dat',status='new')
      do 105 i=1,80
  105 gline(i)='-'
      gline(1)=' '
      read(1,'(1x,a78)')head
      write(*,'(1x,a77)')head
      write(10,'(1x,a77)')head
      write(11,'(5x,a70)')head
      write(12,'(1x,a77)')head
C Don't be confused by this. All units are to be in min, cpm, etc.
      read(1,'(1x,a3)')gunit
      write(*,'(1x,a3)')gunit
      write(10,'(1x,a3)')gunit
      write(11,'(5x,a3)')gunit
      write(12,'(1x,a3)')gunit
      write(*,1)
    1  format(' ')
      write(11,1111)(gline(i),i=1,73)
  110 write(*,1120)
 1120 format(1x,'Do you want a complete result file? (Y/N) : ')
      read(*,'(a1)')ggraf

      if((ggraf.ne.'y').and.(ggraf.ne.'n'))then
      write(*,1190)
 1190 format(1x,'answer y or n')
      goto 110
      endif
      write(*,1195)
 1195 format(1x,'Do you want a plot on the screen and halt',
     %' after each plot? (Y/N): ')
      read(*,'(a1)')halt
      if(halt.eq.'y')write(*,1110)(gline(i),i=1,78)
```

```
      if(ggraf.eq.'y')write(10,1111)(gline(i),i=1,73)
 1110 format(1x,78a1)
 1111 format(4x,73a1)
C Read in the data
C ADTA=counts/min, BDTA=sigma(counts/min)
C CDTA=time at beginning of count, DDTA=length of count
  200 continue
      if(gnew.eq.'e')then
        write(*,1199)
 1199    format(1x,'Enter gamma energy: ')
        read(*,'(f8.0)')enyfind
        if(enyfind.lt.eny) rewind(1)
  201    continue
        read(1,'(1x,a2)',end=999)gok
        if(gok.ne.'--')goto 201
        gprint='y'
        call clrscr
        read(1,1200)eny,ii
 1200    format(1x,f6.1,6x,i2)
        if(eny.eq.0)goto 201
        if(eny.lt.enyfind)goto 201
        gnew=' '
        goto 202
      endif
      gnew=' '
      read(1,'(1x,a2)',end=999)gok
      if(gok.ne.'--')goto 200
      gprint='y'
      call clrscr
      read(1,1200)eny,ii
      if(eny.eq.0)goto 200
  202 if(halt.eq.'y')write(*,1110)(gline(i),i=1,78)
      if(ggraf.eq.'y')write(10,1111)(gline(i),i=1,73)
      backspace(11)
      read(11,'(5x,a3)')gdel
      if(gdel.ne.'---')write(11,1111)(gline(i),i=1,73)
      write(*,1205)eny
      if(ggraf.eq.'y')write(10,1205)eny
 1205 format(/,1x,'analysis of ',f6.1,' kev')
      in=0
      do 205 i=1,ii
      read(1,1208)gdel,enyg,cdt,ddt,adt,bdt
 1208 format(a3,4x,f6.1,4e12.5)
      if(gdel.eq.'   ')then
        in=in+1
        cdta(in)=cdt
```

```
       ddta(in)=ddt
       adta(in)=adt
       bdta(in)=bdt
       endif
  205 continue
C HCOR='N' No corrections for decay during counting
C HCOR='Y' Corrections for decay during counting
      if(hcor.eq.'y')goto 1820
      do 206 i=1,in
  206 cdta(i)=cdta(i)+ddta(i)/2.
      idata=in
      gnew='n'
  207 read(1,1210)i,gz2,gz3,z3,z4,gz1,z5,z1,z6,z2
 1210 format(1x,i2,1x,a8,1x,a1,f7.1,f7.2,a1,e12.4,3e11.4)
 1211 format(1x,i2,1x,a8,1x,a1,f7.1,f7.2,a1,f7.3,5x,3e11.4)
      if(i.ne.99)then
        xths(i)=z1
        xa0s(i)=z2
        xe(i)=z3
        xie(i)=z4
        gxie(i)=gz1
        xthf(i)=z5
        xa0f(i)=z6
        gxid(i)=gz2
        gmd(i)=gz3
        knucf=i
        goto 207
      endif
      inewf=0
  210 read(1,1215)icn,kz(1),kz(2),kz(3),kz(4)
 1215 format(6i3)
  211 continue
      if(icn.eq.9)then
        inewf=1
        goto 980
      endif
      if(ggraf.eq.'y')write(10,1300)
 1300 format(1x,'.....NEW FIT.....')
      if(icn.eq.0)goto 990
      do 222 i=1,10
      hfix(i)=' '
      fram(i)=0
      rfram(i)=0
      efix(i)=0
      gid(i)='xxxnn mm'
  222 continue
```

```
 223 if(icn.lt.6)then
     icom=icn
     if(icom.eq.1)gfit='a'
     if(icom.eq.2)gfit='b'
     if(icom.eq.3)gfit='c'
     if(icom.eq.4)gfit='d'
     goto 224
     endif
     if(icn.lt.10)then
     if(icn.eq.6)then
       gfit='f'
     endif
     if(icn.eq.7)then
       gfit='g'
     endif
     icom=icn-4
     goto 224
     endif
     if(icn.lt.12)then
     icom=icn-6
     goto 224
     endif
     write(*,1409)
 1409 format(1x,'Invalid case number. Enter new number: ')
     read(*,'(i2)')icn
     goto 223
C Input initial values for parameters
 224 continue
       if(icom.eq.1)then
         a01=adta(1)
       endif
       if(icom.eq.2)then
         a02=adta(idata)
         a01=adta(1)-a02
       endif
       if(icom.eq.3)then
         a03=adta(idata)*0.7
         km=idata/2
         a02=adta(km)-a03
         a01=adta1-a02-a01
         if(a01.lt.0.)a01=adta(1)/2.
       endif
       a00(1)=a01
       a00(2)=a02
       a00(3)=a03
       do 225 i=1,icom
```

```
      gid(i)=gxid(kz(i))
      abu(i)=xie(kz(i))
      gabu(i)=gxie(kz(i))
      efix(i)=xe(kz(i))
      x1=xths(kz(i))
      x2=xa0s(kz(i))
      x3=xthf(kz(i))
      x4=xa0f(kz(i))*abu(i)/100.
      if(x2.eq.0.and.x4.eq.0)x2=a00(i)
      if(x1.eq.0)then
        hfix(2*i-1)='y'
        fram(2*i-1)=x3
        else
        hfix(2*i-1)='n'
        fram(2*i-1)=x1
      endif
      if(x2.eq.0)then
        hfix(2*i)='y'
        fram(2*i)=x4
        else
        hfix(2*i)='n'
        fram(2*i)=x2
      endif
  225 continue
    do 230 i=1,2*icom
  230 rfram(i)=fram(i)
    iter=0
    do 240 i=1,icom
  240 fram(2*i-1)=.693147/fram(2*i-1)
    if(gprint.eq.'y')then
      if(ggraf.eq.'y')write(10,1440)
C       if(halt.eq.'y')write(*,1440)
 1440  format(1x,'iter    h.l.#1    i.a.#1    h.l.#2    ',
   x  'i.a.#2    h.l.#3    i.a.#3  ')
      if(ggraf.eq.'y')write(10,1450)'init',(.693147/fram(2*l-1),
   %  fram(2*l),l=1,icom)
C if(halt.eq.'y')write(*,1450)'init',(.693147/fram(2*l-1),
C %  fram(2*l),l=1,icom)
 1450  format(1x,a4,10(1x,e9.3))
      endif
    do 1800 i=1,idata
    bsav(i)=bdta(i)
 1800 ea(i)=adta(i)
    hcor='n'
C Locate and count the variable parameters
    iord=0
```

```
      do 1830 i=1,icom*2
      if(hfix(i).eq.'n')then
      iord=iord+1
      ipr(iord)=i
      endif
 1830 continue
C If corrections are desired, then go do it
 1820 if(hcor.eq.'y')call correc(bsav)
C Go take derivatives and build matrix
      if(icn.lt.6)call deriv
      if(icn.gt.5)call gderiv
C Go solve the matrix
      call matrix(vel,wel,zel,iord)
      iter=iter+1
C Convergence check
      ier=0
      do 2040 i=1,iord
      fram(ipr(i))=fram(ipr(i))+zel(i)
 2040 if(abs(zel(i)).gt.abs(fram(ipr(i)))/10000.)ier=1
C Print out results of iteration
      if(gprint.eq.'y')then
        if(ggraf.eq.'y')write(10,3280)iter,(.693147/fram(2*l-1),
     %fram(2*l),l=1,icom)
c if(halt.eq.'y')write(*,3280)iter,(.693147/fram(2*l-1),
c %  fram(2*l),l=1,icom)
 3280   format(1x,i4,10(1x,e9.3))
        endif
      ika=0
      if(fram(1).lt.0)ika=1
      do 2050 ik=2,icom*2
 2050 if(fram(ik).lt.0.and.hfix(ik-1).eq.'n')ika=1
      if (ika.eq.1)then
        write(*,3283)
 3283   format(1x,'********* PROBLEM IN THE FIT *********')
        if(ggraf.eq.'y')write(10,3283)
        if(halt.eq.'y')goto 2410
        goto 200
        endif
      if(iter.lt.2)goto 1820
      if(iter.gt.50.)goto 2160
      if(ier.eq.1)goto 1820
      goto 2200
 2160 write(*,3290)
 3290 format(1x,'It has not converged after 50 iterations')
      if(ggraf.eq.'y')write(10,3310)
 3310 format(1x,'WARNING . . . WARNING . . . WARNING . . . WARNING')
```

```
      if(ggraf.eq.'y')write(10,3320)
 3320 format(1x,'This fit did not converge')
      if(ggraf.eq.'y')write(10,3310)
 2200 if(halt.eq.'y')write(*,1)
      if(ggraf.eq.'y')write(10,1)
      if(ggraf.eq.'y')write(10,3340)
C     if(halt.eq.'y')write(*,3340)
 3340 format(1x,'nr  t1/2(Fit) Sigma(Fit) Unit',
     %'    T0 Act. Sigma Act.   Fix T1/2 Fix T0Act.')
      m=1
      do 2290 i=1,icom
      if(hfix(2*i-1).eq.'n'.and.hfix(2*i).eq.'n')then
      x1=0.693147/fram(2*i-1)
      x2=.693147*wel(m,m)**.5/fram(2*i-1)**2.
      if(ggraf.eq.'y')write(10,3350)i,x1,x2,gunit,fram(2*i),
     %wel(m+1,m+1)**.5,0.,0.
C if(halt.eq.'y')write(*,3350)i,x1,x2,gunit,fram(2*i),
C  %wel(m+1,m+1)**.5,0.,0.
      m=m+2
      endif
      if(hfix(2*i-1).eq.'y'.and.hfix(2*i).eq.'n')then
      x1=0.693147/fram(2*i-1)
      x2=.693147*wel(m,m)**.5/fram(2*i-1)**2.
      if(ggraf.eq.'y')write(10,3350)i,0.,0.,gunit,fram(2*i),
     %wel(m,m)**.5,x1,0.
C if(halt.eq.'y')write(*,3350)i,0.,0.,gunit,fram(2*i),
C  %wel(m,m)**.5,x1,0.
      m=m+1
      endif
      if(hfix(2*i-1).eq.'n'.and.hfix(2*i).eq.'y')then
      x1=0.693147/fram(2*i-1)
      x2=.693147*wel(m,m)**.5/fram(2*i-1)**2.
      if(ggraf.eq.'y')write(10,3350)i,x1,x2,gunit,0.,0.,0.,fram(2*i)
C     if(halt.eq.'y')write(*,3350)i,x1,x2,gunit,0.,0.,0.,fram(2*i)
      m=m+1
      endif
      if(hfix(2*i-1).eq.'y'.and.hfix(2*i).eq.'y')then
      x1=0.693147/fram(2*i-1)
      x2=.693147*wel(m,m)**.5/fram(2*i-1)**2.
      if(ggraf.eq.'y')write(10,3350)i,0.,0.,gunit,x1,fram(2*i)
C     if(halt.eq.'y')write(*,3350)i,0.,0.,gunit,x1,fram(2*i)
      endif
 3350 format(1x,i2,2e11.4,2x,a3,4e11.4,1x,f4.1)
 2290 continue
C Print a table with the result for each data point
      if(gprint.eq.'y')then
```

```
      if(halt.eq.'y')write(*,1)
C if(halt.eq.'y')write(*,410)
 410 format(1x,'   Rate    Cor. rate   Sigma     Time     Delta T ',
    X'  R Calc    % Error   Chi**2')
C if(halt.eq.'y')write(*,1)
      chi=0.
      do 2400 i=1,idata
      ch2=(abs(tact(i)-ea(i)))**2./bdta(i)**2.
C if(halt.eq.'y')write(*,3430)adta(i),ea(i),bdta(i),cdta(i),
C x  ddta(i),tact(i),1.*(ea(i)-tact(i))*100./ea(i),ch2
 3430   format(1x,7(e9.3,1x),e9.3)
 2400   chi=chi+ch2
      if(ggraf.eq.'y')write(10,1)
C if(halt.eq.'y')write(*,1)
      if(halt.eq.'y')write(*,1)
      if(halt.eq.'y')write(*,1)
      if(idata.eq.2)then
      chir=0
         else
         chir=chi/(idata-iord)
      endif
      if(ggraf.eq.'y') write(10,3440)chi,chir
      write(11,3441)eny,idata,gfit,chir
 3440   format(1x,'Chi squared =',E11.5,', Reduced chi squared =',
   %E11.5)
 3441   format(5x,f6.1,' keV: Nr data points=',I2,', ',A1,' fit, ',
   %  'reduced chi squared= ',E10.4)
      if(ggraf.eq.'y') write(10,1)
         endif
    call clrscr
 2410 call graph(ggraf,chir,halt)
    if(ika.eq.1)goto 977
    itype=0
    if(gfit.eq.'f')itype=1
    if(gfit.eq.'g')itype=1
    if(gfit.eq.'h')itype=1
    if(itype.eq.1) abu(1)=(abu(1)*abu(2)/100)
    m=1
    do 2420 i=1,icom
    if(hfix(2*i-1).eq.'n'.and.hfix(2*i).eq.'n')then
    x1=0.693147/fram(2*i-1)
    x2=.693147*wel(m,m)**.5/fram(2*i-1)**2.
    if(gabu(i).ne.'*') gabu(i)='%'
    if(abu(i).eq.0)then
 3445 format(1x,'Abundens of gamma can not be zero!!!',
   %' It is set to 100%')
```

```
   if(halt.eq.'y')write(*,3445)
   if(ggraf.eq.'y')write(10,3445)
   abu(i)=100.
 endif
 absa(i)=fram(2*i)/abu(i)*100
 sabsa(i)=wel(m+1,m+1)**.5/abu(i)*100
 if(x1.gt.999.)then
 if(halt.eq.'y')write(*,3450)eny,gid(i),efix(i),abu(i),
%gabu(i),x1,absa(i),sabsa(i),gfit
 if(ggraf.eq.'y')write(10,3450)eny,gid(i),efix(i),abu(i),
%gabu(i),x1,absa(i),sabsa(i),gfit
 write(11,3451)gid(i),efix(i),abu(i),gabu(i),x1,x2,absa(i),
%sabsa(i)
 write(12,3450)eny,gid(i),efix(i),abu(i),gabu(i),x1,absa(i),
%sabsa(i),gfit
 else
 if(halt.eq.'y')write(*,3452)eny,gid(i),efix(i),abu(i),
%gabu(i),x1,absa(i),sabsa(i),gfit
 if(ggraf.eq.'y')write(10,3452)eny,gid(i),efix(i),abu(i),
%gabu(i),x1,absa(i),sabsa(i),gfit
 write(11,3453)gid(i),efix(i),abu(i),gabu(i),x1,x2,absa(i),
%sabsa(i)
 write(12,3452)eny,gid(i),efix(i),abu(i),gabu(i),x1,absa(i),
%sabsa(i),gfit
 endif
 m=m+2
 endif
 if(hfix(2*i-1).eq.'y'.and.hfix(2*i).eq.'n')then
 x1=0.693147/fram(2*i-1)
 x2=.693147*wel(m,m)**.5/fram(2*i-1)**2.
 if(abu(i).eq.0)then
   if(halt.eq.'y')write(*,3445)
   if(ggraf.eq.'y')write(10,3445)
   abu(i)=100.
 endif
 absa(i)=fram(2*i)/abu(i)*100
 sabsa(i)=wel(m,m)**.5/abu(i)*100
 if(x1.gt.999.)then
 if(halt.eq.'y')write(*,3450)eny,gid(i),efix(i),abu(i),
%gabu(i),x1,absa(i),sabsa(i),gfit
 if(ggraf.eq.'y')write(10,3450)eny,gid(i),efix(i),abu(i),
%gabu(i),x1,absa(i),sabsa(i),gfit
 write(11,3451)gid(i),efix(i),abu(i),gabu(i),x1,0.,absa(i),
%sabsa(i)
 write(12,3450)eny,gid(i),efix(i),abu(i),gabu(i),x1,absa(i),
%sabsa(i),gfit
```

```
 else
 if(halt.eq.'y')write(*,3452)eny,gid(i),efix(i),abu(i),
%gabu(i),x1,absa(i),sabsa(i),gfit
 if(ggraf.eq.'y')write(10,3452)eny,gid(i),efix(i),abu(i),
%gabu(i),x1,absa(i),sabsa(i),gfit
 write(11,3453)gid(i),efix(i),abu(i),gabu(i),x1,0.,absa(i),
%sabsa(i)
 write(12,3452)eny,gid(i),efix(i),abu(i),gabu(i),x1,absa(i),
%sabsa(i),gfit
 endif
 m=m+1
 endif
 if(hfix(2*i-1).eq.'n'.and.hfix(2*i).eq.'y')then
 x1=0.693147/fram(2*i-1)
 x2=.693147*wel(m,m)**.5/fram(2*i-1)**2.
 absa(i)=fram(2*i)/abu(i)*100
 if(x1.gt.999.)then
 if(halt.eq.'y')write(*,3450)eny,gid(i),efix(i),abu(i),gabu(i),
%x1,absa(i),0.,gfit
 if(ggraf.eq.'y')write(10,3450)eny,gid(i),efix(i),abu(i),
%gabu(i),x1,absa(i),0.,gfit
 write(11,3451)gid(i),efix(i),abu(i),gabu(i),x1,x2,absa(i),0.
 write(12,3450)eny,gid(i),efix(i),abu(i),gabu(i),x1,absa(i),0.,gfit
 else
 if(halt.eq.'y')write(*,3452)eny,gid(i),efix(i),abu(i),gabu(i),
%x1,absa(i),0.,gfit
 if(ggraf.eq.'y')write(10,3452)eny,gid(i),efix(i),abu(i),gabu(i),
%x1,absa(i),0.,gfit
 write(11,3453)gid(i),efix(i),abu(i),gabu(i),x1,x2,absa(i),0.
 write(12,3452)eny,gid(i),efix(i),abu(i),gabu(i),x1,absa(i),0.,gfit
 endif
 m=m+1
 endif
 if(hfix(2*i-1).eq.'y'.and.hfix(2*i).eq.'y')then
 x1=0.693147/fram(2*i-1)
 x2=.693147*wel(m,m)**.5/fram(2*i-1)**2.
 absa(i)=fram(2*i)/abu(i)*100
 if(x1.gt.999.)then
 if(halt.eq.'y')write(*,3450)eny,gid(i),efix(i),abu(i),gabu(i),
%x1,absa(i),0.,gfit
 if(ggraf.eq.'y')write(10,3450)eny,gid(i),efix(i),abu(i),gabu(i),
%x1,absa(i),0.,gfit
 write(11,3451)gid(i),efix(i),abu(i),gabu(i),x1,0.,absa(i),0.
 write(12,3450)eny,gid(i),efix(i),abu(i),gabu(i),x1,absa(i),0.,gfit
 else
 if(halt.eq.'y')write(*,3452)eny,gid(i),efix(i),abu(i),gabu(i),
```

```
     %x1,absa(i),0.,gfit
      if(ggraf.eq.'y')write(10,3452)eny,gid(i),efix(i),abu(i),gabu(i),
     %x1,absa(i),0.,gfit
      write(11,3453)gid(i),efix(i),abu(i),gabu(i),x1,0.,absa(i),0.
      write(12,3452)eny,gid(i),efix(i),abu(i),gabu(i),x1,absa(i),0.,gfit
      endif
      endif
 3450 format(1x,f6.1,1x,a8,f7.1,'kev,',f6.2,a1,',hl=',e10.4,
     %',a0=',e11.5,'+/-',e11.5,1x,a1)
 3451 format(5x,a8,f6.1,'kev,',f6.2,a1,',hl=',e8.2,'+/-',e7.1,
     %',a=',e10.4,'+/-',e9.3)
 3452 format(1x,f6.1,1x,a8,f7.1,'kev,',f6.2,a1,',hl=',f10.4,
     %',a0=',e11.5,'+/-',e11.5,1x,a1)
 3453 format(5x,a8,f6.1,'kev,',f6.2,a1,',hl=',f8.3,'+/-',f7.3,
     %',a=',e10.4,'+/-',e9.3)
 2420 continue
  977 if(halt.eq.'y')then
        write(*,3455)
 3455    format(1x,
     %'Do you like to save this(these) result(s)?(Y/N): Y; ')
        read(*,'(a1)')haltx
        if(haltx.eq.' ')haltx='y'
        if(haltx.eq.'n')then
             if(ika.ne.1)then
            do 978 i=1,icom
            backspace(11)
  978         backspace(12)
            backspace(11)
          endif
          if(ggraf.eq.'y')then
 3460         backspace(10)
            backspace(10)
            read(10,'(1x,a8)')gskip
               if(gskip.ne.'.....new')goto 3460
            backspace(10)
          endif
        endif
      endif
      if(inewf.eq.0)goto 210
  980 continue
  990 continue
C If option "halt" you now can enter new fit information
      if(halt.ne.'y')goto 200
      write(*,1)
      write(*,4120)
 4120 format(1x,'New fit (F), delete data point (D), next energy (C),',
```

```
   %' new energy (E): F;')
    read(*,'(a1)')gnew
    if(gnew.eq.' ')gnew='f'
    if(gnew.eq.'c')goto 200
    if(gnew.eq.'e')goto 200
    if(gnew.eq.'d')then
      do 991 i=1,idata
 991    write(*,4122)i,cdta(i),ddta(i),adta(i),bdta(i)
4122    format(1x,i2,4e13.5)
 992    write(*,4123)
4123    format(1x,'Enter point to delete or 0 for no delete: ')
       read(*,'(i2)',err=992)idel
       j=0
          if(idel.eq.0)goto 982
       do 993 i=1,idata
       if(i.eq.idel)goto 993
       j=j+1
       adta(j)=adta(i)
       bdta(j)=bdta(i)
       cdta(j)=cdta(i)
 993    ddta(j)=ddta(i)
       idata=idata-1
       do 994 i=1,idata
 994    write(*,4122)i,cdta(i),ddta(i),adta(i),bdta(i)
       write(*,4124)
4124    format(1x,'More points to delete?(Y/N): N; ')
       read(*,'(a1)')check
       if(check.eq.' ')check='n'
       if(check.eq.'y')goto 992
    endif
 982 call clrscr
 989 write(*,1205)eny
    if(knucf.gt.22)then
      knuc1=knucf-22
      do 5080 i=1,22
      if(xthf(i).lt.999.)then
      write(*,1211)i,gxid(i),gmd(i),xe(i),xie(i),gxie(i),xthf(i),
   %   xths(i),xa0f(i),xa0s(i)
      endif
      if(xthf(i).ge.999.)then
      write(*,1210)i,gxid(i),gmd(i),xe(i),xie(i),gxie(i),xthf(i),
   %   xths(i),xa0f(i),xa0s(i)
      endif
5080    continue
       write(*,4125)
4125    format(1x,'Return for more: ')
```

```
      read(*,'(a1)')gchech
      do 5081 i=knuc1,knucf
      if(xthf(i).lt.999.)then
      write(*,1211)i,gxid(i),gmd(i),xe(i),xie(i),gxie(i),xthf(i),
     %   xths(i),xa0f(i),xa0s(i)
      endif
      if(xthf(i).ge.999.)then
      write(*,1210)i,gxid(i),gmd(i),xe(i),xie(i),gxie(i),xthf(i),
     %   xths(i),xa0f(i),xa0s(i)
      endif
5081    continue
    else
 995    do 5082 i=1,knucf
      if(xthf(i).lt.999.)then
      write(*,1211)i,gxid(i),gmd(i),xe(i),xie(i),gxie(i),xthf(i),
     %   xths(i),xa0f(i),xa0s(i)
      endif
      if(xthf(i).ge.999.)then
      write(*,1210)i,gxid(i),gmd(i),xe(i),xie(i),gxie(i),xthf(i),
     %   xths(i),xa0f(i),xa0s(i)
      endif
5082    continue
    endif
5083 write(*,4130)
4130 format(1x,'(0)No fit: Type ; (1)single comp./ (2)two comp./',
     %' (3)three comp./ (4)four comp.',/,' (6)growth and decay/',
     %' (7)G. & D. + one comp./ (8)G. & D. + two comp. Type?:  ')
    read(*,'(i2)',err=5083)icn
    if(icn.eq.0)goto 200
    if(icn.eq.10)goto 989
    if(icn.eq.99)goto 999
    if(icn.lt.1)goto 5083
    if(icn.gt.8)goto 5083
    if(icn.eq.5)goto 5083
    iicn=icn
    if(icn.gt.5)iicn=iicn-4
    do 996 i=1,4
 996 kz(i)=0
    do 997 i=1,iicn
    write(*,4151)i
4151 format(1x,'Return or give number for comp. nr ',I1,': ')
    read(*,'(i2)')kz(i)
    if(kz(i).eq.0)then
      knucf=knucf+1
      kz(i)=knucf
      j=knucf
```

```
        write(*,4152)
 4152    format(1x,'  Gues of half-life: ')
        read(*,'(f10.0)')xths(j)
        write(*,4153)
 4153    format(1x,'Gues of A0-activity: ')
        read(*,'(f10.0)')xa0s(j)
        xe(j)=0
        xie(j)=100.
        gxie(j)=' '
        xthf(j)=0
        xa0f(j)=0
        gxid(j)='000xx mm'
        gmd(j)=' '
      endif
  997 continue
      goto 211
  999 stop
      end

SUBROUTINE DERIV
C-------------------------------------------------------------------------------------------------
C This subroutine is used to take the derivatives of the decay curve functions for all
C but the growth and decay derivatives.
C-------------------------------------------------------------------------------------------------
      implicit integer*2(i-n)
      implicit real*8(a-f,r-z)
      common vel,zel,ea,tact,adta,bdta,cdta,ddta,icom,icn,idata,iord
     x,fram,ipr
      dimension vel(10,10),zel(10),tact(200),ea(200)
      dimension adta(200),bdta(200),cdta(200),ddta(200)
      dimension fram(10),ed(10),ipr(10)
C First clear out the old matrix
      do 60 j=1,iord
      do 50 k=1,iord
   50 vel(j,k)=0.
   60 zel(j)=0.
      do 75 i=1,idata
      do 23 j=1,2*icom
   23 ed(j)=0.
      tact(i)=0.
C Now take the derivatives
      do 55 j=1,icom
      texp=exp(-fram(2*j-1)*cdta(i))
      ed(2*j-1)=-cdta(i)*fram(2*j)*texp
      ed(2*j)=texp
   55 tact(i)=fram(2*j)*texp+tact(i)
```

```
C Now build the matrix
      do 100 j=1,iord
      zel(j)=zel(j)+ed(ipr(j))*(ea(i)-tact(i))/bdta(i)**2.
      do 110 k=1,iord
  110 vel(j,k)=vel(j,k)+ed(ipr(j))*ed(ipr(k))/bdta(i)**2.
  100 continue
   75 continue
      return
      end

SUBROUTINE GDERIV
C-------------------------------------------------------------------------------------------------
C This subroutine is to take the derivatives for the growth and decay cases.
C-------------------------------------------------------------------------------------------------
      implicit integer*2(i-n)
      implicit real*8(a-f,r-z)
      common vel,zel,ea,tact,adta,bdta,cdta,ddta,icom,icn,idata,iord
     x,fram,ipr
      dimension vel(10,10),zel(10),tact(200),ea(200)
      dimension adta(200),bdta(200),cdta(200),ddta(200)
      dimension fram(10),ed(10),ipr(10)
C First clear out the old matrix
      do 60 j=1,iord
      do 50 k=1,iord
   50 vel(j,k)=0.
   60 zel(j)=0.
      do 280 i=1,idata
      do 90 j=1,2*icom
   90 ed(j)=0.
      tact(i)=0.
C Now take the derivatives
      j=1
  100 texp1=exp(-fram(4*j-1)*cdta(i))
      texp3=exp(-fram(4*j-3)*cdta(i))
      e1me2=texp3-texp1
      el2ml1=fram(4*j-1)-fram(4*j-3)
      ed(4*j-3)=fram(4*j-2)*fram(4*j-1)/el2ml1*(e1me2/el2ml1-cdta(i)
     x*texp3)
      ed(4*j-2)=fram(4*j-1)/el2ml1*e1me2
      ed(4*j-1)=fram(4*j-2)*fram(4*j-1)/el2ml1*(e1me2/fram(4*j-1)
     x-e1me2/el2ml1+cdta(i)*texp1)-fram(4*j)
     x*cdta(i)*texp1
      ed(4*j)=texp1
      tact(i)=tact(i)+fram(4*j-1)/el2ml1*e1me2*fram(4*j-2)
     x+fram(4*j)*texp1
C If two g&d's then do it again
```

```
      if((icn.gt.9).and.(j.eq.1))then
      j=2
      goto 100
      endif
      if(icn.eq.10)goto 270
      if(icn.eq.6)goto 270
C If any independent components,get their derivatives too
      j=3
      if(icn.eq.11)j=5
      do 260 l=j,icom
      texp=exp(-fram(2*l-1)*cdta(i))
      ed(2*l-1)=-cdta(i)*fram(2*l)*texp
      ed(2*l)=texp
  260 tact(i)=tact(i)+fram(2*l)*texp
  270 continue
C Build the matrix
      do 300 j=1,iord
      zel(j)=zel(j)+ed(ipr(j))*(ea(i)-tact(i))/bdta(i)**2.
      do 310 k=1,iord
  310 vel(j,k)=vel(j,k)+ed(ipr(j))*ed(ipr(k))/bdta(i)**2.
  300 continue
  280 continue
      return
      end

SUBROUTINE MATRIX(VEL,WEL,ZEL,IORD)
C-----------------------------------------------------------------------------------------------
C This is the matrix diagonalization and inversion subroutine.
C VEL(I,J) are the elements of the matrix
C WEL(I,J) are the elemants of the inverse matrix
C ZEL(I)   are the elements of the vector
C IORD is the order of the matrix
C Solution and inversion is done by Gauss-Jordan elimination below the diagonal,
C reflecting through the center, repeating the Gauss-Jordan elimination and re-
C reflecting.
C-----------------------------------------------------------------------------------------------
      implicit integer*2(i-n)
      implicit real*8(a-f,r-z)
      implicit character(g-h)
      dimension vel(10,10),wel(10,10),zel(10),usum(10)
C Scale the matrix, the inverse, and the vector to prevent overflow and underflow and
C to enhance accuracy.
      do 10 iz1=1,iord
      usum(iz1)=0.
      do 20 iz2=1,iord
      usum(iz1)=usum(iz1)+vel(iz1,iz2)
```

```
   20 wel(iz1,iz2)=0.
      do 30 iz2=1,iord
   30 vel(iz1,iz2)=vel(iz1,iz2)*dble(iord)/usum(iz1)
      zel(iz1)=zel(iz1)*dble(iord)/usum(iz1)
   10 wel(iz1,iz1)=dble(iord)/usum(iz1)
      iz4=1
C Check for zeroes on the diagonal
   60 do 210 iz1=1,iord
      if(vel(iz1,iz1).eq.0.)then
      if(iz4.eq.2)goto 415
      do 410 iz5=iz1+1,iord
      do 380 iz6=1,iord
      vel(iz1,iz6)=vel(iz1,iz6)+vel(iz5,iz6)
  380 wel(iz1,iz6)=wel(iz1,iz6)+wel(iz5,iz6)
      zel(iz1)=zel(iz1)+zel(iz5)
  410 if(vel(iz1,iz1).ne.0.)goto 412
      goto 415
  412 endif
C Gauss-Jordan elimination
   75 ebug=vel(iz1,iz1)
      do 110 iz2=1,iord
      vel(iz1,iz2)=vel(iz1,iz2)/ebug
  110 wel(iz1,iz2)=wel(iz1,iz2)/ebug
      zel(iz1)=zel(iz1)/ebug
      if(iz1.eq.iord)goto 220
      do 200 iz2=iz1+1,iord
      if(vel(iz2,iz1).eq.0.)goto 200
      ebug=-vel(iz2,iz1)/vel(iz1,iz1)
      do 180 iz3=1,iord
      vel(iz2,iz3)=vel(iz2,iz3)+ebug*vel(iz1,iz3)
  180 wel(iz2,iz3)=wel(iz2,iz3)+ebug*wel(iz1,iz3)
  200 zel(iz2)=zel(iz2)+ebug*zel(iz1)
  210 continue
C Reflect through the center
  220 if(iord/2.eq.(iord+1)/2)then
      iz1=int(iord/2)
      else
      iz1=int((iord-1)/2)
      endif
      do 290 iz2=1,iz1
      do 270 iz3=1,iord
      store=vel(iz2,iz3)
      vel(iz2,iz3)=vel(iord+1-iz2,iz3)
      vel(iord+1-iz2,iz3)=store
      store=wel(iz2,iz3)
      wel(iz2,iz3)=wel(iord+1-iz2,iz3)
```

```
 270 wel(iord+1-iz2,iz3)=store
     store=zel(iz2)
     zel(iz2)=zel(iord+1-iz2)
 290 zel(iord+1-iz2)=store
     do 296 iz2=1,iz1
     do 295 iz3=1,iord
     store=vel(iz3,iz2)
     vel(iz3,iz2)=vel(iz3,iord+1-iz2)
     vel(iz3,iord+1-iz2)=store
     store=wel(iz3,iz2)
     wel(iz3,iz2)=wel(iz3,iord+1-iz2)
 295 wel(iz3,iord+1-iz2)=store
 296 continue
     iz4=iz4+1
     if(iz4.eq.2)goto 60
     return
C If all else fails, give up
 415 if(ggraf.eq.'y')write(10,420)
     write(*,420)
 420 format(1x,'Matrix wont solve . . . Matrix wont solve')
     stop
     end

SUBROUTINE GRAPH(GPRINT,CHI,HALT)
C-------------------------------------------------------------------------------------------------
C This is a semi-log printer plotter routine.
C-------------------------------------------------------------------------------------------------
     implicit integer*2(i-n)
     implicit character(g-h)
     implicit real*8(a-f,r-z)
     common vel,zel,ea,tact,adta,bdta,cdta,ddta,icom,icn,idata,iord
    x,fram,ipr,nrplot,jplot
     dimension tact(200),ea(200),bdta(200),sil(200),sih(200),cdta(200)
     dimension gr(125),adta(200),ddta(200),vel(10,10),zel(10)
     dimension fram(10),ipr(10),grm(80,20)
C Take logs
     jplot=jplot+1
     do 570 i=1,idata
     if(tact(i).le.0.)then
     tact(i)=-1.
     goto 510
     endif
     tact(i)=log10(tact(i))
 510 if(ea(i)+bdta(i).le.0.)then
     ea(i)=-1.
     sil(i)=-1.
```

```
      sih(i)=-1.
      goto 570
      endif
      sih(i)=log10(ea(i)+bdta(i))
      if(ea(i).le.0.)then
      ea(i)=-1.
      sil(i)=-1.
      goto 570
      endif
      if(ea(i)-bdta(i).le.0.)then
      sil(i)=-1.
      goto 560
      endif
      sil(i)=log10(ea(i)-bdta(i))
  560 ea(i)=log10(ea(i))
  570 continue
C Find extrema xmax,xmin,ymay,ymin
      xmax=cdta(1)
      xmin=cdta(1)
      ymax=ea(1)
      ymin=ea(1)
      do 730 i=1,idata
      if(cdta(i).gt.xmax)xmax=cdta(i)
      if(cdta(i).lt.xmin)xmin=cdta(i)
      if(sih(i).gt.ymax)ymax=sih(i)
      if(tact(i).gt.ymax)ymax=tact(i)
      if(sil(i).eq.-1.)goto 725
      if(sil(i).lt.ymin)ymin=sil(i)
  725 if(tact(i).eq.-1)goto 730
      if(tact(i).lt.ymin)ymin=tact(i)
  730 continue
C Now make the plot line by line
      if(halt.eq.'y')write(*,895)ymin,ymax,xmin,xmax,chi
      if(gprint.eq.'y')write(10,895)ymin,ymax,xmin,xmax,chi
  895 format(1x,'logymin=',f4.2,'/logymax= ',f4.2,'/xmin=',e9.3,
     !'/xmax=',e9.3,'/chi sqrd=',e9.3)
      do 910 i=1,78
      do 900 j=1,20
      grm(i,j)=' '
  900 continue
  910 continue
      do 920 i=1,78
      grm(i,1)='í'
  920 grm(i,20)='í'
      do 930 j=1,20
      grm(1,j)='ο'
```

```
 930 grm(78,j)='º'
     grm(1,1)='é'
     grm(1,20)='è'
     grm(78,1)='»'
     grm(78,20)='¼'
     scx=(xmax-xmin)/73
     scy=(ymax-ymin)/17
     do 1030 i=1,75
     do 1000 iw=1,20
1000 gr(iw)=' '
     do 1010 j=1,idata
     if((cdta(j).ge.xmin+scx*dble(i-1)).and.(cdta(j).lt.xmin+
    xscx*dble(i)))then
     if(sih(j).ne.-1.)gr(int((sih(j)-ymin)/scy+1.))='â'
     if(sil(j).ne.-1.)gr(int((sil(j)-ymin)/scy+1.))='á'
     if(ea(j) .ne.-1.)gr(int((ea(j) -ymin)/scy+1.))='+'
     if(tact(j).ne.-1.)gr(int((tact(j)-ymin)/scy+1.))='*'
     endif
     do 1020 ii=1,18
1020 grm(i+2,20-ii)=gr(ii)
1010 continue
1030 continue
     grm(3,17)='*'
     grm(5,17)='='
     grm(7,17)='c'
     grm(8,17)='a'
     grm(9,17)='l'
     grm(10,17)='c'
     grm(11,17)='.'
     grm(13,17)='d'
     grm(14,17)='a'
     grm(15,17)='t'
     grm(16,17)='a'
     grm(3,18)='+'
     grm(5,18)='='
     grm(7,18)='a'
     grm(8,18)='c'
     grm(9,18)='t'
     grm(10,18)='u'
     grm(11,18)='a'
     grm(12,18)='l'
     grm(14,18)='d'
     grm(15,18)='a'
     grm(16,18)='t'
     grm(17,18)='a'
     grm(3,19)='-'
```

```
      grm(5,19)='='
      grm(7,19)='e'
      grm(8,19)='r'
      grm(9,19)='r'
      grm(10,19)='o'
      grm(11,19)='r'
      grm(13,19)='l'
      grm(14,19)='i'
      grm(15,19)='m'
      grm(16,19)='i'
      grm(17,19)='t'
      do 1040 j=1,20
      if(halt.eq.'y')write(*,1035)(grm(i,j),i=1,78)
 1035 format(1x,78a1)
      do 935 i=1,78
      if(grm(i,j).eq.'í')grm(i,j)='.'
      if(grm(i,j).eq.'º')grm(i,j)=':'
      if(grm(i,j).eq.'é')grm(i,j)='.'
      if(grm(i,j).eq.'è')grm(i,j)=':'
      if(grm(i,j).eq.'»')grm(i,j)='.'
      if(grm(i,j).eq.'¼')grm(i,j)=':'
      if(grm(i,j).eq.'â')grm(i,j)='-'
  935 if(grm(i,j).eq.'á')grm(i,j)='-'
      if(gprint.eq.'y')write(10,1035)(grm(i,j),i=1,78)
 1040 continue
      return
      end

      SUBROUTINE CORREC(BSAV)
C-------------------------------------------------------------------------------------------------
C This subroutine corrects for non-linear decay during the counting intervals.
C-------------------------------------------------------------------------------------------------
      implicit integer*2(i-n)
      implicit real*8(a-f,r-z)
      common vel,zel,ea,tact,adta,bdta,cdta,ddta,icom,icn,idata,iord
     x,fram,ipr
      dimension ea(200),adta(200),bdta(200),cdta(200),ddta(200)
      dimension fram(10),sbar(200),rcor(200),exl(5),exl1(5)
      dimension bsav(200),vel(10,10),zel(10),tact(200),ipr(10)
      if(icn.gt.5)goto 200
C Corrections for independent components
      do 40 i=1,idata
      ea(i)=adta(i)*fram(1)*ddta(i)/(1.-exp(-fram(1)*ddta(i)))
   40 sbar(i)=fram(2)*exp(-fram(1)*cdta(i))*(1.-exp(-fram(1)*
     xddta(i)))/fram(1)/ddta(i)
      if(icn.eq.1)then
```

```
      bdta(i)=abs(bsav(i)/adta(i)*ea(i))
      return
      endif
      do 130 i=1,idata
      rcor(i)=0.
      do 110 j=2,icn
      sbar(i)=sbar(i)+fram(2*j)*exp(-fram(2*j-1)*cdta(i))*(1.-
     xexp(-fram(2*j-1)*ddta(i)))/fram(2*j-1)/ddta(i)
  110 rcor(i)=rcor(i)+fram(2*j)*exp(-fram(2*j-1)*cdta(i))*(1.-
     xfram(1)/fram(2*j-1)*(1.-exp(-fram(2*j-1)*ddta(i)))/
     x(1.-exp(-fram(1)*ddta(i))))
      ea(i)=ea(i)+adta(i)*rcor(i)/sbar(i)
  130 bdta(i)=abs(bsav(i)/adta(i)*ea(i))
      return
C Corrections for growth and decay curves
  200 xl2ml1=fram(3)-fram(1)
      xl4ml3=fram(7)-fram(5)
C Calculate average activities
      do 650 i=1,idata
      do 260 jw=1,5
      exl(jw)=fram(2*jw)*exp(-fram(2*jw-1)*cdta(i))
  260 exl1(jw)=1.-exp(-fram(2*jw-1)*ddta(i))
      ea(i)=adta(i)*fram(3)*ddta(i)/exl1(2)
      sbar(i)=0.
      jw=1
  320 sbar(i)=sbar(i)+fram(jw*4-1)/fram(jw*4-3)/(fram(jw*4-1)-
     xfram(jw*4-3))*exl(jw*2-1)*exl1(jw*2-1)/ddta(i)
      sbar(i)=sbar(i)-fram(4*jw-2)*exp(-fram(4*jw-1)*cdta(i))
     x/(fram(jw*4-1)-fram(jw*4-3))*exl1(jw*2)/ddta(i)
      sbar(i)=sbar(i)+exl(jw*2)/fram(jw*4-1)*exl1(jw*2)/ddta(i)
      if(jw.eq.2)goto 370
      if(icn.gt.9)then
      jw=2
      goto 320
      endif
  370 if(icn.eq.10)goto 460
      if(icn.eq.6)goto 460
      if(icn.eq.11)then
      jw=5
      goto 410
      endif
      jw=3
  410 sbar(i)=sbar(i)+exl(jw)/fram(jw*2-1)*exl1(jw)/ddta(i)
      if(icn.eq.11)goto 460
      if(icn.eq.jw+4)goto 460
      jw=jw+1
```

```
      goto 410
  460 continue
C Done with average activity now calculate the corrections
      rcor(i)=exl(1)*fram(3)/xl2ml1*(1.-fram(3)/fram(1)*exl1(1)
     x/exl1(2))
      if(icn.eq.6)goto 630
      if(icn.gt.9)goto 600
      jw=3
  550 rcor(i)=rcor(i)+exl(jw)*(1.-fram(3)/fram(2*jw-1)*exl1(jw)/
     xexl1(2))
      if(icn.eq.jw+4)goto 630
      if((icn.eq.jw+6).and.(icn.gt.9))goto 630
      jw=jw+1
      goto 550
  600 rcor(i)=rcor(i)+exl(3)*fram(7)/xl4ml3*(fram(3)/fram(7)*exl1(4)
     x/exl1(2)-fram(3)/fram(5)*exl1(3)/exl1(2))
      jw=4
      goto 550
  630 ea(i)=ea(i)+adta(i)*rcor(i)/sbar(i)
  650 bdta(i)=abs(bsav(i)/adta(i)*ea(i))
  660 continue
      return
      end
SUBROUTINE CLRSCR
C-------------------------------------------------------------------------------------------------
C This routine clears the screen and sets the cursor to first position in first line.
C Routine requires ANSI device driver.
C-------------------------------------------------------------------------------------------------
          integer         ilin
          character*4     astr
          data            astr/     ' [2j' /
          astr(1:1)= char(27)
          write( *, * ) astr
9000      continue
                  return
                          end
```

3. Desort.for

```
      PROGRAM DESORT
      dimension ia(2000),enya(2000),enyb(2000),hl(2000),a0(2000),
     %sa0(2000),abe(2000)
      character*78 blank
      character*6 ga(2000)
      character*3 gcheck
      character*1 gb(2000)
      character*75 gx
```

```
      open(1,file='desort.dat',status='old')
      open(10,file='desort.res',status='new')
      do 100 i=1,2
      read(1,'(a78)')blank
  100 write(10,'(a78)')blank
      ii=1
  110 read(1,1010,end=190)enya(ii),ia(ii),ga(ii),enyb(ii),abe(ii),
     %hl(ii),a0(ii),sa0(ii),gb(ii)
      write(*,1011)enya(ii),ia(ii),ga(ii),enyb(ii),abe(ii),hl(ii),
     %a0(ii),sa0(ii),gb(ii)
 1010 format(f7.1,1x,i3,a6,f6.1,4x,f6.2,5x,e10.3,4x,e11.5,3x,e11.5,1x,
     %a1)
  1011 format(1x,f6.1,1x,i3,a6,f6.1,'kev,',f6.2,',hl=',e10.3,',a0=',
     %e11.5,'+/-',e11.5,1x,a1)
      ii=ii+1
      goto 110
  190 continue
      nnucl=ii-1
      do 200 i=1,nnucl
      do 200 j=1,nnucl
      if(ia(i).ge.ia(j))goto 200
      call iexch(ia(i),ia(j))
      call rexch(enya(i),enya(j))
      call g6exch(ga(i),ga(j))
      call rexch(enyb(i),enyb(j))
      call rexch(abe(i),abe(j))
      call rexch(hl(i),hl(j))
      call rexch(a0(i),a0(j))
      call rexch(sa0(i),sa0(j))
      call g1exch(gb(i),gb(j))
  200 continue
      do 205 i=1,nnucl
      ii=i
      if(ia(ii).ne.ia(ii-1))write(10,1020)

 1020 format(/)
      write(*,1011)enya(ii),ia(ii),ga(ii),enyb(ii),abe(ii),hl(ii),
     %a0(ii),sa0(ii),gb(ii)
      write(10,1011)enya(ii),ia(ii),ga(ii),enyb(ii),abe(ii),hl(ii),
     %a0(ii),sa0(ii),gb(ii)
  205 continue
      end

  SUBROUTINE IEXCH(m,n)
      l=m
      m=n
```

```
      n=l
      return
      end

SUBROUTINE G6EXCH(a,b)
      character*6 t,a,b
      t=a
      a=b
      b=t
      return
      end

SUBROUTINE G1EXCH(a,b)
      character*1 t,a,b
      t=a
      a=b
      b=t
      return
      end

SUBROUTINE REXCH(a,b)
      t=a
      a=b
      b=t
      return
      end
```

4. CROSS.for

```
      PROGRAM CRSPLT
      dimension tim(50), cur(50), a0i(50), erri(50), brnchi(50),
     1          fluxi(50), tiab(50), title(8)
      integer z, zp, zgp
      character*10 title,targ,proj
      common / tabl / nat(900), elt(900), isomt(900), z(900), zp(900),
     1               zgp(900), hl(900), hlp(900), hlgp(900), itot
      data blank / 1h /
C-------------------------------------------------------------------------------------------
C Cross calculates cross sections for nuclides based upon the gamma-assignments
C made from decay data. Cross sections may be calculated based upon single gammas
C or upon several gamma lines identified for a given nuclide.  In the first case, the
C input data are not (necessarily) sorted in a particular order, and no separators should
C be used.  In the second case (>= 1 gamma per nuclide) the input data should be
C sorted by nuclide and each set of data for any given nuclide should be separated by a
C blank record.
```

```
C In any case, a summary table is generated by specifying that option. The program is
C terminated with an EOF after the last input card or after the summary table specifier.
C Cross section calculations include variable flux factors. This code does weighted
C mean calculation based upon
C                                        w(i) = br(i) / err(i)**2
C where w(i) is the weight linearly dependant on the branching ratio, br(i) and on the
C square of the error, err(i). The code also uses a correct error analysis and error
C rejection for cross section calculations based upon more than 1 gamma line. The
C standard error is calculated by
C                                    s.e. = sqrt((sum(nu(i)*w(i)) / sum(w(i)))
C where sum indicates a sum over all n members of the sample, w(i) is the weight, nu
C the deviation, x(i)-<x>, and n is the number of lines for a given nuclide.
C  DATA INPUT
C card 1…..Title card (8a10)
C card 2…..Bbdt information card (a10,2f10.4,a10,2f10.1)
C targ…..Target
C tgtwt…..Target thickness (mg/cm**2)
C tgmass…..Target mass
C proj…..Projectile
C hichrg…..Charge of projectile
C tob…..Total time of bombardment (min)
C card 3-n…..Bombardment history cards (2f10.4)
C tim(i) …..Time of i-th beam flux interval (min)
C cur(i) …..Current of i-th interval (microcoul.)
C card n+1…..Blank
C card n+2…..Chemical yield data (2e10.3), yield, error in yield
C cards n+3-m…..Either single tau2 cards with no separators or cards sorted by
C nuclide and separated by blanks.
C card m+1…..After last card a summary table may be generated with a 1.0 in colums
C 1-3.
C This program will output results to "masin.dat" compatible with the input format to
C MASSY. Read in the isotable for decay information to be matched up to cross
C sections in CPREP for generation of MASSY cards.
C-------------------------------------------------------------------------------------------------

     open(5,file='library.dat',status='old')
     i = 0
 100 i = i + 1
       read(5,805) elt(i), nat(i), isomt(i), z(i), zp(i), zgp(i),
    1              hl(i), hlp(i), hlgp(i)
       if(z(i) .ne. 0.0) goto 100
         itot = i - 1
     open(6,file='inputa.dat',status='old')
 105 read(6,800) title
     read(6,801) targ,tgtwt,tgmass,proj,hichrg,tob
       iflag = 0
```

```
      totcur = 0.0
      tottim = 0.0
 i = 1
        write(*,*) 'got here'
110 read(6,802) tim(i), cur(i)
      if(tim(i) .eq. 0.0) goto 120
        fluxi(i) = cur(i)*6.241e12 / (hichrg*tim(i))
        tottim = tottim + tim(i)
        totcur = totcur + cur(i)
        tiab(i) = tob - tottim
    write(*,*) 'entry ok'
        i = i + 1
        goto 110
120 intrvls = i - 1
    tgtn = tgtwt*6.0220e20 / tgmass
    tflux = totcur*6.241e12 / (hichrg*tottim)
        write(*,*)'Go to another place'
    read(6,806) yield, erryld
    if(yield .eq. 0.0) yield = 100.0
    if(erryld .eq. 0.0  .and.  yield .ne. 100.0) erryld = 5.0
    yield = yield / 100.
    erryld = erryld / 100.0
        write(*,*)'Got yield'
    open(7,file='output',status='new')
    write (7,900) title
    write (7,901) targ,proj
    write(7,902) tgtwt,tgmass,totcur,hichrg,tottim,tgtn,tflux,
   1          yield,erryld
130 line = 0
    tsep = 0.0
    hlfsav = 0.0
C-----------------------------------------------------------------------------------------------
C e1…..Measured gamma ray energy
C e2…..Known gamma ray energy
C a0…..Initial activity (cpm)
C err…..Error in a0 (cpm)
C el…..Element symbol
C a…..Mass number
C isom…..m (metastable) or g (ground state). Be careful that your form of 'isom'
C matches isotab.dat
C hlf…..Half-life (day)
C brnch…..Branching ratio of gamma ray(%)
C frac…..Separation time of nuclide from parent. If no chemical separation was made,
C frac=0.0
C  format(1x,f6.1,1x,a3,2a2,2x,f6.1,4x,f6.2,5x,f10.4,4x,e11.5,3x,e11.5)
C-----------------------------------------------------------------------------------------------
```

```
 140 read(6,803)e1,a,el,isom,e2,brnch,hlf,a0,err
     frac=0.0
3334        if(e1 .eq. 0.0) goto 170
         if(e1 .eq. 1.0) goto 200
           decode(3,700,a) c1,c2,c3
           decode(3,701,a) i1,i2,i3
           na = i1*100 + i2*10 + i3
           if(c3 .eq. blank) na = i1*10 + i2
           if(c2 .eq. blank) na = i1
 150        if(line .eq. 0) write (7,903) el,na,isom
           line = line + 1
           if(hlfsav .ne. 0.0) goto 155
             hlfsav = hlf
             elsav = el
             nasav = na
             isomsav = isom
 155         if(hlfsav .ne. hlf) goto 160
             write(7,904) e1,e2,a0,err,el,na,isom,hlf,brnch,frac
             a0i(line) = a0
             erri(line) = err
             brnchi(line) = brnch
             if (frac.gt.tsep) tsep=frac
             goto 140
 160         write (7,905)
           line = line - 1
           iflag = 1
 170 if(line .eq. 1) goto 180
       nlins = line
       call error(a0i,erri,brnchi,a0ave,errave,nlins)
       goto 190
 180 a0ave = a0i(1)
     errave = erri(1)
     nlins = 1
 190 hlf = hlfsav * 1440.
     sum = 0.0
     do 10 i = 1,intrvls
       sum = sum + fluxi(i) * (1.0 - exp(-0.693 * tim(i)/hlf)) *
    1                        exp(-0.693 * tiab(i)/hlf)
  10 continue
     sigma = a0ave*1.0e27 / (sum*tgtn)
     errsig = errave*1.0e27 / (sum*tgtn)
     sigy = sigma / yield
     errsigy = sigy * sqrt((erryld/yield)**2 + (errsig/sigma)**2)
     write (7,906) nlins, line, elsav, nasav, isomsav
     write (7,907) sigma, errsig
     call result(elsav,nasav,isomsav,sigma,errsig,line,nlins,
```

```
     1          sigy,errsigy,tsep,0)
      if(iflag .ne. 1) goto 130
        iflag = 0
        line = 0
        hlfsav = 0.0
        goto 150
   200 call result(elsav,nasav,isomsav,sigma,errsig,line,nlins,
     1          sigy,errsigy,tsep,1)
      goto 105
   298 write (7,908)
   299 stop
C  FORMAT STATEMENTS
   700 format(3a1)
   701 format(3i1)
   800 format(8a10)
   801 format(a10,2f10.4,a10,2f10.4)
   802 format(2f10.4)
C  803 format(1x,f6.1,1x,a3,2a2,2x,f6.1,4x,f5.1,4x,e9.3,4x,e11.5,3x,
C     xe11.5)
   803 format(1x,f6.1,1x,a3,2a2,2x,f6.1,4x,f6.2,5x,f9.4,4x,e11.5,3x,
     x e11.5)
   805 format(1x,a2,i3,a2,i3,2i5,3e10.3)
   806 format(2e10.3)
   900 format(1h1, 10x, 6(10h**********), //, 14x,
     1      'C r o s s   s e c t i o n   c a l c u l a t i o n s',//,
     2      11x,6(10h**********),//,10x,8a10,//)
   901 format(1h0,/,
     1      ' Revised error analysis for finite data set,',/,
     4      ' Cross sections for the reaction of ',/,
     5      5x,a10,'  with  ',a10,///)
   902 format(1h0,10x,'I n p u t   p a r a m e t e r s',//,
     1      10x,'Target thickness   =',f10.4,10h mg/cm**2  ,/,
     2      10x,'Target mass        =',f10.4, /,
     3      10x,'Total beam current =',f10.3,' microcoul.',/,
     4      10x,'Projectile charge  =',f10.3, /,
     5      10x,'Total bbdt time    =',f10.2,' minutes', /,
     6      10x,'Target atoms (n)   =',g12.5,' atoms',/,
     7      10x,'Total beam flux    =',g12.5,' h.i. / min.',/,
     8      10x,'Yield for sample   =',g11.4,' +/- ',g11.4,/////)
   903 format(1h0,'I s o t o p e ...',a2,'-',i3,a2,/)
   904 format(1h ,2f7.1,2(1x,e11.4),1x,1x,a2,'-',i3,a3,
     1      f8.3,f7.1,e10.3)
   905 format(1h0, 'Hey turkey, you need a blank card to separate ', /,
     1      ' the nuclides here, but you are forgiven this time.',//)
   906 format(1h0,3x,i3,' out of',i3,' gamma line(s) were used to ',
     1      'calculate the ‘,a2,'-',i3,a2,' cross section.',/)
```

```
 907 format(1h0,10x,'Cross section= ',g12.5,' +/- ',g12.5,
    1      /,11x,6(7h*******),///)
 908 format(1h0,4(10h**********),/,
    1      ' EOF on card input detected at intermediate stage.',/,
    2      ' PROGRAM ABORTED.')
      End

      SUBROUTINE ERROR(a0i,erri,bri,a0ave,errave,nlins)
C-------------------------------------------------------------------------------------------------
C 'ERROR' is called when there are at least two points in the set of data for a given
C nuclide.  If there are more than two points, then error will test the points for the
C rejection criteria as for sets of data with fewer than 10 measurements, we have
C decided to use the 2-sigma rejection limit since Chauvenets criterion eliminates far
C too many points in small data sets.
C-------------------------------------------------------------------------------------------------
      dimension a0i(1),erri(1),bri(1),a0rej(50),errej(50),chauv(25)
      data chauv/ 0.000, 0.000, 1.380, 1.535, 1.645, 1.730,
     1            1.800, 1.862, 1.915, 1.960, 2.001, 2.038,
     2            2.070, 2.100, 2.127, 2.155, 2.178, 2.200,
     3            2.220, 2.240, 2.260, 2.278, 2.293, 2.310, 2.327/
      n = 0
      irej = 0
      if(nlins .eq. 2) goto 120
      if(nlins .le. 25) crit = chauv(nlins)
      if(nlins .le. 10) crit = 2.0
      if(nlins .gt. 25) crit = chauv(25) + 0.12*(nlins-25)
      call MEAN(a0i,erri,bri,a0ave,errave,nlins)
      write (7,900) a0ave,errave,crit
      do 10 i = 1,nlins
        dev = abs(a0ave-a0i(i))
        if(dev .gt. crit*errave) goto 100
          n = n + 1
          a0i(n) = a0i(i)
          erri(n) = erri(i)
          bri(n) = bri(i)
          goto 10
 100    irej = irej + 1
        a0rej(irej) = a0i(i)
        errej(irej) = erri(i)
  10  continue
      if(irej .eq. 0) goto 110
        write (7,901)
        write (7,902) (a0rej(j),errej(j), j=1,irej)
 110  nlins = n
 120  call MEAN(a0i,erri,bri,a0ave,errave,nlins)
      write(7,903) a0ave,errave
```

```
   return
900 format(1h0,' Calculation of initial mean',/,10x,'Mean = ',G12.5,
  1       5X,'Std. dev.= ',g12.5,5x,'Rejection param.= ',f5.3,/)
901 format(1h0,'Rejected data points, Chauvenets criterion',//)
902 format(2(5x,g12.5))
903 format(1h0,' Final mean= ',g12.5,5x,'Std. dev.= ',g12.5,/)
   End

   SUBROUTINE MEAN(a0i,erri,bri,a0ave,errave,nlins)
   dimension a0i(1), erri(1), bri(1), wti(50)
   sumxw = 0.0
   sumw  = 0.0
   sumwnu = 0.0
   if(nlins .gt. 1) goto 100
     a0ave = a0i(1)
     errave = erri(1)
     return
100 do 10 i = 1,nlins
     wti(i) = bri(i) / erri(i)**2
     sumw = sumw + wti(i)
     sumxw = sumxw + a0i(i)*wti(i)
 10 continue
   a0ave = sumxw / sumw
   do 20 i = 1,nlins
     sumwnu = sumwnu + wti(i) * (a0ave-a0i(i))**2
 20 continue
   errave = sqrt(sumwnu / sumw)
   return
   end

   SUBROUTINE RESULT(el,na,isom,sig,erc,nf,nu,y,ey,
  1                  tsep,iend)
   dimension eln(300),nan(300),isomn(300),sign(300),esign(300),
  1          ngamf(300),ngamu(300),csy(300),ecsy(300),trec(300)
   data n/0/
   if(iend .eq. 1) goto 100
     n = n + 1
     eln(n) = el
     nan(n) = na
     isomn(n) = isom
     sign(n) = sig
     esign(n) = erc
     ngamf(n) = nf
     ngamu(n) = nu
     csy(n) = y
     ecsy(n) = ey
```

```
      trec(n) = tsep
      return
100     write(7,900)
    do 10 i = 1,n
      write(7,901) eln(i),nan(i),isomn(i),sign(i),esign(i),
   1             ngamf(i),ngamu(i),csy(i),ecsy(i)
 10 continue                                                  280
    call CPREP(eln,nan,isomn,csy,ecsy,trec,n)
    iend = 0
    n = 0
    return
900 format(1h1,1x,'Results of  ',//,1x,'isotopes',2x,'Cross-',
   1       'section(mb)',5x,'Error(mb)',5x,'Gammas found, used',
   2       2x,'Yield(mb)',5x,'Error(mb)',//)
901 format(1x,a2,1x,i3,a2,4x,2(e10.4,10x),i2,10x,i2,2(5x,e10.4),/)
    End

    SUBROUTINE CPREP(eln,nan,isomn,sign,errn,trec,n)
    dimension eln(300), nan(300), isomn(300), sign(300),
   1          errn(300), trec(300)
    integer z, zp, zgp
    common / tabl / nat(900), elt(900), isomt(900), z(900), zp(900),
   1                zgp(900), hl(900), hlp(900), hlgp(900), itot
    write (7,902)
    do 10 i = 1,n
      do 20 j = 1,itot
        if(eln(i) .eq. elt(j)  .and.  nan(i) .eq. nat(j)  .and.
   1       isomn(i) .eq. isomt(j)) goto 100
 20   continue
      write (7,900) eln(i),nan(i),isomn(i)
      goto 10
100   if(hlp(j) .eq. -0) hlp(j) = 0.0
      if(hlgp(j) .eq. -0) hlgp(j) = 0.0
    open(8,file='massyin',status='new')
    write(8,901) elt(j),nat(j),isomt(j),z(j),zp(j),zgp(j),hl(j),
   1             hlp(j),hlgp(j),sign(i),errn(i),trec(i)
    write (7,901) elt(j),nat(j),isomt(j),z(j),zp(j),zgp(j),hl(j),
   1             hlp(j),hlgp(j),sign(i),errn(i),trec(i)
 10 continue
    return                                                    394
900 format(' $$$$$$$$$$missing nuclide from isotable  ',a2,'-',i3,a2)
901 format(1x,a2,i3,a1,i4,2i5,5e10.4,1x,f8.4)
902 format(1h1, '  massy card images',/)
    end
```

5. Handanal.for

```
      program handanal
C-------------------------------------------------------------------------------------------------
C This program reads in ascii spectra from the 2006 triumf expt and calculates peak
C areas and uncertainties.
C Variables:
C lb1=left ch # bkg #1
C lb2=left ch # bkg #2
C lp1=left peak ch #
C rp1=right peak ch #
C rb1=right bkg ch # 1
C rb2=right bkg ch #2
C-------------------------------------------------------------------------------------------------

      dimension dummy(12),spe(8192)
      integer lb1,lb2,lp1,rp1,rb1,rb2
      character atit,dummy
      write(*,*)'input filename'
      read(*,*)atit
      open(1,file='70zn4us06.Spe',status='old')
      open(2,file='output',status='new')
      do 69 i=1,12
      read(1,*)dummy(i)
69    continue
      do 699 i=1,8191
      read(1,*)spe(i)
699   continue
      write(*,*)'input lb1,lb2,lp1,rp1,rb1,rb2'
      read(*,*)lb1,lb2,lp1,rp1,rb1,rb2
      peak=0.0
      right=0.0
      xleft=0.0
      do 10 i=lp1,rp1
      peak=peak+spe(i)
10    continue
      do 11 i=lb1,lb2
      xleft=xleft + spe(i)
11    continue
      do 12 i=rb1,rb2
      right=right+spe(i)
12    continue
      xlc=(lb2-lb1)+1
      xrc=(rb2-rb1)+1
      xlb=xleft/xlc
      xrb=right/xrc
      pc=rp1-lp1+1
```

```
bkg=pc*(xlb+xrb)/2
area=peak-bkg
uarea=sqrt(peak+bkg)
write(2,*)'peak analysis report'
write(2,*)'integration parameters'
write(2,*)lb1,lb2,lp1,rp1,rb1,rb2
write(2,*)'the peak area is ',area,'+/-',uarea
end
```

APPENDIX C

Sub-barrier fusion of ^{9}Li with ^{70}Zn

W. Loveland,[1] A. M. Vinodkumar,[1] R. S. Naik,[1] P. H. Sprunger,[1] B. Matteson,[1] J. Neeway,[1] M. Trinczek,[2]
M. Dombsky,[2] P. Machule,[2] D. Ottewell,[2] D. Cross,[2,4] K. Gagnon,[2,3] and W. J. Mills[2,3]
[1]*Department of Chemistry, Oregon State University, Corvallis, Oregon 97331, USA*
[2]*TRIUMF, Vancouver, British Columbia, Canada V6T 2A3*
[3]*Department of Physics, Simon Fraser University, Burnaby, British Columbia, Canada V5A 1S6*
[4]*Department of Chemistry, Simon Fraser University, Burnaby, British Columbia, Canada V5A 1S6*
(Received 1 September 2006; published 13 December 2006)

The cross section for the fusion of ^{9}Li with ^{70}Zn was measured for seven projectile energies spanning the sub-barrier and near-barrier region (*E*c.m. ranging from 9.7 to 13.4 MeV) using the ISAC facility at TRIUMF. γ –ray spectroscopy of the irradiated target foils along with β counting of the chemically separated Ge and As evaporation residues were used to measure the fusion cross sections. Statistical model calculations were used to correct for the yields of any unobserved nuclei. The observed fusion excitation function shows significant sub-barrier fusion enhancement with a large deduced value of the fusion radius, R_B =12.1±1.0 fm. Coupled-channels calculations do not account for the observed sub-barrier enhancement. The implications of this finding for understanding the fusion of ^{11}Li are discussed.

DOI: 10.1103/PhysRevC.74.064609 PACS number(s): 25.70.Jj, 25.60.Pj, 25.85.−w

I. INTRODUCTION

The nuclear structure and nuclear reactions of ^{9}Li are of interest for three reasons. (a) It is the core nucleus of the two-neutron halo nucleus 11Li that is of great current interest and an understanding of ^{9}Li is important for an understanding of ^{11}Li. (b) ^{9}Li is itself a very neutron-rich nucleus (N/Z = 2) with a significant neutron skin [1] and an understanding of its reactions may be helpful in understanding the interactions of very neutron-rich nuclei. (c) ^{9}Li is a well-characterized nucleus with a simple shell-model structure, which should be helpful in modeling its interactions. In this article, we focus on a study of the fusion excitation function of ^{9}Li interacting with an intermediate mass, neutron rich nucleus ^{70}Zn. The study was undertaken to gain insight into the fusion of a very neutron-rich projectile with a neutron rich target nucleus and to serve as a precursor of a study of the fusion of ^{11}Li with this nucleus. Previous studies have been made, at intermediate energies, of the elastic scattering of ^{9}Li [2] and the total interaction cross section of ^{9}Li interacting with intermediate mass nuclei, such as Cu [3]. Both nuclear interactions and electromagnetic dissociation were observed with the interaction radius of ^{9}Li being normal. The fusion of ^{9}Li with Si at 11.2 *A*–15.2 *A* MeV was studied at RIKEN [4] by measuring the evaporation residues

and any associated neutrons. In contrast to similar studies with ^{11}Li, the neutron spectra associated with the ^{9}Li interactions had the shape of fusion evaporation spectra. However, no detailed information on the fusion cross sections or an analysis of them is available. The fusion of ^{9}Li with ^{209}Bi (at a projectile energy of 36 MeV) was also studied at RIKEN [5]. The ratio of the production cross sections for the evaporation residues ^{214}Rn and ^{215}Rn was measured but no fusion cross section was measured. With this in mind, we undertook a study of the fusion of ^{9}Li with ^{70}Zn at the ISAC facility at TRIUMF. [We also attempted, unsuccessfully (see Appendix), to measure the fusion cross section of ^{11}Li interacting with ^{70}Zn.] In Sec. II of this article, we describe the experimental apparatus; our results are presented and discussed in Sec. III. Conclusions are given in Sec. IV.

II. EXPERIMENTAL METHODS

The measurement of the fusion cross sections for the ^{9}Li+^{70}Zn reaction was carried out at the ISAC facility at TRIUMF. Proton beams (500 MeV) with intensities ranging from 50–85 μA struck Ta metal production targets. Beams of radioactive ^{9}Li were extracted with energies up to 18.4 keV, mass separated by passage through two dipole magnets and accelerated to their final energy by radiofrequency quadrupole and drift tube linear accelerators. The details of the production of these secondary beams are discussed elsewhere [6,7]. After acceleration, the beam was delivered to the HEBT straight-through beam line in the ISAC facility. The experiment was carried out in a large-volume (~40 L) scattering chamber, known as the Laval chamber, at the end of this beam line. The beams struck ^{70}Zn targets mounted in the chamber. Beam intensities were monitored by detecting elastic scattering at ±16.2° with additional monitoring of the beam by a suppressed Faraday cup at the end of the beam line. The experiments were carried out in two separate runs, August–September 2005 and May–June 2006. In the 2005 experiments, the primary proton beam was 50 μA and the average on-target ^{9}Li intensity was 5×10^{6} particles/s. In the 2006 experiments, higher proton currents were used (50–85 μA) and the average on-target beam intensity was slightly less, 4×10^{6} particles/s. ^{70}Zn was chosen as the target for this study because of its neutron-richness and because the predicted evaporation residues (As or Ge nuclei) were easily detected using radiochemical techniques and because it is possible to get above the interaction barrier with the ISAC ^{9}Li beam, which has a maximum energy of ~1.71 A MeV. Targets of ~95% enriched ^{70}Zn (thickness ~0.8–1.1 mg/cm^2) were prepared by electrodeposition on Al backing foils (0.54–0.71 mg/cm^2). Si detectors (300 mm^2) were mounted ~40 cm from the target at ±16.2° to monitor the ^{9}Li elastic scattering during each irradiation. Another measure of the beam intensity was a shielded, suppressed Faraday cup at the end of the beam line, which agreed roughly with the Rutherford scattering estimates of the beam doses. ^{9}Li is 178 ms β emitter with a Q_β ~13.6 MeV with ~50% of the decays resulting in neutron emission. Because we were not sure how the Faraday cup would respond to the high-energy β decays, we chose Rutherford/elastic scattering as the primary monitor of the beam intensity. A 0.008m^3 shield of 5% boron-loaded paraffin was used to reduce the neutron emission from the Faraday cup to acceptable levels. Before discussing the results of the measurement of the evaporation residue yields, it might be useful to discuss what we

might expect. In Fig. 1, we show the predicted cross sections for the various nuclides formed in this reaction. These simulations were done using the statistical model codes PACE v. 4.13 [8] and HIVAP [9].

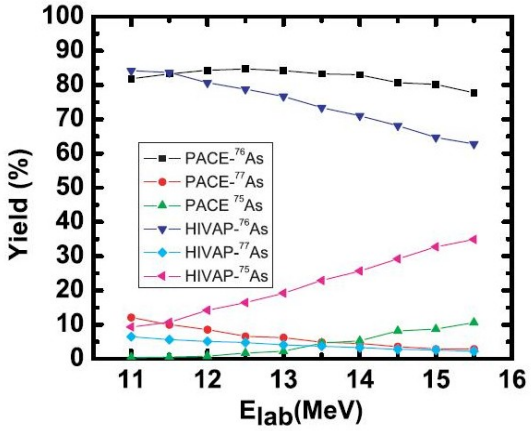

FIG. 1. (Color online) Statistical model simulations of the expected yields of various nuclides in the reaction of ^{9}Li with ^{70}Zn.

The entire evaporation residue cross section is predicted to be concentrated in the three isotopes of As, stable ^{75}As, 1.09-day ^{76}As, and 38.8h ^{77}As. Both simulations show the largest predicted component is ^{76}As. ^{77}As, a minor component of the yield, has the further complication that its β branch to the excited states of the daughter is small, causing the characteristic decay γ -ray line at 239 keV to be present in only 1.6% of the decays. For each of the ^{9}Li energies studied, a fresh ^{70}Zn target was installed in the scattering chamber and it was irradiated for 1–3 days. In the 2006 run, the irradiated target foil was counted with a Ge γ -ray spectrometer for about 1 day prior to commencing a radiochemical analysis of the target. The Ge γ -ray spectrometer consisted of a large-volume Ge detector (efficiency ~80% of NaI) connected to digital signal processing electronics (ORTEC DSPEC). The efficiency of the detector was measured with NIST calibrated γ -ray standards. The γ -ray spectra were analyzed using DECHAOS [10] to give absolute end of bombardment activities. Cross sections were calculated for the observed residue nuclei taking into account the temporal variation of the beam intensity during the irradiations.

Following γ -ray spectroscopy, the irradiated target foil and backing material were dissolved in acid and the As and Ge residues were separated by standard radiochemical separations [11]. Then the As and Ge fractions were assayed using a Tennelec LB1000 Low Background Beta Counter (efficiency ~52.5%) and the decay of the sample was followed for several days. The yields of the As chemical separation ranged from 27 to 100% (average yield = 63%), whereas the yields of the Ge separations ranged from 3 to 32% (average yield = 22%). (These yields were determined by post irradiation neutron activation analysis of the samples.) The residue nuclei were identified by their atomic number (established by chemistry) and their observed decay half-life. The decay curves for the β counting were resolved using the DECHAOS software. A typical decay curve is shown in Fig. 2.

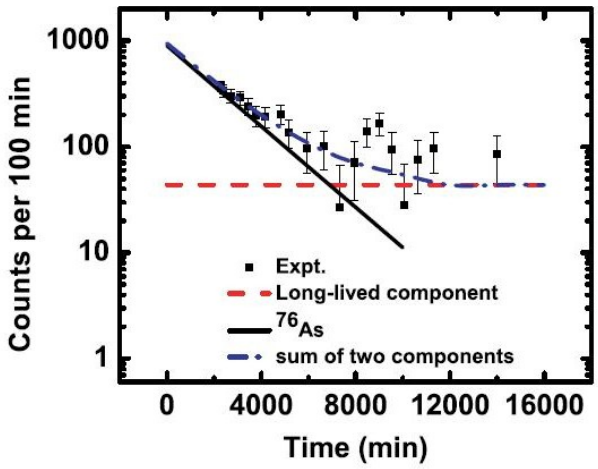

FIG. 2. (Color online) Decay curve for β counting of As chemical fraction from the reaction of 14.7 MeV ^{9}Li+^{70}Zn. The decay curve is resolved into two components: that due to ^{76}As decay (solid line) and that due to a long-lived background activity (dashed line). The sum of the two components is shown as a dash-dotted line.

The only detected activity in any irradiation was ^{76}As. Upper limits (2σ) for the production of ^{77}Ge and ^{77}As were ~0.1 mb. After correction for chemical yields, branching ratios, detector efficiency, temporal variation of the beam intensity during the irradiations, etc., the production cross sections for the residue nuclei were calculated. In Table I, we summarize the details of each irradiation. (E_{cot} is the center-of-target beam energy.)

TABLE I. Details of the ^{9}Li irradiations.

E_{lab} (MeV)	E_{cot} (MeV)	t_{irr} (min)	Dose (particles)	Method of assaying samples
11.5	11.0	848	3.4×10^{11}	β
12.5	12.0	5099	2.6×10^{11}	β, γ
13.5	13.0	1006	2.3×10^{11}	β
14.0	13.7	2395	6.5×10^{11}	β, γ
14.5	14.1	2577	5.9×10^{11}	β, γ
15.1	14.7	2062	4.2×10^{11}	β, γ
15.4	15.0	1196	3.9×10^{11}	β

Where a cross section was determined by both γ -ray spectroscopy and β counting, the results were averaged to get the final cross section. To get the fusion cross sections from the observed radionuclide yields, a correction for unobserved products must be made. That correction was taken as the average value of the ratio of the fusion cross section to the ^{76}As production cross section as computed using the statistical model

codes PACE v. 4.13 [8] and HIVAP [9]. These corrections ranged from 0.72 to 0.83 for the different projectile energies.

III. RESULTS AND DISCUSSION

The observed fusion cross sections are tabulated in Table II and plotted as a function of beam energy in Fig. 3.

TABLE II. Measured fusion cross sections for the reaction of ^{9}Li with ^{70}Zn.

E_{cot} (MeV)	$E_{c.m.}$ (MeV)	Cross section (mb)
11.0	9.7	34.1 ± 6.6
12.0	10.6	51.7 ± 23.1
13.0	11.5	79.2 ± 12.1
13.7	12.1	178.1 ± 16.7
14.1	12.5	214.8 ± 15.6
14.7	13.	391.3 ± 22.3
15.0	13.4	$341. \pm 36.3$

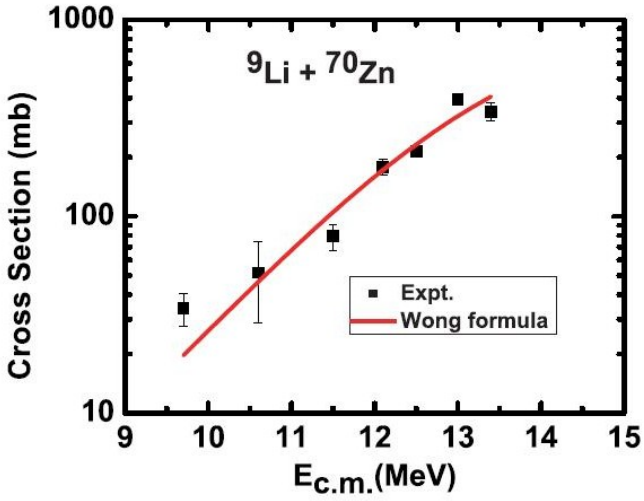

FIG. 3. (Color online) The measured fusion excitation function for the ^{9}Li+^{70}Zn reaction. The line is the result of fitting the data with the Wong one-dimensional barrier penetration model with $V_B = 12.5$ MeV, $R_B = 12.1 \pm 1.0$ fm, and $\hbar\omega = 5.7 \pm 0.8$ MeV.

The uncertainties in the cross sections reflect the uncertainties in the measured activities (primary uncertainty) and the systematic uncertainties, such as detector efficiencies, beam integration, decay branching ratios, correction for missing activities, etc. To place these data in the context of other similar measurements of fusion excitation functions for Li interacting with Zn, we show in Fig. 4 the reduced fusion excitation functions for the ^{6,7}Li+^{64}Zn [12] and the ^{9}Li+^{70}Zn reactions.

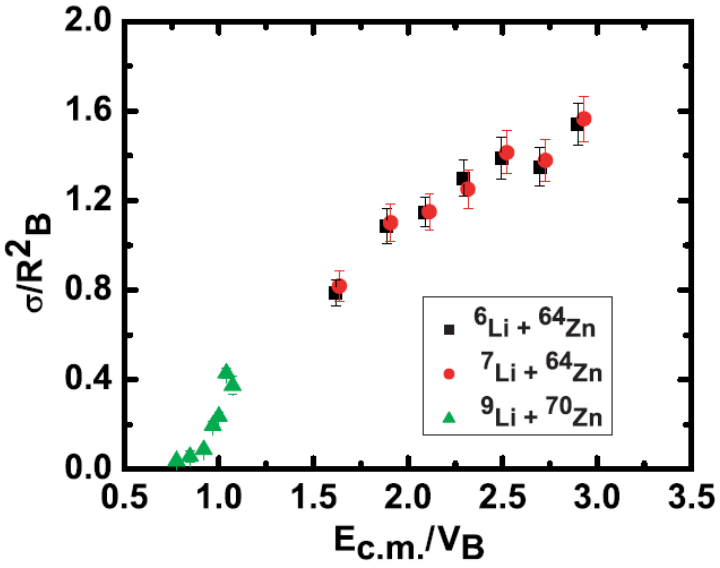

FIG. 4. (Color online) The reduced fusion excitation functions for the reaction of ^{6,7}Li with ^{64}Zn and ^{9}Li with ^{70}Zn.

In making this plot we divided the center-of-mass (c.m.) beam energy by the value of the fusion barrier height, V_B, for each system as derived from the semi empirical Bass model [13] and divided the cross section by the square of the Bass model fusion radius, R_B. (Use of another semi empirical prescription [14] for V_B and R_B would change the values of the scaling parameters by 3–4%.) We see, immediately, that the projectile energies used in this work are sub- and near barrier, whereas the studies with ^{6,7}Li were at a much higher energy. The Bass model barrier height for the ^{9}Li+^{70}Zn system is 12.5 MeV, with most of our data being taken in the sub-barrier region. To describe this sub-barrier fusion, we anticipate that the nuclear structure of ^{9}Li will be important. ^{9}Li has a charge radius, r_c = 2.217 fm [15], a matter radius of 2.44± 0.08 fm [16], and a neutron radius of 2.59 fm [16]. As such, the nucleus is described [16] as having a neutron skin of thickness 0.48 fm. The density distribution for ^{9}Li, although not as large as for ^{11}Li, does show a significant tail to large radii with $\rho = 10^{-4}$ nucleon/fm^3 at 6.5 fm [17]. ^{9}Li has been described in the shell model [18] as a combination of ^{4}He, ^{3}H, and two neutrons. The Q value for two-neutron transfer (^{9}Li + ^{70}Zn → ^{7}Li + ^{72}Zn) is large (+8.612 MeV). All of these factors lead us to expect a large fusion radius for ^{9}Li involving the interaction of the skin neutrons with neutron-rich ^{70}Zn. A simple way to demonstrate this effect numerically is through the use of the Wong formula [19]. The Wong formula represents the fusion barrier as a parabola and, in a semiclassical expression, describes the fusion cross section, σ_W, as

$$\sigma_W = \frac{\hbar\omega_B R^2{}_B}{2E} \ln\left\{1+\exp\left[\frac{2\pi}{\hbar\omega_B}\left(E-V_B\right)\right]\right\} \qquad (1)$$

in terms of the fusion barrier height V_B, fusion radius R_B, and barrier curvature $\hbar\omega_B$. We fixed the value of V_B at 12.5 MeV [13] and fit the data by varying R_B and $\hbar\omega_B$ giving values of R_B = 12.1 ± 1.0 fm and $\bar{}\hbar\omega B$ = 5.7±0.8 MeV. The data are well described (Fig. 3). (Allowing all parameters to vary produced R_B = 18±29 fm, V_B =

13.8±4.9 MeV, and $\hbar\omega_B$ = 6.8±2.5 MeV. Because that fit is not statistically meaningful, we constrained V_B to be the value represented by the semiempirical Bass model.) The deduced value of R_B, 12.1 fm, is substantially larger than the simple touching radius ($2.44 + 1.2 \times 70^{1/3} = 7.44$ fm) and presumably reflects the interaction of the large tail of the ^{9}Li density distribution with that of ^{70}Zn. ^{9}Li is moderately deformed ($\beta_2 = -0.235$) [18], whereas ^{70}Zn has $\beta_2 = 0.228$ [20]. It is traditional to evaluate sub-barrier fusion cross sections, such as those measured in this work, using a coupled channels calculation. We used the code CCFULL [21] to make this calculation. We included the inelastic excitation of the first vibrational 2+ and 3− states in ^{70}Zn [20] and the rotational states in ^{9}Li [20]. We assumed a potential with V_0 = 105 MeV, r_0 = 1.12 fm and a diffuseness parameter a = 0.65 fm. We also included the two-neutron transfer channel described earlier (coupling strength = 0.3). In Fig. 5, we compare the measured data with the CCFULL calculations. There is a large sub-barrier fusion enhancement that is not described by the coupled-channels calculation. It is clear that the sub-barrier fusion of ^{9}Li is not easily described in conventional models of fusion. What are the consequences of this for understanding the fusion of ^{11}Li?

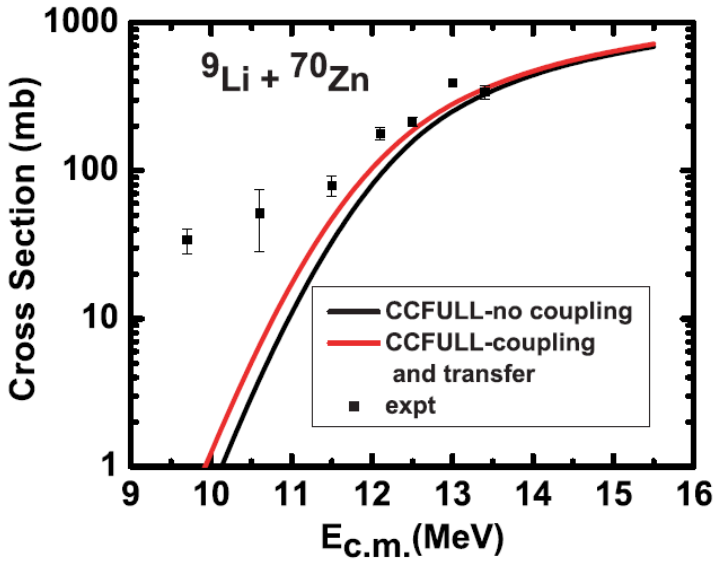

FIG. 5. (Color online) Comparison of the measured fusion excitation function for the ^{9}Li+^{70}Zn reaction and the predictions of a coupled-channels calculation.

As a schematic illustration of the difficulties posed by the data measured in this work, we show, in Fig. 6, the fusion excitation function for ^{9}Li+^{70}Zn "scaled up" to the ^{9}Li+^{208}Pb reaction. To do the "scaling," we have simply assumed the reduced excitation functions for the two systems are the same, and scaled projectile energies by the Bass barrier heights and the cross sections by the Bass model fusion radii.

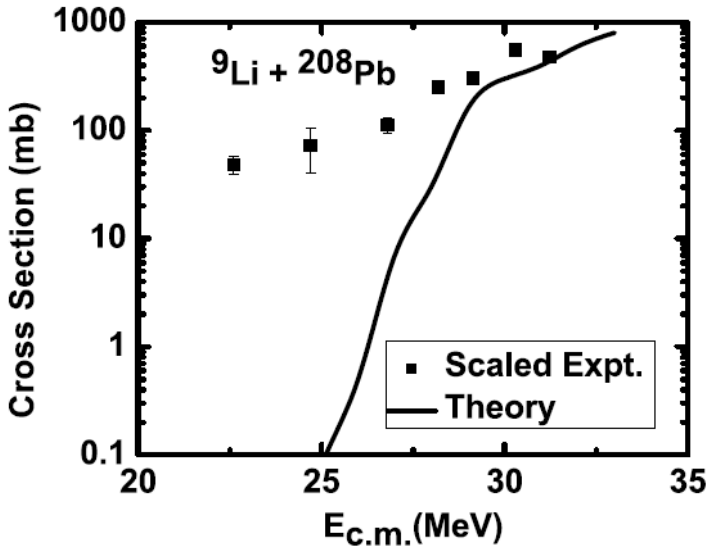

FIG. 6. Schematic comparison of the fusion excitation function for the ^{9}Li+^{208}Pb reaction as scaled from the data measured in this experiment and a calculation [22] of this excitation function.

We also show a sample theoretical calculation of the expected fusion cross section associated with the fusion of ^{9}Li with ^{208}Pb [22]. The observed sub-barrier fusion enhancement is not predicted and if this enhancement occurs for the fusion of the ^{9}Li core in the ^{11}Li reactions, it will complicate the description of these reactions. For example, the central issue in the fusion of ^{11}Li with ^{208}Pb [23] is the effect of the breakup of ^{11}Li prior to fusion. One measure of whether this occurs is the observation of sub-barrier fusion enhancement, i.e., if no breakup occurs, one expects [23] that the sub-barrier fusion of ^{11}Li with ^{208}Pb will be greatly enhanced by the halo nucleons. But if the ^{9}Li core already shows this sub-barrier fusion enhancement independent of the presence or absence of the halo nucleons, determining the effect of the breakup of ^{11}Li will be more difficult.

IV. CONCLUSIONS AND SUGGESTIONS FOR FUTUREWORK

What have we learned from this study? We conclude that: (a) It is possible to measure fusion excitation functions for light and intermediate mass nuclei using current ^{9}Li radioactive beams. (b) The fusion excitation function for the ^{9}Li+^{70}Zn reaction shows a large sub-barrier fusion enhancement that is not accounted for by current coupled channel calculations. (c) The large fusion radius, R_B = 12.1±1.0 fm, deduced from fitting the observed excitation function may be due to the neutron skin and extended neutron density distribution of ^{9}Li. (d) The analysis of ^{11}Li fusion reactions will need to take into account the unexpected sub-barrier fusion enhancement associated with the ^{9}Li core. Possible extensions of this work include: (a) actually performing the study of the fusion of ^{9}Li with ^{208}Pb to verify that the behavior predicted by excitation function scaling actually occurs and (b) extension of future studies of the fusion of ^{9}Li to lower energies to determine the limits of the sub-barrier fusion.

ACKNOWLEDGMENTS

We thank the operations staff of the cyclotron and ISAC, in particular, Chris Payne and Marco Marchetto, for providing the ^{9}Li beams. This work was supported in part by the Director, Office of Energy Research, Division of Nuclear Physics of the Office of High Energy and Nuclear Physics of the U.S. Department of Energy under grant DE-FG06-97ER41026 and TRIUMF and the Natural Sciences and Engineering Research Council of Canada.

APPENDIX

One of the original goals of this experiment was to measure the fusion excitation function for the ^{11}Li+^{70}Zn reaction. Three separate irradiations of ^{70}Zn targets with beams of ^{11}Li were made in hopes of detecting evaporation residues. The ^{11}Li beams were produced in a similar manner to that described for the production of ^{9}Li beams. Proton beam currents of 50 μA (2005) and 100 μA (2006) were used to produce ^{11}Li beams. The average on-target beam intensities were 680 particles/s (2005) and 740 particles/s (2006). At these incident beam intensities, detection of evaporation residues, even using sensitive radiochemical techniques, is difficult. The details of the irradiations are given in Table III.

TABLE III. Details of the ^{11}Li irradiations.

E_{lab} (MeV)	E_{cot} (MeV)	t_{irr} (min)	Dose (particles)
17.5	17.0	2546	1.04×10^{8}
17.5	17.0	3647	2.16×10^{8}
16.5	16.1	2840	7.78×10^{7}

Following each irradiation, the ^{70}Zn targets and backing foils were dissolved in acid and As and Ge chemical fractions were isolated using the same methods employed in the ^{9}Li irradiations. Upper limits on cross sections were calculated for each irradiation and are summarized in Table IV.

TABLE IV. Measured upper limit ($2\ \sigma$) cross sections for the ^{11}Li+^{70}Zn reaction.

E_{lab} (MeV)	Upper limit cross section (b)
17.5	31
17.5	27
16.5	55

The values of these upper limits are so large as to be meaningless. The currently available energetic ^{11}Li beams are not sufficiently intense to do studies of fusion reactions.

[1] G. F. Bertsch, B. A. Brown, and H. Sagawa, Phys. Rev. C **39**, 1154 (1989).
[2] D. Peterson, J. J. Kolata, P. Santi, J. von Schwarzenberg, D. Bazin, and B. M. Sherrill, Phys. Rev. C **67**, 014601 (2003).
[3] B. Blank *et al.*, Nucl. Phys. **A555**, 408 (1993).
[4] M. Petrascu *et al.*, Phys. Lett. **B405**, 224 (1997).
[5] A. Yoshida *et al.*, in *Heavy Ion Fusion: Exploring the Variety of Nuclear Properties*, edited by A. M. Stefanini, G. Nebbia, S. Lunardi, and G. Montagnoli (World Scientific, Singapore, 1994), pp. 311–318.
[6] P. Bricault, M. Dombsky, A. Dowling, and M. Lane, Nucl. Instrum. Methods Phys. Res. B **204**, 319 (2003).
[7] M.Dombsky, P.Bricault, andV. Hanemaayer,Nucl. Phys. **A746**, 32c (2004).
[8] O. B. Tarasov and D. Bazin, Nucl. Instrum. Methods Phys. Res. B **204**, 174 (2003).
[9] W. Reisdorf, Z. Phys. A **300**, 227 (1981).
[10] K. Aleklett, J. O. Liljenzin, andW. Loveland, J. Radioanal. Nucl. Chem. **193**, 187 (1995).
[11] NAS-NS-3002(rev), Radiochemistry of Arsenic, p. 34 (1965).
[12] I. Padron *et al.*, Phys. Rev. C **66**, 044608 (2002).
[13] R. Bass, *Nuclear Reactions with Heavy Ions* (Springer, New York, 1980).
[14] L. C. Vaz, J. M. Alexander, and G. R. Satchler, Phys. Rep. **69**, 373 (1981).
[15] R. Sanchez *et al.*, Phys. Rev. Lett. **96**, 033002 (2006).
[16] A. V. Dobrovolsky *et al.*, Nucl. Phys. **A766**,1 (2004).
[17] A. Bhagwat, Y. K. Gambhir, and S. H. Patel, J. Phys. G **27**, B1 (2001).
[18] D. Borremans *et al.*, Phys. Rev. C **72**, 044309 (2005).
[19] C. Y. Wong, Phys. Rev. Lett. **31**, 766 (1973).
[20] The energy levels for the nuclei in question were taken from the ENSDF files at the National Nuclear Data Center (http://www.nndc.bnl.gov), whereas the deformations were taken from S. Raman, C. W. Nestor, and P. Tikkanen, At. Data Nucl. Data Tables **78**, 1 (2001); R. H. Spear, At. Data Nucl. Data Tables **42**, 55 (1989).

[21] K. Hagino, N. Rowley, and A. T. Kruppa, Comput. Phys. Commun. **123**, 143 (1999).
[22] N. Takigawa, M. Kuratani, and H. Sagawa, Phys. Rev. C **47**, R2470 (1993).
[23] C. Signorini, Nucl. Phys. **A693**, 190 (2001).